# Melt Decontamination of Radioactive Stainless Steel by Electroslag Remelting

Joanna Meredith Robertson Buckentin

B.S., Metallurgical Engineering,
University of Arizona, 1981
M.S., Mineral Processing Engineering,
Montana College of Mineral Science and Technology, 1983

A dissertation submitted to the faculty of the
Oregon Graduate Institute of Science & Technology
in partial fulfillment of the
requirements of the degree
Doctor of Philosophy
in
Materials Science and Engineering

April 1996

The dissertation "Melt Decontamination of Radioactive Stainless Steel by Electroslag Remelting" by Joanna M.R. Buckentin has been examined and approved by the following Examination Committee:

---

Dr. David G. Atteridge
Thesis Advisor
Professor, Materials Science and Engineering
Oregon Graduate Institute of Science & Technology

---

Dr. Brian K. Damkroger
Department Manager (Acting)
Liquid Metal Processing Department
Sandia National Laboratories

---

Dr. Jack H. Devletian
Professor, Materials Science and Engineering
Oregon Graduate Institute of Science & Technology

---

Dr. Robert H. Frost
Associate Professor, Metallurgical Engineering
Colorado School of Mines

---

Mr. Ronald E. Mizia
Engineering Fellow
Idaho National Engineering Laboratory

---

Dr. Milton R. Scholl
Assistant Professor, Materials Science and Engineering
Oregon Graduate Institute of Science & Technology

# Acknowledgments

I would like to acknowledge the faculty and staff of Oregon Graduate Institute of Science and Technology for my excellent educational experience. Special thanks goes to Professor Jack Devletian, for his skillful teaching of Solidification Mechanics and Ternary Phase Diagrams, Dr. Lemmy Meekisho, for giving me a foundation in Finite Element Analysis, Dr. Tony Bell of the Physics Department, for his through treatment of Classical Thermodynamics, and Dr. David Atteridge, for his detailed treatment of the relationship between free energy and phase diagrams. Very special and heart felt thanks goes to Dr. Atteridge for all his work as an organized and practical thesis advisor and to both he and his wonderful wife, Jessie, for being my friends.

Several individuals at Idaho National Engineering Laboratory were very helpful, especially Ron Mizia, who was an excellent program manager, and Dr. Glen Kessinger, who helped with the thermodynamics. This work could not have been completed without the capabilities of the analytical lab at Teledyne Wah Chang, Albany. I am also very grateful to ESCO for their work in material preparation and especially to Dan Danks, for providing analysis of many ingot sections.

I would like to thank the personnel of the Liquid Metals Processing Laboratory at Sandia National Laboratories for all their help, encouragement, and support. Sam Giron carefully helped prepare the many batches of slag needed for this research. Bob Davis and Marty Gonzales did an excellent job of installing thermocouples in the water jacket. Thanks also goes to the ESR team: Greg Shelmidine, Eric Schlienger, and Dave Melgaard. I am very grateful to Greg for his help with setting up the furnace and running the melts. This work could not have been completed without Greg's enthusiasm for it. The control strategy designed by Eric allowed the melting experiments to be run in a precise manner, and the control and monitoring software written by Dave allowed real-time observation of experimental parameters. I would like to thank Jim Maroone for his help and advice. I am very grateful to Dr. Brian Damkroger for all the time he spent with me during the time I was analyzing my data and writing this thesis. He asked thought provoking questions from which I learned a great deal.

Finally, and most especially, I am grateful to my family for their love. My sons, John and Patrick, are the lights of my life. My very special and wonderful parents, John and Peggy Robertson, always believed in me. I would especially like to thank my dad for teaching me about the magic of metallurgy and for the wonderful gift of his friendship.

# Dedication

This work is dedicated to

Noelle Margaret Robertson, my sister

and to

Amanda Jo Buckentin, my daughter

*"Be not forgetful to entertain strangers,*

*for thereby some have entertained angels unawares"*

*Hebrews 13:2*

# Table of Contents

# List of Figures

# List of Tables

# Abstract

Joanna Buckentin
Supervising Professor: Dr. David Atteridge

This research was directed at the recycling of radioactively contaminated stainless steel by Electroslag Remelting. Factors influencing ingot quality and elemental partitioning between stainless steel and slag were studied. Stainless steel (304L) electrodes measuring 2.5 inches in diameter were coated with blends of rare earth element oxides to simulate surface contaminated scrap metal. These electrodes were melted into a 3.75 inch diameter round mold using thirteen different slags representing a factor space on the ternary $CaF_2/CaO/Al_2O_3$ phase diagram. Samples of each ingot, slag cap, and slag skin were analyzed for the presence of the surrogate elements. During each melt, changes in current, voltage, power, and impedance were electronically recorded. Thermochemical modeling was used to predict the partitioning of elements between the metal and the slag and to provide insight into the chemical mechanisms by which certain elements are captured by a slag. Analysis of the remelted steel showed that, for each slag tested, the level of surrogate elements was less than the detection limit of 1 ppm, except when the choice of slag caused oxide entrapment on the ingot surfaces. Slag chemistry was shown to influence the final chemistry of the ingot produced, as well as its surface quality. Most of the slags tested did not cause the steel to deviate from the chemistry for 304L, and, in fact, resulted in a decrease in the levels of elements such as sulfur and silicon. In particular, slag chemistry was shown to influence the partitioning of surrogates between the slag skin and the slag cap. This partitioning may be explained by studying the mechanisms by which slag skins are formed and the prevalent surrogate bearing species present in slags of different chemistries. Ideally, radionuclides would be partitioned to the slag cap, which could easily be disposed of at the end of the melt.

# Chapter 1
# Introduction

## 1.1 Purpose of the Research

The downsizing or discontinuation of domestic nuclear operations, both defense related and commercial, has led to a growing stockpile of radioactively contaminated scrap metal, much of which is stainless steel. Due to initial design requirements for nuclear operations, this steel, which contains large quantities of strategic elements such as nickel and chromium, is the product of complex processing operations and thus represents a valuable domestic resource. Burial of this material would be wasteful and expensive, since long term monitoring would be necessary in order to minimize environmental risk. Melt decontamination of this material would maintain the chemical pedigree of the stainless steel, allowing its controlled reuse within the nuclear community. This research addresses the melt decontamination of radioactively contaminated stainless steel by electroslag remelting (ESR). This melting technique, which is industrially used for the production of specialty steels and superalloys, maintains the specified chemistry and mechanical properties of the original material while capturing the radioactive transuranic elements in a stable slag phase.

## 1.2 Experimental Overview

This research is centered about the use of Electroslag Remelting as a process for the melt decontamination of stainless steel and the consolidation of radioactive elements into a small volume of chemically stable slag. The partitioning of elements such as sulfur and phosphorous to a slag has been shown to be dependent on the thermochemical properties of the slags used. The specific purpose of this study was to determine the effects of slag chemistry on the melt decontamination efficiency achieved when 304L stainless steel was melted in contact with various slags having different ratios of $CaF_2/CaO/Al_2O_3$. Selected

non-radioactive rare earth elements were used in these experiments to simulate the presence of radioactive transuranic elements. Thermodynamic modeling was performed in order to predict the differences which could be expected in the behaviors of the surrogate elements and the actual radionuclides in a high temperature environment.

### 1.2.1 Melting Experiments

In order to simulate the melting of surface contaminated reactor piping, stainless steel bars were plasma spray coated with various mixtures of surrogate oxides. The rare earth elements lanthanum, cerium, and neodymium were chosen to act as surrogates in this study because of the thermochemical similarity of these elements to the transuranic elements. The surrogates were applied as oxides because the chemical affinity of the transuranic elements for oxygen would insure their presence as oxides in the layers of corrosion product which adhere to the walls of reactor piping. The coated stainless steel bars were then electroslag remelted using slags containing various ratios of calcium fluoride, calcium oxide, and alumina. After melting, the resulting stainless steel was analyzed in order to determine the extent to which it had been decontaminated as well as the changes in its base chemistry which had been brought about by melting. Samples of the slag cap and the slag skin were analyzed in order to determine how the surrogate elements were partitioned during melting.

### 1.2.2 Modeling Experiments

Because this study was conducted using surrogates in place of actual radionuclides, thermochemical modeling was undertaken in order to determine how well each slag would be expected to remove transuranic elements from stainless steel. A free energy minimization model was used to predict the residual levels of surrogate elements present in each ingot after remelting using a slag of known chemistry. Predictions were also made concerning the remelting of uranium contaminated stainless steels. The accuracy of the free energy minimization model was determined by a comparison of the predicted changes in levels of major alloying elements with the actual changes caused by remelting. Free energy minimization was also used to predict the types and quantities of chemical species formed in the slag. The levels of thermochemically dominant surrogate bearing species were also predicted using an ionic Temkin slag model.

## 1.3 Summary of the Results

Melting results showed that the rare earth elements were removed from the bulk of the stainless steel to levels below the detectable limit of 1 ppm regardless of the chemistry of the slag employed. In agreement with this result, free energy minimization studies predicted that bulk surrogate levels would be much less than 1 ppm in the remelted steels, but that some slags would achieve more effective decontamination than others. In cases where the chosen slag resulted in poor surface quality, however, entrapped slag inclusions caused increased levels of surrogates on the ingot surfaces. Slag chemistry was shown to influence surface quality as well as melting efficiency.

Interestingly, this study showed that, by changing the slag chemistry, the rare earth elements used to simulate radionuclides could be partitioned to either the slag skin or to the slag cap. This result may be explained by looking at the solidification trace for each slag in conjunction with the rare earth phases predicted by the thermochemical model. When a molten slag comes in contact with a cold copper jacket, the component of the slag with the highest melting point may be assumed to solidify out first. The rare earth bearing compounds may be present as low melting point fluorides or higher melting point oxides or aluminates, depending on the chemistry of the slag. The chemical form taken by the rare earth elements may be predicted by use of the thermochemical slag model. If the highest melting point component in the slag is a rare earth compound, the rare earth element will be concentrated in the slag skin. If, on the other hand, the rare earth is present in a form with a lower melting point than the oxide-fluoride mix predicted by the phase diagram, the rare earth will tend to be present in the slag cap because it would be among the last phases to solidify.

## 1.4 Ramifications

Electroslag remelting was shown to be an excellent process for the melt decontamination of radioactive stainless steel. The process could easily be enclosed, facilitating the capture of volatile dust and gases. Slag chemistry could be adjusted in order to optimize the capture of radionuclides and other undesirable elements from the steel while allowing the retention of property dependent alloying elements. At the end of each melt, radioactive elements are present in a solid, mineral-like slag which is easily handled and stored.

In order to insure optimum decontamination levels, remelting operations should utilize a slag which effectively captures radioactive elements and facilitates the production of ingots having excellent surface quality. Good ingot surface minimizes the possibility of radioactive slag inclusions and eliminates the need for surface treatment prior to forming. The capture of radionuclides in a monolithic slag cap would provide for ease of handling and storage and would minimize the level of surface contamination present on the ingots.

Thermodynamic modeling suggests that, while the transuranic elements are thermochemically similar to the rare earth surrogates used in this study, they will probably not behave in an identical manner during electroslag remelting operations. It is thus recommended that pilot studies be carried out using actual radioactive elements and that an optimum slag be selected for each type or mixture of contaminants present in each batch of scrap to be melted.

# Chapter 2
# Background

## 2.1 Overview

Nuclear operations involving transuranic (TRU) elements have resulted in the accumulation of large quantities of contaminated metallic waste which are stored at various DOE, DOD, and commercial sites under the control of DOE and the Nuclear Regulatory Commission (NRC). This waste will accumulate at an increasing rate as commercial nuclear reactors built in the 1950s reach the end of their projected lives, as existing nuclear powered ships become obsolete or unneeded, and as various weapons plants and fuel processing facilities, such as the gaseous diffusion plants, are dismantled, repaired, or modernized.

The life expectancy of a commercial nuclear power plant is about 40 years. Those plants which began operation in the 1950s will be reaching the ends of their projected lives in the 1990s and additional plants are scheduled for shutdown through the year 2020. Each of these plants will produce 40,000 to 50,000 tons of metal waste when dismantled. Much of the LLCMW (low level contaminated metal waste) recovered during decommissioning of a commercial nuclear reactor will be in the form of low carbon stainless steel pipe and tubing ranging in size from 1 to 4 inches to 24 to 36 inches in diameter, although larger and smaller diameters will be encountered.[1] The amount of metal contained in this waste represents a substantial resource, especially when the content of such strategic metals such as nickel and chromium are considered.

Contaminated metal waste represents a considerable storage volume as well as a significant cost since it must be maintained and monitored indefinitely in secure storage. Alternatively, this material may be disposed of by burial, with current commercial costs being in the range of $450.00 per cubic foot.[2] The resulting financial and environmental burden will continue to be a problem as quantities of contaminated waste increase while the space available for disposal continues to decrease. The high cost of either disposal or

storage requires that the volume of material be minimized. Melting and casting into ingots of convenient shape reduces the volume of the material. However, if sufficient decontamination were achieved during melting, controlled reuse of the metal may be possible. Such reuse is an attractive option for many reasons, both economic and environmental. Published results show that melt refining can be an effective technique for decontamination, as well as volume reduction, when the proper slags, refractories, and melting techniques are used. The currently used technology, on the other hand, of surface decontamination by means of an acid leach or electrolytic technique, produces an additional contaminated liquid waste stream. Surface decontamination is also ineffective in decontaminating parts with cracks (a common fault in reactor steam tubes) or complex shapes.

## 2.2 Sources and Types of Radioactive Scrap Metal

Radioactively contaminated scrap metal arises from several different types of operation . The material composition and the type, level, and chemical form of contaminant present will vary depending on its source. In addition to requiring different processing schemes and/or parameters for optimum decontamination these differences will also affect environmental, safety, and health concerns for material handling and process operation. A review of the measurement of radiation, the various types and the associated hazards of each is presented in Appendix I.

The problems associated with recycling contaminated stainless steel are strongly related to the types, properties, and concentrations of the various radioisotopes which are present, hence on the source of the radioactive scrap metal (RSM). Stainless steel scrap will be contaminated by radioactive isotopes that originate from three major sources: fission, activation, and transmutation.[1] Fission products which result from the usually asymmetric splitting of the original nuclei, are typically isotopes with atomic mass numbers between 95 and 138. Activation products are usually unstable isotopes of the original alloying elements, such as cobalt and manganese, in the case of stainless steel. In commercial reactors, activation products result when neutrons from the nuclear reaction collide with the nuclei of the atoms that make up these components. Activation products are contained more or less homogeneously within the volume of the structures in which they were formed but may be transported by the primary coolant as a corrosion products and deposited on surfaces throughout the system. Transmutation, which occurs within the nuclear fuel itself as a result of neutron capture, generates the transuranic (TRU) elements,

defined as elements with atomic numbers above 92. TRUs characteristically have long half lives.

The greatest portion of the radionuclides of concern are present in the form of surface contamination.[3] An example is the oxidized material which is known to adhere tenaciously to the internal surfaces of reactor piping. This material is composed of corrosion products from anything with which the water has come in contact, including activated structures in the vicinity of the reactor core or fuel fragments which have escaped through cladding breaches.

Evaluating the radionuclides present in radioactive scrap metal also includes a consideration of the time between operation and recycling. Some radionuclides are short lived and the passage of time greatly decreases their levels. Dyer[3] has assumed that it would take at least 1000 days before any reactor material would enter the recycling process and therefore has limited his consideration to radionuclides with half-lives longer than 50 days. Another concern is the type of nuclear emissions associated with particular nuclides. Gamma emitters will be a major problem in any recycling effort because the radiation they emit will not be decreased by most shielding. Conversely, alpha and beta emitters are less of a problem but must be controlled in the working area to prevent ingestion by workers.

Virtually all facilities which have been sites of nuclear activity will, at some point, become sources for radioactive scrap metal. One of the largest sources of radioactive scrap metal are commercial nuclear power plants, which were built in the 1950s and typically have a projected 40 year lifespan. Commercial nuclear power plants are by no means the only source of radioactive scrap metal, however. Each step in uranium beneficiation processes results in uranium contaminated equipment. The utilization of this uranium for the production of power or weapons results in equipment contaminated not only with uranium, but with fission and activation products. Fuel handling, storage, and reprocessing result in yet more contaminated metal. The following overview of some of the processes which result in contaminated metals describes the decontamination challenges which may be encountered at some specific nuclear sites.

### 2.2.1 Uranium Beneficiation and Purification Plants

Naturally occurring uranium ore typically contains only a few pounds of uranium per ton, of which $^{235}U$ is the only fissile isotope. Naturally occurring uranium is typically 99.27 atom percent $^{238}U$, 0.72 a/o $^{235}U$, and 0.0056 a/o $^{234}U$, which results from the decay of $^{238}U$. Each isotope decays by a series of decay reactions, yielding various daughter

products in the process, many of which are radioactive in their own right. Fresh uranium emits mainly alpha activity, but as uranium ages, beta and gamma activity develop owing to the growth of the first two decay products of $^{238}U$, $^{234}Th$ and $^{234}Pa$. After about a month, these approach saturation activity which remains constant for hundreds of years due to the long half life of $^{230}Th$, the first daughter of $^{234}U$. Purified uranium, freed from the decay products of $^{234}U$ is much less toxic than the uranium ores and the tailings of uranium mills. The most dangerous products of the decay of $^{234}U$ are $^{230}Th$, $^{210}Po$, and radium, long lived alpha emitters, as well as radium's gaseous daughter radon which disperses radioactivity in uranium mines and near mill tailings piles. These daughter products, more than the uranium itself, are responsible for the radioactive hazard associated with uranium mines and concentrating plants, which are one source of radioactive scrap metal.[4]

The uranium in the ore is concentrated by several processes including leaching, precipitation, solvent extraction, and ion exchange. Uranium concentrates are known commercially as yellow cake because the sodium diuranate or ammonium diuranate commonly produced by uranium mills is a bright yellow solid.[5] Uranium mining and beneficiation facilities include earth moving equipment, railroad cars, leach tanks, and various vessels and piping. Much of this equipment is likely to be composed of carbon and stainless steel and will be contaminated with various forms of uranium.

Light water reactors must be supplied with uranium having a higher content of fissile material than the 0.71 w/0 $^{235}U$ present in natural uranium. Uranium concentrates are shipped to a refinery or conversion plant where impurities are removed prior to the production of uranium hexafluoride, which is the feed material for a gaseous diffusion isotope separation process. In this process, $UF_6$ gas at high pressure flows along the inner walls of porous tubes whose outer wall is maintained at lower pressure. Because of the pressure differential, the gas flowing through the tube wall becomes slightly enriched in $^{235}U$.[4] Because the number of stages required to obtain a useful degree of separation is large, these plants contain vast amounts of nickel, carbon steel, stainless steel, aluminum, copper and other metals contaminated with uranium.

Finally, enriched $UF_6$ is shipped to a plant for the fabrication of reactor fuel elements where it is converted to $UO_2$ or other forms of uranium used in reactor fuel. For light water power reactors in the United States, $UO_2$ is pressed and sintered into pellets, which are loaded into zircaloy tubing. These individual fuel rods are sealed and assembled into bundles and the fuel elements are shipped to the reactor. During each component of the process leading up to the manufacture of reactor fuel, facilities may have become contaminated to some degree with uranium and its fission products.

## 2.2.2 Nuclear Power Reactors

In the nuclear fission process used in power reactors reaction, the $^{235}U$ nucleus splits into two radioactive fission products, releasing energy and several new neutrons to sustain the process. To keep the rate of the reaction constant, neutrons are allowed to leak from the reactor, or are absorbed by nonfissionable materials such as boron or $^{238}U$. Also, some of the neutrons absorbed by $^{235}U$ produce the isotopes $^{236}U$, $^{240}Pu$, or $^{234}U$ rather than causing fission.

The fission of $^{235}U$ can take place in a number of ways as long as the contents of the $^{235}U$ nucleus, 92 protons and 143 neutrons plus the reactant neutrons, are maintained. For example, the products may be $^{144}Ba$ (56 protons and 88 neutrons), $^{89}Kr$ (36 protons and 53 neutrons), and three extra neutrons. The fission fragments are often unstable themselves and undergo radioactive decay, converting neutrons to protons, which remain in the nucleus, and electrons, which constitute beta radiation. In this case, four neutrons in the $^{144}Ba$ are successively converted into protons and electrons resulting in $^{144}Nd$ and beta radiation. Similarly, three neutrons in the $^{89}Kr$ may be converted, resulting in $^{89}Y$ as the end product. In addition to $^{235}U$, $^{239}Pu$ and $^{233}U$ can be used as fuel in nuclear fission reactors.[4]

Since the radioactive fission products have half-lives ranging from fractions of a second to millions of years, the emission of beta particles and delayed gamma rays takes place over a long period of time after a reactor has been shut down, but at a diminishing rate. As a result, a broad range of contaminants can be produced in fission reactors.

The two most common commercial reactor types in the United States are the pressurized water reactor (PWR) and the boiling water reactor (BWR). In these reactors, fuel and moderator ordinarily remain in place, and coolant flows through the reactor to remove heat. In a pressurized water reactor, the coolant/moderator is pressurized to 150 bar so that it remains liquid at the highest temperature (300°C) to which it is heated in the reactor. Hot coolant flows from the reactor to a steam generator where it is cooled by heat exchange with feedwater and returned to the reactor. In the process, the feedwater is converted to steam to drive the turbine. The steam is then condensed, preheated and recircualted as feedwater to the steam generator. In a boiling water reactor, the water is at a lower pressure (around 70 bar) so that it boils and is partially converted to steam as it flows through the reactor. Coolant leaving the reactor is separated into water which is recycled and steam, which is sent directly to the turbine.

In a reactor, primary water comes in contact with the nuclear core and becomes contaminated with radioactive nuclides by two means. The first is by the breaching of fuel elements, which permits the escape of radioactive elements. Primary water also contains corrosion products from the stainless steel pipes through which it passes. These corrosion products pass through the reactor core and become activated. Once the primary water is contaminated, it contaminates all the reactor components with which it comes in contact, often by depositing radioactive corrosion products on the surfaces. The situation is particularly acute in a boiling water reactor which no external steam generator. Nearly all of the components of a boiling water reactor come in contact with the primary water, and thus are contaminated with either fission products from the fuel or activated corrosion products, or both. These components include the reactor water piping, the steam turbine, the steam condenser, the reactor pump, and the reactor water cleanup system.[3]

Dyer[3] surveyed the radionuclides found in commercial nuclear power reactors in the United States and found that the radionuclide types and amounts differ according to reactor type. Radionuclides resulting from activation of iron, cobalt, and zinc were shown to be present at similar levels in pressurized water reactors and boiling water reactors, unlike the activation nuclides for nickel and tin. The nuclides resulting from the activation of nickel, $^{58}Co$ and $^{63}Ni$, were found to be present at a higher level in pressurized water reactors. The tin activation nuclide, $^{125}Sb$, was present at higher levels in boiling water reactors due to the dissolution of tin from the condenser tubes. Isotopes of radiocesium, $^{134}Cs$ and $^{137}Cs$ were shown to be two orders of magnitude higher in pressurized water reactors than in boiling water reactors, while isotopes of radiostrontium, $^{89}Sr$ and $^{90}Sr$ were found to be present at the same level in the two reactor types.

Analysis of pressurized water reactor coolant indicated that 90% of the radionuclide activities were radiocesium fission products and 10% were iron and cobalt activation products ($^{55}Fe$ and $^{60}Co$). A similar analysis of boiling water reactor coolant revealed about 91% of the activities were from $^{125}Sb$, with the other 9% represented by $^{55}Fe$ and $^{60}Co$. A survey of reactor parts showed that the radionuclides which accounted for 1% or more of the total activity were $^{54}Mn$, $^{55}Fe$, $^{60}Co$, $^{65}Zn$, $^{125}Sb$, $^{134}Cs$, and $^{137}Cs$. The most significant surface contamination of the primary cooling was found to be that related to surface oxide formation on the inside surface of loop components. The corrosion and activation chemistry that leads to such contamination varies with the reactor type. A reducing environment causes surface corrosion and oxide deposition in PWR reactors while an oxidizing environment results in deposits of different chemistry in BWR reactors. PWR cooling systems have been shown to contain phases of the type $Ni_xFe_yCo_zO$ and $Cr_aFe_bO_3$

where x+y+z=1and a+b=2. The BWR cooling system is constructed of stainless steel and is subjected to steam during normal operations. In this oxidizing environment the system contains $Fe_2O_3$ and $Fe_3O_4$ deposits as well as $NiFe_2O_4$ and $NiO_a(OH)_b$.[6,7]

### 2.2.3 Fuel Storage and Reprocessing Plants

The fuel processing operations used in conjunction with a nuclear reactor are yet another source of radioactive metal. Factors that typically require fuel to be discharged from the reactor include deterioration of the cladding due to fuel swelling, thermal stresses, or corrosion, and loss of nuclear reactivity as a result of depletion of fissile material and buildup of neutron absorbing fission products. The typical fuel lifetime of a fuel bundle is approximately three years. Reprocessing is used to recover and recycle uranium and plutonium and to reduce radioactive wastes to more compact form. Spent fuel is usually held in cooled storage basins at the reactor site to allow some of the radioactivity to decay prior to reprocessing. These storage basins, fuel racks, and the associated handling equipment may be candidates for melt recycling.

Spent fuel from a reactor contains uranium and plutonium as well as a very large number of fission product isotopes which are listed in Table 2.1, which due to its length is located at the end of this chapter. Several of these isotopes must be addressed when considering melt decontamination of fuel handling facilities and storage racks.

Fuel elements also contain radionuclides formed by neutron activation in the zircaloy cladding, stainless steel end fittings, and Inconel spacers. A typical three year irradiation of the metallic fuel cladding produces the radionuclides listed in Table 2.2 at the end of this chapter. Major contributors to the cladding radioactivity are $^{60}Co$ $^{55}Fe$, $^{58}Co$, and $^{68}Ni$. Ten years after discharge, appreciable radioactivity remains, so irradiated cladding is treated as long lived radioactive waste. When fuel cladding is composed of 316 stainless, as in the case of fast breeder reactors, the resultant radionuclides include $^{54}Mn$, $^{55}Fe$, and $^{60}Co$. Fuel cladding will also contain uranium, plutonium, and other transuranic radionuclides as contaminants on the inner surfaces of the cladding.[4]

## 2.3 Options for the Disposition of Radioactive Scrap Metal

As nuclear facilities close or their components are replaced, decisions must be made regarding the disposal or recycle of radioactive scrap metal. While some technologies approach the problem of radioactive scrap metal strictly from a disposal viewpoint, other

technologies incorporate ways to both minimize the volume of radioactive waste which will require storage and to decontaminate strategic radioactive metals so that their chemical pedigree is maintained. These decontaminated metals could then be available for controlled reuse within the DOE and/or commercial nuclear community, as opposed to being disposed of, allowing their strategic and economic values to be utilized.

### 2.3.1 Size Reduction, Packaging and Burial

As currently being performed, this option only requires that pieces of radioactive metal be torch cut or consolidated by melting to sizes small enough to fit within a waste container. When full, these containers are sealed and permanently stored in a monitored repository. While this method of scrap metal disposal may be performed with relative ease, there are many reasons why this is not the best option when long term costs and environmental factors are considered. Perhaps the most compelling of these reasons lies in the wealth of strategic alloying elements contained in radioactive scrap metal. As shown in Table 2.3 below, America's stockpile of radioactive scrap metal represents a large domestic resource for elements such as nickel, chromium, and manganese.[2] Unless decontaminated and recycled, this resource is lost.

**Table 2.3 Uses of and Sources of Strategic Elements Present in Radioactive Scrap Metal**

| | Chromium | Nickel | Manganese |
|---|---|---|---|
| **Uses** | Present in the 18-20% range to inhibit corrosion in stainless steel and nickel based alloys | Base for Inconel and other nickel base alloys,<br>Alloying element in stainless steel | Alloying element in steel production |
| **Sources of Virgin Material** | South Africa<br>Former Soviet Union<br>Turkey<br>Zimbabwe<br>Philippines<br>Cuba<br>Yugoslavia | Canada<br>New Caledonia<br>Former Soviet Union<br>South Africa<br>Burma<br>East Indies | Ukraine<br>South Africa<br>India<br>Ghana |

### 2.3.2 Methods for Decontamination of Radioactive Scrap Metal

The goal of radioactive scrap metal decontamination is the removal of radioactive contaminants to a level such that the decontaminated metal may be handled safely or reused. In some cases, this may be achieved by use of surface decontamination techniques. There are, however, distinct advantages to the use of melt decontamination techniques.

#### 2.3.2.1 Surface Decontamination

Surface decontamination may be performed by either mechanical (sand blasting), chemical (acid attack), or electrochemical (anodic dissolution) removal of radioactive contaminants from the surfaces of metal parts or structures. These methods are inexpensive, uncomplicated, and relatively effective for the removal of surface contamination of parts with simple geometries. Surface decontamination may provide partial decontamination of piping assemblies without the need for disassembly. However, these techniques do nothing to remove bulk contamination and are ineffective for complex geometries, or for removal of contamination from cracks, a common flaw in reactor steam and heat exchanger tubes. Because these methods employ the principle of physical or chemical scouring to remove contamination, they result in a contaminated waste stream of scouring agent such as water, acid, or a sand slurry. The creation of this secondary waste stream creates further handling and disposal problems.

#### 2.3.2.2 Melt Decontamination

Melt decontamination of radioactive scrap metal has been widely studied and has several inherent advantages. These processes operate above the melting point of the scrap metal so that decontamination reactions take place either between two liquid phases or between a liquid phase and a gas phase, making the reaction kinetics involved very rapid. The high temperature at which these processes operate also aids their kinetic efficiency. When the radionuclide to be removed has a higher vapor pressure than its host metal, melting technologies can take place under vacuum in order to facilitate the removal of these species. Some melting technologies support the use of slags or fluxes which interact thermochemically and electrochemically with the liquid metal to specifically capture radionuclides. When properly formulated, these slags act as a low volume, stable containment for radioactive species. The basic operations of several processes are described

below, as are design requirements necessary for each process to be used for radioactive materials.

### 2.3.2.2.1 Descriptions of Melting Technologies

The technologies which have been investigated for the melt decontamination of radioactive scrap metals include electric arc melting, air induction melting, vacuum induction melting, plasma melting, and electroslag remelting. In the following sections, each technique is described and the inherent advantages or disadvantages regarding the use of each as a decontamination strategy are briefly discussed.

#### 2.3.2.2.1.1 Electric Arc Melting

In electric arc melting, the charge is heated and melted due to the heat passed between an electrode and the charge (in direct current melting) or indirectly between three electrodes (in three phase alternating current melting). Electric arc furnaces consist of a refractory lined hearth and a water cooled roof section, with holes to allow the electrodes to be lowered into place. The roof section may be lifted or swung away to permit feedstock to be loaded into the furnace. The roof section is then replaced, the electrodes are lowered and power is applied to melt the charge. After melting, the furnace is tilted, slag is tapped, and the molten metal is poured into a ladle. This process produces a great deal of dust and fume. Due to the logistics of scrap loading and molten metal removal, these furnaces are difficult to enclose. In order to safely use electric arc melting as a decontamination strategy, consideration must be made so that volatile elements and dust are captured and contained. In addition, spent refractory from the furnace hearth and from ladles used to transport molten metal becomes a radioactive waste stream. Slag handling is complex, because radioactive slags must be handled in a molten condition, at or above 1400°C, and slow cooled in such a way that their physical integrity is maintained.

#### 2.3.2.2.1.2 Air Induction Melting

An induction furnace is an AC electric furnace in which the primary conductor generates, by electromagnetic induction, a secondary current that develops heat within the metal charge. Once the charge is molten, this current may also be used to stir the melt. Induction melting permits, but does not require the use of a slag. Induction furnaces are

refractory lined, so reactions between the refractory and the metal and the refractory and the slag will occur. Such reactions increase the risk of cross contamination between melts and may cause the presence of contaminated refractory particles in the melt. Molten slag is removed by skimming, often manually. Because these furnaces may be opened for molten slag removal, sealing them is difficult and fumes and dust will escape during the slag skimming process. Induction furnaces favor good melt agitation , relatively easy fume control, and rapid heatup. Induction melting is not as inherently as dusty a process as electric arc melting, producing only 20% as much effluent dust as an electric arc furnace of similar capacity.[8] When used as a melt decontamination strategy, the overall process must include plans for capture of those radionuclides which will report to the fume and dust. Additionally, plans must be made for disposal of contaminated furnace and ladle refractory and for the solidification and containment of spent slag.

### 2.3.2.2.1.3 Vacuum Induction Melting (VIM)

Vacuum induction melting is based on the same principle as air induction melting, except that melting is performed in a vacuum, facilitating the capture of dust and fume. When performed in a vacuum, induction melting is usually done without a slag layer. Vacuum induction melting is an optimum decontamination strategy for the removal of volatile radionuclides, but, because it is performed without a slag, does not provide a mechanism for the removal of non-volatile radioactive species, except by means of inclusion formation, flotation, and agglomeration.

### 2.3.2.2.1.4 Plasma Melting

Plasma melting uses an intense and controllable stabilized electric arc discharge as the source of energy. Furnace designs incorporating both single and multiple plasma torches have been developed. One design features a dual hearth system with a torch operating in the transferred arc mode to each water cooler copper section. Material to be melted is fed into an upper water cooled copper hearth where primary melting is carried out. Heavy inclusions separate under gravity and molten material overflows into a water cooled withdrawal section. This section is equipped with a second torch for superheating which vaporizes or dissolves the low density inclusions floating on the surface of the melt. This process has no refractories to interact with the melt. Plasma melting has the capacity to incorporate a slag if desired, although its presence may complicate the process. As a

decontamination technique, the process is flexible, in that many types of scrap may be melted at once, with organic wastes being volatilized by the plasma. In addition, the process is a "one step" operation, with scrap being fed in, consolidated and decontaminated, and formed into a finished ingot. Removal of nonvolatile radionuclides may not be as efficient in plasma melting as in other melting technologies, due to the presence of the cold hearth, which reduces the average superheat and may thus have a detrimental effect on reaction kinetics.[9]

### 2.3.2.2.1.5 Electroslag Remelting

Electroslag Remelting, or ESR, is a consumable electrode process in which heat is generated by the passage of electric current through a conductive slag, which is resistively heated. As the electrode melts, the droplets of metal are refined by contact with the slag. The droplets collect at the bottom of a water cooled copper crucible and consolidate to form an ingot with low residual impurities, very few nonmetallic inclusions, and excellent surface quality. ESR produces a metal ingot in the form of a cylinder or a slab, which may be directly formed into a useful product by rolling or forging. Because the ESR process may be controlled remotely, it is easily contained and the volatile radionuclides which are removed from the metal may be effectively captured. During the ESR process, many decontamination mechanisms come into play. Radionuclides may be transferred from metal to slag at three sites: at the molten metal/slag interface present at the electrode tip, at the metal droplet/molten slag interface, and at the interface between the not yet solidified ingot and the slag. In addition, due to the presence of an electric current, two of these surfaces are electroactive, and the flow of electrons may be used to optimize decontamination reactions. At the completion of melting, the slag containing the radionuclides is removed as a solid, which is much easier and safer than the handling of liquid slag required by other processes. When performed in its usual mode as a consumable electrode process, ESR requires electrodes to be solid and continuous. Pieces of scrap may be welded together to accomplish this, as long as electrical contact between electrode sections is maintained. Alternately, the ESR process may be used in tandem with another melting process which would consolidate scrap, producing ESR electrodes.

## 2.4 Melt Decontamination Studies

The problem of radioactive scrap metal decontamination and disposal is of concern throughout the industrialized world. Researchers in many countries have conducted work, individually and as cooperative research groups, to develop safe and effective methods for the melt densification and decontamination of radioactive scrap metal. After the success of early melt decontamination trials, various melt decontamination strategies were studied on a laboratory scale. In several countries, full scale technical demonstrations have been followed by the completion of industrial melt decontamination facilities.

### 2.4.1 Early Trials

Interest in decontamination of steels began in the 1950s when the accumulation of uranium contaminated scrap at some locations increased to an onerous level. The first production scale steel decontamination project described in the literature involved 6000 tons of low level contaminated metal waste and was undertaken by the National Lead Company of Ohio[10]. Their efforts focused on monitoring the exposures of foundry personnel that resulted from processing this waste. A commercial steel mill used an electric arc furnace to melt the scrap which consisted of discarded uranium extraction equipment and baled drums which had been used for shipping uranium concentrate. The ingots averaged less than 3 ppm U and the slag contained 2.12 % U. The slag weight constituted 8.5% of the weight of the steel melted. By calculation, the average original uranium content of the scrap was 2000 ppm. The level of contained uranium in the ingots was below regulatory concern and they were sold on the commercial scrap market while the slag was shipped to Oak Ridge for disposal. In 1958, the same process was applied to 350 tons of radium contaminated scrap. After melting, the ingots averaged $9.0 \times 10^{-13}$ g Ra/ g steel and the slag averaged $1.47 \times 10^{-9}$ g Ra/ g steel.[11]

In 1956, Atomic Energy Commission policy permitted free disposal of uranium-contaminated steel when certain radioactivity restrictions were met. Kelvin and Harris[12] did a study with the purpose of demonstrating that, within certain limits, uranium contaminated iron and steel could be released into normal trade channels. Uranium contaminated scrap metals were obtained from various AEC uranium production sites, analyzed for alpha activity and uranium content, and were then induction remelted in a manner similar to that used in industrially treated scrap. Stainless-steel, copper, nickel, and nickel-steel ingots

were made by melting 20-30 lbs. of scrap in a magnesia or graphite crucible and casting into molds. Dust samples were taken directly above the crucibles in order to evaluate the health hazard of uranium carrying dust. After remelting, surface alpha-activity measurements were made on the individual ingots. The authors concluded that "air-dust samples revealed that no hazard should exist from dust or fumes during such remelting operations" because, with "a single exception, all samples taken during the remelting processes indicated atmospheric uranium concentrations below 10 dpm/$m^3$ (decays per minute) or less than 1% of the maximum permissible concentration". However, the one high sample showed a concentration of 80 alpha dpm/$m^3$. Nevertheless, the researchers concluded that "the remelting of large quantities could be safely accomplished." The research did show that uranium contaminated stainless steel, nickel, and copper was decontaminated down to about 1 ppm by remelting, although the ingot surfaces showed higher concentrations . Other conclusions, surprising by today's standards included: "The remelting of this type of material can be accomplished without hazard to personnel." Also "The contaminated slag contains significantly less uranium than a very low-grade ore, such as phosphate rock, and disposal should be permitted on normal slag dumps."

The Y-12 plant at Oak Ridge supervised the melting of a 20 year accumulation of low level contaminated metal waste in a 10 ton electric arc furnace; 27000 tons of scrap were melted requiring 2037 heats for the carbon steel scrap and 218 heats for the stainless steel scrap. The mild steel ingots averaged 0.4 ppm with 94.3% of the heats containing 1 ppm or less of uranium while the stainless heats averaged 0.6 ppm with 79.8% of the heats containing 1 ppm or less. The slags for the carbon steel heats averaged 2630 ppm uranium. This production scale work was reported by Mautz in 1975 in a handbook which provided up to date information on uranium decontamination of common metals by smelting.[13]

### 2.4.2 Developmental Studies

Bench scale melting tests for the removal of uranium and transuranics have been conducted by several researchers. At Argonne National Laboratory, Seitz, Gerding, and Steindler[14] studied the decontamination of mild steel, stainless steel, and nickel contaminated with 400-1400 ppm of plutonium oxide. Contaminated metals were melted in a resistance furnace in the presence of silicate slags of various compositions. Several crucible materials were tested to determine their ability to contain molten slag and steel without chemical attack or cracking. Magnesium oxide crucibles were attacked by a calcium silicate slag, while calcia stabilized zirconia crucibles were subject to cracking. The best

crucible material tested was recrystallized alumina. After melting, the major source of activity remaining within the ingots was found to be due to the incomplete separation of the silicate slag from the steel. In all experiments performed, the plutonium was shown to be effectively captured by the slag. The chemistry of various slags tested had some effect on plutonium extraction. Partition coefficients (plutonium in slag/plutonium in steel) of $7x10^6$ were measured with borosilicate slag and $3 \times 10^6$ for calcium-magnesium-silicate slag. The researchers noted that some of the borosilicate slags were inhomogeneous with higher plutonium and chromium concentrations in regions of high alumina content.

Staged melting was found to improve decontamination efficiencies. Staged melting was done on one heat where portions of two previously melted ingots were remelted using a clean slag. This resulted in an even greater reduction in plutonium content. The initial content of the charge was reported as about 0.1 ppm Pu while the ingot resulting from this melt averaged 0.002 ppm Pu. This reduction was postulated to be the result of the removal of Pu containing inclusions. The possibility was considered that a similar result could have been obtained in the primary melt by a longer holding time in the crucible to allow time for the oxide inclusions to coalesce and float into the slag. The inclusions still trapped in the first melt (which had a duration of one hour) had an additional hour to float to the surface in the second melt. Two other single melts held for two hours under a borosilicate slag yielded similarly low Pu contents, leading to a conclusion that longer holding times may be nearly as effective as staged melting.

In 1978, Copeland, Heestand, and Mateer[15] of Oak Ridge National laboratory published a report which detailed both the theoretical thermodynamics and the practical engineering aspects of planned metal melt decontamination research. In fulfillment of these plans, researchers[16, 17, 18] studied the effect of slag composition and other processing variables on the degree of decontamination achieved in the melt refining of metals contaminated with $UO_2$. Samples were contaminated by addition of $UO_2$ to the flux, which was added to the metal in a crucible. Melting was then performed at approximately 1600°C in an induction furnace and time was allowed for slag metal equilibration. After cooling, samples were taken of the metal and the slag. The degree of decontamination was not reported to be highly dependent upon slag composition although low efficiencies were associated with high silica slags. In general, highly fluid basic oxidizing slags were found to be more effective in the decontamination of stainless steel.

A logical continuation of the melting work performed at Oak Ridge involved a potential disposal method for the resulting contaminated slags. The feasibility of size-reducing and disintegrating slags was studied. Solidified slags generated in melt refining

were crushed and reduced in size to less than 3 mm. The size reduced slags were mixed with cement and found to form stable grout mixtures.[19]

A six ingot scoping study was performed at Hanford[20,21] by Hobbick, Schatz, and Aden who used an induction furnace to make 5 lb. melts. The charge for each melt consisted of five uncontaminated stainless steel bars, two of which were then contaminated as follows: one bar was painted with a slurry containing $PuO_2$ so that the bar contained 0.8 to 1.0 g of Pu (an addition to the total melt of 350 to 440 ppm) and another bar was dipped into an acidified solution of beta-gamma source from Hanford "tank waste" and was thus coated with $^{60}Co$, $^{137}Cs$, and $^{155}Eu$. A flux resembling the borosilicate glass composition was used, but the high SiO2 content caused attack of the MgO crucibles. After melting, autoradiographs showed that the ingot contamination was concentrated on the surface of the ingots and in inclusions. Ingot analysis by wet chemistry showed levels of residual Pu in the 0.1 to 0.085 ppm range, while an approximate 98% reduction of beta, gamma, and actinide levels was achieved.

Uda, Iba, and Tsuchiya[22] investigated the effect of slag chemistry on the melt refining of mild steel. In a related study, Abe, Uda, and Iba[23] melted samples of uranium contaminated mild steel, 304 stainless steel, and copper under various $SiO_2$-CaO-$Al_2O_3$ slags. Other variables included in these studies were contamination levels and melting times and temperatures. The aim of this research was to establish an optimized decontamination strategy for various metal types. Rods of the metals to be melted were contaminated by dipping in a uranyl nitrate solution of known concentration and were subsequently heated to decompose the uranyl nitrate $UO_2$ . Samples were then melted in an enclosed furnace under an argon atmosphere. The results of various tests revealed that slag chemistry is an important factor in decontamination efficiency.

The ionic character of a slag may be represented by its basicity, which is defined as the moles of basic oxide (CaO) divided by the total moles of acidic oxide ($SiO_2$ + $Al_2O_3$). The most effective slag basicity was around 1.5. Fluxes containing $CaF_2$ were more effective, possibly because as fluorides break the bonds of the silicate network present in $SiO_2$ containing slags,[24] additional $SiO_4^{4-}$ anions are produced which could combine with uranyl cations at the slag metal interface, causing uranium capture in the slag according to the following reaction:

$$2UO_2^{2+} + SiO_4^{4-} \leftrightarrow (UO_2)_2 SiO_4$$

Slags containing NiO also proved to be effective because the oxide breaks down to yield free oxygen ions which also break down the silicate network causing the formation of

acid slag anions. Using their optimum conditions, these researchers produced ingots with levels of uranium near the levels of the metal prior to contamination and melting.

In another study of the effect of slag basicity, researchers Ren, Liu, and Zhang[25] conducted 100 gram melt tests in order to determine suitable flux composition and process parameters for the effective removal of uranium from copper, nickel, and mild steel. Using a slag with a composition of 38.1% $SiO_2$, 41.4% CaO, 3.8% MgO, 2.6% $Fe_2O_3$, and 14.1% $Al_2O_3$ and a basisity of approximately 1.1 as a base, slag basisity was varied from a 0.25 to 1.95. Optimum decontamination was achieved with a flux having a basicity of 1.1.

Research performed at the Montana College of Mineral Science and Technology[26] by Worcester, Twidwell, Paolini, and Weldon involved small scale (two pound) air induction melts of stainless steel contaminated with cerium, lanthanum, and neodymium to simulate the presence of radionuclides. This research showed that the ability of a slag to collect contaminants from a molten metal bath is both time and temperature dependent and thus is kinetically controlled.

Researchers at Kobe Steel, Ltd. and Power Reactor and Nuclear Fuel Development Corporation[27,28] investigated the use of electroslag refining to decontaminate plutonium contaminated waste. This melting method was expected to have advantages as a process for treating radioactive metallic waste. Because melting and solidification take place in the same water cooled copper mold, no refractories are necessary, equipment needs are simplified, and volume reduction and radionuclide immobilization are accomplished simultaneously. Radioactive particles on the surface of the metallic waste can be transferred to the melted slag. Testwork was performed using $HfO_2$ as a surrogate for $PuO_2$, because of the similarity of properties. A 10 kg pilot scale furnace was used to become familiar with ESR operations, after which a 100 kg furnace was constructed and used for simulated decontamination tests. The furnace featured a rectangular copper mold and two 50 mm tungsten bars which served as non-consumable electrodes. The slag used had a composition of 47% CaO, 48% $Al_2O_3$, and 5% $B_2O_3$ and was selected on the basis of mechanical strength to insure stability in long term storage. The furnace was fed with pieces of surrogate treated metal (67 ppm Hf) by use of a bucket mechanism which moved up and down, receiving pieces of metal in the upper position then descending over the melted slag and depositing the metal into the melted slag. Upon evaluation of both ingot and slag for hafnium content, it was found that the solidified slag containing 298 ppm Hf and the ingot contained 2.53 ppm Hf, yielding a decontamination factor of about 25.

Electroslag refining was also the subject of a study by Uda, Ozawa, and Iba[29] who investigated the potential of this method for melting of uranium contaminated metal

cylinders. Electroslag refining was selected because many metallic wastes in the forms of rods, cylinders, and tubes can be melted without cutting them into pieces. The aim of this study was to establish ESR melting conditions for metal cylinders in which the cross section ratio of electrode to mold was less than the usual industrial ratio of 0.3 to 0.6 while comparing the decontamination efficiency of ESR with that for a resistance furnace. The ESR test equipment consisted of a 60 mm water cooled copper mold, an AC power supply, an electrode position controller and an off gas line and filter for removal of fume from the enclosed melting chamber. Cylinders of iron and aluminum were prepared for melting by application of a uranium containing solution to their surfaces so that the resultant uranium concentration was 500 ppm. The flux composition used for the experiments was 40% SiO2 -30% CaO- 20% Al2O3 - 10% CaF2 for the iron, and 14% LiF - 76% KCl - 10% BaCl for the aluminum. The decontamination effect achieved with ESR was better than that obtained with a resistance furnace and was shown to be independent of melt rate. The final ingot concentrations of the iron were 0.01 to 0.015 ppm which were less than the as received specimen before contamination, although ingot levels for the aluminum were 3 to 3.5 ppm which were a few times higher than in the as received condition, before the application of contaminants.

A feasibility study conducted by Atteridge[30] at the Oregon Graduate Institute revealed that the electroslag refining process could be effectively used to directly melt assemblies of stainless steel piping without an initial electrode consolidation step. Using this technology, contaminated reactor piping could be cut to suitable electrode lengths and directly melt decontaminated by ESR. Such a strategy would greatly reduce the need to manually torch cut contaminated material and could have advantages both in terms of processing costs and worker safety.

### 2.4.3 Full Scale Technical Demonstrations

Stainless steel scrap melting work at the Idaho National Engineering Laboratory[31] was concerned primarily with reducing the volume of the scrap to conserve dwindling waste storage capacity. The Waste Experimental Reduction Facility (WERF) was established to process a variety of low-level beta/gamma contaminated waste. A 750 kW induction furnace was used to demonstrate that melting the scrap and casting into 680 kg ingots was a safe and effective method for achieving at least a 10 fold reduction in volume while converting the scrap into a readily packagable form and stabilizing any radioisotopes

remaining in the ingots. The contaminated feedstock was generated by various INEL facilities and consisted mostly of salvaged reactor and test support components that were surface contaminated only. The major contaminants were $^{60}Co$, $^{90}Sr$, and $^{137}Cs$. Because the radioactivity level of the ingots produced had been too low to formulate a basis for the prediction of the dispersion of isotopes resulting from melting, three intentionally contaminated melts were made using sub-sized (200-300 kg) heats. Known quantities of $^{60}Co$, $^{85}Sr$, and $^{137}Cs$ were added to uncontaminated stainless steel. $^{85}Sr$ was used instead of $^{90}Sr$ because $^{85}Sr$ is a gamma emitter and therefore easier to detect in minute quantities. After melting, 91-100 % of the cobalt, 0-15% of the cesium, and 0-4% of the strontium remained in the ingots. Most of the strontium was collected in the high silica slag used, while most of the cesium vaporized and was collected by the air filtration system. Distributions in the slag were difficult to measure because slag remained attached to the ingot and the dipping tools, while some reacted with the furnace refractory and remained in the furnace.

The European community has been active in treating radioactive scrap by melting techniques. Lacroix and Talliez published a study of the melting of portions of a rejected carbon steel heat exchanger from the Chinon A power plant.[32] The activity of the incoming metal was between 10 and 20 mCi per metric ton. The purpose of the test was to determine the behavior and final distribution of radionuclides after melting as well as to evaluate the potential contamination of the surroundings due to the melting and casting processes. The study used a refractory lined graphite electric arc furnace of 4 to 5 metric ton capacity equipped with a mobile hood for fume capture. After melting, the total weight of the ingot was 3660 kg. The weight of the slag was 200 kg and that of the dust was 30 kg. The activity of each of the products was measured and 76 mCi was found in the ingots, 217 μCi in the slag, 148 μCi in the filter dust, and 38 μCi in the molding sand. Radiation checks in the vicinity of the furnace during operation revealed that the atmospheric activity did not exceed the maximum permissible level for public exposure of 10 $pCi/m^3$. The report concluded that the dose rates are sufficiently insignificant to permit the operation of a 4000 metric ton operation in complete safety.

British Steel Corporation[33] conducted a study to determine the practicality of releasing properly treated and characterized RSM to commercial electric furnace operations. The scrap used in this study was composed of contaminated steel from three different reactor systems which was mixed in various ratios with uncontaminated steel. The study consisted of 16 heats, six of which were melted in 50 kg or 0.5 tonne induction furnaces and ten of which were melted in a 5 tonne electric arc furnace. The radionuclides of interest

were $^{60}Co$, $^{134}Cs$, and $^{137}Cs$. Because of its chemical similarity to iron, the cobalt consistently partitioned to the steel castings while the cesium was captured in the slag and the fume. The partitioning of cesium between slag and fume was reported to be a function of the melting technique, the slag composition and the type of scrap melted. After analysis, all the ingots produced in this study were diluted in 300 tonne basic oxygen furnaces to less than 10-5 μCi/g. In a continuation of this work, experiments were undertaken in which europium ($^{152}Eu$ and $^{154}Eu$) contaminated steel was melted in a 500 kg induction furnace as well as in a 3 tonne arc furnace. It was found that the europium was contained wholly in the slag under both oxidizing and reducing conditions and that none was detectable in either the steel or the off gasses. The conclusion drawn from this research was that, although the process could be operated within published safety criteria, the cost of controlling and monitoring the scrap would out weigh its value. This research program was concluded in 1988 with no plans of future work.[34]

Decontamination technology for use in decommissioning the Japan Power Demonstration Reactor (JPDR) has been the object of research by the Japan Atomic Energy Research Institute (JAERI).[35] The objectives of tests performed by JAERI have been to investigate and assess the behavior of radionuclides during melting and casting and their influence on the working environment. Design of test equipment took place in 1987 and installation was completed by the end of March, 1990.[36] The melting equipment includes a 500 kg high frequency induction furnace equipped with an air tight hood. Melting and casting equipment are enclosed in a steel chamber which is kept at a slightly negative pressure to minimize the spread of radionuclides. Following equipment installation, cold tests on non-radioactive carbon and stainless steels were performed.

By September 1991, two heats of 304 stainless steel and four heats of carbon steel recovered from JPDR had been conducted. A series of five stainless steel test melts were performed using gamma emitting tracers as surrogates for nuclides commonly found in contaminated material from light water reactors, $^{54}Mn$, $^{60}Co$, $^{65}Zn$, $^{85}Sr$, and $^{137}Cs$. In a second series of tests, $^{63}Ni$ was used as a beta emitting radionuclide. Experimental variables included the type of contamination, the $CaO/SiO_2$ ratio in the flux, and melting temperature. The study examined the work place radiation dose, radionuclide partitioning among ingot, slag, dust, and offgas, and the final distribution of radioactivity within an ingot. It was found that 99.5% of the cobalt, 91% of the manganese, and 75% of the zinc remained in the ingot and were uniformly distributed. None of the strontium or the cesium was found in the ingots. Slag analysis showed that no cobalt was present, while 1% of the zinc, 7% of the manganese, 39% of the cesium, and 73 % of the strontium were present.

Accuracy of the fume analysis was questioned because 7% of the zinc, 27% of the strontium, and 23% of the cesium remained unaccounted for. This problem could have been caused by condensation of the fume before it reached the sampling location.[37]

### 2.4.4 Industrial Operations

Jacquet-Francillon and co-researchers[38] reported the development of a cold crucible induction melting operation designed to melt contaminated zircaloy and stainless steel hulls from the pilot nuclear facility at Marcoule. An industrial scale facility designed to process 15 ingots/year began production in 1993. In addition, a three phase, 15 tonne arc furnace has been used since April of 1992 for the melt consolidation for the treatment of ferrous materials recovered from the dismantling of the $CO_2$ systems from the graphite moderated, $CO_2$ cooled plutonium production and power generation reactors at Marcoule. By April 1993, an estimated 2580 tonnes of cast iron had been produced for reuse within the nuclear industry.[39,40]

Melt consolidation of ferrous scrap from dismantling nuclear power plants began at the Siempelkamp foundry in Krefeld, Germany in 1984.[41] While the first melts were performed using a modified 20 tonne coreless induction furnace, a new facility became operational in 1990. This facility consists of a 3.2 tonne 300-500 Hz coreless induction furnace with a melting capacity of 2 tonne/hr. The furnace facility is equipped with a fume system which provides negative pressure to the melting enclosure.[42] This facility was used to melt 500 tonnes of steel scrap from decommissioning the Gundremmingen Unit A (KRB A) nuclear power plant. Mies[43] reports that samples taken from remelted scrap are within permissible levels of activity, that the slag is disposed of at normal industrial waste facilities, and the filter dust is stored as low level waste.

In Sweden, radioactive scrap metal of Swedish and German origin was melted at Studsvik AB. By the end of 1988, over 400 tonnes of low activity scrap metal had been melted, of which approximately 90% was carbon steel and the remainder was stainless steel. The induction furnace employed has a capacity of 1.5 tonne/hr. Analytical results showed that Co, Mn, Zn, Ag, and Sb remained in the steel while Cs partitioned to the slag and dust.[44]

In the United States, Scientific Ecology Group, Inc. (SEG)[45] currently performs RSM consolidation in a 20 ton, 7200 kW induction melting furnace. During one melting campaign, 2735 tons of carbon steel material was melted and cast into shield blocks. In a

second campaign, 2200 tons of carbon steel was consolidated into shield blocks for nuclear operations.[46]

## 2.5 Recycling and Reuse of Decontaminated Metal

While many countries have recently begun melting of radioactive scrap metal for densification and limited reuse for low technology applications, there is, as yet, no plan in place for the recycle of specialty metals for high technology applications. The stockpile of contaminated metals in the United States is composed of valuable alloys which could be decontaminated and reused for nuclear related applications with their original properties intact. The alternative is the costly disposal and long term monitoring of these materials. The choice to dispose of contaminated strategic metals leads to the use of virgin materials for use in nuclear applications. These virgin materials will become contaminated, adding to the problem. If, however, the alternative of decontamination and recycle is chosen, storage costs are greatly reduced and the need for materials to be used in present or future nuclear applications is met.

It is theoretically possible to simply release melt decontaminated RSM into the non-nuclear community scrap metal market place, and this is being done overseas. However, present use-restriction rules in the US do not allow remelt RSM to be mixed with non-radioactively contaminated scrap, no matter how low the level of residual contamination. These rules dictate that RSM scrap remain separate, and not be used for general domestic/industrial use. It can, however, be used for nuclear community-specific applications, and, indeed there are multiple possible uses within the nuclear community for remelted RSM. These vary from low-tech waste burial boxes and barrels to high-tech transportation and interim/permanent waste storage canisters for high level radioactive waste.

### 2.5.1 Waste Canisters: A Possible Product

High level waste (HLW), a by product of the many facets of nuclear activities, is a hazard which must be permanently disposed of. Current plans for disposal of this material include conversion of HLW into a non-leachable glass or ceramic which would be contained within 304L stainless steel canisters for permanent disposal in a secure repository. The tonnage of stainless steel needed to produce the required number of canister

is considerable, but could be met by the LLCMW (low level contaminated metal waste) inventory if successful technologies can be developed to convert this waste into acceptable canisters. Nearly 26,000 tons of stainless steel will be needed to produce the canisters deemed necessary to accommodate current and projected quantities of HLW.[1] By recycling the material now in the form of contaminated stainless steel piping, the supply of contaminated stainless steel waste could meet the demand for the large number of waste canisters without placing an additional burden on our natural resources or strategic materials. Additionally, if the stainless steel that is classified as LLCMW could be converted into a product that is suitable for the requirements of the HLW storage containers, the cost of storing and monitoring the LLCMW would be eliminated. If contaminated stainless steel waste is to be recycled into canisters, technologies must be developed to remove the contamination or to reduce it to very low levels. Three major problems must be confronted when melting contaminated stainless steel waste for recycling into waste containers: the removal and control of the radioactive contamination, achieving the desired stainless steel composition, and controlling the nonmetallic inclusion content to achieve desired mechanical properties and long term corrosion resistance.

# Chapter 2 Tables

**Table 2.1**
**Fission Products Found in Spent Reactor Fuel**

| Heavy Elements | | Neutron Absorbing fission products | | Long lived radioactive fission products | |
|---|---|---|---|---|---|
| Uranium | 235,236,238 | Technetium | 99 | Krypton | 85 |
| Plutonium | 239,240,241 | Rhodium | 103 | Strontium | 89,90 |
| | | Xenon | 131,133,135 | Yttrium | 90,91 |
| | | Neodymium | 143,145 | Zirconium | 95 |
| | | Samarium | 149,151 | Niobium | 95 |
| | | Europium | 155 | Molybdenum | 99 |
| | | Gadolinium | 155 | Technetium | 99 |
| | | | | Ruthenium | 103,106 |
| | | | | Rhodium | 106 |
| | | | | Tellurium | 129 |
| | | | | Iodine | 129,131 |
| | | | | Xenon | 133 |
| | | | | Cesium | 137 |
| | | | | Barium | 140 |
| | | | | Lanthanum | 140 |
| | | | | Cerium | 141,144 |
| | | | | Praseodymium | 143,144 |
| | | | | Neodymium | 147 |
| | | | | Promethium | 147 |

**Table 2.2**
**Radionuclides Found in Irradiated Fuel Cladding**

| Radionuclide | Half life | Radionuclide | Half life |
|---|---|---|---|
| $^{10}Be$ | $2.5x10^6$ yr. | $^{91}Y$ | 58.8 days |
| $^{22}Na$ | 2.60 yr. | $^{93}Zr$ | $1.5X10^6$ yr. |
| $^{32}P$ | 14.3 days | $^{95}Zr$ | 65 days |
| $^{33}P$ | 25 days | $^{92m}Nb$ | 10.16 days |
| $^{45}Ca$ | 165 days | $^{93m}Nb$ | 13.6 yr. |
| $^{46}Sc$ | 83.9 days | $^{95}Nb$ | 35 days |
| $^{49}V$ | 330 days | $^{93}Mo$ | >100 yr. |
| $^{51}Cr$ | 27.8 days | $^{99}Tc$ | $2.12X10^5$ yr. |
| $^{54}Mn$ | 303 days | $^{117m}Sn$ | 14.0 days |
| $^{55}Fe$ | 2.6 yr. | $^{119m}Sn$ | 250 days |
| $^{59}Fe$ | 45 days | $^{121}Sn$ | 76 yr. |
| $^{58}Co$ | 71.3 days | $^{123}Sn$ | 125 days |
| $^{60}Co$ | 5.26 yr. | $^{124}Sn$ | 60 days |
| $^{59}Ni$ | $8X10^4$ yr. | $^{125}Sb$ | 2.7 yr. |
| $^{63}Ni$ | 92 yr. | $^{125m}Te$ | 58 days |
| $^{89}Sr$ | 52 days | | |

# Chapter 2 References


[1] Reimann, G.A. "Technical Assement of Processes to enable Recycling of Low-Level Contaminated Metal Waste," EGG-WTD-10056, Idaho National Engineering Laboratory, (1992).

[2] Buckentin, J. M., Damkroger, B. K., Schlienger, M.E. "Radioactive Scrap Metal Decontamination Technology Assesment Report and Research Proposal," Unpublished Report, Sandia National Laboratories, Albuquerque, New Mexico, (1995).

[3] Dyer, N. C., Bechtold, T.E. (Editor), "Radionuclides in United States Commercial Nuclear Power Reactors," WINCO-1191, INEL-DOE, (1994).

[4] Benedict, M., Pigford, T., Levi, H., Nuclear Chemical Engineering, McGraw Hill, New York, (1981), 1-35.

[5] Rosenqvist, T. Principles of Extractive Metallurgy, McGraw Hill, New York, (1974), 454-456.

[6] Smee, J.L., "Dissolution Characteristics of Metal Oxides in Water Cooled Reactors," in Decontamination and Decommissioning of Nuclear Facilities, M.M. Osterhut, Editor, Plenum Press, New York, (1980), 281.

[7] Kessinger, G., Idaho National Engineering Laboratory, Idaho Falls, Idaho. Private Communication, January, 1995.

[8] Worcester, S.A., Twidwell, L.G., Paolini, D.J., Weldon, T.A., Mizia, R.E. (Ed.) "Decontamination of Metals by Melt Refining/Slagging, An Annotated Bibliography: Updiate on Stainless Steel and Steel," INEL-95/0123, INEL-DOE, (January, 1995).

[9] Schlienger, E., Sandia National Laboratory, Albuquerque, New Mexico. Private Communication, May, 1995.

[10] Starkey, R.H., McKekvey, J.W., Held, B.J., Alpaugh, E.L., "Health Aspects of the Commercial Meltng of Uranium-Conaminated Ferrous Metal Scrap," *American Industrial Hygiene Association Journal*, Vol. 21, (1960), 178-181.

[11] Starkey, R.H., Quigley, J.A., McKelvey, J.W., "Health Aspects of the Commercial Meltng of Radium-Conaminated Ferrous Metal Scrap," *American Industrial Hygiene Association Journal*, Vol. 22, (1961), 489-493.

[12] Klevin, P.B. ; Harris, W.B. "Remelting May Permit Reclaiming Uraninum-Contaminated Metals" *Nucleonics*, Vol. 14, (April 1956), 93-96.

[13] Mauutz, E.W., Briggs, G.G., Shaw, W.E., and Cavendish, J.H., Uranium Decontamination of Common Metals by Smelting: A Review (Handbook), NSA 3204, National Lead Company of Ohio, Cincinnati, Ohio, (1975).

[14] Seitz, M.G., Gerding, T,J., Steindler, M.J., "Decontamination of Metals Containing Plutonium and Americium" ANL-78-13, UC-70, UC-10, Argonne National Laboratory, (June 1979).

[15] Copeland, G.L., Heestand, R.L., Mateer, R.S., "Volume Reduction of Low-Level Contaminated Metal Waste by Melting: Selection of Method and Conceptual Plan," ORNL/TM-6388, Oak Ridge National Laboratory, (June, 1978).

[16] Heshmatpour, B., Copeland, G.L., "The Effects of Slag Composition and Process Variables on Decontamination of Metallic Wastes by Melt Refining," ORNL/ TM-7501, UC-70, Oak Ridge National Laboratory, (Jan., 1981).

[17] Heshmatpour, B., Copeland, G.L., "Metallurgical Aspects of Waste Metal Decontamination by Melt Refining," *Nuclear and Chemical Waste Management*, Vol. 2, (1981), 25-31.

[18] Heshmatpour, B., Copeland, G.L., Heestand, R.L., "Decontamination of Transuranic Waste by Melt Refining" ORNL/TM-7951, 1981; *Nuclear and Chemical Waste Management*, Vol. 4, (1983), 129-134.

[19] Heshmatpour, B., Copeland, G.L., Heestand, R.L. "Granulation of Slags and Metals After Melt Refining of Contaminated Metallic Wastes," *Nuclear and Chemical Waste Management*, Vol. 2, (1981), 33-37.

[20] Hobbick, C.W., Schatz, D.R., Aden, G.D., "Distribution and Removal of Radionuclides in Molten Stainless Steel," RHO-CD-1444, (June, 1981).

[21] Deichman, J.L., "Contaminated Metallic Melt Volume Reduction Testing," ORNL/NFW-81/34, Oak Ridge National Laboratory, (1981).

[22] Uda, T., Iba, H., Tsuchiya, H., "Decontamination of Uranium-Contaminated Mild Steel by Melt Refining" *Nuclear Technology*, Vol.73, (April 1986), 109-115.

[23] Abe, M., Uda, T., and Iba, H., "Melt Refining Method for Uranium-Contaminated Steels and Copper," Waste Management 85, Proceedings of the Symposium on Waste Management at Tucson, Arizona, Mar. 24-28, No. 3, (1975), 375-379.

[24] Turkdogan, E.T., Physical Chemistry of High Temperature Technology, Academic Press, New York , (1980), 140.

[25] Ren, X.W., Liu, W.C., Zhang, Y., "Melt Refining of Uranium Contaminated Copper, Nickle, and Mild Steel," Proceedings of the International and Topical Meeting on Nuclear and Hazardous Waste Management, Spectrum 94, Atlanta, GA, August 14-18, ANS.

[26] Worcester, S.A., Twidwell, L.G., Paolini, D.J., Weldon, T.A., Mizia, R.E. (Ed.) "Decontamination of Metals by Melt Refining/Slagging,: First Year Progress Report," WINCO-1138, INEL-DOE, (1995).

[27] Kitagawa, K., Nagura, K., Noura, T., "Treatment of Radioactive Metallic Waste by the Electro-slag Melting Method," *Kobe Steel Engineering Reports*, Vol. 33, No. 1, (Jan. 1983), 1-6.

[28] Ochiai, A., Kitagawa, K., Sawada, Y., Isuhara, S., Ohtsuka, K., "Treatment of Plutonium-Contaminated Metallic Waste by the Electro-slag Melting Method," IAEA-SM-261/20; EDB-84-020441, Japan: Kobe Steel, (June, 1982).

[29] Uda, T., Ozawa, Y., Iba, H., "Melting of Uranium-Contaminated Metal Cylinders by Electroslag Refining," *Nuclear Technology*, Vol.79, (1987), 328-337.

[30] Atteridge, D.A., Buckentin, J., Carter, J., Davis H.L., Devletian, J.H., Scholl, M.R., Turpin, R.B., Webster, S.L., Mizia, R.E. (Ed.), "Refining Technology for the recycling of stainless Steel Radioactive scrap Metals: FY 94 Bi-Annual Report," INEL-DOE, WINCO-1224, (1994), 1-97.

[31] Reimann, G.A. "Technical Assement of Processes to enable Recycling of Low-Level Contaminated Metal Waste," EGG-WTD-10056, Idaho National Engineering Laboratory, (Jan., 1992).

[32] Lacroix, J.P.; Tailliez, M. "STMI's Industrial Experience in Low Activity Steel Waste Processing by Melting," Waste Mangement 86, 3, R.G. Post (ed.), (1986), 547-552.

[33] Gomer, C.R., Lambley, J.T., "Melting of Contaminated Steel Scrap Arising in the Dismantling of Nuclear Power Plants," EUR-10188, Commission of the European Communities, (1985).

[34] Harvey, D.S., "Melting of Contaminated Steel Scrap from Decommissioning," or Advances in Ceramics, Vol. 20. *Nuclear Waste Management II*, 1986 Decommissioning of Nuclear Installations-1990, Brussels, Pfulgrad, et. al. editors, (1990), 473-481.

[35] Fujiki, K., Hirabayashi, T., Kanazazawa, K., Yasunaka, H., "Decontamination and Melting Test for Metal Waste in JPDR Decommission Project-Toward recycling of LLW," Proceedings Waste Management, Tucson, AZ, USA, (1991), 171-178.

[36] Nakamura, H., Fujiki, K., "Radioactive Metal Melting Test at Japan Atomic Energy Research Institute," Proceedings Waste Management 1993, Vol 2., (1993), 1683.

[37] Nakamura, H., Kanazawa, K., Sato, T., Yamate, K., Fujiki, K., "Fundamental Research on Melting of Radioactive Metal Materials," Japan Atomic Energy Research Institute, Shirakata-shirane, Tokaimura, Ibaraki-ken, 319-11, Proceedings of the International Topical Meeting on Nuclear and Hazardous Waste Management, Spectrum 94, Atlanta, GA, August 14-18, ANS, 206-210.

[38] Jacquet-Francillon, N., Jouan, A., Moncouyoux, Sombret, C., "Melting: A Promising Technique for Processing Metallic Decladding Materials from Irradiated Nuclear Fuels", ICCN 91, Bombay, India, (1991).

[39] Peulve, J., "Treatment of Dismantled Materials by Fusion," Techno-992-022, Commissarit A L'Energie Atomique Report, (1992).

[40] Peulve, J., et. al., "Dismantiling of Nuclear Facilities Scrap Steel Management of G2 and G3 Reactors at Marcoule," UDIN, Commissarit A L'Energie Atomique, Marcoule ie Apr. 16, (1993).

[41] Sappok, M., Tarcza, G.A., "Results of Metallic Waste Treatment by Melting," Siemplekamp Giesserei GmbH & Co., Germany; CONF-874048 Vol. 1, Westinghouse Hanford, Oct., (1987), 115-127.

[42] Sappok, M., Rettig, G., "Results of Melting Large Quantities of Radioactive Metallic Scrap," Proceedings of the International Topical Meeting on Nuclear and Hazardous Waste Management, Spectrum "92," American Nuclear Society, La Grange Park, Illinois, (1992), 120.

[43] Mies, H.P., Stang, W., "Decommissioning of Nuclear Power Plant Gundremmingen Unit A," Company Report: Kernkraftwerke Gundremmingen Betriebsgesellschaft, Germany, (1991).

[44] Menon, S., Hernborg, G., Andersson, L., "Melting of Low-Level Contaminated Steels," Decomissioning Nuclear Installations-1990, Studsvik AB, Sweden, (1990), 497.

[45] Scientific Ecology Group, Inc., (SEG) SEG Commercial Phamplet on "Metal Processing," and Industrial Portfolio, Scientific Ecology Group P.O. Box 2530, 1560 Bear Creek Road, Oak Ridge, TN 37830, (1993).

[46] Worcester, S.A., Twidwell, L.G., Paolini, D.J., Weldon, T.A., Mizia, R.E. (Ed.) "Decontamination of Metals by Melt Refining/Slagging, An Annotated Bibliography: Update on Stainless Steel and Steel," INEL-95/0123, INEL-DOE, (January, 1995).

# Chapter 3
# The Thermodynamics of Melt Refining

Melt refining is the process of removing unwanted elements or compounds from an alloy during a melting operation. The kinetics of melt refining are typically favorable because reactions take place between either a liquid and a gas or between two liquids, usually at elevated temperature. When an element to be removed has a higher vapor pressure than the host alloy, melting at a reduced pressure will encourage selective evaporation, otherwise the use of a slag is necessary. Slags are molten mixtures of metal oxides which may also contain silicates, phosphates, borates, or halides, depending on their application. In melt refining processes, slags are used as cleansing agents and are less dense than the alloy being melted so they float on top of the surface of the melt and protect it from oxidation and heat loss. The effectiveness of a slag depends on the affinity of unwanted elements in the metal for chemical components in the slag as well as the density of the resultant compounds. In general, compounds formed between tramp elements and elements in the slag (such as oxygen) have low densities and therefore remain with the slag. Therefore, a knowledge of the compounds which may be formed and their properties is critical. It is also important to access the relative stabilities of the compounds formed as well as the degree to which they form in preference to similar compounds involving the host metal or an important alloying element. These considerations become important in designing melt refining systems that selectively remove tramp elements from the metal while allowing an alloy to retain its valuable components.

A thermodynamic feasibility study was performed in order to determine the probability of removing radionuclides from molten stainless steel. The thermodynamic properties of various elements were compared so that suitable nonradioactive surrogates could be chosen for use in melting studies. Thermodynamic models were used to describe the molten stainless steel solution and the liquid slag. Interactions between the two liquids,

as well as the behaviors of surrogate elements and radionuclides, were modeled by use of free energy minimization techniques.

## 3.1 Thermodynamic Principles

The thermodynamic principle which makes melt refining possible is the fact that an element will partition between a metal and a slag toward an equilibrium in which its activity is the same in both phases.[1] In an ideal solution the activity of a component is equal to its concentration. Most solutions are not ideal, therefore activity may be thought of as the effective concentration of a component in solution, or the degree to which the component is available to participate in chemical reactions. The activity of a given component in solution may vary from its apparent concentration as a result of the complex way in which charged particles interact with one another in solute-solute and solute-solvent interactions.[2] In order to obtain the true activity, $a_b$ , of a component b in solution the molecular or ionic concentration, $X_b$, must be multiplied by an activity coefficient, $\gamma$, thus:

$$a_b = \gamma_b X_b$$

When a metal is melted, its chemical constituents are free to react with other constituents of the molten metal or the molten slag. The degree to which a contaminant may be removed from a metal by melting depends on the stability of compounds which may be formed by this contaminant and the constituents of the slag phase. When an element forms a stable compound which is collected into the slag phase, its activity in the slag is decreased and more of the element must partition to the slag from the metal to balance the activities. Thus its activity in the metal is decreased as well. This process continues until equilibrium is reached or until the process is halted kinetically. The degree to which an element will partition between a metal and a slag is governed, therefore, by the stability of the compounds it is thermodynamically permitted to form with the constituents of the slag and by the extent to which the system achieves equilibrium.

If kinetically permitted to do so, a melt refining system will approach equilibrium by seeking its lowest total free energy. This occurs when the free energy of the products and the free energy of the reactants are equal and $\Delta G$ is equal to zero. The value of $\Delta G$ is an indication of the energy available to do useful work or to bring about chemical change.

The position of equilibrium, and thus the degree of melt refining possible, for any metal/slag system is affected by several factors. These factors include the concentrations of the products and reactants present, the pressure (if reactions involve gas phases as they often do at the high temperatures associated with melt refining), and temperature. For the general reaction:

$$pA + qB = rC + sD$$

where p, q, r, and s are the numbers of moles of A, B, C, and D respectively, the extent to which this reaction proceeds is governed by the rate of the forward reaction as well as the rate of the reverse reaction, and may be described by an equilibrium constant, $K_c$:

$$K_c = \frac{a_C^r \, a_D^s}{a_A^p \, a_B^q}$$

By convention, the activities of pure solids or liquids (substances in their standard states) are equal to one. If $K_c$ is greater than one, equilibrium lies to the right (since products predominate and the numerator is greater than the denominator), and the reaction will proceed as written. If, on the other hand, $K_c$ is less than one, equilibrium lies to the left and the reaction will proceed "backwards". If the concentration of any one of the reactants or products is altered, the concentration of the others must change to keep $K_c$ constant. Changes in pressure will not affect the position of equilibrium when only solids or liquids are involved or in gaseous reactions with no volume change. Changes in concentration and pressure affect the position of equilibrium but they do not influence the value of $K_c$, as temperature is able to do. $K_c$ is temperature dependent because a temperature change influences the rates of both forward and reverse reactions, but seldom to the same extent.

The relationship between the free energy available to bring about a chemical reaction and the equilibrium constant for that reaction may be written as follows:

$$\Delta G = \Delta G^\circ + RT \ln K_c$$

where T is the absolute temperature and R is the gas constant. $\Delta G^\circ$, the standard free energy change, is the maximum work obtainable from the system when the change is performed reversibly. The standard free energy change of a reaction is equal to the sum of the standard free energies of the products minus the sum of the standard free energies of the

reactants. An element in its standard state at 298°K has a standard free energy of zero. The standard free energy of a compound is equal to the standard free energy change of formation for the compound, $\Delta G^{\circ}_{f}$, which is the free energy change when one mole of a compound is formed from its elements at 298°K and one atmosphere of pressure.

When a reaction has reached equilibrium, $\Delta G$ is equal to zero and the standard free energy change associated with the reaction may be expressed as a function of the equilibrium constant, thus:

$$\Delta G^{\circ} = -RT \ln K_c$$

When K is greater than one, $\Delta G^{\circ}$ will be negative and a reaction will proceed as written, when K is less than one, $\Delta G^{\circ}$ will be positive, indicating that a reaction will not take place as written, but will proceed in reverse. Hence, calculation of $\Delta G^{\circ}$ gives valid information regarding the initial and final points of a reaction and predicts the feasibility and equilibrium position possible. For reactions in progress, however, $\Delta G$ should be used because the system is not at equilibrium.[2]

## 3.2 Thermodynamic Tools

Although the thermodynamics of melt refining systems is complex, the feasibility of using a slag to remove an element from a liquid metal may be estimated by employing various simplifications. The following sections describe two thermodynamic tools, Ellingham diagrams and predominance area diagrams, which may be used to access the behavior of elements in a melt refining system.

### 3.2.1 Ellingham Diagrams

The tendency of an element to partition to the slag depends on the stability of compounds which may be formed. The standard free energy may be used to indicate the favorability of a reaction. Ellingham diagrams are plots of standard free energy versus

temperature. They are often used to compare the relative stabilities of oxides of various elements which may be present in the melt refining system.

For any chemical reaction, the free energy change as a function of temperature may be written as:

$$\Delta G^{o}_{T} = \Delta H^{o}_{T} - T\Delta S^{o}_{T}$$

$$= \Delta H^{o}_{298} + \int_{298}^{T} \Delta c_p dT - T\Delta S^{o}_{298} - T\int_{298}^{T} \frac{\Delta c_p}{T} dT$$

where $\Delta H^{\circ}$ is the standard enthalpy change for the reaction and $\Delta S^{\circ}$ is the standard entropy change. The heat capacity at constant pressure of each product or reactant may be written as:

$$c_p = a + bT + cT^{-2}$$

The thermodynamic equation for the variation of free energy with temperature is expressed as:

$$\Delta G^{\circ} = IT + \Delta H^{O} - \Delta aT \ln T - \frac{\Delta bT^{2}}{2} - \frac{\Delta c}{2T}$$

Where I is an integration constant which may be determined if the equilibrium constant at any temperature is known.[3]

Ellingham[4] plotted experimentally determined free energy versus temperature relationships for the oxidation and sulfidation of a series of metals and discovered that the relationships could be approximated by straight lines over the temperature range in which no physical change occurred. He showed that the relationship between free energy and temperature could be approximated by means of the equation for a straight line:

$$\Delta G^{\circ} = A + BT$$

The constant A is identified with the standard enthalpy change of the reaction, $\Delta H^{\circ}$ and the constant B is identified with the negative standard entropy change of the reaction, $-\Delta S^{\circ}$.[3]

The value of $\Delta G^{\circ}$ for an oxidation reaction is a measure of the chemical affinity of the metal for oxygen. A highly negative free energy value indicates a high probability that a stable oxide will be formed. Ellingham diagrams, plots of the variation of $\Delta G^{\circ}$ with T at

constant pressure, may be plotted showing various reactions of interest (all normalized to a per mole of oxygen basis) in order to determine the relative stabilities of various oxides. Ellingham diagrams may also be plotted to compare the stabilities of compounds formed by other types of reactions, such as sulfidation or fluoridation.[5]

As an example, an Ellingham diagram may be used to compare the stability of $UO_2$, uranium dioxide, with the oxides of other metals, as shown in Figure 3.1.

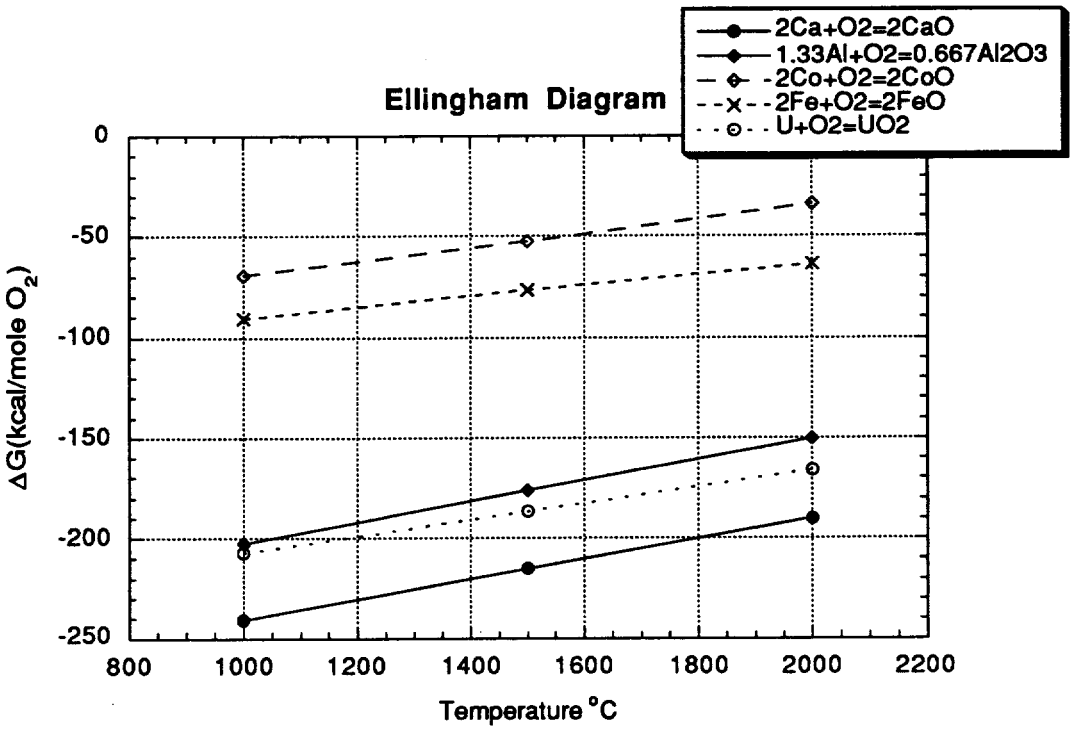


**Figure 3.1**
**The Stabilities of Various Oxides Compared by Means of an Ellingham Diagram**

The diagram shows that CaO, calcia, is the most stable oxide of those plotted, with $UO_2$ being only slightly less stable. $UO_2$ is shown to be more stable than alumina, $Al_2O_3$ which indicates that in a melt refining system in which alumina was present in the slag, uranium would rob aluminum of oxygen, and would thus partition to the slag as an oxide. If, however, uranium were present in a slag composed of calcia, the diagram predicts that uranium would be unable to partition to the slag as an oxide because oxygen would be preferentially tied up with the calcium. The diagram also shows that uranium dioxide is much more stable than iron oxide and so it is feasible to remove uranium from iron by

selective oxidation. Conversely, cobalt is less easily oxidized than iron, so the feasibility of removing radioactive cobalt from an iron bearing alloy by selective oxidation is low.

### 3.2.2 Kellogg Diagrams (Predominance Area Diagrams)

The Kellogg diagram, also known as the predominance area diagram, was first used to study the equilibrium relations in a system containing metal, sulfur, and oxygen. The gas phase for this system contains $O_2$ and $SO_2$ and, at a given temperature; the composition of the gas mixture is defined by the partial pressure of any two gaseous components. Also, for a fixed gas composition the composition of the condensed phases is fixed. The phase relations in a ternary system at constant temperature may be described in a two dimensional diagram where the two coordinates are the partial pressures of two of the gaseous components. The lines on the diagram describe equilibrium between any two condensed phases and define the region in which any given compound is predominantly present. For example, when a metal Me is present under a gas composed of $O_2$ and $SO_2$ the following reaction may occur:

$$Me + SO_2 \rightarrow MeS + O_2$$

which has an equilibrium constant

$$K = \frac{p_{O_2}}{p_{SO_2}}$$

so that

$$\log p_{O_2} - \log p_{SO_2} = \log K.$$

This equation may be plotted on a graph having axes $\log_{pO2}$ and $\log p_{SO2}$. The metal, Me, will be predominant on the low sulfur side of the line and the sulfide, MeS, will be predominant on the high sulfur side of the line. Other lines may be plotted to determine the equilibrium of other possible phases, resulting in a diagram which describes which compound will predominate under any combination of partial pressures.[6] These diagrams,

which have traditionally been used in the design of roasting systems, are often called Kellogg diagrams.[7,8]

In thermodynamics, partial pressures of gaseous species are analogous to activities of species present in a solution. Therefore, in this research, a type of diagram analogous to the predominance area diagram has been used to show the relationships between the activities of two dissolved species in the slag and the types of compounds which may be formed. Although melt refining systems tend to be complex, containing many species, predominance area diagrams can be a useful tool for evaluating the feasibility for separating elements on the basis of selectively complexing one of them into a compound involving three elements. Such diagrams are also useful for the prediction of the activities of species which may be necessary in order to effect the partitioning of a particular element into the slag as a stable species, as is the case in melt refining. Figure 3.2, generated with HSC Chemistry for Windows, shows the uranium species which may be formed in a slag containing ions of oxygen and fluorine at 1600°C.[9]

This diagram shows that uranium forms various oxides and fluorides depending on the activity of oxygen and fluorine in solution. In order to examine the feasibility of selectively partitioning uranium to a slag, the diagram above must be compared with a predominance area diagram for the major constituent of the metal to be decontaminated, in this case the iron in stainless steel. A predominance area diagram for iron in an environment containing oxygen and fluorine ions at 1600°C is shown in Figure 3.3.[9]

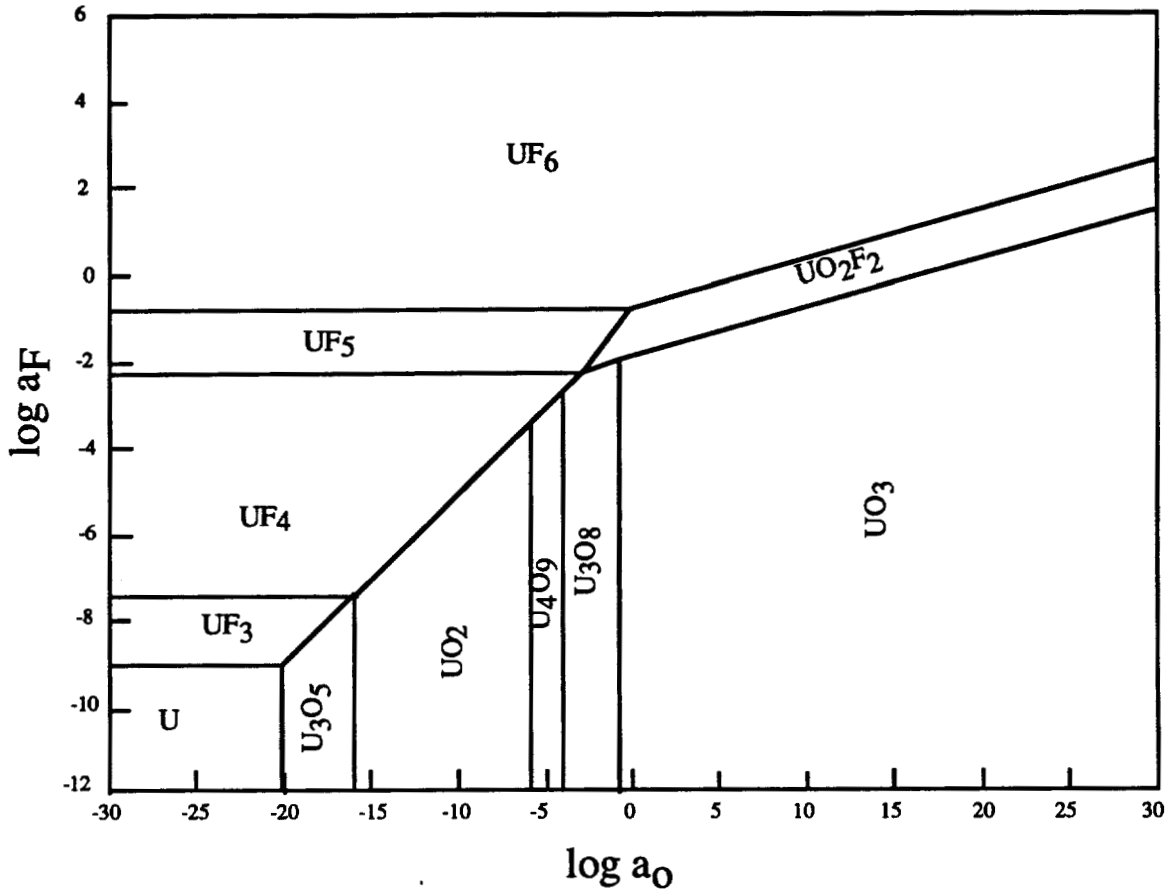


**Figure 3.2**

**The Effect of the Activities of Oxygen and Fluorine in the Slag on the Predominant Uranium Bearing Species Which are Formed**

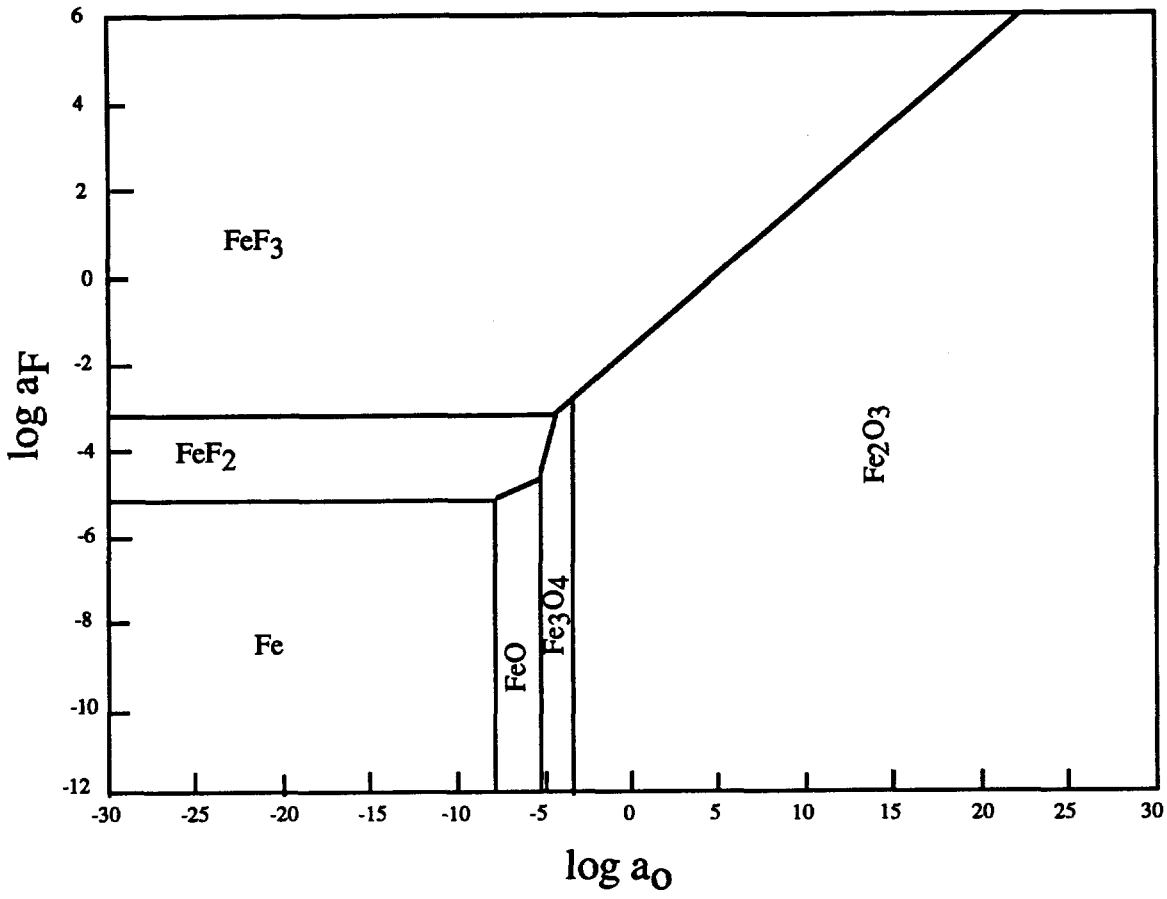


**Figure 3.3**

**The Effect of the Activities of Oxygen and Fluorine in the Slag on the Predominant Iron Bearing Species Which are Formed**

Comparison of the two diagrams shows that uranium forms both oxides and fluorides at lower activities of oxygen and fluorine than iron. Uranium may therefore be selectively removed from iron alloys. This is not the case for all radionuclides, however, as the following predominance area diagram for cobalt in the presence of oxygen and fluorine, Figure 3.4, indicates.[9]

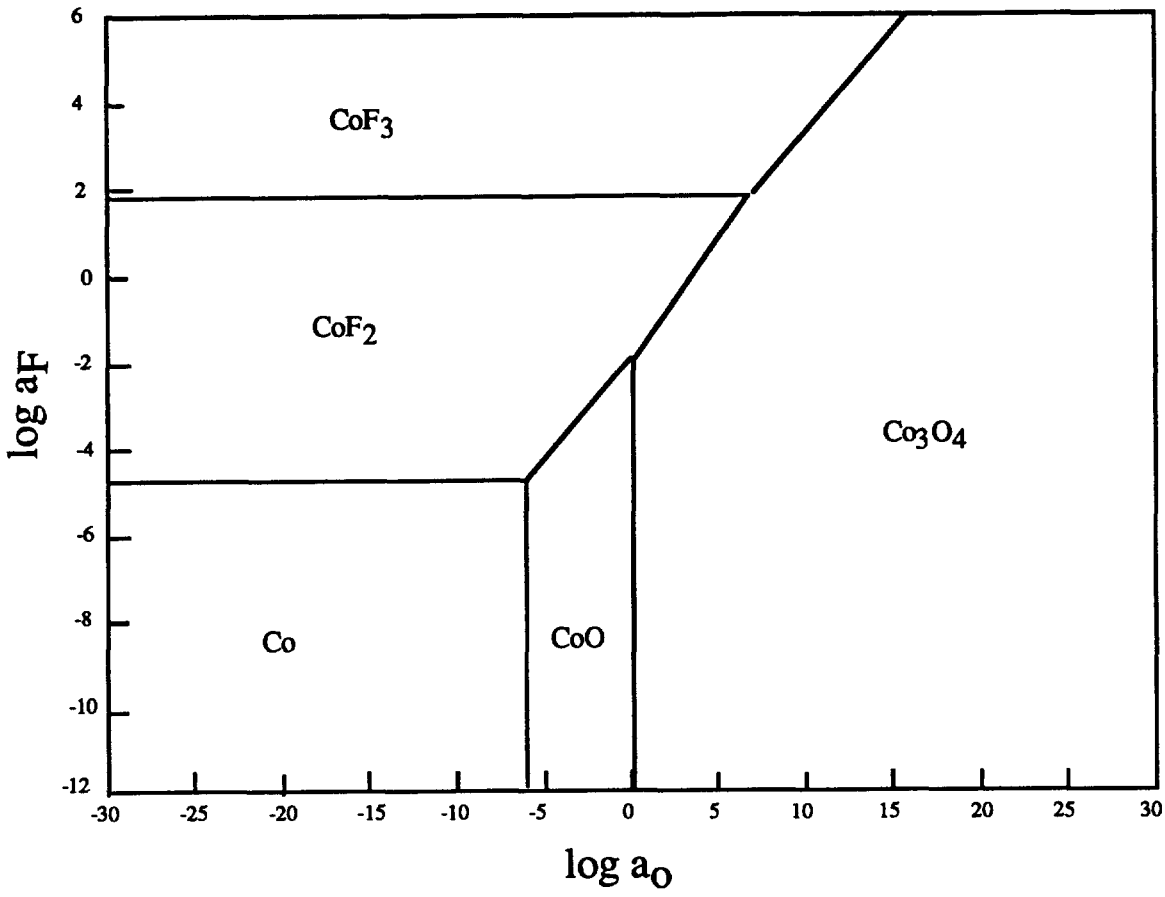


**Figure 3.4**

**The Effect of the Activities of Oxygen and Fluorine in the Slag on the Predominant Cobalt Bearing Species Which are Formed**

Comparison of the diagram for cobalt with the one for iron shows that at the oxygen or fluorine activities necessary to oxidize or fluoridize cobalt, iron would also be reacted. It would therefore be unlikely that cobalt would be partitioned into a slag in contact with a stainless steel melt. In order to effect melt partitioning of elements such as cobalt, which are very similar to iron, it would be necessary to form a stable complex between cobalt and one or more constituents of the slag. Furthermore, in order for this melt partitioning to be effective, the complex must form in preference to any stable iron bearing complex.

Predominance area diagrams, in conjunction with Ellingham diagrams, suggest that it is feasible to remove some radionuclides from stainless steel. These diagrams do not, however, predict the extent to which an element may partition to a slag or show how this partitioning may change in the presence of other elements.

## 3.3 Thermodynamic Calculations

Although kinetic and electrochemical effects play an important role in melt refining, equilibrium thermochemical calculations provide a basis for predicting the occurrence of reactions as well as the conditions under which they may occur. In order to understand the refining capability of slags in contact with molten metals, it is necessary to understand the general thermochemistry governing the interactions between these phases. Element transfer between slag and metal is dependent to a great extent on the thermodynamics of the slag phase. Because of difficulties encountered in performing thermochemical studies on liquid slags at very high temperatures, however, accurate thermochemical data is sparse. Never the less, various researchers have used thermodynamic approximations to forecast the partitioning of radionuclides between a molten metal and a slag.

The strong oxide forming tendency of plutonium and other TRU elements will favor removal as oxides from the parent metal. Oxygen may enter the slag from the atmosphere, from oxidation present on scrap to be remelted, or from oxygen present in the flux components. The resultant oxides are either captured by the slag or form ingot inclusions.[10]

Studies by Heshmatpour and Copeland[11,12] and Copeland, Heestand, and Mateer[13] examined the partitioning of uranium between liquid iron and a slag. The authors assumed that uranium removal was accomplished by reaction with oxygen and that complete thermochemical equilibrium was established. The slag was assumed to behave as an ideal solution. A feasible oxygen exchange between the iron oxide in the slag and the uranium in the melt was written as:

$$U_{(l)} + 2FeO_{(slag)} \leftrightarrow UO_{2(slag)} + 2Fe_{(l)}$$

The liquid metal solution was assumed to be composed of only iron and uranium, and at infinite dilution the activity of uranium was approximated by its weight percent. The standard free energy associated with this reaction was be expressed as follows:

$$\Delta G^{o} = \Delta G^{o}_{(UO_2)} - 2\Delta G^{o}_{(FeO)} - RT\ln\left[\left(2.364\times10^{-3}\right)\gamma^{o}_{(U)}\right]$$

$$= -RT\ln\frac{X_{(UO_2)}X^{2}_{(Fe)}}{X^{2}_{(FeO)}(wt.\%U)}$$

Substitution of known or assumed quantities into this equation allowed the derivation of a relationship between the equilibrium concentration of uranium in the liquid iron and its activity coefficient, $\gamma^{o}_{(U)}$, which was unknown.

At 1900°K, the standard free energies of formation of $UO_2$ and FeO are as follows:

$$\Delta G^{o}(FeO) = -140.9 \text{ kJ/mol } (-33.670 \text{ kcal/mol})$$
$$\Delta G^{o}(UO_2) = -738.7 \text{ kJ/mol } (-176.550 \text{ kcal/mol})$$

Taking 1 wt. % as the standard state for uranium in liquid iron, the atom fraction of uranium was calculated to be:

$$X(U) = \frac{wt.\%U}{(100 - wt.\%U)\left[\frac{M(U)}{M(Fe)}\right] + wt.\%U} = 2.364\times10^{-3}$$

Where wt. % U is the weight percent of uranium in the solvent metal and M(U) and M(Fe) are the molecular weights of iron and uranium, respectively. Because the solution was composed of iron and uranium only, at infinite dilution the activities of iron and uranium were assumed to be approximately equal to their atom fractions. The authors assumed that both FeO and $UO_2$ behaved ideally in a slag composed of 50% CaO, 44% $SiO_2$, 5% FeO, and 1% UO2. The atomic fractions of FeO and $UO_2$ in the slag were calculated to be:

$$X(FeO) = 4.10\times10^{-2}$$
$$X(UO_2) = 2.18\times10^{-2}$$

By substitution of the proper quantities, the equilibrium weight percent of uranium in the iron was found to be:

$$wt.\%U=\frac{(1.5\times10^{-10})}{\gamma^{o}(U)}$$

The partition ratio, $\lambda$, is defined as the amount of contaminant in the slag divided by the amount of contaminant in the metal and is a quantity which may be readily measured in a melt refining experiment. At equilibrium, the activity of the solute species in the two phases will be equal, though their analytical concentrations will not. This phenomena reflects the difference in the chemical potential of the species in their respective environments.[14] In order to determine a partition ratio for this system, the authors assumed the final slag weight to be 5% of the weight of the liquid iron. Therefore, for 100 grams of metal, the slag weight was 5 grams, and contained 1 wt.% (0.05g) $UO_2$, so the mass of uranium in the slag is equal to:

$$m(U)(slag)=\frac{M(U)}{M(UO_2)}m(UO_2)=\left(\frac{238.07}{270.07}\right)0.05=0.4408\ g.$$

and the mass of uranium in the melt is:

$$m(U)(melt)=m(metal)(wt.\%U)=100(wt.\%U)$$

The partition ratio is therefore:

$$\lambda=\frac{m(U)(slag)}{m(U)(melt)}=(2.95\times10^{6})\gamma^{o}(U)$$

Because a value for the activity coefficient of uranium in liquid iron was not available, the authors examined values of the activity coefficient of uranium at infinite dilution in some other solvents[15] and on the basis of these values, proposed that the activity coefficient of a dilute solution of uranium in iron probably lies between 0.1 and $10^{-5}$. Results of associated melting studies on uranium contaminated mild steel showed that a sample of mild steel melted under 10 grams of $CaO\text{-}Al_2O_3\text{-}FeO$ flux results in an average uranium concentration of 1 ppm in the steel and 1000 ppm in the slag, representing a value of 100 for the partition coefficient. These studies indicate that $\gamma o(U)$ in liquid iron has a value on the order of $10^{-3}$ to $10^{-4}$.

In a related study, Heshmatpour, Copeland, and Heestand[16] performed a thermodynamic analysis of a simple melt refining system and calculated the extent to which

plutonium could be removed from liquid iron, assuming that the contaminant combined with oxygen and entered a slag, which was presumed to act as an inert solvent for the resulting oxide. Their treatment assumes complete thermodynamic equilibrium between the liquid iron and an iron oxide bearing slag. The oxidation of plutonium was expressed as:

$$Pu + 2FeO_{(slag)} \leftrightarrow PuO_{2(slag)} + 2Fe_{(liq)}$$

The authors considered the liquid iron to be in contact with a slag composition of 50 wt.% CaO, 44 % $SiO_2$, 5% FeO, 1%$PuO_2$ at a temperature of 1900°K. Melting tests performed in conjunction with their work indicated that the partition ratio was approximately 300. Although they were unable to find a reported value for $\gamma o$(Pu) in liquid iron, their results yield a value of $2x10^{-4}$ for $\gamma o$(Pu) and about $3x10^{-6}$ or 0.03 ppm for the wt. % plutonium in liquid iron.

Another thermochemical study was performed by Joyce and Lally of Los Alamos National Laboratories in conjunction with Ozturk and Fruehan of Carnegie-Mellon University[17]. They identified the radioactive partitioning between the metal and the slag phases as a key issue in liquid metal recycle and waste treatment, and a thermochemical scoping study was performed with this in mind. The basis of their thermodynamic analysis was the removal of transuranic elements from steel by combining them with oxygen and transferring the oxygen to a slag phase. Depending on the chemical potential of the oxygen, species such as $UO_2$, $UO_3$, $U_4O_9$, and $U_3O_8$ were predicted to form, as the valence of uranium changes with oxygen potential. Under steelmaking conditions, however, the uranium in the slag was expected to exist primarily as $U^{+4}$, although it could exist as $UO_3^{2-}$, $UO^{+2}$, or $UO_4^{-4}$. The authors point out that a knowledge of the form of uranium present in a slag should aid in the selection of its chemistry.

Molten oxides forming a slag are dissociated into cations and anions. These oxides are present as two main types: basic oxides which cause the donation of $O^{2-}$ ions to the slag and acidic oxides which accept $O^{2-}$ ions. If the uranium in the slag occurs as $U^{+4}$ or $UO^{+2}$ the reactions which show basic behavior are:

$$[U] + 2[O] \rightarrow U^{4+} + 2O^{2-}$$
$$[U] + 2[O] \rightarrow UO^{2+} + O^{2-}$$

Such reactions could be driven further to the right by the selection of an acidic slag which accepts $O^{2-}$ ions. If however the uranium is of the form $UO_3^{-2}$ or $UO_4^{-4}$, their acidic behavior would result in the decreased activity of $O^{2-}$ in the slag:

$$[U] + 2[O] + O^{2-} \rightarrow UO_3^{2-}$$
$$[U] + 2[O] + 2O^{2-} \rightarrow UO_4^{4-}$$

These reactions could be encouraged by use of a basic slag, able to donate $O^{2-}$ ions.

Abe, Uda, and Iba[18] carried out a study which verified that slag basicity has an effect on the efficiency of uranium removal from molten metal. The ionic character of a slag may be represented by basicity, which is defined as[19]:

$$\text{basicity} = \frac{\text{moles of basic oxide (CaO)}}{\text{moles of acidic oxide } (SiO_2 + Al_2O_3)}$$

The maximum decontamination obtained in this study was at a slag basisity of 1.5. It was proposed that this was due to the production of acidic oxide ions such as $SiO_4^{4-}$ or $Al_2O_5^{4-}$ which combined with $UO_2^{2+}$ ions and were captured in the slag:

$$2UO_2^{2+} + SiO_4^{4-} \leftrightarrow (UO_2)_2SiO_4$$

These thermodynamic studies show that, by making some assumptions and incorporating experimental data, it is possible to predict the decontamination possible in a very simple melt. The extent of decontamination possible in a more complex system would be much more difficult to predict due to the presence of several elements in the melt and the thermochemical competition of the reactions which may go on between these elements and the reactive elements in the slag.

## 3.4 Thermodynamic Modeling

In order to model a complex system, such as the interaction between molten stainless steel and a multicomponent slag, appropriate solution models must be developed for the molten metal and for the slag. In order to predict the outcomes of the interactions between these two phases, free energy minimization techniques are used.

### 3.4.1 Models for Liquid Metal Solutions

The thermodynamic properties of a liquid metal depend on the components present in solution. Partial molar quantities are those which relate to each individual component of the solution. For example, in a liquid metal solution containing iron and uranium, iron will have its own thermodynamic functions denoted by $\overline{H}_{Fe}$, $\overline{S}_{Fe}$, and $\overline{G}_{Fe}$ and uranium will have similar functions. A partial molar quantity is defined as any thermodynamic function which is characteristic of the state of the system and which depends on the amount of the substance present in the system. The liquid metal solution also has total or integral thermodynamic functions of enthalpy, entropy, volume, and free energy which depend on the partial thermodynamic functions, for example:

$$G = \sum_{i=1}^{r} n_i \overline{G}_i$$

Where $n_i$ is the number of moles of component i in a system where r components are present. The integral molar function is determined by dividing by the total number of moles:

$$G_m = \frac{G}{n_{total}} = \sum_{i=1}^{r} \frac{n_i}{n_{total}} \overline{G}_i = \sum_{i=1}^{r} N_i \overline{G}_i$$

where Gm is the integral molar free energy and Ni is the mole fraction of i in a system with r components.

When there is more than one solute present, there may be, and usually is, interaction between them. Interaction coefficients indicate the effect of each solute on the one under consideration, but, as a first approximation, the assumption is made that the interaction between the other solutes is negligible. When a liquid metal contains several solutes in dilute solution, the relationship of the activity coefficient, $\gamma$, of solute 1 due to the interaction of solute 2 may be represented by:

$$\log \gamma_1^2 = \varepsilon_1^2 N_2$$

where $\varepsilon_1^2$ is the interaction coefficient of solute 2 on solute 1. In similar fashion, when four solutes are present and the activity coefficient of solute 1 alone in solution at infinite dilution is $\gamma_1^1$, then the activity of solute one in the multicomponent solution will be:

$$\log\gamma_1^2 = \varepsilon_1^2(N_2)$$
$$a_1 = \gamma_1^1\gamma_1^2\gamma_1^3\gamma_1^4(N_1)$$
$$\log a_1 = \log\gamma_1^1 + \varepsilon_1^2 N_2 + \varepsilon_1^3 N_3 + \varepsilon_1^4 N_4 + \log N_1$$
$$\log\frac{a_1}{N_1} = \log\gamma_1 = \log\gamma_1^1 + \varepsilon_1^2 N_2 + \varepsilon_1^3 N_3 + \varepsilon_1^4 N_4$$

The interaction coefficient of solute 2 on solute 1 ($\varepsilon_1^2$) will be negative if solute 1 reacts more strongly with solute 2 than with the solvent, since the amount of solute 1 which is free to react (its activity) will be decreased. If however, solute 1 reacts more strongly with the solvent than with solute 2, the interaction coefficient will be positive, resulting in an increase in activity of solute 1.

The concept of activity becomes increasingly complex as the number of components in solution increases. In real solutions, the activity of a component in solution is not only a function of the interactions between itself and the other solutes, but is also influenced by the interactions among the other solutes. The interaction parameter formalism first proposed by Wagner[20] is frequently used for representing the thermodynamic properties of dilute solutions, especially iron based alloys.

If a system consists of r solutes numbered 1 through r and a solvent, it has a total of r+1 components. The Wagner formalism for each solute may be written as:

$$\ln\frac{\gamma_i}{\gamma_i^o} = \sum_{j=1}^{r}\varepsilon_{ij}N_j \quad [i=1,2,...,r]$$

Where $\varepsilon_{ij}$ are the first order inter action parameters given by:

$$\varepsilon_{ij} = \left( \frac{\partial \ln \gamma_i}{\partial N_j} \right)_{N_{solvent}=1} \quad \text{and} \quad \varepsilon_{ij} = \varepsilon_{ji}$$

Mole fractions are denoted by $N_i$ and activity coefficients by $\gamma_i$. The activity coefficient of a solute at infinite dilution (when $N_{solvent}=1$) is denoted by $\gamma_i^o$, where:

$$\lim_{N_i \to 0} \left( \frac{a_i}{N_i} \right) = \gamma_i^o$$

The Wagner formalism is inconsistent except in the case of infinite dilution. Pelton and Bale[21] proposed a simple modification of the interaction parameter formalism for the thermodynamics of dilute solutions which reduces to the standard formalism at infinite dilution. In the modified formalism, the numerical values of the interaction parameters are the same as in the original formalism. The modified formalism is thermodynamically consistent at finite concentrations. In the modified formalism, if component 1 is the solvent, then for solutes i=2,3,4,...r:

$$\ln \gamma_i = \ln \gamma_i^o + \sum_{j=2}^{r} \varepsilon_{ij} N_j + \sum_{j,k=2}^{r} \varepsilon_{ijk} N_j N_k + \sum_{j,k,l=2}^{r} \varepsilon_{ijkl} N_j N_k N_l + \ln \gamma_{solvent}$$

where

$$\ln \gamma_{solvent} = -\frac{1}{2} \sum_{j,k=2}^{r} \varepsilon_{jk} N_j N_k - \frac{2}{3} \sum_{j,k,l=2}^{r} \varepsilon_{jkl} N_j N_k N_l - \frac{3}{4} \sum_{j,k,l,m=2}^{r} \varepsilon_{jklm} N_j N_k N_l N_m$$

The first order interaction parameters, εij, have been determined for many binary solutions. Data for second and third order interaction parameters is not nearly as common.

When two or more liquid metals are mixed there is a change in both the integral and partial thermodynamic functions of the resultant solution. If the free energy of the mixed solution is less than the sum of the free energies of its components, complete mixing occurs. Otherwise, the solutions are immisible. When two liquids are mixed to produce an ideal solution there is no change in either internal energy, U, or in enthalpy, H, on mixing and the physical properties of the components are additive. As most real solutions are not ideal, the concept of regular solutions was developed. Regular solutions vary slightly from ideal behavior in that the entropy change is the same as for an ideal solution and the change in the integral molar free energy is given by:

$$\Delta G^{m} = RT\sum_{i=1}^{r} N_i \ln a_i$$

### 3.4.2 Models for Liquid Slags

Liquid slags, composed of mixed oxides, silicates, aluminates and fluorides are ionic in nature, and thus are composed of cations and anions. In order to characterize a slag, the activities of its components must be determined. Several theories allow calculation of the activities of slag components from calculation of their thermodynamic functions. Slag theories may be classified into molecular or ionic theories. The ionic theories apply mainly to basic slags such as those used in ESR. None of the theories is truly accurate, however, which leads to a need to determine activities experimentally.

#### 3.4.2.1 Temkins's theory

According to Temkin[22], slag is composed of cations and anions. Ions with opposite signs are the closest neighbors in a molten slag, with each cation surrounded by anions and each anion surrounded by cations. The slag, therefore, may be viewed as being composed of two ideal solutions of cations and anions. It is also assumed that all ion species in the slag are known. Because slags are assumed to be composed of ions, ionic fractions are used instead of mole fractions. If, for example, a slag is composed of two species, $CaF_2$

and $Al_2O_3$, which dissociate completely into ions $Ca^{2+}$, $Al^{3+}$ , $AlO^{3-}$, and $F^-$ the cation fractions are:

$$x_{Ca^{2+}} = \frac{n_{Ca^{2+}}}{n_{Ca^{2+}} + n_{Al^{3+}}} \quad \text{and} \quad x_{Al^{3+}} = \frac{n_{Al^{3+}}}{n_{Ca^{2+}} + n_{Al^{3+}}}$$

and the anion fractions are:

$$x_{F^-} = \frac{n_{F^-}}{n_{F^-} + n_{AlO_3^{3-}}} \quad \text{and} \quad x_{AlO_3^{3-}} = \frac{n_{AlO_3^{3-}}}{n_{F^-} + n_{AlO_3^{3-}}}$$

where n is the number of ions in solution. The numbers of ions are related to the number of molecules of $CaF_2$ and $Al_2O_3$ in the original slag as follows:

$$nCaF_2 \rightarrow nCa^{2+} + 2nF^-$$

$$nAl_2O_3 \rightarrow nAl^{3+} + nAlO_3^{3-}$$

For the ideal mixing of components the change in enthalpy is zero, therefore, the change in free energy on mixing is:

$$\Delta G^m = -T\Delta S^m$$

where the entropy of mixing the ions is:

$$\Delta S^m = \Delta S_+^m + \Delta S_-^m$$

The change in entropy for the ideal mixing of cations, $\Delta S^m_+$ , and of anions, $\Delta S^m_-$, are calculated thus:

$$\Delta S_+^m = -R(x_{Ca^{2+}} \ln x_{Ca^{2+}} + x_{Al^{3+}} \ln x_{Al^{3+}})$$

$$\Delta S_-^m = -R(x_{F^-} \ln x_{F^-} + x_{AlO_3^{3-}} \ln x_{AlO_3^{3-}})$$

The sum of which yields:

$$\Delta S^m = -R(x_{Ca^{2+}} \ln x_{Ca^{2+}} + x_{Al^{3+}} \ln x_{Al^{3+}} + x_{F^-} \ln x_{F^-} + x_{AlO_3^{3-}} \ln x_{AlO_3^{3-}})$$

So that

$$\Delta G^m = RT(x_{Ca^{2+}} \ln x_{Ca^{2+}} + x_{Al^{3+}} \ln x_{Al^{3+}} + x_{F^-} \ln x_{F^-} + x_{AlO_3^{3-}} \ln x_{AlO_3^{3-}})$$

The relative partial molar free energy of $CaF_2$ in the slag may be defined as

$$G^M_{CaF_2} = \left( \frac{\partial G^m}{\partial x_{CaF_2}} \right)_{x_{Ca^{2+}}, x_{F^-}}$$

Performing the partial differential yields the following equality:

$$G^M_{CaF_2} = RT\,(\ln x_{Ca^{2+}} + 2\ln x_{F^-}) = RT \ln (x_{Ca^{2+}} x^2_{F^-})$$

and

$$G^M_{AL_2} = RT \ln a_{CaF_2}$$

so that

$$a_{CaF_2} = x_{Ca^{2+}} x^2_{F^-}$$

This is known as Temkin's Rule, which states in more general terms that the activities of components in a molten, ionized mixture are related to the ion fractions of the components. The rule is most applicable to fused salt mixtures, but may also be applied to slags. If a solution contains $A_iL_j$ and $B_pM_r$, the activities of these components may be calculated as follows:

$$a_{A_iL_j} = (x_{A^{j+}})^i (x_{L^{i-}})^j$$

where

$$x_{A^{j+}} = \frac{n_{A^{j+}}}{\sum n_{cations}} \quad \text{and} \quad x_{L^{i-}} = \frac{n_{L^{i-}}}{\sum n_{anions}}$$

$$a_{B_pM_r} = (x_{B^{r+}})^p (x_{M^{p-}})^r$$

### 3.4.2.2 Electrically Equivalent Ion Fraction

When slags are composed of ions of mixed valency, a provision may be made to maintain electrical neutrality at cation and anion sites. The number of cation and anion sites is assumed to be constant, with only cations being allowed to occupy cation sites and only anions being allowed to occupy anion sites. For example, if the cations in the slag are $A^+$ and $B^{2+}$, the $B^{2+}$ ions may occupy the $A^+$ sites only if a vacant cation site is generated. The anions may also exhibit different valences, as in the case of mixing oxides with halides. In order to consider the formation of electrically neutral species, the electrically equivalent ion fraction may be calculated. In a mixture of $A^+$, $B^{2+}$, $C^{3+}$, and $D^{4+}$ ions, the electrically equivalent ion fraction, x', may be defined as:

$$x'_{B^{2+}} = \frac{2n_{B^{2+}}}{n_{A^+} + 2n_{B^{2+}} + 3n_{C^{3+}} + 4n_{D^{4+}}}$$

The activities of the ions are not proportional to the mole fractions and are not a linear function of the concentrations of the ions. The basis of this slag model is the assumption that the slag has some short range order, and, while this may not be true, the use of x' in place of x in a Temkin analysis provides a way of estimating the activities of slag constituents which form from ions of different valences.

### 3.4.3 Free Energy Minimization Modeling

This method of determining the composition of a system at equilibrium is based on the fact that at equilibrium the total Gibbs free energy of the system has its minimum value. A system may be thought of as being composed of a certain number of moles of each of several substances reacting at a certain temperature. The total Gibbs free energy of the system can be expressed in terms of partial molar Gibbs free energies and number of gram moles, x:

$$G = \sum x_i \overline{G}_i$$

Where $\overline{G}i$, the partial molar free energy of the ith species, is

$$\overline{G}_i = G_i^o + RT \ln a_i$$

where $G_i^o$ is the molar free energy of the ith component in the standard state and $a_i$ is the activity of the ith component . So that

$$G = \sum x_i G_i^o + \sum RT x_i \ln a_i$$

Complex systems have one or more condensed phases and solid or liquid solutions in addition to a gas phase. The total free energy for such a system is given by:

$$\frac{G}{RT} = \frac{1}{RT}\sum x_i^g G_i^{og} + \sum x_i^g \ln a_i^g + \frac{1}{RT}\sum x_i^l G_i^{ol} + \sum x_i^l \ln a_i^l + \frac{1}{RT}\sum x_i^s G_i^{os} + \sum x_i^s \ln a_i^s$$

where the superscripts s, g, and l denote the solid, gas and liquid phases. Several free energy minimization principles have been published in the literature, for which the underlying principle is essentially the same[23]. The function G/RT is minimized subject to two types of constraints. Firstly, that the atom balance relations be satisfied and secondly that the number of gram moles of each species have positive values at equilibrium. A reduced free energy function, F is defined that is equal to G/RT:

$$F = f(x_1, x_2, ....., x_n)$$

The equilibrium state corresponds to the minimum in F, and at equilibrium:

$$\frac{\partial F}{\partial x_i} = 0$$

$$i = (1,2,3....n)$$

The n species that compose the system ($CaF_2$, $Al_2O_3$, CaO, $CeO_2$, $La_2O_3$, etc) are constituted from m elements (Ca, F, Al, O. Ce, La). Because each kind of atom is conserved, there will be m constraining equations that can be represented in the form of a matrix:

$$\begin{bmatrix} q_{11} & q_{12} & \cdots & q_{1n} \\ q_{21} & q_{22} & \cdots & q_{2n} \\ \vdots & & & \vdots \\ q_{m1} & q_{m2} & \cdots & q_{mn} \end{bmatrix} \begin{bmatrix} x_1 \\ x_2 \\ \vdots \\ x_n \end{bmatrix} = \begin{bmatrix} b_1 \\ b_2 \\ \vdots \\ b_m \end{bmatrix}$$

$$b_j = \sum_{i=1}^{n} q_{ji} x_i \quad 1 \le j \le m$$

Here $b_j$ is the number of gram atoms of element j given by the initial composition. For example, the number of moles of calcium present may be calculated from the known amounts of calcium fluoride and calcium oxide that make up each slag. In the above equation, $q_{ji}$ is the number of gram atoms of element j in 1 gram mole of species i. For example, in the $CaF_2$ system if j is Ca and i= $CaF_2$ then $q_{ji} = 1$. The values of q are defined by the types of species expected to form from the atoms present. This is why any species which is expected to be present in a solution at the pressure and temperature of interest should be included in the calculation. This necessitates some knowledge of the system of interest before free energy minimization is performed. To some extent, the species expected to be present may be determined by examination of the free energies of formation of each species expected to be present. If the free energy of formation is negative, the possibility exists that the species will be present.

Using linear algebra, if n is less than m, the elements $b_1$ through $b_m$ are linearly dependent. In our case n will usually be greater than m because for each kind of atom

present, more than one compound can usually form, so m is less than n (fewer equations than unknowns) and the system has a non trivial solution. In this case there are m dependent variables, with the others (of number n-m)being independent.[24]

The final solution will give values for $x_i$ through $x_n$ (the number of moles of each substance formed) that will minimize the free energy for the system. In order to do this, most of the commercial software available follows an iterative process which includes the following stages: From the matrix above, m equations can be written. The m dependent variables are then expressed in terms of the n-m independent variables. Additionally, a constraint is observed that each dependent variable, $x_1$ - $x_m$, have a value greater than zero. Because $x_1$ - $x_m$ have already been written in terms of $x_{m+1}$ - $x_n$, a series of equations results which may be solved for $x_{m+1}$ in terms of the other independent variables. If the values for each dependent variable in these equations are chosen arbitrarily, we obtain a set of values for $x_{m+1}$ for which the lower and upper limits for $x_{m+1}$ may be found.

### 3.4.3.1 Mechanics of the F*A*C*T* Computer Program

In this research, free energy minimization was performed by use of the Facility for the Analysis of Chemical Thermodynamics[25] (F*A*C*T*) EQULIB computational software. The F*A*C*T* program includes an extensive thermodynamic database. It is possible to access the database directly using the COMPOUND program. EQULIB requires thermochemical data to be retrieved, as needed, from the database, or, if desired, from a personal database assembled by the user and used in conjunction with the built-in database. The code EQULIB is the most recent version of the chemical equilibrium code, SOLGASMIX.[26] EQULIB calculates the equilibria of chemical systems by free energy minimization considering condensed species of invariant composition and solutions of species which could be present under equilibrium conditions. These solutions may be specified by the user to behave ideally or to conform to a given solution model, of which there are several to choose from in the SOLUTION section of the code, such as the modified interaction parameter model, detailed above.

Based upon the values of the stoichiometric coefficients of each species initially present, a list of possible products is generated from which the user may construct solutions. Each solution is then assigned a specific solution model, the rules of which govern the behavior of the solution. For example, in this research, gas species were combined to form an ideal gas. Metallic species, present as liquids at the temperatures

given, were grouped to form a liquid solution and were assigned to behave according to the modified dilute interaction parameter model. Oxygen and fluorine bearing species, which were liquid at the temperatures given, were allowed to form a slag phase which behaved as an ideal solution. Components of the system which were predicted to be solids at the temperature given were taken to be condensed phases of invariant composition.

Initially, the free energy of the reactants of the system is calculated. The molar quantities of the invariant phases and the solution components are varied by the code and the free energy is calculated again. Adjustment of the stoichiometric coefficients, followed by free energy composition is repeated again and again until the free energy of the system is at a minimum.[27]

#### 3.4.3.1.1 Limitations of Predictions

Kessinger[27] performed a verification study in which EQUILIB was benchmarked against published phase diagrams, the results of hand calculations, and the results of the F*A*C*T REACT code. Although the program produced results that are in agreement with thermochemical data, several deficiencies were observed. The most notable of these deficiencies is that the code extrapolates data for species and phases beyond the acceptable stability ranges. This creates problems when the data for a solid is extrapolated to a temperature above its stability range and there is no data for a liquid species of the same chemistry present in the database. Because the standard free energy of formation of the solid may be more negative than the sum of the free energies of the liquid species that form when the solid melts, unreliable results may be reported.

Another deficiency was encountered with the extent of the database, as data for many phases was not available, although it could be manually added when it could be found in the literature. It was, in fact, the lack of thermochemical data which limited the use of F*A*C*T* for this research. The systems at hand were quite complex, with a number of invariant phases possible for which no thermochemical data existed.

## 3.5 Summary

While thermodynamics is a powerful tool for the prediction of the partitioning of radionuclides during melting, thermodynamic predictions are only as good as the assumptions made to generate them and the accuracy of the data used in the calculations.

Thermodynamic data for many of the compounds formed by radioactive compounds are difficult to generate. The chemistry of many highly alloyed metals does not allow the assumption of infinite dilution important to many solution models, but neither are these solutions ideal, although the extent of deviation from ideality is not often known as values for activity and interaction coefficients have not been generated. While thermochemical measurements of liquid metals at high temperatures are difficult, such measurements on liquid slags are more difficult still, due to the corrosive nature of the slags and their complex chemistries. Nevertheless, thermochemical predictions have been shown to agree with empirical data for less complex systems, so as the understanding of metal-slag interactions becomes more complete, the thermodynamic predictions for melt partitioning will doubtless increase in accuracy.

# Chapter 3 References


[1] Heshmatpour, B., Copeland G.L., Heestand, R.L., "Decontamination of Transuranic Contaminated Metals by Melt Refining," *Nuclear and Chemical Waste Management*, Vol. 4, (1983), 129-134.

[2] Moore, J.J. Chemical Metallurgy, Butterworth-Heinemann Ltd., Jordan Hill, Oxford, (1990).

[3] Gaskell, D.R. Introduction to Metallurgical Thermodynamics, McGraw-Hill, New York, (1973), 253- 276.

[4] Ellingham, H.J.T., "Reducibility of Oxides and Sulfides in Metallurgical Processes", *J. Soc.Chem. Ind.*, Vol. 63 (1944).

[5] Twidwell, L.G. Physical Chemistry of Iron and Steelmaking, Montana College of Mineral Science and Technology, Butte, Montana, (1980).

[6] Rosenqvist, T. Principles of Extractive Metallurgy, McGraw-Hill book Company, New York. (1974), 245-248.

[7] Kellogg, H.H., Basu, S.K., "The Roasting of Sulfide Ores," *Transactions. AIME*, Vol. 218: (1960), 70-81.

[8] Pehlke, R.D. Unit Processes of Extractive Metallurgy, Elsevier, New York, (1973).

[9] Roine, A. HSC Chemistry for Windows-Chemical Reaction and Equiblibrium Software with Extensive Thermochemical Database, Version 1.10, Outokumpu Research Oy, Pori, Finland, (1993).

[10] Nafziger, R.H., The Electroslag Melting Process, United States Department of the Interior, Bureau of Mines Bulletin 669, (1976).

[11] Heshmatpour, B., Copeland, G.L. "The Effects of Slag Composition on Decontamination of Metallic Waste by Melt Refining", ORNL/TM-7501, Oak Ridge National Laboratory, Oak Ridege, Tennissee, (1981).

[12] Heshmatpour, B., Copeland, G.L. "Metallurgical Aspects of Waste Metal Decontamination by Melt Refining" *Nuclear and Chemical Waste Manangement*, Vol.2, (1981), 25-31.

[13] Copeland, G.L., Heestand, R.L., Mateer, R.S., "Volume Reduction of Low Level Contaminated Metal Waste by Melting-Selection of Method and Conceptual Plan", ORNL/TM-6388, Oak Ridge National Laboratory, Oak Ridege, Tennissee, (1978).

[14] Miller, R.L., Reimann, G.A. "Thermodynamics of Gas-Metal-Slag Equilibria for Applications in In Situ and Ex Situ Vitrification Melts" EGG-MS-10613. Idaho National Engineering Laboratory, (May, 1983).

[15] Dealy, J.M., Pehlke, R.D., "Activity Coefficients in Binary Liquid Metallic Solutions at Infinite Dilution," *Transactions of the Metallurgical Society of AIME*. 227, (1963), 131.

[16] Heshmatpour, B., Copeland, G.L., Heestand, R.L., "Decontamination of Transuranic Contaminated Metals by Melt Refining", *Nuclear and Chemical Waste Management*, Vol. 4, (1983), 129-134.

[17] Joyce, E.L., Lally, B.R., Fruehan, R.J., Ozturk, B., "Liquid Metal Recycle and Waste Treatment: Liquid Metal Melt-Slag Technology Evaluation for MWIP" LA-UR Report 93-3026. Submitted to DOE-EM50. (1993)

[18] Abe, M., Uda, T., Iba, H., "A Melt Refining Method for Uranium Contaminated Steels and Copper" Waste Management 85, Proceedings of the Symposium on Waste Management at Tucson, Arizona, March 24-28, No. 3, Ed. R.G. Post and M.E. Wacks, (1985), 375.

[19] Uda, T., Iba, H., Tsuchiya, H. "Decontamination of Uranium-Contaminated Mild Steel by Melt Refining" *Nuclear Technology*, Vol 73,.(April 1986), pp. 109-115.

[20] Wagner, C., Thermodynamics of Alloys, Addison Wesley, Reading, MA, (1962), p. 51.

[21] Pelton, A.D., Bale, C.W., "A Modified Interaction Parameter Formalism for Non-Dilute Solutions", *Met. Trans.*, 17A, (1986), 1211-1215.

[22] Temkin, M., "Title is in Russian", *Acta Physicochemica URSS*, Vol. 20, (1945), 411.

[23] Rao, Y.K., Stoichiometry and Thermodynamics of Metallurgical Processes, Cambridge University Press, (1985), 765-773.

[24] Rabenstein, Albert L., Elementary Differential Equations with Linear Algebra, Academic Press Subsidiary, Harcourt Brace Jovanovich Publishers, New York, (1975).

[25] F*A*C*T* is a copyrighted product of Thermfact Ltd./Ltee., 447 Berwick Ave., Mount-Royal, Quebec, CANADA, H3r IZ8.

[26] Eriksson, G., "SOLGASMIX,"*Chemica Scr.*, Vol. 8, (1975), 100.

[27] Kessinger, G.F., "Verification of Thermodynamic Codes React and Equilib for the Study of Non-Aqueous Inorganic Systems", WINCO-1105 Westinghouse Idaho Nuclear Corporation Report, (September 1992).

# Chapter 4
# Electroslag Remelting: Process Configuration and Slag Chemistry

Electroslag remelting, often referred to as ESR, is a secondary melting technique which may be used for a variety of metals and alloys if appropriate fluxes, control strategies, and melting parameters are used. The ESR process is widely used among producers of specialty metals and alloys because it is capable of producing very clean material with an absence of pipe and porosity. Material produced by ESR has uniform structure and chemical composition and thus exhibits excellent mechanical properties. Optimized control strategies and correct slag selection result in smooth ingot surfaces, eliminating the need for surface treatment before working.

## 4.1 Process and Equipment Description

A schematic diagram of an ESR furnace is shown in Figure 4.1. The electrode, which is usually consumable and composed of the metal to be melted, is welded to a stub of metal which is, in turn, attached to a movable water cooled copper electrode support. This electrode bearing assembly is connected to a power supply which may be either single phase AC, DC straight polarity (negative), or DC reverse polarity (positive). Before the beginning of the melt, a base plate and turnings of the metal or alloy to be melted are placed on a water cooled copper base plate, to which a power return cable may be connected. Melting takes place in a water cooled copper crucible to which another power return may be connected. Prefused flux is charged into the bottom of the crucible prior to initiation of the melt. At the beginning of the melt, an arc is struck between the electrode and the baseplate. This arc is immediately quenched by the melting flux. During the melt, additional flux may be charged through the top of the furnace, in the case of an open air melt, or through a feeder in a closed furnace melt.

When the flux is completely melted, the power is increased and the temperature of the molten slag, which is restively heated, reaches and exceeds the liquidus temperature of the electrode. As the electrode melts, drops of molten metal fall through a slag layer which completely surrounds the molten drop, oxidizing the most reactive species and capturing them into the slag. Metal droplets collect in a pool which solidifies on the water cooled copper base plate. As melting proceeds, an ingot is built up. The top of this ingot is a pool of molten metal which is in contact with molten slag. As melting proceeds, the molten slag is continuously displaced in an upward direction. When the rising slag meets the cooled mold, selective solidification takes place, forming a shell or skin of solid slag between the crucible and the solidifying ingot. This slag skin serves as a protective coating for the copper crucible and its characteristics influence the surface quality of the ingot produced. Near the end of an ESR melt, the power may be adjusted to eliminate the formation of pipe and centerline porosity in the ingot.[1]

Refining takes place due to reactions between the metal and the slag at three stages, during the formation of a droplet on the electrode tip, as the detached droplet falls through the slag, and after the molten metal has collected in a pool at the top of the ingot. Removal of impurities from the ingot may be accomplished by promotion of chemical reactions with components of a chosen slag. Alternately, slags may be selected to inhibit the removal of elements that are to be retained for alloying purposes. Non-metallic inclusions may be removed by encouraging physical flotation and by chemical extraction with the slag.[2]

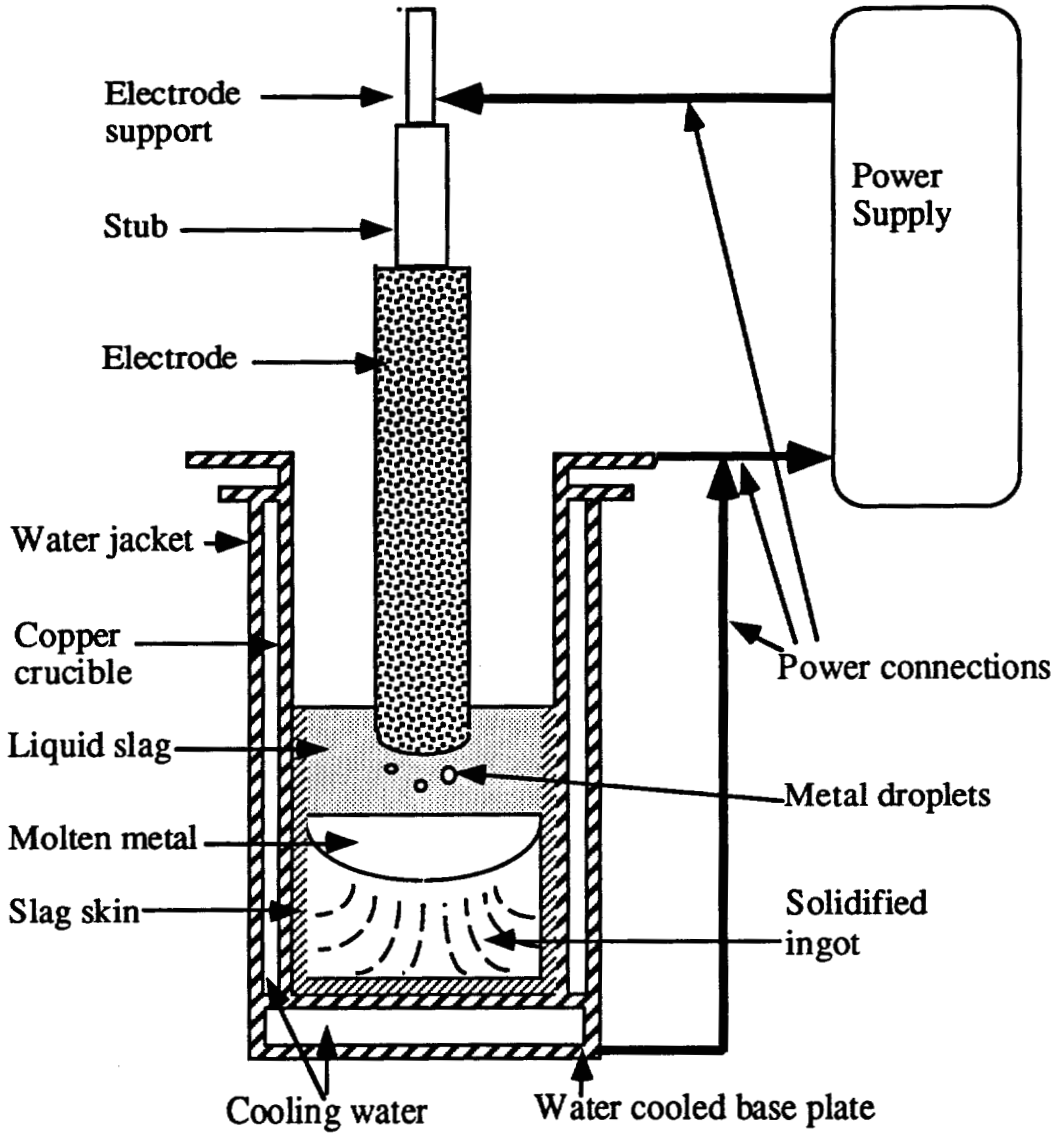


**Figure 4.1**
**Schematic of Electroslag Remelting Furnace**

### 4.1.1 Electrical Behavior of the System

The heat required to operate the ESR process is generated by the joule effect in the slag bath. For practical purposes it is assumed that the slag behaves as a resistance element whose cross sectional area is intermediate between that of the electrode and that of the mold. If the normal laws of electricity are applied, the following equation may be used to describe this situation:

$$l = \frac{VA}{I\rho}$$

where l is the effective resistance path length roughly equal to the slag depth or to the distance between electrode tip and molten metal surface, V is the voltage drop across the slag, A is the effective cross section of the current path (taken by some as the electrode area and by others as the mold area), I is the current, and ρ is the effective value of the slag resistivity. The actual circuit is more complex. The distribution of current within the slag bath is not uniform due to the effects of temperature differentials, stirring effects, and the presence of metal droplets which are of lower resistivity than the slag. The slag bath is in a state of motion due to thermal convection effects and electromagnetic effects, which are dependent on current density and hence on electrode diameter. Because the presence of metal droplets will reduce the resistance it is expected that, other things being equal, the resistance will be lower at higher melt rates because of the higher volume of metal in transit at any time. The dependence of bath resistance on electrode immersion has been demonstrated to show that resistance changes rapidly with depth of immersion at shallow immersion and as immersion increases the slope is not as steep. This phenomena has been used as the basis of a controller to maintain constant immersion.[2]

### 4.1.2 Thermal Behavior of the System

The generation and transfer of heat in ESR influences product quality as well as process efficiency. Of the total heat supplied by Joule heating of the slag, only a small proportion is used in melting the metal, the remainder being transferred to the cooling water through the mold or lost by radiation from the slag surface. Mitchell[3] found that a dynamic heat balance of the ingot pool region shows that the liquid metal accounts for only 10-30% of the heat input, depending on ingot diameter. The boundaries of the heat transfer system are the slag-gas surface, the slag or metal-slag skin-crucible, and the ingot. The heat transfer taking place at the slag or metal-slag skin-crucible has an effect on the thickness and consistency of the slag skin, which, in turn, affects the surface quality of the ingot. The dynamic heat balance in the molten ingot pool, which determines the solidification structure of the ingot, is greatly influenced by the presence of liquid slag above it. The

energy efficiency of an ESR process may be calculated as the ratio of the heat used to melt the metal to the total electric power supplied. The heat used to melt the metal can be estimated from multiplying the heat capacity and heat of fusion of the metal by the melt rate.[2]

## 4.2 ESR Slags

The slag phase in ESR performs many functions. The chemistry of the slag influences such important physical properties as resistivity and heat capacity, as well as density, viscosity, and surface tension. The physical properties of the slag, in turn, influence the performance of the entire melting process. If, for example, due to its chemistry, a slag has insufficient resistivity at melting temperatures it will be difficult to maintain the slag superheat necessary for melting operations, and efficiency will suffer. The functions of ESR slags, their chemistries, the resultant physical properties, and their influence on the ESR process will be discussed in the following sections.

### 4.2.1 Functions of the Slag Bath

The slag bath, which is responsible for melting and refining the metal, is a very important part of the electroslag remelting system. The slag performs several important functions:

1. It acts as the heating element. As the element of the electrical circuit which has the greatest resistivity, it is responsible for the conversion of electrical energy into heat by the Joule effect. During melting, a dynamic balance between the slag resistance and applied voltage is achieved, compatible with the characteristics of the power supply. The relationships between current, voltage, slag depth and resistivity are complex and optimized adjustment is essential to ESR operation.

2. The slag dissolves and captures non metallic material. Inclusions which do not react with the slag and are immisible in the steel are removed, by flotation and adhesion, into the slag. Other inclusions may be dissolved by the slag.

3. The slag is the refining agent of the process. Reactions between the slag and the metal may be used to effect the removal of tramp elements while promoting the retention of valuable alloying constituents.

4. The slag protects the metal from contamination. Because it is melted and solidified under a slag, the molten metal never comes into contact with the atmosphere and the direct oxidation that may cause problems in conventional metal melting is not experienced in ESR. The slag may however provide a vehicle for the transport of reactive components such as oxygen or moisture so that an inert gas cover may be required.

5. The slag forms a mold lining. Because the temperature of the mold wall is maintained below the melting point of the slag, a crust of solid slag forms between the molten slag bath and the mold walls. This slag skin serves as a mold liner in which the ingot forms and solidifies. The thickness and heat conduction characteristics of this slag skin influence the solidification mechanics and thus the final structure of the ingot. The surface tension between the molten metal and the slag skin influence the surface quality of the ingot produced.[2,4]

### 4.2.2 Chemistry

The chemistry of ESR slags is based on the mix of the major constituents, the addition of special additives, and the presence of impurities. The most widely used slag systems in ESR are the fluoride-oxide slag systems, namely those in the calcium fluoride-lime-alumina system. Special additives for the control of slag chemistry and properties may include magnesia, magnesium fluoride, barium fluoride, barium oxide, rare earth oxides, titania, zirconia, and chromium oxide. Impurities often include silica and iron oxide.

Salt[5] suggested a notation to describe slag composition. Calcium fluoride is listed first followed by the remaining constituents in the order of lime, magnesia, alumina, and silica (which is the order of decreasing basicity) giving their percentage compositions only. The general formula is (a/b/c/d/e) where a=% calcium fluoride, b=% lime, c= % magnesia, d=% alumina, and e=% silica. Slag compositions within the ternary calcium fluoride-lime-alumina system are abbreviated by the shorthand of writing (%$CaF_2$/% CaO/% $Al_2O_3$), for

example a slag of composition 60% calcium fluoride, 20% calcium oxide, and 20% alumina would be denoted a (60/20/20) slag.

### 4.2.2.1 Phase Diagram

Slags made from the raw materials $CaF_2$, CaO, and $Al_2O_3$ do not melt in the normal sense when heated. Instead, the calcium fluoride melts at 1423°C , followed by the melting and dissolution of the remaining components following a pattern defined by the established phase diagrams. The rate of dissolution of CaO and $Al_2O_3$ is determined by temperature and the stability of intermediate phases.[6]

The constitution diagram of the ternary calcium fluoride-lime-alumina system has been extensively investigated and the diagram shown in Figure 4.2, prepared by Zhmodin[7], is considered to be the most reliable version. The main feature is a trough corresponding to compositions with roughly equal proportions of lime and alumina. These slags have liquidus temperatures in the range 1350-1500°C which makes them suitable for melting a range of steels and superalloys. Another important feature of the system is a two liquid zone in the high fluoride low lime region. There are two congruently melting ternary compounds $3CaO•3Al_2O_3•CaF_2$ denoted $C_3A_3F_1$ and $11CaO•7Al_2O_3•CaF_2$ denoted $C_{11}A_7F_1$. Table 4.1 lists the invariant points associated with the ternary diagram.

The binary calcium fluoride lime system has been used where a large degree of desulfurization is required. High lime contents incur a risk of moisture retention or pickup. Many commonly used slags have compositions with $CaO/Al_2O_3 = 1$ such as (60/20/20) and (70/15/15) These lie along the low melting point trough, have acceptable values of electrical resistance (0.5 ohm cm.) and have a high degree of fluidity. If it is desired to increase the temperature of operation, or to increase the melt rate for a given power output, slag resistance can be increased by increasing the alumina content of the slag. In order to do this without increasing the liquidus temperature, compositions may be chosen from within the low temperature trough, such as (50/25/25).[8]

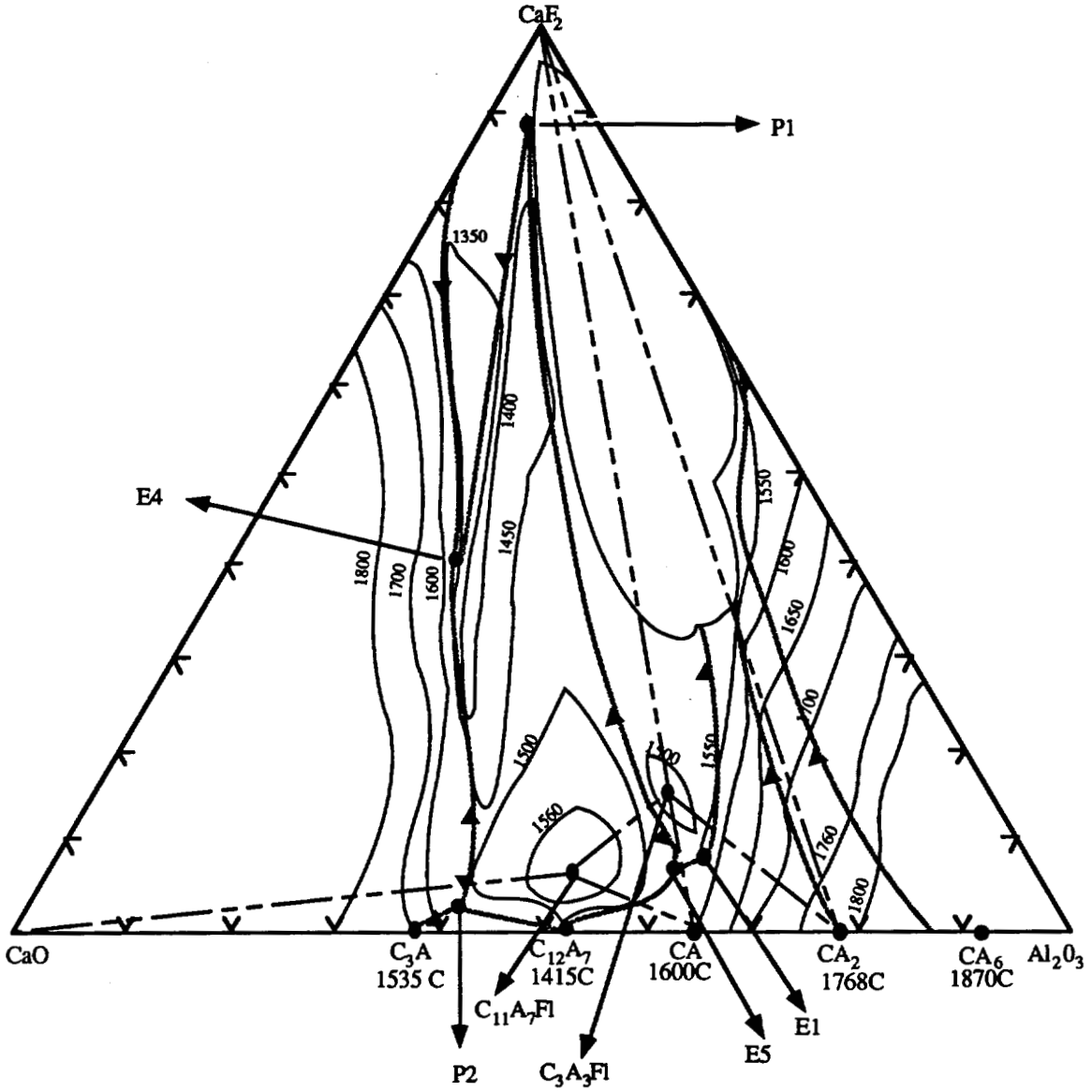


**Figure 4.2**

**Ternary Phase Diagram for the System $CaF_2$-CaO-$Al_2O_3$**

**Table 4.1**

**Invariant points in the system $CaO-Al_2O_3-CaF_2$**

| Point | Type | CaO % | $Al_2O_3$ % | $CaF_2$ % | Temp. °C | Nature of Equilibrium |
|---|---|---|---|---|---|---|
| E1 | Eutectic | 31.0 | 61.0 | 8.0 | <1498 | $L = CA + C_3A_3Fl + CA_2$ |
| E2 | Eutectic | 0.4 | ~2 | 97-98 | ~1390 | $L = CA_2 + CaF_2 + CA_6$ |
| E3 | Eutectic | 0.9 | ~2.5 | 96-97 | ~1385 | $L = C_3A_3Fl + CaF_2 + CA_2$ |
| E4 | Eutectic | 38.0 | 22.0 | 40.0 | 1230 | $L = CaO + C_{11}A_7Fl + CaF_2$ |
| E5 | Eutectic | 35.0 | 58.5 | 6.5 | <1475 | $L = CA + C_{11}A_7Fl + C_3A_3Fl$ |
| P1 | Peritectic | 6.0 | 6.0 | 88 | 1355 | $L + C_3A_3Fl = C_{11}A_7Fl + CaF_2$ |
| P2 | Peritectic | 56.2 | 42.5 | 1.3 | 1460 | $L + CaO = C_3A + C_{11}A_7Fl$ |
| $CaF_2$ | Invariant | 0.0 | 0.0 | 100.0 | 1422 | Congruent Melting |
| $C_3A_3F_1$ | Invariant | 30.5 | 55.4 | 14.1 | 1507 | Congruent Melting |
| $C_{11}A_7F_1$ | Invariant | 43.7 | 50.7 | 5.5 | 1577 | Congruent Melting |

### 4.2.2.1.1 Consequences of the Phase System

The phase system is important in determining a slag's suitability for ESR processing. Regardless of any chemical requirements that may exist, in order to provide a suitable melting medium the slag should have a liquidus temperature about 100°C below that of the metal, but must also form a primary solid phase on freezing which has a melting point higher than that of the metal.[9] The slag skin, which solidifies on the cold metal crucible must contain a small pool of liquid metal. If the slag film has a low melting point, it will be melted to some degree, depending on the temperature of the molten metal with which it is in contact. Fluctuations in the temperature of the molten metal cause changes in the amount of slag which is melted back before a skin of metal forms. Such changes may result in undesirable laps on an ingot surface.[10] It is possible, however, for slag systems which include low melting point phases to give good ingot surfaces. This result may be obtained when a component of the surface skin melts and forms a liquid which has a low interfacial tension with the steel, resulting in a smooth ingot surface.[11] While the phases

formed by a slag upon solidification influence the composition of the skin and its thickness, the thermal conductivity of the resultant slag skin influences the heat transfer rate through the skin and thus the solidification structure of the ingot. As an ESR melt proceeds, the bulk slag composition changes due to the selective solidification of the phases which make up the skin. The location of the starting slag on the phase diagram determines the composition of the phases which make up the skin and the stability of the chemical makeup of the bulk slag.

### 4.2.2.2 Slag Preparation

Slag to be used in the ESR process is usually prefused to refine the slag and reduce the content of components which are detrimental to the production of high quality metal. The removal of water is the most important aspect of slag fusion. Water in the slag, which is mainly associated with lime, can react with hot metal to produce hydrogen which gives rise to ingot porosity and hydrogen cracking. During fusion there is a substantial reduction in the content of water and other undesirable constituents. Slag fusion allows the lime in the slag to combine with other constituents and reduces its tendency to rehydrate. Adequate prefusion, in which the slags are held molten at 1650 to 1750°C, is essential if ingot porosity and hydrogen cracking are to be avoided.

During prefusion, pyrohydrosysis of some of the calcium fluoride always takes place if there is any water present. Pyrohydrolysis takes place by the reaction:

$$CaF_2 + H_2O \rightarrow 2HF + CaO$$

According to this reaction, even when lime has not been included in the raw materials, the fused slag will contain 2-5% CaO.

The fusion of slag may be performed in either an induction furnace with a graphite crucible in which the graphite acts as both furnace lining and susceptor, or a graphite electrode arc furnace, either single phase or three phase. Carbon is picked up by all slags to some extent, which is a function of the fusion time and the surface area of the graphite in contact with the melted slag. The greatest amount of carbon pickup is associated with slags which contain free lime, which react with the graphite to form carbides:[6]

$$CaO + 3C \rightarrow CaC_2 + CO$$

During subsequent ESR melting, the ingot may pick up carbon from the slag.

### 4.2.2.3 Changes in Slag Chemistry During Melting

Slags based on $CaF_2$ are used almost exclusively in electroslag remelting. Chemical reactions cause changes in the composition of the slag, along with the evolution of volatile fluorides and oxides. Most ESR slags are fluxed with calcium fluoride and therefore some losses occur from the slag pool during melting as fluorine bearing vapor species. These losses often have the effect of increasing the CaO content of the slag, which in turn changes its melting point and properties such as conductivity, so that production (melt rate) is affected, as are ingot chemistry and properties.[8] Vaporization loss from the calcium fluoride, calcium oxide alumina melts is due primarily to the formation of the volatile species $AlF_3$:

$$3(CaF_2) + (Al_2O_3) \rightarrow 3(CaO) + 2AlF_3(g)$$

Other vapor losses include:

$$(CaF_2) \rightarrow CaF_2(g)$$
$$2(CaF_2) + (SiO_2) \rightarrow 2(CaO) + SiF_4(g)$$
$$(CaF_2) + H_2O \rightarrow (CaO) + 2HF(g)$$

### 4.2.3 Properties

The chemical makeup of a slag determines its physical and chemical properties. Some relevant properties are vapor pressure, electrical conductivity, viscosity, density, and surface tension. The overall efficiency of the melting operation is governed to a certain

extent by the physiochemical properties of the liquid slag. To establish optimum operating conditions for an ESR system, a knowledge of slag properties is required.[12]

Slag chemistry is specified so that certain specific property specifications are met and maintained. Because process operating temperatures measured in the slag bath between the electrode tip and the molten metal pool lie in the range of 1600 to 2500°C, the slag components must have a low vapor pressure. The slag must be stable at operating temperatures higher than the melting point of the metal. Resistivity is a function of composition and may be adjusted within limits, provided that the chemical requirements are met. The composition should allow desired reactions to take place rapidly and the reaction products retained in the slag or discharged to the atmosphere, as in the case of undesirable components such as sulfur. The slag should also inhibit the removal of valued alloying elements. Viscosity affects the residence time of metal droplets in the slag, the rate of escape of gasses, the degree of stirring in the slag, the kinetics of mass transfer, and the thickness of the slag crust.[13,14] The difference in density between the slag and the metal also has an effect on the residence time and size of droplets. The interfacial tension between slag and metal should have a low value to increase mass transfer rate and facilitate the production of small droplets, but this can reduce the ability of slag and metal to separate and thus encourage slag entrapment. Surface tension also affects the mechanism of solution of inclusions as well as the surface quality of the ingot produced.

Numerical values for the physical properties of slags have been accumulated by Mills and Keane[12]. For practical purposes Mills[15] has produced a master diagram shown in Figure 4.3 covering compositions in the calcium fluoride lime alumina system. Although lines of constant properties are shown, Mills points out that the experimentally determined values usually show a decrease in value through the two liquid region. This is attributed to the fact that, when making measurements in this region, the values obtained refer primarily to the lighter of the two liquids. The figure shows that as the amount of calcium fluoride in a slag is decreased, the electrical conductivity decreases, the viscosity, density, and surface tension increase and the total normal emissivity decreases.

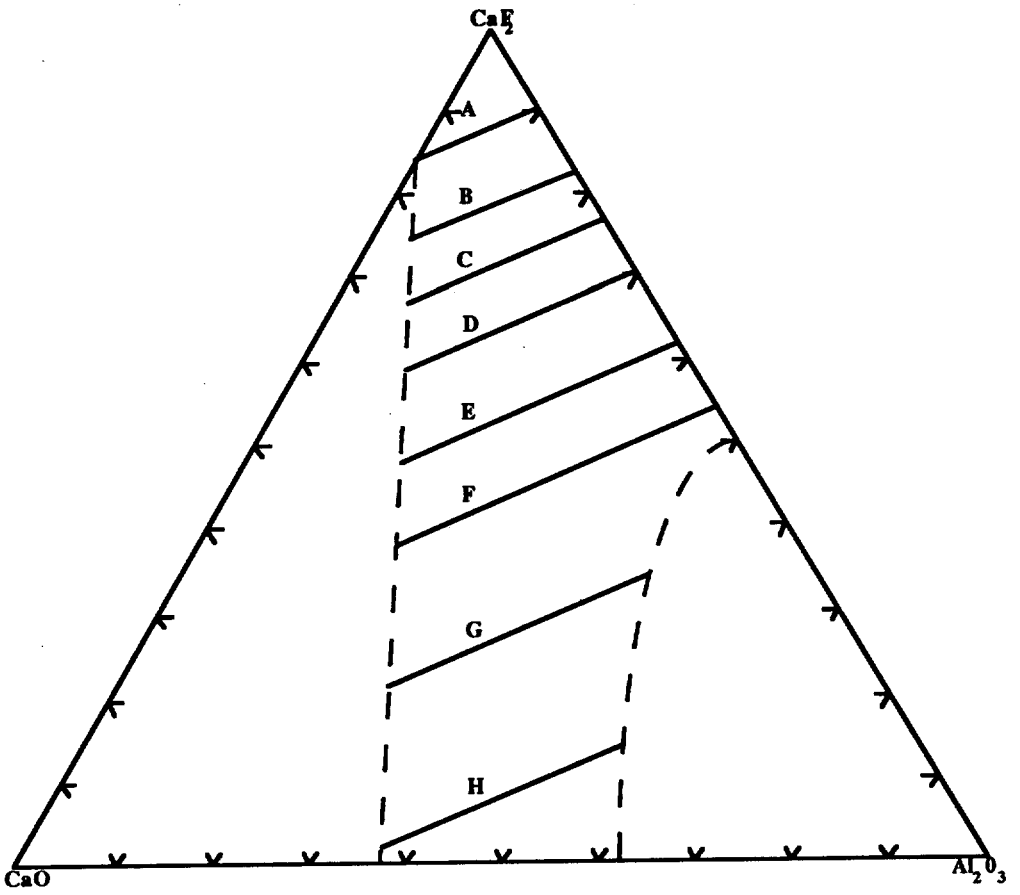


| Contour | Electrical Conductivity $\kappa$ ($ohm^{-1}$ $cm^{-1}$) | Viscosity $\eta$ ($10^{-1}$Ns/m) | Density $\rho$ ($g/cm^3$) | Surface Tension $\sigma$ (mN/m) | Total normal emissivity $\varepsilon_{TN}$ |
|---|---|---|---|---|---|
| A | 6 | 0.15 | 2.47 | 285 | 0.96 |
| B | 5 | 0.2 | 2.48 | 300 | |
| C | 4 | 0.25 | 2.49 | 310 | |
| D | 3.5 | 0.3 | 2.5 | 320 | 0.9 |
| E | 3 | 0.4 | 2.55 | 335 | |
| F | 2.5 | 0.6 | 2.6 | 350 | 0.85 |
| G | 2 | 0.8 | 2.7 | 400 | |
| H | 1 | 1.0 | 2.8 | 450 | 0.81 |

**Figure 4.3**
**Properties of Slags in the System $CaF_2$-CaO-$Al_2O_3$**

### 4.2.3.1 Vapor Pressure

Of the fluorides of aluminum, barium, magnesium, strontium, and calcium, calcium fluoride has the lowest vapor pressure and hence is the least volatile. Most of the oxides, except those of the alkali metals, such as sodium and potassium, have a lower vapor pressure than calcium fluoride. The loss of oxides from the slag due to vaporization is, therefore, not as significant a problem as is the loss of fluorides. Only those oxides having very low vapor pressures such as lime, alumina, and zirconia, may be used, however, because the vapor pressure of an oxide is proportional to the partial pressure of oxygen in solution in the slag. The higher the partial pressure of oxygen in the slag then the higher will be the concentration of oxygen in the metal. The oxides of those elements commonly existing in more than one oxidation state, such as the oxides of titanium, vanadium, chromium, manganese, iron, cobalt, nickel, and copper may, if present, facilitate the transfer of oxygen between the atmosphere and the metal.[14]

### 4.2.3.2 Electrical Conductivity

In ESR, the slag bath is the source of heat for melting as the liquid slag acts as a resistive medium for conversion of electrical energy into thermal energy. The conductivity of the slag will control the temperature of the slag phase and thus the melt rate of the metal to be refined. In an ESR the power P dissipated by the slag when a current I is passed under a potential difference V is given approximately by the relation:

$$P=VI=\frac{V^2 A\kappa}{d}$$

where A is the cross sectional area of the slag bath, d is the path length of the resistor, or the depth of the slag pool, and $\kappa$ is the electrical conductivity of the slag. Although a high melt rate would give a high production rate, large temperature gradients would be generated across the molten metal pool and this would result in a deep melt pool and preferential solidification in a radial direction rather than the desired axial solidification. A melt rate which is too low, however, produces ingots with a coarse crystalline structure and poor surface quality.

Specific electrical conductivity is a function of both composition and temperature. At a given temperature, the electrical conductivity of an ionic melt is a function of both the ionic mobilities of the cations and their concentrations. Cation mobilities depend on the degree of bonding between the anions and cations present in solution and are related to the ionic dimensions as well as the melt viscosity. Pure molten $CaF_2$ can generally be considered to be a completely simple ionic melt in which the ions are completely free to move randomly. Electric charges are conducted through a melt of pure $CaF_2$ by the passage of $Ca^{2+}$ and $F^-$ ions. Dissolution of oxides in the melt would be expected to decrease the conductivity because although the $F^-$ ions and the $O^{2-}$ ions are of similar ionic radii, the double charge on the oxygen anion results in a stronger ability to bond with cations, thus making them less mobile. Oxides with partial polar bonding such as $Al_2O_3$ and $TiO_2$ are expected to decrease the conductivity more than oxides having purely ionic bonds such as CaO and MgO because the more polar oxides tend to form aggregates of complex ions such as $Al_3O_7^{5-}$, $AlO_3^{3-}$, $AlO_2F_2^{3-}$, and $AlOF_2^-$ which have low mobilities due to their large size.[8]

Mitchell and Cameron[16] showed that the addition of CaO lowers the conductivity of calcium fluoride with a slight change in the temperature dependence. They attribute this to the decrease in ion mobility, possibly because of the clustering of complex oxide ions. These researchers also found that a small amount of $Al_2O_3$ produced a large decrease in the conductivity of calcium fluoride. The isothermal kinematic viscosity remains nearly constant throughout the range of alumina contents from 0-5%, leading the authors to conclude that the decrease in conductivity is due to a chemical complexing effect. This is also evidenced by the unchanged temperature dependence. The contribution of the fluoride ion to the total ionic mobility is thought to be reduced by the reaction:

$$Al_2O_3 + 4F^- \rightarrow AlO_2F_2^{3-} + AlOF_2^-$$

As alumina content is increased, conductivity is decreased in a nonlinear fashion. The authors suggest that the charge transfer mechanism in these liquids is by movement of calcium ions through a complex oxyfluoride network. This network also accounts for the increase in viscosity observed after 10% alumina has been added to calcium fluoride.

The principle effect of addition of lime to solutions containing calcium fluoride and alumina may be to replace the fluoride part of the complex ions, thus releasing the fluoride ion as charge carriers:

$$AlO_2F_2^{3-} + O^{2-} \rightarrow AlO_3^{3-} + 2F^-$$

$$AlO_2F_2^- + O^{2-} \rightarrow AlO_2^- + 2F^-$$

Thus, relatively small amounts of lime produce substantial increases in the conductivity of calcium fluoride, alumina liquids. Based on this mechanism, it seems likely that charge in ESR slags is carried, not only by the calcium cation, but by the fluoride anion as well.

Literature reports of results of conductivity measurements in the ESR slag systems show some discrepancies which may be accounted for by crucible slag interaction or by the use of DC methods to estimate cell resistance. The work of Hara, Hashimoto, and Ogino[17] shows a regular variance in conductivity with composition:

$$\kappa = \exp\left[1.911 - 1.38N_x - 5.69N_x^2\right] + 0.0039\left[T - 1700\right]$$

where $\kappa$ is the conductivity of the slag, T is in degrees centigrade, and Nx is:

$$N_x = N_{Al_2O_3} + 0.75N_{SiO_2} + 0.5\left[N_{TiO_2} + N_{ZrO_2}\right] + 0.2\left[N_{CaO} + 2N_{CaS}\right]$$

This equation supports the theory that changes in conductivity due to the addition of alumina to calcium fluoride slags is due to the formation of complex ions which have low mobility and a tendency to form networks. These complex ions may have a tendency to cluster, leading to decreased mobility of fluoride ions as well as increased resistance to the migration of Ca+.[18] The presence of silica, which is also a network forming compound in slag, also decreases conductivity. The more ionic compounds, especially calcium oxide, were shown to have less effect on conductivity.

### 4.2.3.3 Viscosity

Viscosity is the property of a fluid that determines the resistance offered to a shearing force under laminar flow conditions. The coefficient of dynamic viscosity of a

fluid is defined as the tangential force on a unit area of either of two parallel planes at a unit distance apart when the space between them is filled with the fluid and one of the planes moves relative to the other with unit velocity in its own plane.

The viscosity of the molten slag in an ESR influences melting performance. Slag viscosity influences the kinetics of reactions at the slag metal interface. A low viscosity slag encourages a strong stirring motion resulting from electromagnetic or Lorenz forces which enables gas removal at the slag metal interface. Slag viscosity also influences the thickness of the slag skin. A low viscosity slag favors formation of a thin slag skin over the surface of the refined ingot.

The terminal velocity of the metal droplets (and hence their residence time in the slag) is also affected. According to Stokes' Law, the terminal velocity of a particle descending in molten slag under the influence of the acceleration due to gravity, g, is directly proportional to the square of the radius of the metal droplet, the density difference between the particle and the slag and inversely proportional to the viscosity;

$$V = \frac{2gr^2(\rho_{particle} - \rho_{slag})}{9\eta}$$

where V is the terminal velocity at which the particle is sinking or floating in the slag without the contribution of slag motion, g is the acceleration due to gravity, r is the radius of the molten metal droplet or inclusion, $\rho_{particle}$ is the density of the particle and $\rho_{slag}$ is the density of the molten slag and $\eta$ is the coefficient of dynamic viscosity. A high viscosity slag would increase the residence time of metal drops in the slag bath, providing greater time for chemical exchanges to occur between the metal and the slag. The viscosity also influences the flotation and capture of any undissolved inclusions.

The two parameters which affect the viscosity the most are slag composition and temperature. Considering viscosity as a function of temperature, Frenkel developed the following relationship:

$$\eta(T) = A\exp\left(\frac{B}{kT}\right)$$

where $\eta$ is the coefficient of dynamic viscosity, k is the Boltzmann constant, T is the absolute temperature and A and B are constants.[2]

In molten slag systems, the number and strength of chemical bonds influences viscosity. An increase in temperature reduces the number of bonds present, thus reducing viscosity. The bonding forces depend on the concentration of various species in the melt. As the simple ions combine, the viscosity changes because the size of the resulting complex ions is increased and their mobility is decreased. In general, the addition of oxide to $CaF_2$ melts increases viscosity. Slags which do not contain calcium fluoride are highly viscous due to the size and low mobility of aggregates of complex ions present. Addition of $F^-$ anions results in a breakdown and consequent reduction in the size of these complex structures and the viscosity of the slag is decreased. Eutectic compositions may be associated with lower viscosities due to the presence of a larger temperature range for fluidity.

### 4.2.3.4 Density

During melting, liquid metal droplets detach themselves from the electrode tip and fall through the slag. The terminal velocity of a spherical metal drop is related to the difference in density between the liquid metal and the slag by Stokes law. A small density difference results in a low terminal velocity for the metal drops and a greater residence time for chemical exchanges between the drop and the slag. However, a small density difference also results in the formation of large drops, which may not be as efficient for chemical exchange. The ideal situation, as far as driving chemical reactions is concerned, would be to have a slag with a large density difference from the metal (yielding small drops) and a high viscosity (yielding a low terminal velocity for the metal droplets). A large density difference between molten slag and molten metal also enhances the separation of the slag and metal, thus inhibiting the possibility of slag entrapment. [14]

A knowledge of the density of molten slag at elevated temperatures is important in that enables the calculation of the minimum mass of slag required knowing the minimum depth of slag, d, required. The density of a slag depends on both composition and temperature. The density of a slag at any temperature may be empirically calculated by assuming a linear law of addition:

$$\frac{1}{\rho_{(T^\circ C)}} = V = \frac{M_1}{\rho_{1(T^\circ C)}} + \frac{M_2}{\rho_{2(T^\circ C)}} + \frac{M_3}{\rho_{3(T^\circ C)}} + \ldots$$

Experimental data indicate that adding lime and alumina to calcium fluoride slag increases slag density. Alumina is more effective than lime in increasing slag density. The density of a slag composed of 70% $CaF_2$ and 30% CaO was measured to be 2.66 g/cm$^3$ at 1450°C while that of a slag composed of 70% $CaF_2$ and 30% $Al_2O_3$ was measured to be 2.88 g/cm$^3$.[14]

### 4.2.3.5 Surface Tension

The surface tension between a slag phase and a metal phase with which it is in contact determines the effectiveness of removal of impurities from the metal across the two liquid interface. The magnitude of the interfacial tension $\gamma_{ms}$ between the metal and the slag has a great effect on the mass transfer between the metal and the slag. The interfacial tension is related to the surface tension of the metal $\gamma_m$ and the surface tension of the slag $\gamma_s$. A low value of $\gamma_{ms}$ favors an increase in mass transfer across the boundary and also promotes emulsification of the two media by facilitating the formation of small droplets. While low surface tension results in large surface area between the metal and the slag and thus good refining capability, a low value of $\gamma_{ms}$, or a high work of adhesion, encourages entrapment of slag droplets in the liquid metal. The work of adhesion is expressed by the following relationship:

$$W_{ms} = \gamma_m + \gamma_s - \gamma_{ms}$$

The work of cohesion of the slag may be expressed as:

$$W_s = 2\gamma_s$$

The tendency for slag to become entrapped within the metal increases with the increase in the difference between $W_{ms}$ and $W_s$. The tendency for entrapment increases as the spreading coefficient, S, becomes more positive, where

$$S = W_{ms} - W_s.$$

Selection of a refining slag is a compromise between a good refining capacity favored by low $\gamma_{ms}$ and a minimum entrapment of slag particles favored by high $\gamma_{ms}$.

While some refining in ESR is done by ionic transfer between phases, the surface properties of the slag are important in the removal, either by dissolution or by physical separation, of non-metallic inclusions from the metal. The free surface energy conditions necessary for the complete removal of a thin lamina-shaped particle from the metal surface are as follows:

$$\gamma_{mi} > \gamma_{si} + \gamma_{ms}$$

where $\gamma_{mi}$ is the interfacial tension between the inclusion and the liquid metal and $\gamma_{si}$ is the interfacial tension between the inclusion and the liquid slag.[12]

## 4.2.3.6 Complications in Property Measurement

Slag properties reported in the literature vary greatly from study to study and large discrepancies are often present in published figures and graphs. These discrepancies may be caused by the reactivity of the molten slags with the materials used to contain them, compositional changes taking place during an experiment which result from the reactions between the fluorides and the oxides in the slag, limitations of the experimental and computational methods used, or measurements conducted in two phase regions.

Slags made up of $CaF_2$ with oxide additions react with most materials. This creates a puzzle for researchers looking for an inert material in which to contain a molten slag so that an experiment may be performed. The only materials which remain reasonably inert in the presence of these slags are Pt and its alloys, Mo, W, and Ir and even these materials may react with slags containing FeO. While graphite crucibles have been used, it has been

shown that $CaF_2$-$Al_2O_3$ melts form $CaC_2$, $Al_4C_3$, and carbon in the liquid.[12] Ogino, et al.[17], have shown that electrical conductivity appears to be lower when it is measured in graphite cells.

Molten $CaF_2$ will react with water and some metal oxides to form CaO and some gaseous fluorides, as shown in the following equations:

$$CaF_2 + H_2O \rightarrow CaO + 2HF_{(g)}$$
$$3CaF_2 + Al_2O_3 \rightarrow 3CaO + 2AlF_{3(g)}$$

Similar reactions occur with $SiO_2$ or $TiO_2$. The composition of a slag changes continuously as a result of these reactions, especially in an open furnace or crucible. The CaO formed by one of the above reactions may react with other components in the melt:

$$CaO + 6Al_2O_3 \rightarrow CaO \cdot 6Al_2O_3$$

The first two describe an increase in the activity of CaO, while the last describes a decrease in the activity of alumina.

In comparing the effect of composition or temperature on a particular property, it is important that measurements be taken of homogenous systems. Two phase regions such as miscibility gaps and regions in which both solids and liquids may be present will yield data which should not be compared with data taken in single phase regions. Because of the extensive region of immisibility in the calcium fluoride-lime-alumina system, it may be impossible to obtain accurate property measurements in this region.

## 4.3 Slag Selection

The physical and chemical properties of a slag influence the process efficiency and operation as well as the quality and suitability of the final product. Optimum properties of a slag include a heat of fusion low enough for easy melting, a low thermal conductivity to provide an insulating cap for the ingot, and a viscosity low enough to permit effective

stirring for gas removal at the slag/gas interface yet high enough for maximum droplet exposure for maximum possible refining. The slag should be chemically stable and have a low vapor pressure at the high temperatures obtained during the electroslag process. The flux should be stable at high temperatures and be compatible with the metal to be melted. The slag should also have sufficient resistivity to insure efficient melting without detriment to product quality.[1] The attainment of desired slag properties is achieved by the adjustment of slag chemistry.

The major components of ESR slags, calcium fluoride, lime, and alumina, have high temperature stability and low vapor pressure. The proportions of these major components determine the essential chemical and physical properties of the slag and thus directly influence not only the efficiency of the melting process but the soundness of the ingot produced. The role of calcium fluoride in the slag is to reduce the solidus and liquidus temperatures, increase the electrical conductivity, and decrease the viscosity and surface tension of the slag. The lime is added primarily as a desulphurizing agent which also reduces the electrical conductivity slightly. The function of alumina is to increase the electrical resistance of the slag but it can give rise to an increase in the oxygen content of the metal to be melted. Replacing part of the alumina by either lime or magnesia reduces this risk of oxygen pickup. Slags containing more than 15% magnesia, however, are difficult to operate due to increased slag viscosity.

### 4.3.1 Chemistry Adjustment for Process Efficiency

The proportions of calcium fluoride, lime, and alumina present in a slag determine its liquidus temperature and electrical resistance. For melting to take place, the slag must be completely liquid and at a temperature higher than that of the metal to be melted. Slags with liquids temperatures at, below or above the liquidus temperature of the metal may be used. If the liquidus temperature of the slag is at or below that of the metal, only sufficient energy to raise the temperature of the slag above the liquidus temperature of the metal is needed. This is the most energy efficient option. If the liquidus temperature of the slag is above the liquidus temperature of the metal, enough energy must be applied to melt the slag. Generally no advantage is gained by having the slag liquidus above the metal liquidus.[2] The temperature attained in the slag bath is essentially a function of the resistance of the slag and the current passing through it as well as the rate heat is extracted by conduction,

convection, radiation and latent heat of fusion of the metal. Slags with high alumina content have high electrical resistance and promote high melt rate and increased productivity.

### 4.3.2 Chemistry Adjustment for Product Quality

Although slags with high alumina contents promote high melt rate and increased productivity, they may adversely affect ingot yield. Ingot yield is compromised by slag entrapment, center looseness, piping, porosity, hydrogen cracking, and poor surface. If slag resistance is increased to much the melt rate will be high but the metal pool will deepen with solidification becoming more radial causing increasing center looseness, piping and poorer cleanliness. Slow melt rates also favor vertical solidification patterns which reduce the risk of non metallic material enriched metal freezing in the center of the ingot before the nonmetallic material has had time to enter the slag phase. Slow melt rates associated with slags containing only small or moderate amounts of alumina encourage maximum cleanliness. Inclusion removal is favored by slow melt rate due to the increased time available for slag metal reactions to take place. Lime is added to slags to promote sulfur removal however lime poor slags are less prone to cause hydrogen cracking than are lime rich slags. Slag chemistry should be optimized to strike a balance between high throughput and high product quality.

#### 4.3.2.1 Deoxidation Additions

Various slag deoxidation methods may be used to aid in the selective partitioning of elements between the metal and the slag in electroslag remelting and to minimize the activity of oxygen in the metal so that alloying elements are retained. The oxygen activity in the metal is directly related to the square root of the oxygen activity in the slag. Deoxidants may be added either during slag fusion or continuously during remelting. Aluminum is a suitable and inexpensive deoxidant, as are calcium, titanium, and the rare earths. These metals may also be added in order to retain necessary quantities of them in the metal. During ESR it is quite usual to experience oxidation loss of alloying elements, particularly the reactive elements such as aluminum, titanium, and silicon. The degree of reactivity of an element with oxygen may be predicted theoretically from the free energy of formation of its oxides. The predicted order of element reactivity in order of decreasing reactivity with oxygen in the ESR process is:

**La, Ca, Ce, U, Zr, Ba, Al, Mg, Ti, Si, B, V, Mn, Nb, Cr, Fe, W, Co, Sn, Pb, Zn, Ni, Cu.**

In any alloy containing more than one of the above elements, those to the left of the list will tend to be oxidized in preference to those towards the right. For example, in the electroslag refining of an alloy containing aluminum and titanium, so long as some aluminum is present after ESR, titanium losses will be negligible.

Using a slag of low oxygen potential is the best method of minimizing oxidative losses of alloying elements and promoting deoxidation of the metal or alloy. Low oxygen potential may be achieved in slags by minimizing the presence of those oxides which have a low negative free energy of formation such as the oxides of

**K, Pb, Cu, Na, Co, Ni, Sn, Zn, Mn, Fe, Cr, W, V, Nb, B, and Si**

with those at the beginning of the list being the most detrimental.

It is also necessary minimize the presence of oxides of elements which may exist in more than one oxidation state such as:

**Ti, V, Cr, Mn, Fe, Co, Ni, and Cu.**

The oxide of any element which exists in more than one oxidation or valence state such as the transition element oxides is capable of acting as a medium for oxygen transfer between the atmosphere and the metal. Considering iron oxides as the transfer media, then at the gas/slag interface the following reaction takes place:

$$2FeO_{(slag)} + \frac{1}{2}O_{2(atmosphere)} \leftrightarrow Fe_2O_{3(slag)}$$

and at the slag metal interface this leads to:

$$Fe_2O_{3(slag)} + Fe_{(metal)} \leftrightarrow 3FeO_{(slag)}$$

which leads to an increase in oxygen activity in the metal as follows:

$$FeO_{(slag)} \leftrightarrow Fe_{(metal)} + O_{(metal)}$$

Free oxygen in the metal can combine with essential alloying elements, thus reducing their useful levels and producing nonmetallic inclusions. When alloying elements combine with oxygen, they no longer fulfill their purpose of chemically or mechanically modifying the alloy, and because they exist as nonmetallic inclusions, are a detriment to its properties as they magnify stresses and initiate cracks.

## 4.4 ESR as a Decontamination Strategy

As a process for the safe, economical removal of radionuclides into a slag phase, ESR has many benefits. The slags in ESR tend to be hotter than in other melting processes, which may have a beneficial effect on reaction kinetics. In addition, metal/slag contact in ESR is very good in terms of promoting completion of reactions. There are no refractories in ESR to become contaminated, thereby forming another type of radioactive waste. A lack of refractories also means that there are no refractory interactions to compete with metal/slag interactions. Ease of slag removal is also a benefit of ESR. Because most of the slag simply solidifies on the top of the ingot when the melt is finished, it would be easy to package and store the radioactive slag robotically, to avoid human exposure. This would be much more difficult and expensive if a liquid slag were involved, as would be the case in other processes. Ease of fume capture in ESR would permit the effective capture of volatile isotopes such as $^{137}Cs$ and $^{85}Sr$. Nafsiger noted that the partitioning of elements between the metal and the slag is different under AC and DC conditions. By studying the effect of current type, current density, and voltage on various partition coefficients, the ESR process may be controlled so that the radioactive species are pushed into the slag.

# Chapter 4 References


[1] Nafziger, R.H., The Elecroslag Melting Process. Bulletin 669, U.S. Bureau of Mines, Washington, (1976).

[2] Hoyle, G., Electroslag Processes, Applied Science Publishers, London, (1983).

[3] Mitchell, A. "Theory and Practice of Electroslag Melting" *The Journal of Vacuum Science and Technlogy*, Volume 7, Number 6. (Nov.-Dec., 1970). 863-873.

[4] Lloyd, G.W., Owen, T.A., Baker, L.A. "Mechanism of Electroslag Refining" *Journal of the Australian Institute of Metals*; Volume 16, Number 1, (Feb. 1971), 17-25.

[5] Salt, D.J. Electroslag Refining, London, Chapman and Hall. (1969).

[6] Mitchell, A., Smailer, R.M. "Practical Aspects of Electroslag Remelting Technology" International Metals Reviews, Nos. 5 and 6, (1979), 231-264.

[7] Chatterjee, A.K., Zhmodin, G.I. "The Phase Equilibrium Diagram of the System CaO-Al2O3-CaF2" *Journal of Materials Science*, Vol. 7, (1972), 93-97.

[8] Turkdogan, E.T. Physicochemical Properties of Molten Slags and Glasses. The Metals Society, London. (1983), 460-473.

[9] Mitchell, A. "The Chemistry of ESR Slags" *Canadian Metallurgical Quarterly*, Vol. 20, No. 1, (1981),101-112.

[10] Mitchell, A., Etienne, M. "The Solidification of Electroslag Fluxes" *Transactions of The Metallurgical Society of AIME*, Vol. 242, (July, 1968), 1462-1464.

[11] Bell, M., Mitchell, A., "Some Observations on the Surface Quality of Electroslag Ingots" *Journal of the Iron and Steel Institute*, Vol. 209, Part 8, (Aug., 1971), 658-670.

[12] Mills, K.C., Keene, B.J. "Physicochemical Properties of Molten $CaF_2$ based slags" *International Metals Reviews*, No. 1, (1981), 21-69.

[13] Schwerdtfeger, K, "Some aspects on the kinetics of reactions occurring in the ESR process", Proceedings of the 5th International Conference of Vacuum Metallurgy and ESR, Munich Germany (Oct., 1976), 1393-1399.

[14] Duckworth, W.E. and Hoyle, G. Electro-slag Refining, Chapman and Hall Ltd. London, (1969).

[15] Mills, K. C., "The physicochemical properties of slags', NPL Report Chem. 65, National Physical Laboratory, London, HM Stationery Office (Feb. 1977).

[16]Mitchell, A., Cameron, J. "The Electrical Conductivity of Some Liquids in the System CaF2 + CaO + Al2O3" *Metallurgical Transactions*, Vol. 2, (December, 1971), 3361-3366.

[17] Hara, S., Hashimoto, H., Ogino, K. "Electrical Conductivity of Molten Slags for Electroslag Remelting" *Transactions ISIJ*, Vol. 23, (1983), 1053-1058.

[18] Chiho, W., Shunhua, X. "Electrical Conductivity of Molten Slags of CaF2+Al2O3 and CaF2+Al2O3+CaO Systems for ESR" *ISIJ International*, Vol., 33 (1993), 239-244.

# Chapter 5
# Experimental Rationale and Procedures

The goal of the melting experiments performed in this research was to determine the effect of slag composition on the removal of surface contamination from stainless steel. The experimental procedures described in this chapter include the application of surrogates by plasma spray to the surface of stainless steel ingots and the subsequent electroslag remelting of the sprayed ingots. Slags of different chemistries were blended and prefused specifically for this research. After melting was complete, samples of the remelted metal ingots and the slags were prepared and submitted for chemical analysis. Details of the experimental procedures used are presented in the first part of this chapter.

In order to insure that the results of this study could be used in the design of a melt decontamination facility, a great deal of thought was given to the choices of experimental feedstock and variables. Suitable non-radioactive surrogates were chosen, on the basis of physical and chemical similarity, to represent radioactive contaminants. The choice of surrogate elements was one of the most important aspects of this research because of the expectation that, in a melt refining environment, these elements behave in a similar manner to the radioactive species which they represent. Of equal importance was the decision to apply the surrogates to the feedstock in a manner mimicking the presence of a layer of oxidized surface contamination. The slags used in the melting studies were chosen to represent a range of physical and thermochemical properties postulated to have an effect on the capture of radionuclides. The choices which were made in this research and the various rationale which were considered are presented in the latter part of this chapter.

## 5.1 Experimental Procedures

In this section, the preparation of melting feedstock, the application of surrogate elements, the blending and prefusion of slags, and the actual electroslag remelting of the coated ingots are described.

### 5.1.1 Preparation of Master Melt Heats E1, E2, and E3

Three approximately 2,000 pound induction melts utilizing austenitic steel scrap metal from the INEL were completed at ESCO, a commercial stainless steel casting company in Portland, Oregon, in order to produce small diameter billets that were subsequently used for remelt studies. The first melt (E1) of approximately 1,800 pounds was melted August 1993 and cast into forty 2.5" diameter billets; twenty billets were two feet long and twenty were approximately one foot long. Extra feed stock was added to the second and third melts which each resulted in twenty billets two feet long and twenty billets one and one-half to two feet long. This resulted in the production one hundred and twenty billets for subsequent remelting studies.

#### 5.1.1.1 Chemistry of Starting Material

Table 5.1 (located at the end of this chapter) shows the chemistries of each of the heats produced. Values for nickel and molybdenum varied the most, with the weight percent of nickel being slightly higher in the E1 melt than is called out in the standard for 304L stainless steel . The percentage of carbon in heat E2 was found to exceed the ASTM maximum standard for 304L. In general, the percentages of molybdenum were also shown to be higher than is usual in 304L. The conclusion was therefore reached that the steel received from the INEL must have been mixed with another alloy. Analysis of unmelted material showed that the tubing received contained Nitronic 50 as well as 304L.

Samples of each heat were analyzed for the presence of rare earth elements by Instrumental Neutron Activation analysis at Oregon State University. Table 5.2 shows the results of these analysis.

**Table 5.2**
**Rare Earth Chemistry Analysis of OGI Master Melt Base Metal.**
Analysis performed by Instrumentational Neutron Activation Analysis (INAA)

| Sample | Cs (ppm) | La (ppm) | Ce (ppm) | Nd (ppm) |
|---|---|---|---|---|
| E1 Master Melt | <5.1/<5.4 * | 0.11/0.12 * | <81/<78 * | <100/<140 * |
| E2 Master Melt | <4.5 | 0.13 | <75 | <100 |
| E3 Master Melt | <6.6/<5.1 * | 0.14/0.2 * | <75/<78 * | <100/<130 * |

* Duplicate Analysis

The starting material for the melting study was comprised of bars from heats E2 and E3. Unfortunately, the bars were not identified before plasma spraying and so the identity of individual bars was lost.

## 5.1.2 Application of Surrogates

At Oregon Graduate Institute, simulated radioactive scrap metal was manufactured by applying oxides of chosen surrogate elements to the surfaces of stainless steel bars by means of plasma spray. In a related study, performed at the Montana College of Mineral Science and Technology, surrogate elements were incorporated into stainless steel by means of plasma melting.

### 5.1.2.1 External Application by Plasma Spray

Stable oxides of the three chosen surrogates, lanthanum, cerium, and neodymium, were applied to the surfaces of stainless steel bars by means of plasma spray. Plasma spraying was performed at Oregon Graduate Institute and sprayed bars were shipped to Sandia National Laboratories for remelting. Different amounts and mixtures of surrogates were used to test the effects of radionuclide concentration and the presence of multiple radioactive elements.

Plasma-sprayed coatings are formed by the accumulation of molten and semi-molten particles on a substrate surface. In plasma-spraying, particulate feedstocks are injected into a hot gas plasma where they are heated and accelerated towards the substrate. Bonding to the substrate, and to other impacted particles, is a function of both temperature and velocity of the particle. Plasma temperatures are sufficient to melt all materials and consequently plasma-spray systems are used routinely to deposit oxide based coatings. The velocity of

the particles results from acceleration in the hot plasma gas jet. Plasma flame velocities are normally above sonic velocities, yielding near-sonic or sonic particle velocities with particles of 50 micron diameter or less.

The plasma spray facility of the Materials Science and Engineering Department of the Oregon Graduate Institute consists of a Plazjet II 200KW plasma spray system with an associated three channel mass flow control, a powder feeder, wire feeder, and various fixtures for holding and manipulating samples. This is housed in a 300 square foot acoustic room fitted with a six foot water curtain. The Plazjet II plasma-spray system uses a gun which is quite different in design from the traditional plasma-spray gun. The Plazjet works at high voltages, 300-450V, and low currents, 200-500A, yielding up to 225 kilowatts of power. Most plasma-spraying systems, i.e. 'conventional' systems, operate at nominally 40-60 volts and up to 1800 amps, yielding power levels of 40 to 100 KW. Most research on plasma gun dynamics and behavior has been performed using a "conventional" gun designed to operate at the lower voltages and high currents. The high working voltage of the Plazjet gun design increases the electric arc length within the body of the gun. This allows greater heating of the plasma forming gases. The long dwell time of the gas within the arc, coupled with high gas flow rates, generates hot plasma gas exit velocities which greatly exceed sonic velocities. Shock waves can be observed in the plasma plume. The power conversion efficiency of this gun is also quite high, having been measured at over 75%. In practical terms, this means that there is more thermal energy available at the gun exit than in a conventional gun, which in turn means that greater quantities of material can be melted and sprayed. The high gas exit velocities and the high gas mass flow rates mean that melted materials can also be accelerated to higher velocities. Thus this gun design can increase both the thermal energy and the kinetic energy of sprayed materials. The high power level also means that multiple feed-stocks of powder, wire, or both, can be utilized efficiently.[1] One of the greatest advantages of this system lies in this versatility.

In order to insure production of a tenacious, non-friable, coating surrogate oxide powders were co-sprayed along with a stainless steel wire addition. Different ratios of powder to metal change the capture efficiency because the metal droplets capture the rare earth oxides in flight. In order to change the deposited amount, either the rate of spray or the duration of spray may be increased in order to increase the coating thickness. The weight of surrogates to be applied was calculated on an as metal basis and corrected for the correct weight of the oxide to spray. Despite attempts to calibrate the plasma spray process, uncertainty resulted from the agglomeration of powders which led to uneven coating thicknesses.

A test matrix, presented in Table 5.3, was designed for the purposes of studying changes in melt refining which would be induced by changes in radionuclide concentration and the types of radionuclide present in scrap metal feedstock. In addition, a set of 13 bars with identical coatings were requested for use in slag chemistry studies.

**Table 5.3**
**Planned Feedstock Matrix**

| Coating on Bar | Approximate Amount (metal basis) | Waste Simulated | Purpose of Test Set |
|---|---|---|---|
| $CeO_2$ | 1000 ppm | 0.1 wt. % Pu or U | Study the effect of concentration and slag loading |
| | 5000 ppm | 0.5 wt. % Pu or U | |
| | 10000 ppm | 1 wt. % Pu or U | |
| $CeO_2$ | 5000 ppm | One radionuclide | Study of multiple element effects |
| $CeO_2 + La_2O_3$ | 2500 ppm each | Two radionuclides | |
| $CeO_2 + La_2O_3 + Nd_2O_3$ | 1333 ppm each | Multiple elements | |
| $CeO_2 + La_2O_3$ (13 identical bars) | 2500 ppm each | U and Pu present | Study the effects of slag chemistry |

## 5.1.2.2 Incorporation of Surrogates by Plasma Melting

In a closely related study, researchers at Montana Tech in Butte, Montana incorporated surrogate elements into the bulk of a stainless steel ingot by plasma cold hearth melting. Surrogate elements were sealed into stainless steel envelopes in a vacuum chamber. These envelopes were then welded down the length of a pipe which was nested within a larger diameter pipe before plasma melting. The resultant ingot was sliced into bars, one of which was shipped to Sandia National Laboratories for remelting by ESR. Table 5.4 (at the end of the chapter) shows the chemistry of one sample of the Montana Tech master ingot. The surrogate concentration of this ingot was analyzed by two methods, ICP Mass Spec and Instrumental Neutron Activation Analysis (INAA). The table shows that the surrogate level in the ingot was reported to be higher when the ICP Mass Spec was used than when INAA was used.

### 5.1.3 Slag Manufacture

This research was centered about the effect of slag chemistry on the efficiency of melt decontamination by electroslag remelting. In order that this might be accomplished, slags of various chemistries were blended, prefused, and size reduced at Sandia National Laboratory.

#### 5.1.3.1 Slag Chemistry Test Matrix

The slags investigated in this work were made up of ternary mixtures of calcium fluoride, calcium oxide, and alumina. A matrix of chemistries, shown graphically in Figure 5.1, was developed around a central point. The slag represented by this center point, 50/25/25, was used in melts in which slag chemistry was not varied, namely, the melts to determine the effects of surrogate concentration and the melts to determine the effects of surrogate mixtures. Each of the other melts was conducted using a slag whose chemistry corresponded to a point on the ternary matrix. The chemistry of the slag used for each of the melts performed in this research are listed in Table 5.5.

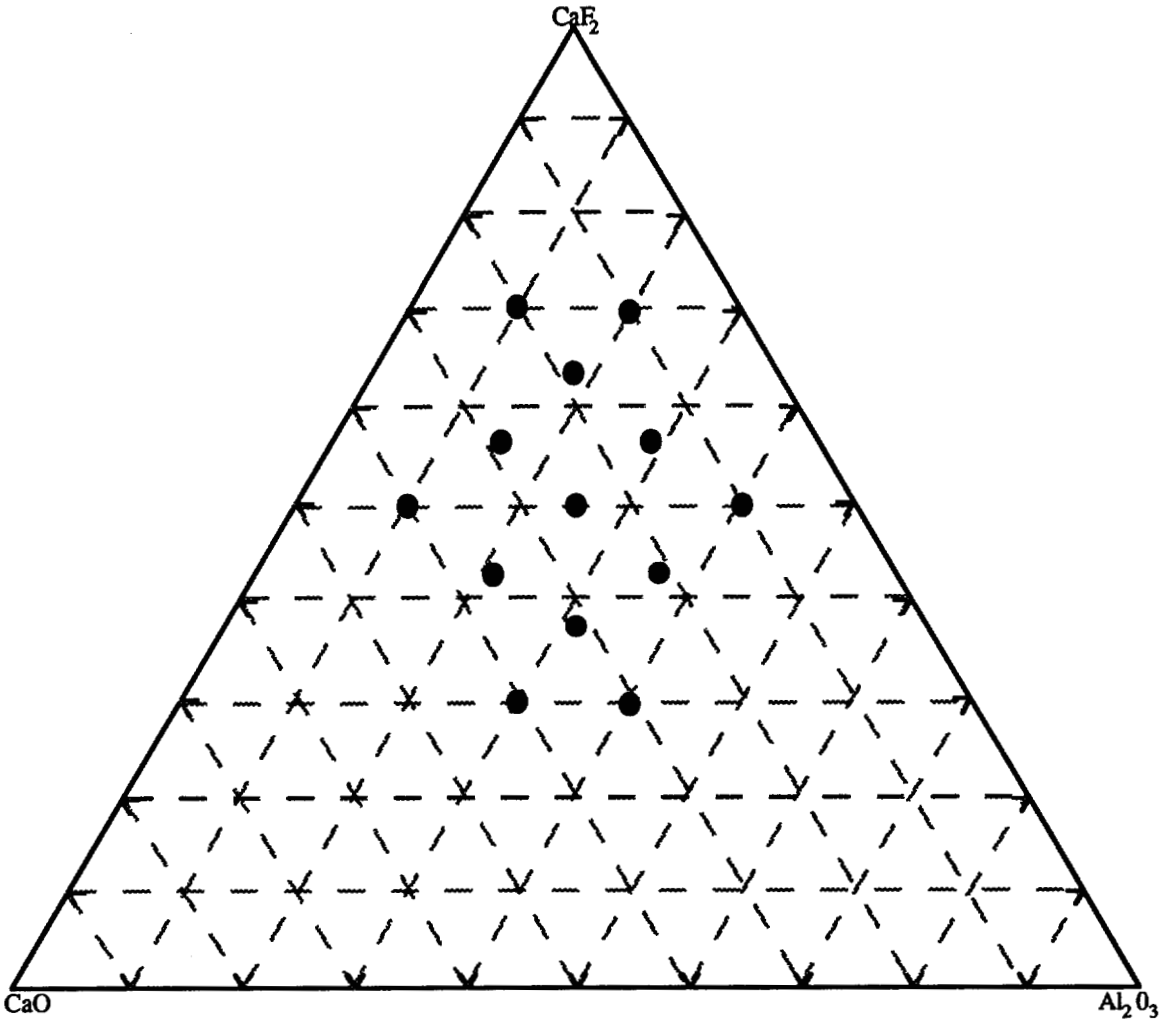


**Figure 5.1**
**Slag Chemistries Plotted on Ternary Grid**

**Table 5.5**
**Chemistry of Slag Used for Each Heat**

| Concentration of Surrogates (Requested) | Slag Used $CaF_2/CaO/Al_2O_3$ | Heat Number |
|---|---|---|
| Ce low level (1000 ppm) | 50/25/25 | 89 |
| Ce mid level (5000 ppm) | 50/25/25 | 93 |
| Ce high level (10,000 ppm) | 50/25/25 | 90 |
| Ce, La 2500 ppm each | 50/25/25 | 74 |
| Ce, La 2500 ppm each | 50/40/10 | 75 |
| Ce, La 2500 ppm each | 36.6/31.7/31.7 | 76 |
| Ce, La 2500 ppm each | 56.7/15/28.3 | 77 |
| Ce, La 2500 ppm each | 30/30/40 | 78 |
| Ce, La 2500 ppm each | 63.4/18.3/18.3 | 79 |
| Ce, La 2500 ppm each | 50/10/40 | 80 |
| Ce, La 2500 ppm each | 50/25/25 | 81 |
| Ce, La 2500 ppm each | 70/20/10 | 82 |
| Ce, La 2500 ppm each | 43.3/35/21.7 | 83 |
| Ce, La 2500 ppm each | 43.3/21.7/35 | 84 |
| Ce, La 2500 ppm each | 30/40/30 | 85 |
| Ce, La 2500 ppm each | 56.7/28.3/15 | 86 |
| Ce, La 2500 ppm each | 70/10/20 | 91 |
| Ce, La 2500 ppm each | 50/25/25 | 88 |
| Ce, La, Nd 1666 ppm each | 50/25/25 | 92 |
| Ingot from Montana Tech | 50/25/25 | 94 |

### 5.1.3.2 Slag Preparation

Slags of various chemistries needed for this research were blended using an industrial 70/15/15 slag as a base. Prefusion was performed in order to prevent hydration of the calcium oxide and to produce slags as much like those used in industry as possible. Prefused slags were crushed so that they could be fed into the annulus between the electrode and the crucible during remelting.

### 5.1.3.2.1 Slag Blending

A cost estimate revealed that it would be quite expensive to purchase the raw materials necessary for the production of all the slag necessary for this research, as four pounds of slag were needed for each melt. The slags were therefore made by adding

known quantities of components to a given weight of 70/15/15 industrial slag. An additional benefit of this method was the efficiency of the prefusion operation. Because the industrial slag lies along the low melting point trough of the phase diagram, it was melted first and superheated before the other components were added. Table 5.6, located at the end of this chapter, lists the weights of the individual components of each slag that were blended for this research. Analysis of the 70/15/15 slag (lot number 8-2193) which was used as a base for the other slag chemistries tested was provided by the manufacturer, American Flux and Metal, and is presented in Table 5.7. A sample of the 70/15/15 slag was analyzed by ICP Mass Spec for the presence of Ce, La, and Nd so that slag enrichment could be properly calculated. The slag was found to contain 490 ppm Ce, 240 ppm La, and 240 ppm Nd. The rare earth elements are found in the minerals which make up the slag components. Chemical analysis of the 70/15/15 base slag allowed the starting chemistry of each slag used to be calculated by mass balance, as presented in Table 5.8.

#### 5.1.3.2.2 Slag Prefusion

In order to insure that the industrial slag and the added components were well mixed and that the CaO did not hydrate in unpredictable ways, the slag was prefused. Prefusion was performed in four pound batches in an air induction furnace. Prior to melting each batch of slag, a graphite crucible was placed in the refractory lined induction chamber of the furnace. The power supply of the furnace was set to approximately 15 KW until the graphite crucible began to heat up, at which point a specified amount of low melting industrial slag was added. Upon melting and superheating the eutectic slag, measured amounts of high melting point oxides were added to bring the slag composition to the required point on the ternary phase diagram. The power was adjusted between 20 and 40 KW until all oxides had melted in and induced stirring had homogenized the mixture. Power adjustments were necessary in order to insure completion of melting without the mixture becoming greatly overheated. At this time, power was turned off and the mixture was allowed to solidify. This procedure was followed for 18 slag melts of four pounds each.

### 5.1.4 Electroslag Remelting Experiments

Before melting tests could be accomplished, the Sandia's ESR unit was modified to accommodate a small water jacket necessary for performing the pilot scale melts planned for this research. In addition, modifications were made to the copper mold and water jacket manufactured by Oregon Graduate Institute. Several preliminary melts were performed in order to test the equipment and choose a control strategy. After these preliminary steps, melting experiments were initiated.

#### 5.1.4.1 Equipment Preparation

Before melting experiments could be performed, several pieces of equipment had to be modified. The ESR furnace at Sandia National Laboratories was made to accommodate the small copper mold and water jacket necessary for melting 2.5" diameter ingots. Cooling water lines were rerouted and a fume collection system was put in place. Two steel shafts were machined for use as electrode extensions. In order to make the saturable core reactor power supply controllable at the low power outputs needed, an SCR firing board was installed.

The copper mold and water jacket assembly mold received from Oregon Graduate Institute was disassembled. Diagrams of the water jacket and copper mold are presented in Appendix II. The outside of the copper mold showed evidence of boiling water and scorching, which led to a decision to modify the water jacket and to install thermocouples in the copper mold. The copper mold was accurately measured so that wall thickness could be determined, slots were machined in the outer wall, and Type K thermocouples were inserted in a spiral pattern along the length of the mold. Thermocouples were held in place and protected from the cooling water by covering the slots with a water resistant sealant. A wire feed plug was inserted into the top of the copper mold and the thermocouple leads were fed through it. The annulus of the inside water jacket was reduced to 0.5" from 0.62". Set screws were installed in order to keep the copper mold centered within the water jacket at all times, and a baffle was added next to the water inlet which insured that cold incoming water was directed upward to draw heat away from the copper mold.

Many of the plasma sprayed bars received from OGI arrived in one foot sections which were welded together in order to make two foot long electrodes which could be

electroslag remelted in order to yield an ingot approximately 13-14 inches high. The ingot slice from Montana Tech was approximately triangular in cross section (2 inches across at its widest point) and 23.5 inches long. A 2.5 inch diameter by 1 foot long bar of 1018 steel was welded onto one end of the ingot slice prior to remelting so that steady state conditions could be reached prior to the introduction of surrogates into the slag.

### 5.1.4.2 Melting Experiments

Before each melting experiment, the coated electrode to be melted was welded onto the extension stub which remained attached to a load cell at the top of the furnace. A jig was devised to hold the electrode concentrically in the mold while welding was taking place so that concentricity could be assured during melting. The mold was raised and a starter plate was installed between the bottom of the mold and the water cooled base plate. Small pieces of scrap steel were placed under the electrode in order to direct and concentrate the arc at the onset of melting. Approximately 150 grams of slag was fed in around the electrode before the start of the melt. After performing safety checks, melting was initiated.

In order to decrease the probability of systematic error, the melting experiments were performed in random order. At the beginning of each melt, the electrode was lowered until an arc was struck between the electrode and the steel scraps. At this point slag was added slowly and the electrode was lowered manually until some of the slag was melted. Melting control was handed over to a computer which monitored and controlled current. Slag addition continued until all the slag had been added. When the slag had melted, a control strategy was implemented to keep melt rate constant at 0.4 kg/min. This control strategy was chosen in order to keep the amount of molten steel in contact with the molten slag constant throughout the melt. Because the resistivity of each slag was different, the voltages, currents, and power requirements were different for each slag used. Values of current, voltage, power, and impedance were recorded. During the course of each melt, thermocouple data was observed and recorded. Temperatures exceeding 200°C at the outside of the copper mold were deemed to be dangerous and cause for discontinuation of a melt. When each melt had been completed and allowed to cool, the mold was raised, slag was collected and the ingot was removed and marked with a steel stamp. The surface quality of each ingot was observed.

### 5.1.5 Sampling and Chemical Analysis

At the completion of each melt, the slag skin and the slag cap were collected separately and weighed. Skin thicknesses were measured and the slag was examined for the presence of interesting structures. These slag samples were crushed and ground so that accurate sampling could be performed. Representative samples were split from each larger sample and sent to Teledyne Wah Chang, Albany, for trace element analysis by Inductively Coupled Plasma Mass Spectrometry (ICP-MS).

For each ingot produced, a slice was cut two thirds of the way from the bottom of the ingot, at a location where steady state melting had been achieved and electrode heating had not yet begun. Each slice was drilled from the outer radius in. Drill turnings from the first quarter inch of drill travel were collected for surface chemistry. Drill turnings for the subsequent one half inch of travel were collected for bulk chemistry. Selected samples were sent to Teledyne Wah Chang, Albany for analysis of La, Ce, and Nd. One quarter of the ingot slice was sent to ESCO for spectrographic analysis of the major elements.

## 5.2 Experimental Rationale

Throughout this study, much consideration was given to the choices of experimental feedstock and variables, with the goal of mimicking, as closely as possible, the melt decontamination of actual radioactive metal components. The selection and application of surrogate elements were important considerations. Surrogates were plasma sprayed as oxides onto stainless steel bars prior to remelting in order to simulate the presence of tenacious oxidized crud prevalent on inside surfaces of reactor tubing components. The selection of slag chemistries and manufacturing techniques was also important.

### 5.2.1 Surrogate Selection

This pilot scale research was aimed at the optimization of the removal of radioactive elements from stainless steel by remelting. Due to complications involved with work involving radioactive materials, surrogates were chosen which mimic, as accurately as possible, the chemical and thermodynamic behavior of the radionuclides of interest. The

choice of surrogate elements is a function of a variety of considerations, including the chemical, physical, and thermochemical properties of the surrogate elements (and those of phases formed by reaction with other elements), availability, ease of handling, and ease of detection. Of these considerations, those related to the physical and thermochemical properties are the most important, and thus were used as criteria to choose surrogates for the present work. Of equal importance was the selection of a method of incorporating the surrogate elements into the metal to be melted. Because much of the radioactive scrap metal, especially that in nuclear power reactors, is surface contaminated and because this research is aimed directly at the melt decontamination of such material, the presence of oxidized radionuclides present in a layer of surface contamination was simulated by mixtures of surrogate oxides applied by plasma spray to the surfaces of stainless steel ingots prior to remelting.

### 5.2.1.1 Radionuclides and their Surrogates

The choice of surrogates for this work was based on various comparisons between radionuclides which have been identified as being of concern to the nuclear community and non-radioactive elements which are similar to these radionuclides. The chemistry and physical properties of important radionuclides and possible surrogate elements was compared. Additional comparisons were made between stable compounds radionuclides would be expected to form in the electroslag environment and those compounds which would be formed by surrogates. On the basis of these comparisons, the surrogates for this work were chosen.

#### 5.2.1.1.1 Radionuclides of Interest

In a study sponsored by the Mixed Waste Integrated Project of the DOE, Stockdale, et al.[2] examined reported experience with radioactive surrogates and suggested a simplified list of materials for use in tests of thermal treatment systems. The chief radionuclides of concern in the treatment of mixed waste were identified as $^{239}Pu$, $^{238}U$, $^{235}U$, $^{137}Cs$, $^{103}Ru$, $^{99}Tc$, and $^{90}Sr$. The radionuclides of interest in this work are fission products which include rare earth elements, cesium, strontium and actinide elements, primarily uranium, thorium, plutonium, and americium. These nuclides are largely by products of uranium beneficiation, enrichment, reactor fuel reprocessing, and weapons program activities.

### 5.2.1.1.2 Radionuclide Chemistry

Many of the elements of importance in nuclear operations are found within the sixth and seventh periods of the periodic system. The sixth period consists of the rare earth fission products from lanthanum to dysprosium, known as the lanthanide series. Most rare earth elements are found naturally in minerals and soils. The only rare earth element which does not occur naturally is promethium, which is formed by the irradiation of neodymium. These elements are so similar that they are difficult to separate from each other by chemical means. Their close similarity in chemical properties is related to their electronic structure, as the chemical behavior of elements is determined by the behavior of electrons in the outermost shells. For example, the chemical properties of cesium and barium are different because of the different numbers of electrons in their outer shells: while the 6s shell is filled for barium, for lanthanum the next electron is added to the previously empty 5d shell. Electrons for most of the elements with higher atomic numbers through lutetium are added to the 4f shell, which is so deep within the atoms as to have little influence on the chemical properties of these elements. The 4f shell is filled for lutetium and succeeding elements, hafnium, tantalum, tungsten, add electrons to the 5d shell. The 5d electrons are not strongly bound, so that each member of the sixth period transition series, hafnium through tungsten is quite distinct from its neighbors.

The seventh period of the periodic table is occupied by a similar series called the actinide series. After the alkaline earth radium, additional electrons are added to the 6d and 5f shells, beginning the actinide series. At the beginning of the actinide series electrons are added to the 6d shell rather than to the 5f shell, so actinium and thorium behave chemically as homologues of lanthanum and hafnium, respectively. Beginning with actinium, the 5f electron shell is populated in a manner analogous to filling the 4f electron shell in the lanthanide series. This type of analysis provides a basis for the selection of nonradioactive surrogates for studies which preclude the use of radioactive materials. Other considerations come into play in surrogate selection, but elements of similar electronic structure are often similar chemically and thermodynamically as well. For gaseous elements the 5f shell is preferred beginning with protactinium, while for metallic crystals at room temperature the 6d shell is preferred as far as uranium . The chemical properties of the actinides are much less similar to each other than those of the lanthanides because the additional electrons added to the 5f and 6d are bound less tightly than those of the 4f and 5d shells of the lanthanides. Tables 5.9 and 5.10 show the configuration of the elements in the sixth and seventh periods and their oxidation states:[3]

Uranium compounds have been prepared with positive valence states of 3,4,5, and 6. Uranium dioxide, $UO_2$, has a melting point of 2760°C, is a stable ceramic and the form in which uranium is most commonly used as a reactor fuel for light water, heavy water, and fast breeder reactors. It does not react with water so that it is not chemically affected by leakage of cladding in water cooled reactors, although fracture of fuel pellets may result in uranium being carried throughout the cooling loop, where it may adhere to piping as one component of radioactive crud. Uranium trioxide, $UO_3$, is made by igniting uranyl nitrate $UO_2(NO_3)_2 \bullet 6H_2O$ or $UO_4 \bullet 2H_2O$, the two principal forms in which uranium purified in aqueous solution is prepared. $U_3O_8$, which occurs naturally as the mineral pitchblende, can also be made by oxidizing $UO_3$ . $UF_4$ is an important intermediate in the production of $UF_6$ and uranium metal. It is made by reacting $UO_2$ with an excess of HF vapor. $UF_6$, the only compound of uranium volatile at room temperature, is used as working fluid in the gaseous diffusion, gas centrifuge, and aerodynamic processes for uranium enrichment.[4]

Although plutonium chemistry has been the subject of many investigations since the 1940s, many aspects of plutonium chemistry are not well defined, one of these being its high temperature chemistry. This is due in part to the complex electronic configuration of the plutonium atom which has a higher binding energy at the 6d level than the 5f level. While thorium, for example, achieves a +4 oxidation state through the loss of the two 7s and two 6d electrons, in plutonium the +4 oxidation state results from the loss of two 7s and two 5f electrons. The energies of the 5f, 6d, 6p, and 7s orbitals have almost comparable binding energies in plutonium and since these orbitals overlap spatially, bonding can involve any or all of these orbitals and the electronic structure of plutonium, in a given oxidation state, may vary between its compounds. Plutonium forms ionic, covalent, or metallic bonds with other elements. The radius of plutonium varies with each type of bond and the oxidation state may be determined by the radius of the element plutonium is bonding with.[5] Important isotopes are $^{236}Pu$ through $^{244}Pu$, which are produced in nuclear reactors. In reactors fueled with uranium and plutonium, $^{239}Pu$ is the principal isotopic component but $^{238}Pu$ contributes the greatest amount of alpha activity. All plutonium isotopes are alpha emitters except $^{241}Pu$ and $^{243}Pu$, which are beta emitters. Plutonium forms the oxides $Pu_2O_3$, $PuO_2$, $PuO_{1.52}$, $PuO_{1.61}$, and PuO. $PuO_2$ is the form of plutonium commonly used in power reactors and like $UO_2$, it has a high melting point: 2400°C. In most plutonium fueled reactors, the fuel is a mixture of uranium and plutonium oxides. The mixed uranium plutonium oxides form a continuous solid solution from $UO_2$ to $PuO_2$, with the fcc fluorite structure. $PuF_3$ and $PuF_4$ are important intermediates in the production of plutonium metal.[5]

### 5.2.1.1.3 Rare Earth Elements as Surrogates

Surrogates should mimic as closely as possible the physical and chemical properties of the radionuclides. Surrogates should be of minimum toxicity, inexpensive, and easily handled and fed to the system. Unlike cesium, strontium, ruthenium, and iodine for which stable, nonradioactive isotopes of the same elements may be used as surrogates, other elements have unique chemical and physical properties, so for complete accuracy there may be no substitutions. The situation is further complicated by the degree of complexity which may be encountered under actual treatment conditions where many substances are present and reaction conditions may vary from point to point. A substance which is an excellent surrogate at one temperature may not mimic the properties of the radionuclide at another. For use as surrogates in high temperature incineration, Stockdale and coworkers recommend ruthenium for technetium and cerium for plutonium and uranium. [2] The choice of Ce as a surrogate for actinide elements is a common one; the suitability of Ce as a plutonium surrogate has recently been discussed by Raraz, Mishra and Averil[6]. In aqueous chemistry rare earth elements have been used as simulates for plutonium and other actinide elements. In these carefully controlled aqueous environments the simulates have worked well. In the high temperature environments created by melting, the chemical environment is not predictable. McAtee and Beal[7] performed a comprehensive review of the high temperature chemistry and thermodynamic properties of plutonium and the rare earth elements. The results of their evaluation show the feasibility of using rare earth elements as plutonium surrogates. A comparison was made of thermal, thermodynamic, and chemical properties of the rare earth elements and the similarity of the rare earths to plutonium was reported as follows:

**neodymium>lanthanum>praseodymium>gadolinium>ytterbium>**
**dysprosium>erbium>europium>terbium>lutetium>samarium.**

### 5.2.1.1.4 Surrogates Used in Present Research

The surrogate elements used in this research were chosen to imitate the chemistry of specific fission products and actinides. Some radioactive elements may be easily replaced without changing the chemical reactivities which influence the interaction of species during melting. These elements are those that have naturally occurring, non radioactive isotopic mixtures, including cesium, strontium, and the rare earth elements (except promethium).

Cesium and strontium are both elements with high vapor pressures which would be removed by any melting treatment done for the purposes of scrap consolidation, especially if the melt was performed in a vacuum. This was demonstrated by Worcester and his coworkers who sought to incorporate the elements Ce, La, Nd, Cs, and Sr into stainless steel by sealing the envelopes in steel packets welded within a pipe. The pipe was plasma melted in a controlled atmosphere and the resulting melt was analyzed. While the steel was found to contain significant amounts of the rare earth elements, the cesium and strontium were not found and were presumed to have vaporized.[8] Rare earth elements are the most abundant fission products. The choices of Ce, La, and Nd as substitutes for all rare earths were reasonable because in general the reactivities and thermochemical properties of the rare earths are quite similar to one another.

The elements with atomic numbers greater than 83 have no non-radioactive isotopes, therefore surrogate elements must be used if these are to be studied in a non-radioactive environment. The rare earth elements cerium, lanthanum, and neodymium were used as surrogates for uranium, plutonium, and the other actinide elements. Cerium was chosen to imitate the chemistry of uranium and plutonium; neodymium was chosen to imitate the chemistry of americium and curium and because it is itself present as a fission product in spent fuel; La was chosen to demonstrate the general behavior of the rare earths.[9]

### 5.2.1.2 Comparison of Surrogates and Radionuclides

The suitability of the surrogates chosen may be demonstrated by a comparison of the properties of the elements themselves as well as the stable compounds they are likely to form in a melt refining environment. Elemental properties of importance are to a great degree governed by electronic structure: the possible oxidation states and the electronegativity, which determine the stable compounds which form. Important properties of compounds include thermochemical stability, melting point, and density. It is likely that the conclusions drawn from individual comparisons would be that different elements are appropriate for mimicking different aspects of the behavior of a given element .[9]

#### 5.2.1.2.1 Elemental Properties

The suitability of a surrogate may be determined by a comparison of a physical or chemical property of the radionuclide of interest with that of the surrogate. The electronic

structure governs the physical and chemical properties of an element as well as the types of bonding it may engage in with the other elements.

The prevalent oxidation state of an element determines the types of compounds that the element may form. The lanthanides all form trivalent ions in solution. In certain high energy environments cerium, praseodymium and terbium also exhibit quadravalent oxidation states and for samarium and europium, bivalent states may be obtained. The multiple valence levels stem from the tendency of the element to try to reach a stable 4f shell containing 0, 7, or 14 electrons. The energy required to remove the outer valence electrons increases as more electrons are removed. The +3 oxidation state of cerium is more stable at lower temperatures. At temperatures greater than the melting point, there may be sufficient thermal energy to achieve the +4 oxidation state. Many of the actinides, including uranium and plutonium exhibit a +4 oxidation state. Electronegativity is defined as a measure of the attraction exerted by an atom upon its own and other electrons in its valence shell. This attraction and that of the other elements making up a compound determine the type of bond that is formed. A numerical value of electronegativity has been assigned to each element. These numerical values semiquantitatively express the tendency of an atom to appropriate available electrons to take part in bonding. In one electronegativity scale, Pauling assigned the value of 0 to the noble gasses and the value of 4 to fluorine, the element whose atoms have the greatest attraction for electrons. The other elements fall between these limits.[10] Table 5.11 lists available oxidation states and electronegativities for the radionuclides of interest and their chosen surrogates.[11] This data indicates that the rare earth elements represent the actinide elements fairly well.

### 5.2.1.2.2 Formation of Stable Compounds

It is important that the compounds formed by the surrogates and other common elements in the melt refining system (oxygen, sulfur, and fluorine, for example) are of the same type and have comparable free energies of formation and physical properties as those compounds formed by the radionuclide. The oxide forms of the rare earth elements are a result of their temperature dependent valence state. All of the rare earth elements form stable sesqioxides or a dioxide. At lower temperatures the +3 valence state of $Ce_2O_3$ is the more stable oxide for cerium. High temperature chemistry data suggest that the +4 oxide state of cerium is the favored state at high temperatures as exhibited by the formation of $CeO_2$. Many of the actinides, including uranium and plutonium exhibit a +4 oxidation state and form stable dioxide compounds. Stable fluorides may also be formed. A knowledge of the electronegativity differences between the elements forming a compound enables the

prediction of its bonding. When the difference in electronegativity between two elements is greater than 1.7, an ionic bond is formed, while differences less than about 1.7 indicate the formation of covalent bonds.[10] The electronegativity of oxygen is 3.5 and that of fluorine is 4.0 indicating that most of the oxide and fluoride species formed between either the rare earths or the actinides will exhibit ionic bonding.

## 5.2.1.2.2.1 Properties of Compounds Formed in Melt Refining

The thermochemical and physical properties of the compounds formed in melt refining directly influence the partitioning of the elements which make up these compounds between a metal and a slag. The thermochemical stability of compounds, shown by the negative free energy of formation of these compounds, determines the degree to which a particular element may be scrubbed from the metal being melted, kinetics permitting. The densities and melting points of the compounds formed influence their physical separation to, and capture by, the slag.

### 5.2.1.2.2.1.1 Thermochemical Properties

The manner in which reactions take place in the high temperature environment of a melt refining system determines the extent to which any element will partition between the metal and the slag. The thermochemistry of the system as a whole determines which compounds will be formed and the subsequent behavior of these compounds.

In melt refining, the most common way in which an element partitions to a slag is by reacting with oxygen to form a stable oxide which may be captured by and incorporated into the slag. Based on the standard free energies of formation of the common rare earth elements Ce, La, and Nd, it can be inferred that their behavior should be quite similar when reacting with oxygen and that they should form a ($Re_2O_3$) oxide. Cerium and lanthanum are strong deoxidizers which lower the activity and solubility of oxygen in liquid iron in much the same way as aluminum does. In the presence of 0.05 to 0.1 wt % of cerium in liquid iron the solubility limit of oxygen is about 10 ppm. The interaction coefficients $e^j_o$ are estimated to be within -3 to-5.[12]

Rare earths are the strongest deoxidizers available in steelmaking because only the rare earths have boiling points high enough to allow retention of effective residuals in solution. Other frequently used deoxidizers, calcium and magnesium oxides have highly

negative free energies of formation but have low boiling points so that they are not retained in solution. Neodymium is also an effective deoxidizer, but its chemistry has been less completely documented than cerium and lanthanum. The standard free energy of formation of $CeO_2$ is more positive than the standard free energy of formation of $Ce_2O_3$ but from examination of the standard free energy values alone it is impossible to predict which will form in a complex system.[13] The oxide of cerium which will be present is determined by the amounts of oxygen and cerium available for reaction (activity). Cerium and oxygen may combine as follows:

$$Ce + O_2 \rightarrow CeO_2 \qquad \Delta G_{1700^\circ C} = -163.398 \text{ kcal/mole}_{CeO_2}$$

$$2Ce + \frac{3}{2}O_2 \rightarrow Ce_2O_3 \quad \Delta G_{1700^\circ C} = -302.192 \text{ kcal/mole}_{Ce_2O_3}$$

Combination of these equations yields:

$$Ce_2O_3 + \frac{1}{2}O_2 \rightarrow 2CeO_2 \quad \Delta G_{1700^\circ C} = -24.604 \text{ kcal/mole}$$

$$\Delta G_{1700^\circ C} = -RT \ln \frac{(a_{CeO_2})^2}{(a_{Ce_2O_3})(a_{O_2})^{1/2}}$$

As the amount of available oxygen decreases, the reaction becomes less favorable until, at some amount of available oxygen, it cannot proceed at all. Thus, the amount of oxygen available determines the oxide which forms. At even lower oxygen pressures, the ratio of oxygen to metal can drop to 1.85 or even 1.75. Plutonium behaves in much the same manner.[14]

Nevertheless, comparisons of the free energies of formation of thermodynamically stable oxides of radionuclides and their surrogates by means of an Ellingham diagram may aid in the selection of suitable surrogates. Figure 5.2 shows the free energy of formation of various stable oxides, normalized per mole of oxygen.

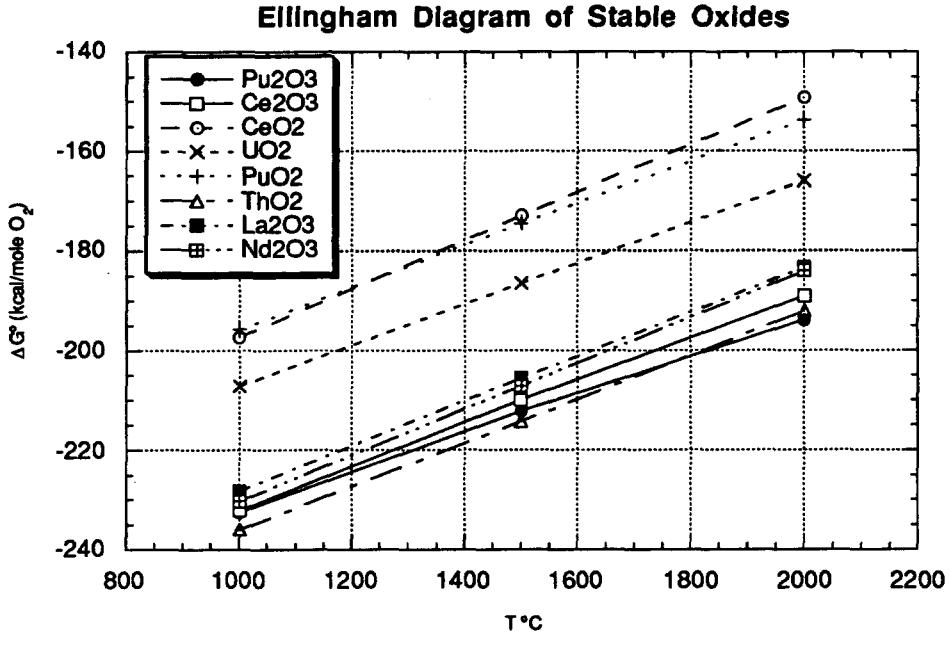


**Figure 5.2**
**Comparison of the Stabilities of Oxides of Radionuclides and Surrogates**

The diagram shows the great stability of the oxides of both the radioactive elements and their rare earth surrogates. The diagram may also be used to determine how closely the surrogates are likely to mimic the radionuclides in their tendency to form stable oxides. If, for example, plutonium exists in its +4 oxidation state, it is well represented by cerium in its +4 oxidation state. If plutonium is present in its +3 oxidation state it may be represented by either cerium in its +3 state, or by lanthanum or neodymium. The free energy of $ThO_2$ is comparable to those of $La_2O_3$ and $Nd_2O_3$, but its oxidation state is different. According to the free energy versus temperature diagram, uranium is best represented by cerium in its +4 oxidation state.

In ESR, elements may also enter the slag by forming fluorides or complex oxides which may incorporate sulfur, aluminum, or other elements. Predominance area diagrams are useful for comparing the stable phases which will be formed by an element in an environment in which there are two other elements with which it could react. This is the case for elements participating in reactions in ESR slags where they may react with either oxygen or fluorine. Figure 5.3 shows the phases formed by cerium in an environment

containing oxygen and fluorine at 1700°C. Figure 5.4 shows the phases formed by plutonium under similar conditions.

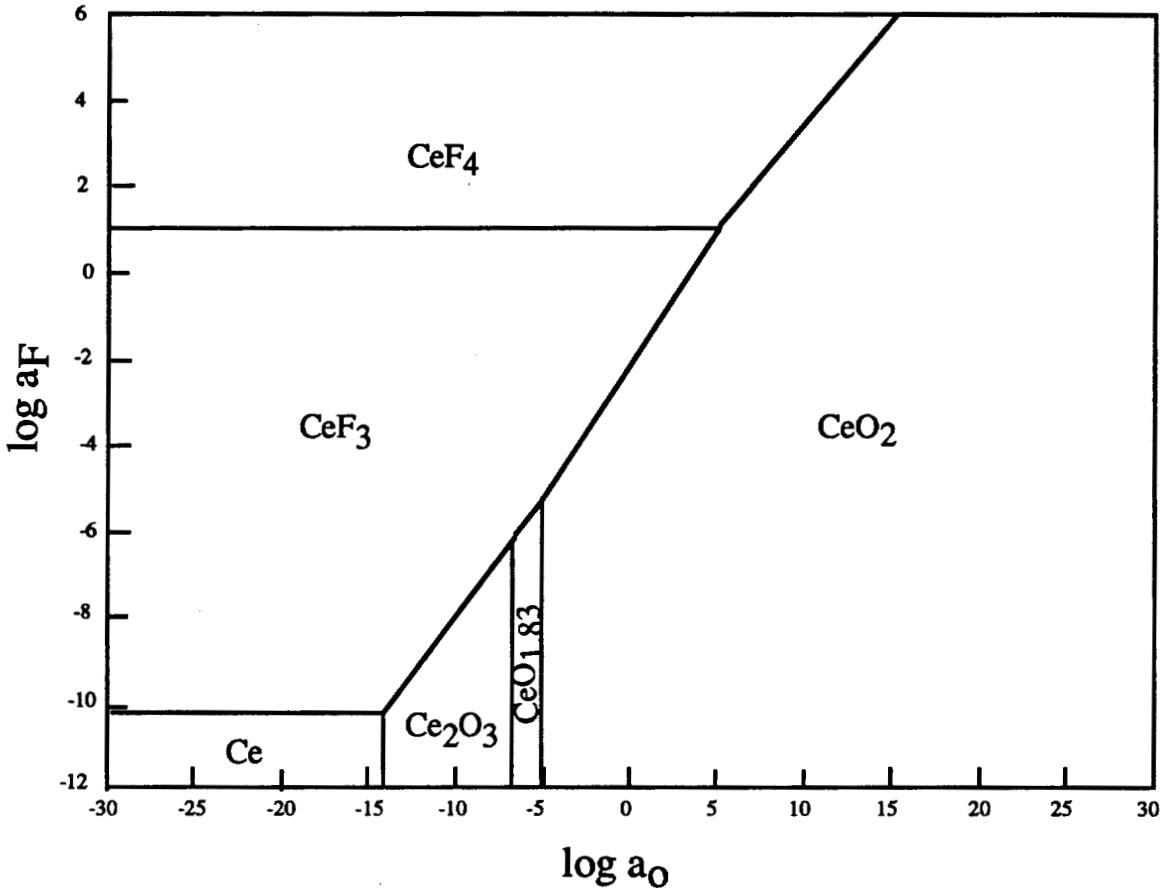


**Figure 5.3**
**Phase Stability Diagram for Cerium in the Presence of Oxygen and Fluorine at 1700°C**

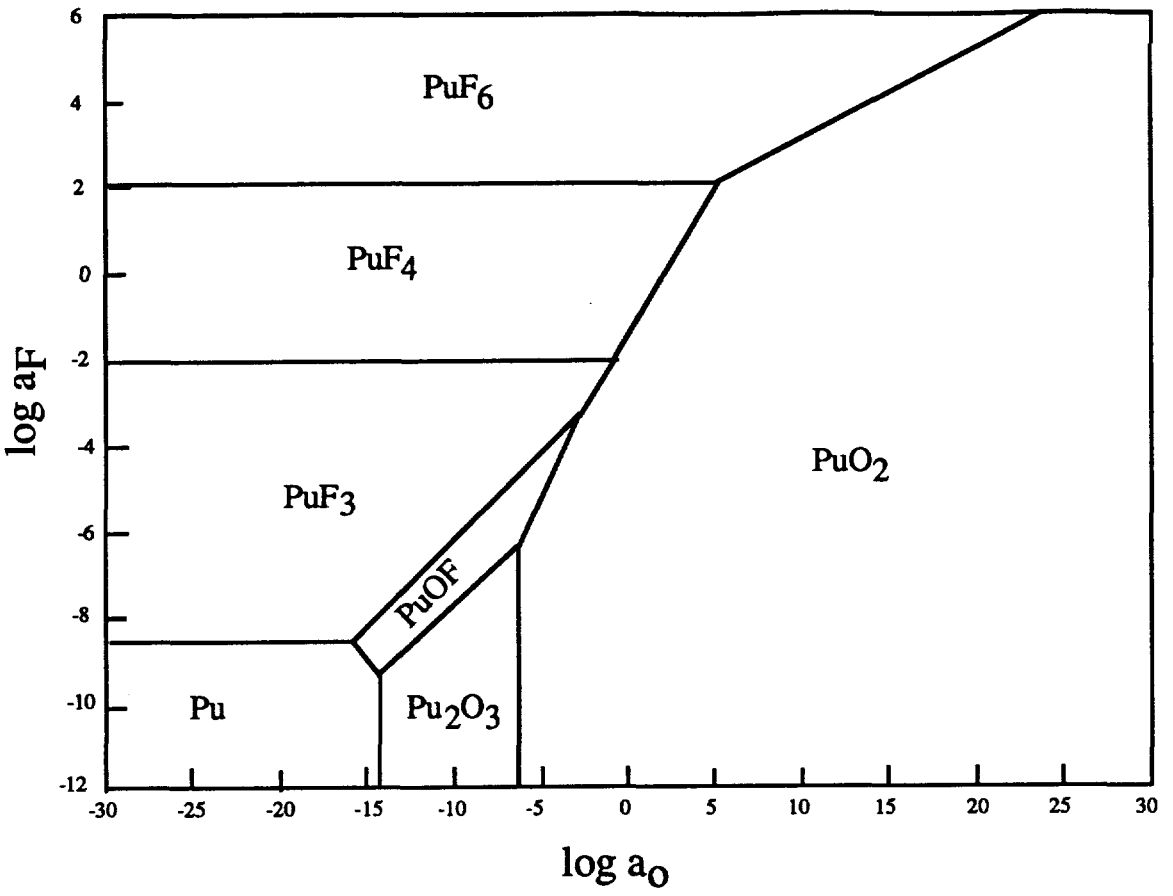


**Figure 5.4**
**Phase Stability Diagram for Plutonium in the Presence of Oxygen and Fluorine at 1700°C**

A comparison of these two diagrams shows that cerium and plutonium are quite similar in their capacity to form oxides and fluorides. There are some differences in the compounds which are predicted. Plutonium forms an oxyfluoride phase which is not predicted for cerium. The diagram for cerium shows an intermediate oxide between $Ce_2O_3$ and $CeO_2$. A similar phase exists for plutonium, although thermodynamic data is not available. Given the assumption that oxygen and fluorine bearing species report to the slag, stiochiometric differences in the compounds which form should not make great differences in the melt partitioning of cerium and plutonium.

The thermodynamics of rare earth oxides, sulfides, and oxysulfides have been studied in relation to their applications in ferrous metallurgy. The rare earths have been shown to form oxysulfides of the form $(RE)_2O_2S$. The negative free energy of formation of these compounds are less than 10 kilocalories less negative than the free energies of formation of common RE oxides at 3000°F and so are highly likely to form. Examination

of inclusions in rare earth deoxidized steel showed that oxysulfides formed in preference to oxides. Rare earths added as deoxidizers to aluminum killed steel were also found to form oxyaluminates of the type $(RE)AlO_3$. Kay[15,16] tabulated the thermochemical properties of cerium and lanthanum compounds containing oxygen and sulfur. Given the affinity of the rare earth surrogates for sulfur and oxygen, a question arises as to whether this affinity is shared by the radioactive elements. The properties of various oxysulfides were studied by Eastman, Brewer, et al[17]. One oxide sulfide compound of each of the elements cerium, thorium and uranium exists and the nomenclature to be used is based on the crystal structure. If an oxide sulfide has the same crystal structure as the pure oxide then it is called a thio-oxide to indicate the replacement of an oxygen by a sulfur. If it has the same crystal structure as the pure sulfide, it is called an oxy-sulfide. If the crystal structure is different from both the oxide and the sulfide it is called a sulfoxide. $Ce_2O_2S$ has the same crystal structure as $Ce_2O_3$ and is called cerium thio-oxide. As ThOS has a crystal structure different from both $ThO_2$ and $ThS_2$ it is thorium sulfoxide. Uranium forms UOS, uranium sulfoxide. Brewer found no other oxide sulfides of these elements, and no direct or indirect evidence for others. Zachariasen[18] carried out studies of the crystal structure of $Ce_2O_2S$, $La_2O_2S$, and $Pu_2O_2S$ and found that the compounds are isostructural with one stoichiometric molecule per hexagonal unit cell. Other lanthanide elements as well as actinium and americium may be expected to form oxy-sulfides which are isostructural with $Ce_2O_2S$. Oxysulfides of thorium, neptunium, and uranium have a different crystal structure. Thermodynamic data for UOS, $Pu_2O_2S$, and ThOS was not found. However, the search for thermodynamic data for these compounds did result in the location of data for other compounds of interest containing oxygen and sulfur. These compounds are of the form $X(SO_4)^2$ where X can be Pu, Th, or U. At similar activities of oxygen and sulfur, the rare earth elements form $X_2(SO4)_3$ type compounds where X is Nd, Ce, or La. These compounds may not be stable at high temperature, however.

## 5.2.1.2.2.1.2 Physical Properties: Melting Points and Densities

The physical properties of the compounds which are formed by the radionuclides and surrogates during melt refining effect the partitioning of these elements between the molten metal and the slag. In ESR, elements in the metal may react with free oxygen and fluorine in the slag at one of three interfaces, forming nonmetallic particles. As the electrode melts, a thin film of liquid forms in contact with the slag. Particles formed may either be swept into the metal droplets or collected by the slag, where they may either remain as solid

particles, be melted (depending on their melting point), or be dissolved in the hot, ionic slag. As metal droplets fall through the slag and are stirred by the presence of Lorentz forces, their surfaces become dynamic reaction sites at which radionuclides may be transferred to the slag. The droplets collect in a liquid metal pool at the top of the ingot. Particles formed at this interface may be transferred to the slag by flotation or turbulent slag stirring. Radionuclides remaining in the liquid metal may react with free oxygen to form deoxidation inclusions, which, if they are less dense than the liquid metal, will float, and be captured in the slag. The density of liquid iron is about 7.6 g/cm$^3$. The densities and melting points of several compounds of the radionuclides and their surrogates are presented in Table 5.12. While the densities of the compounds formed by the surrogates are less than that of liquid iron, the densities of the radioactive compounds tend to be much greater. This difference could affect the mechanics of melt partitioning and thus its efficiency.

**Table 5.12**
**Densities and Melting Points of Radionuclide and Surrogate Compounds**

| Compound | Density (g/cm3) | Melting Point °C |
|---|---|---|
| $CeO_2$ | 7.132 | 2600 |
| $Ce_2O_3$ | 6.86 | 1692 |
| $CeF_3$ | 6.16 | 1460 |
| $La_2O_3$ | 6.51 | 2307 |
| $LaF_3$ | No data | No data |
| $Nd_2O_3$ | 7.24 | 1900 |
| $NdF_3$ | No data | 1410 |
| $PuO_2$ | 11.46 | 2280 |
| $PuF_4$ | 7.0 | 1037 |
| $PuF_3$ | 9.32 | 1425 |
| $ThO_2$ | 9.86 | 3220 |
| $ThF_4$ | 6.32 | >900 |
| ThOS | 6.44 | decomposes |
| $UO_2$ | 10.96 | 2878 |
| $UF_4$ | 6.70 | 960 |

## 5.2.2 Slag Selection

The range of slag chemistries to be studied was determined by a study of industrially used slags and examination of the ternary $CaF_2$-CaO-$Al_2O_3$ phase diagram, shown in Figure 5.5.

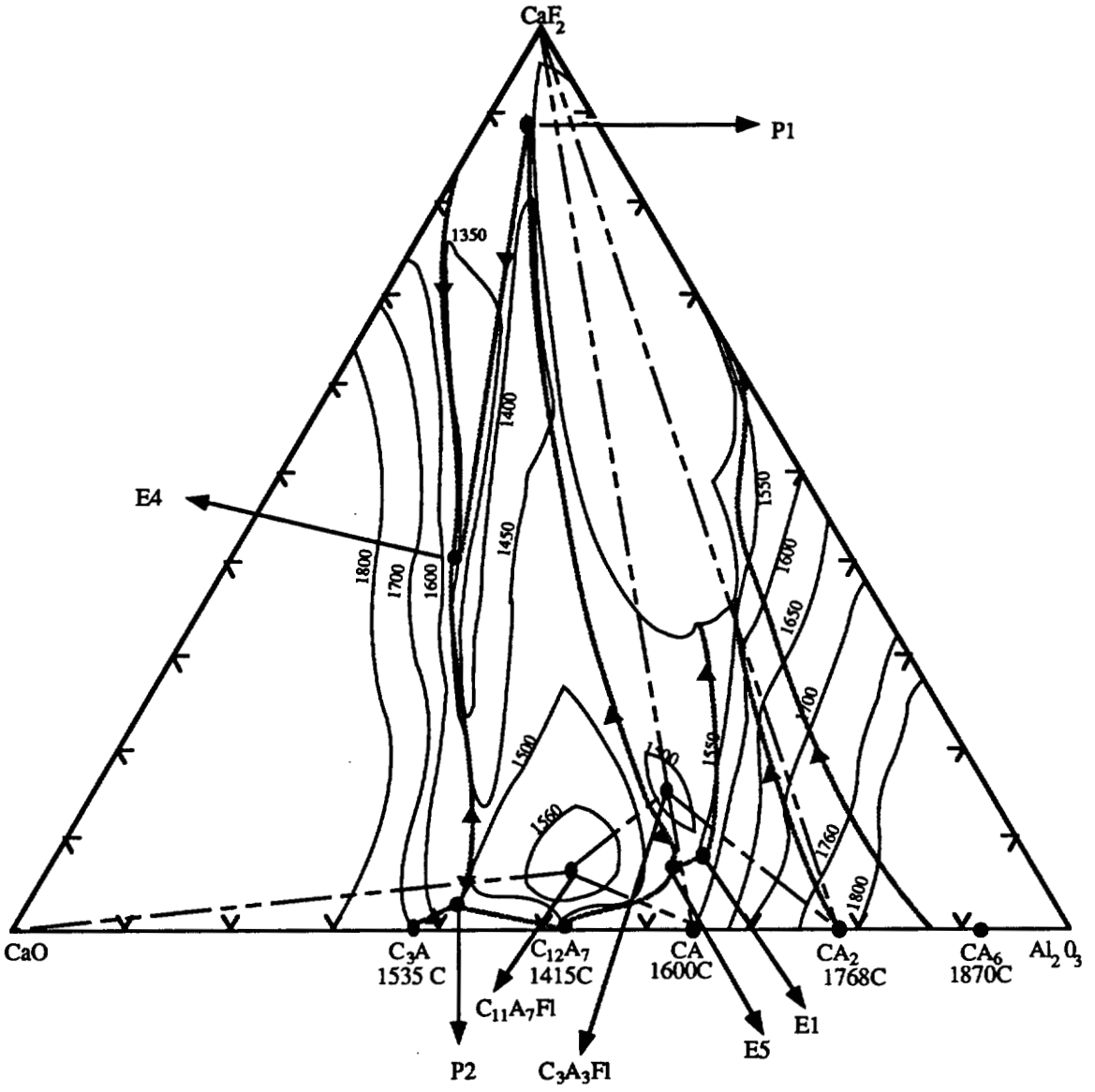


**Figure 5.5**
**Phase Diagram for the System $CaF_2$-CaO-$Al_2O_3$ at 1600°C**

The diagram has two important features that played a role in determining the range of chemistries to be studied. There is a large region of liquid immisibility near the $CaF_2$-$Al_2O_3$ binary. A matrix was chosen that included points within this region in order to determine the effect of immisible liquids in the slag on its ability to capture the surrogates. A second feature is the trough of slags having low liquidus temperatures that extends roughly down the middle of the diagram. The chemistries of most industrial slags fall in or near this trough and have equal amounts of calcium oxide and alumina. The test matrix

included slags with low liquids temperatures, much like those slags used in industry. Due to the variation in the amounts of $Al_2O_3$ contained in the slags, it was expected that each slag would exhibit a unique electrical conductivity. The physical and chemical properties represented by each slag were expected to affect the melt refining process, and thus the test matrix was designed to include slags with very different chemistries.

# Chapter 5 Tables

**Table 5.1**
**Chemistry Analysis of OGI Master Melt Base Metal.**
(Analysis performed by DC plasma, C and S analyzed by Leco Combustion)

| Element Percent | OGI Master Melts | | | 304L ASTM Standard Required Maximum Chemistry | |
|---|---|---|---|---|---|
| | E1 | E2 | E3 | Wrought | Cast |
| Cr | 17.14 | 17.50 | 17.29 | 18-20 | 17-21 |
| Ni | 12.13 | 11.09 | 9.88 | 8-12 | 8-12 |
| Mn | 1.31 | 1.13 | 1.25 | 2.0 | 1.5 |
| Si | 0.69 | 0.41 | 0.63 | 0.75 | 2.0 |
| Mo | 1.12 | 0.94 | 0.55 | NA | NA |
| Cu | 0.22 | 0.25 | 0.16 | NA | NA |
| S | 0.011 | 0.011 | 0.012 | 0.030 | 0.04 |
| P | 0.005 | 0.005 | 0.005 | 0.045 | 0.04 |
| C | 0.025 | 0.034 | 0.030 | 0.03 | 0.03 |

**Table 5.4**
**Chemistry of Sample taken from the Montana Tech Master Melt Ingot**

| | Analysis Method | | |
|---|---|---|---|
| Element | DC Plasma | ICP-MS | INAA |
| Cr | 17.99 % | - | - |
| Ni | 10.25 % | - | - |
| Mn | 1.27 % | - | - |
| Si | 0.43 % | - | - |
| Mo | 0.25 % | - | - |
| Cu | 0.072 % | - | - |
| S | 0.0066 % | - | - |
| P | trace | - | - |
| C | 0.039 % | - | - |
| Ce | - | 1000 ppm | 640 ppm |
| La | - | 670 ppm | 398 ppm |
| Nd | - | 840 ppm | 440 ppm |

**Table 5.6**
**Weights of Individual Slag Components**

| Slag Composition | Number of melts | Grams of slag | Grams of $CaF_2$ | Grams of CaO | Grams of $Al_2O_3$ | Total Weight |
|---|---|---|---|---|---|---|
| 50/25/25 | 6 | 1297 | 0 | 259.4 | 259.4 | 1815.8 |
| 50/40/10 | 1 | 1211 | 60.5 | 544.8 | 0 | 1816.3 |
| 30/30/40 | 1 | 783 | 0 | 425.8 | 607.4 | 1816.2 |
| 30/40/30 | 1 | 783 | 0 | 607.4 | 425.8 | 1816.2 |
| 70/20/10 | 1 | 1211 | 423.7 | 181.6 | 0 | 1816.3 |
| 70/10/20 | 1 | 1211 | 423.7 | 0 | 181.6 | 1816.3 |
| 50/10/40 | 1 | 1211 | 60.5 | 0 | 544.8 | 1816.3 |
| 36.6/31.7/31.7 | 1 | 949 | 0 | 433.3 | 433.3 | 1816.0 |
| 43.3/21.7/35 | 1 | 1123 | 0 | 224.5 | 465.9 | 1813.4 |
| 56.7/15/28.3 | 1 | 1472 | 0 | 53.0 | 294.3 | 1819.3 |
| 63.4/18.3/18.3 | 1 | 1645 | 0 | 85.5 | 85.5 | 1816.0 |
| 56.7/28.3/15 | 1 | 1472 | 0 | 294.3 | 53.0 | 1819.3 |
| 43.3/35/21.7 | 1 | 1123 | 0 | 465.9 | 224.5 | 1813.4 |
| Total | 18 | 15491 | 968.4 | 3575.5 | 3575.5 | 23610.8 |

**Table 5.7**
**Analysis of 70/15/15 Slag**

| Component | Percent |
|---|---|
| $CaF_2$ | 69.10 |
| CaO | 14.45 |
| MgO | 0.136 |
| $Al_2O_3$ | 14.90 |
| $SiO_2$ | 0.76 |
| C | 0.019 |
| S | 0.017 |
| $MnO_2$ | 0.012 |
| Fe | 0.051 |
| $TiO_2$ | 0.041 |
| P | <0.01 |

**Table 5.8**
**Chemistry of the Slag Used in Each Heat as Calculated by Mass Balance**

| Heat | $CaF_2$ % | CaO % | $Al_2O_3$ % | MgO % | $SiO_2$ % | C % | S % | $MnO_2$ % | TiO % | Ce ppm | La ppm | Nd ppm |
|---|---|---|---|---|---|---|---|---|---|---|---|---|
| 74 | 49.52 | 24.68 | 25.01 | 0.097 | 0.544 | 0.013 | 0.012 | 0.008 | 0.029 | 351 | 172 | 172 |
| 75 | 49.55 | 39.75 | 9.965 | 0.090 | 0.508 | 0.012 | 0.011 | 0.008 | 0.027 | 327 | 160 | 160 |
| 76 | 36.20 | 31.49 | 31.73 | 0.071 | 0.398 | 0.009 | 0.008 | 0.006 | 0.021 | 256 | 125 | 125 |
| 77 | 56.97 | 14.88 | 27.25 | 0.112 | 0.626 | 0.015 | 0.014 | 0.009 | 0.033 | 403 | 197 | 197 |
| 78 | 29.85 | 29.73 | 39.94 | 0.058 | 0.328 | 0.008 | 0.007 | 0.005 | 0.017 | 211 | 103 | 103 |
| 79 | 62.86 | 17.87 | 18.28 | 0.123 | 0.691 | 0.017 | 0.015 | 0.010 | 0.037 | 445 | 218 | 218 |
| 80 | 48.83 | 9.522 | 40.93 | 0.089 | 0.500 | 0.012 | 0.011 | 0.007 | 0.027 | 322 | 158 | 158 |
| 81 | 49.52 | 24.68 | 25.01 | 0.097 | 0.544 | 0.013 | 0.012 | 0.008 | 0.029 | 351 | 172 | 172 |
| 82 | 69.61 | 19.69 | 9.965 | 0.090 | 0.508 | 0.012 | 0.011 | 0.008 | 0.027 | 320 | 160 | 160 |
| 83 | 42.91 | 34.74 | 21.67 | 0.084 | 0.472 | 0.011 | 0.010 | 0.007 | 0.025 | 304 | 149 | 149 |
| 84 | 42.91 | 21.39 | 35.02 | 0.084 | 0.472 | 0.011 | 0.010 | 0.007 | 0.025 | 304 | 149 | 149 |
| 85 | 30.15 | 40.15 | 29.22 | 0.059 | 0.331 | 0.008 | 0.007 | 0.005 | 0.017 | 213 | 104 | 104 |
| 86 | 56.12 | 27.97 | 15.02 | 0.110 | 0.617 | 0.015 | 0.013 | 0.009 | 0.033 | 397 | 194 | 194 |
| 88 | 49.52 | 24.68 | 25.01 | 0.097 | 0.544 | 0.013 | 0.012 | 0.008 | 0.029 | 351 | 172 | 172 |
| 89 | 49.52 | 24.68 | 25.01 | 0.097 | 0.544 | 0.013 | 0.012 | 0.008 | 0.029 | 351 | 172 | 172 |
| 90 | 49.52 | 24.68 | 25.01 | 0.097 | 0.544 | 0.013 | 0.012 | 0.008 | 0.029 | 351 | 172 | 172 |
| 91 | 69.61 | 9.664 | 19.99 | 0.090 | 0.508 | 0.012 | 0.011 | 0.008 | 0.027 | 327 | 160 | 160 |
| 92 | 49.52 | 24.68 | 25.01 | 0.097 | 0.544 | 0.013 | 0.012 | 0.008 | 0.029 | 351 | 172 | 172 |
| 93 | 49.52 | 24.68 | 25.01 | 0.097 | 0.544 | 0.013 | 0.012 | 0.008 | 0.029 | 351 | 172 | 172 |

**Table 5.9**
**Electronic Structure of the Lanthanides**

| Element | Oxidation States | Atomic number | Number of electrons | | | | | | | | |
|---|---|---|---|---|---|---|---|---|---|---|---|
| | | | Shell 1,2,3 | 4s | 4p | 4d | 4f | 5s | 5p | 5d | 6s |
| Cesium | 1 | 55 | 28 | 2 | 6 | 10 | – | 2 | 6 | – | 1 |
| Barium | 2 | 56 | 28 | 2 | 6 | 10 | – | 2 | 6 | – | 2 |
| Lanthanum | 3 | 57 | 28 | 2 | 6 | 10 | – | 2 | 6 | 1 | 2 |
| Cerium | 3,4 | 58 | 28 | 2 | 6 | 10 | 2 | 2 | 6 | – | 2 |
| Praseodymium | 3 | 59 | 28 | 2 | 6 | 10 | 3 | 2 | 6 | – | 2 |
| Neodymium | 3 | 60 | 28 | 2 | 6 | 10 | 4 | 2 | 6 | – | 2 |
| Promethium | 3 | 61 | 28 | 2 | 6 | 10 | 5 | 2 | 6 | – | 2 |
| Samarium | 2,3 | 62 | 28 | 2 | 6 | 10 | 6 | 2 | 6 | – | 2 |
| Europium | 2,3 | 63 | 28 | 2 | 6 | 10 | 7 | 2 | 6 | – | 2 |
| Gadolinium | 3 | 64 | 28 | 2 | 6 | 10 | 7 | 2 | 6 | 1 | 2 |
| Terbium | 3 | 65 | 28 | 2 | 6 | 10 | 9 | 2 | 6 | – | 2 |
| Dysprosium | 3 | 66 | 28 | 2 | 6 | 10 | 10 | 2 | 6 | – | 2 |
| Holmium | 3 | 67 | 28 | 2 | 6 | 10 | 11 | 2 | 6 | – | 2 |
| Erbium | 3 | 68 | 28 | 2 | 6 | 10 | 12 | 2 | 6 | – | 2 |
| Thulium | 3 | 69 | 28 | 2 | 6 | 10 | 13 | 2 | 6 | – | 2 |
| Ytterbium | 2,3 | 70 | 28 | 2 | 6 | 10 | 14 | 2 | 6 | – | 2 |
| Lutetium | 3 | 71 | 28 | 2 | 6 | 10 | 14 | 2 | 6 | 1 | 2 |
| Hafnium | 3,4 | 72 | 28 | 2 | 6 | 10 | 14 | 2 | 6 | 2 | 2 |

**Table 5.10**
**Electronic Structure of the Actinides**

| Element | Oxidation States | Atomic number | Number of Electrons | | | | | | | | |
|---|---|---|---|---|---|---|---|---|---|---|---|
| | | | Shell 1-4 | 4s | 4p | 4d | 4f | 5s | 5p | 5d | 6s |
| Francium | 1 | 87 | 60 | 2 | 6 | 10 | – | 2 | 6 | – | 1 |
| Radium | 2 | 88 | 60 | 2 | 6 | 10 | – | 2 | 6 | – | 2 |
| Actinium | 3 | 89 | 60 | 2 | 6 | 10 | – | 2 | 6 | 1 | 2 |
| Thorium | 4 | 90 | 60 | 2 | 6 | 10 | 2 | 2 | 6 | 2 | 2 |
| Protactinium | 4,5 | 91 | 60 | 2 | 6 | 10 | 3 | 2 | 6 | 1 | 2 |
| Uranium | 4,5,6 | 92 | 60 | 2 | 6 | 10 | 4 | 2 | 6 | 1 | 2 |
| Neptunium | 3,4,5,6,7 | 93 | 60 | 2 | 6 | 10 | 5 | 2 | 6 | 1 | 2 |
| Plutonium | 3,4,5,6,7 | 94 | 60 | 2 | 6 | 10 | 6 | 2 | 6 | – | 2 |
| Americium | 3,4,5,6 | 95 | 60 | 2 | 6 | 10 | 7 | 2 | 6 | – | 2 |
| Curium | 3,4 | 96 | 60 | 2 | 6 | 10 | 7 | 2 | 6 | 1 | 2 |
| Berkelium | 3,4 | 97 | 60 | 2 | 6 | 10 | 9 | 2 | 6 | 1 | 2 |
| Californium | 3 | 98 | 60 | 2 | 6 | 10 | 10 | 2 | 6 | – | 2 |
| Einsteinium | 3 | 99 | 60 | 2 | 6 | 10 | 11 | 2 | 6 | – | 2 |
| Fermium | 3 | 100 | 60 | 2 | 6 | 10 | 12 | 2 | 6 | – | 2 |
| Mendelevium | 2,3 | 101 | 60 | 2 | 6 | 10 | 13 | 2 | 6 | – | 2 |
| Nobelium | 2,3 | 102 | 60 | 2 | 6 | 10 | 14 | 2 | 6 | – | 2 |
| Lawrencium | 3 | 103 | 60 | 2 | 6 | 10 | 14 | 2 | 6 | 1 | 2 |

**Table 5.11**
**Comparison of Oxidation States and Electronegativities for Radionuclides and Surrogates**

| Element | Oxidation States | Pauling Electronegativity |
|---|---|---|
| Ce | 3,4 | 1.12 |
| La | 3 | 1.10 |
| Nd | 2,3,4 | 1.14 |
| U | 2,3,4,5,6 | 1.38 |
| Th | 2,3,4 | 1.3 |
| Pu | 2,3,4,5,6,7 | 1.28 |
| Ru | 1,2,3,4,5,6,7,8 | 2.2 |
| Tc | 4,5,6,7 | 1.9 |
| Am | 2,3,4,5,6 | 1.3 |
| Cm | 2,3,4 | 1.3 |

# Chapter 5 References


[1] Atteridge, D.A., Buckentin, J., Carter, J., Davis H.L., Devletian, J.H., Scholl, M.R., Turpin, R.G., Webster, S.L., Mizia, R.E. (Ed.), "Refining Technology for the Recycling of Stainless Steel Radioactive Scrap Metals: FY 94 Bi-Annual Report," INEL-DOE, WINCO-1224, (1994).

[2] Stockdale, J., Bostick, W., Hoffman, D., Lee, H. "Surrogate Formulations for Thermal Treatment of Low-Level Mixed Waste, Part I: Radiological Surrogates" Prepared for the Mixed Waste Integrated Program, US Department of Energy, DOE/MWIP-15.

[3] Emsley, John. The Elements, Clarendon Press, Oxford, (1992).

[4] Benedict, M., Pigford, T., Levi, H. Nuclear Chemical Engineering, McGraw Hill, New York, (1981).

[5] O.J. Wick, ed. The Plutonium Handbook: A Guide to the Technology, Volumes 1 and 2, The American Nuclear Society, La Grange Park, Illinois, (1980).

[6] Raraz,A., Mishra, B., Averil, W.A., "Application of Surrogate Materials in Process Study of Actinides" Rockwell International, Rocky Flats Plant, Golden, Colorado. DOE Report Holdings, RFP--4628.(1993).

[7] McAtee, R.E., Beal, M. "Comparison of the High Temperature Chemistry of Plutonium and Rare Eaths: A Review Study" Idaho National Engineering Laboratory, EG&G Idaho, Inc. EGG-WTD-9801, (September 1991).

[8] Worcester, S.A., et. al., Mizia, R.E. (ed) Decontamination of Metals by Melt Refining/Slagging: First Year Progress Report, DOE, Idaho Operations Office, Westinghouse Idaho Nuclear Company Inc., WINCO-1198 UC-510,( March 1994).

[9] Kessinger, G. Private Communication to R.E. Mizia, Idaho National Engineering Laboratory, August 9, 1993.

[10] Lippencott, W.T., Garrett, A.B., Verhoek, F. H., Chemistry: A Study of Matter, John Wiley and Sons, New York, (1977).

[11] Emsley, John. The Elements, Clarendon Press, Oxford, (1992).

[12] Fruehan, R.J. " The Effect of Zirconium, Cerium, and Lanthanum on the Solubility of Oxygen in Liquid Iron" *Metallurgical Transactions*, Volume 5, (February 1974), 345-347.

[13] Wilson, W.G., Kay, D.A.R., Vahed, A. "The Use of Thermodynamics and Phase Equilibra to Preduct the Behavior of the Rare Earth Elements in Steel." *Journal of Metals*, (May, 1974), 14-23.

[14] Brewer, L. University of California, Berkeley. Private communication. November 10, 1995.

[15] Kay, D.A.R., Wilson, W.G., Jalan, V. "High Temperature Thermodynamics and Applications of Rare Earth Compounds Containing Oxygen and Sulphur in Fuel Gas Desulphurization and SOx and NOx removal" *Journal of Alloys and Compounds*, Vol. 192, (1993), 11-16.

[16] Kay, D.A.R. "High Temperature Thermodynamics and Applications of Rare Earth Oxides and sulphides in Ferrous Metallurgy" *Mineral Processing and Extractive Metallurgy Review*, Volume 10, (1992), 307-323.

[17] Eastman, E.D., Brewer, L., Bromley, L. Gilles, P., Lofgren, N. "Preparation and Properties of the Oxide Sulfides of Cerium, Zirconium, Thorium, and Uranium" *Journal of the Americal Chemical Society*, Vol. 73, (1951), 3896.

[18] Zachariasen, W.H. "Crystal Chemical Studies of the 5f Series of Elements VII. The Crystal Structure of $Ce_2O_2S$, $La_2O_2S$. and $Pu_2O_2S$." *Acta Cryst.*, Vol. 2, (1949), 60-62.

# Chapter 6
# Experimental Results

During the preparation of the slag for the melting experiments and while performing the ESR melts, several interesting observations were made regarding the character of the slag and its effect on the process. After all melting experiments had been completed, samples of steel were analyzed in order to determine both the changes in bulk chemistry effected by electroslag remelting and the degree of decontamination achieved. Samples of slag (skin and cap) were analyzed for the amount of surrogate elements contained in each. Details of the observations and findings of this research are presented in this chapter.

## 6.1 Analysis of Stainless Steel After Melting

Each stainless steel ingot produced was analyzed in order to determine how melting in contact with various slags had changed the chemistry of the alloy. Additionally, each ingot was analyzed for the presence of surrogate elements, both on the surface and in the bulk metal.

### 6.1.1 Major Elements

A slice from the steady state region of each ingot produced was subjected to spectrographic analysis at ESCO for determination of the major elements. These analysis, presented in Table 6.1 (located at the end of this chapter along with selected other chapter tables), were compared with spectrographic analysis of the material before remelting. The amount of copper present in the final ingots may be used to trace

whether each bar melted was from heat E2 or from heat E3, the identity of the individual bars having been lost during the thermal spray process. Copper is an excellent signature element because it is less easily oxidized than iron and will not partition to a slag to any great extent. Figure 6.1 shows that heats 82, 83, 84, 85, 89, 90, and 92 were made up of steel from master melt E2 and the other heats were made up of steel from master melt E3.

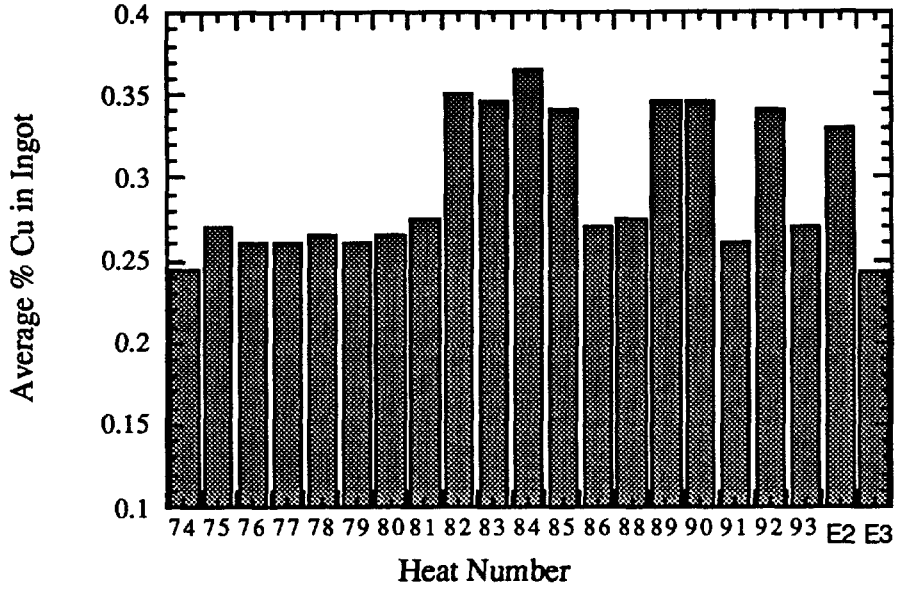


**Figure 6.1**
**Percentage of Copper in Each Ingot and in Master Melt Heats E2 and E3**

Once the starting chemistry of the steel was known for each heat, the differences in elemental concentrations were calculated and these differences are presented in Table 6.2. The tendency of elements to partition between the metal and the slag as a function of slag composition was observed. Table 6.2 shows that all ingots had higher manganese, sulfur, and silicon concentrations in the starting material than in the final ingot, leading to a positive concentration difference. Nickel, copper, and cobalt, however, were higher in the final product than in the starting material, leading to a negative concentration difference. The results for other elements were mixed. The steel samples were also analyzed for oxygen and nitrogen. The results of this analysis are presented in Table 6.3 .

### 6.1.2 Rare Earth Elements

Each steel ingot was analyzed for rare earth elements in order to determine the extent to which they had been removed by electroslag remelting. Samples of each ingot were submitted for the determination of residual levels of Ce, La, and Nd in the bulk material by ICP Mass Spec. These samples consisted of drill turnings taken from the material at radial depths between 0.25" and 0.75". In addition, for three of the ingots, surface samples were taken from radial depths between the surface and 0.25". Of the three ingots for which surface samples were submitted, heat number 91 had excellent surface, heat number 85 had marginal surface with some associated roughness, and heat number 75 had very poor surface with a great deal of entrained slag. The results of this analysis are presented in Table 6.4.

This data shows that the surrogates were removed from the bulk of the plasma sprayed steel to below detectable limits regardless of the amount of surrogate present, the types and mixtures of surrogates applied, or the slag used. The data also shows that, when slag is entrained on the surface of the ingot, incomplete decontamination may be achieved. Surrogate levels in the bulk of the remelted Montana Tech ingot (heat 94) remained appreciable. A comparison of surrogate levels in heat 94 before and after ESR, shown in Table 6.5, reveals that remelting reduced the level of surrogates present in the steel to about half.

**Table 6.5**
**Montana Tech Ingot Before and After Remelting**

| Element | Surrogate Level Before ESR ppm | Surrogate Level After ESR ppm | Amount Removed by ESR (ppm) |
|---|---|---|---|
| Ce | 1000 | 510 | 490 |
| La | 670 | 380 | 290 |
| Nd | 840 | 360 | 480 |

### 6.1.2.1 Surface Quality

As the melt tests proceeded, it was observed that some ingots had very smooth surfaces while others had rougher surfaces and two ingots, from heats 75 and 85, had slag entrained on their surfaces. Figure 6.2 shows two ingots, one with an excellent

surface and one with a very poor surface. A comparison of the observed surface quality of the ingots produced is presented in Table 6.6.

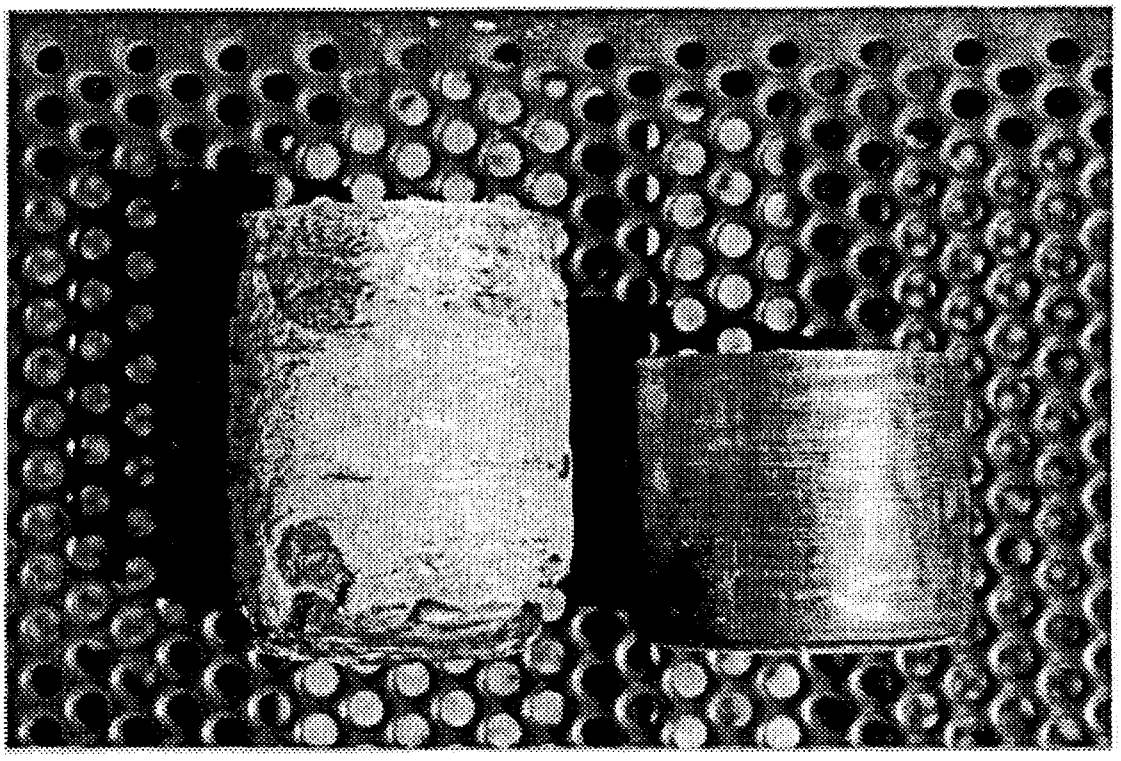

**Figure 6.2**
**Ingot Sections From Heat 75 (left) and Heat 91 (right)**

## 6.2 Slag Behavior

The chemistries of the slags used in this research are plotted on a ternary grid in Figure 6.3. The number next to each design point on the grid is the heat number of the melt performed with that particular slag. An overlay of this grid may be placed on the ternary $CaF_2$-CaO-$Al_2O_3$ phase diagram, as shown in Figure 6.4. During the course of this work, several interesting observations were made regarding the behavior of $CaF_2$-CaO-$Al_2O_3$ slags. Differences in the behaviors of the various slags first became evident as slags were being prepared for use by prefusion. During ESR melts, slag chemistry was observed to affect the relationships between voltage, current and power. Analysis of the slag skins and the slag caps from the various melts performed showed that slag chemistry affected slag skin thickness as well as the manner in which the surrogate elements were distributed between the slag skin and the slag cap.

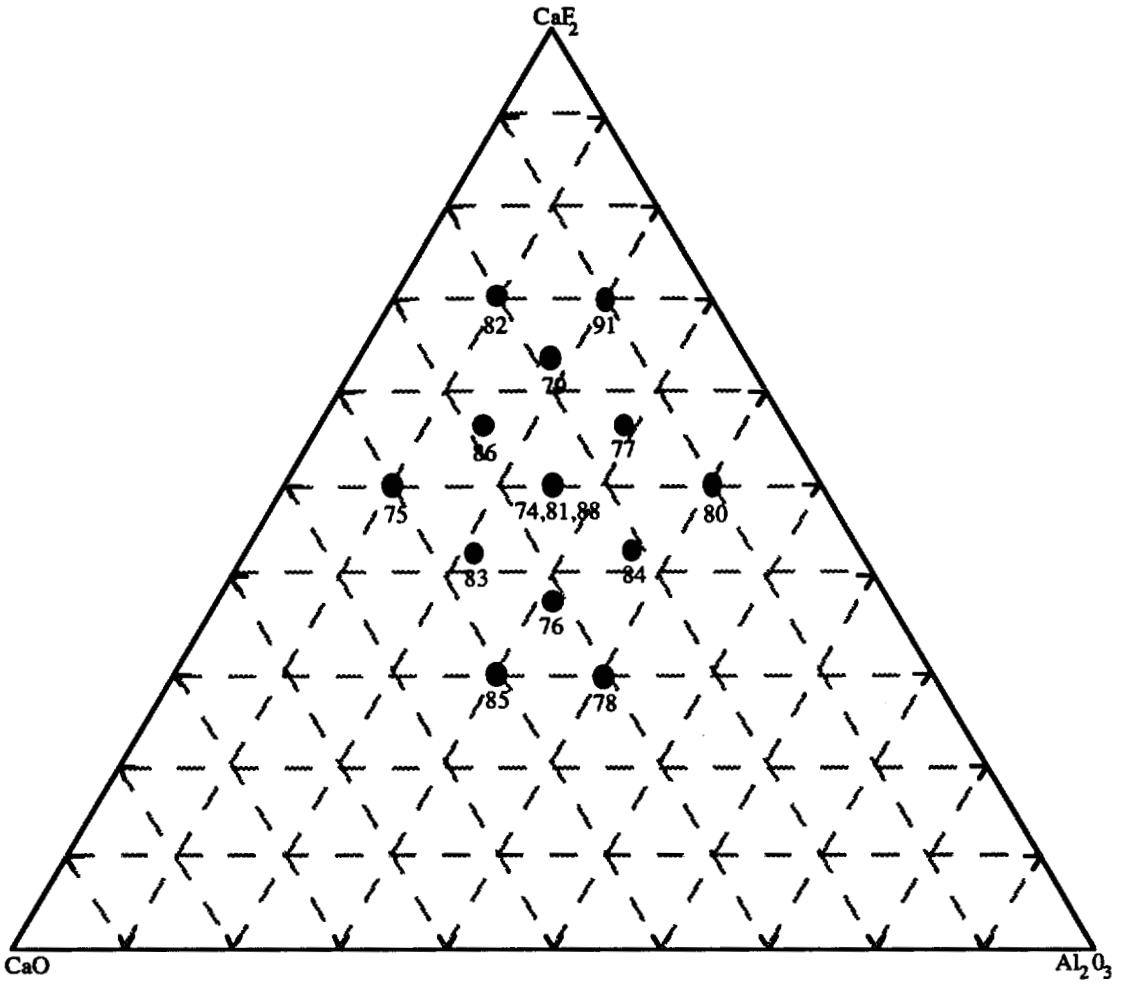


**Figure 6.3**
**Chemistries of Slags Plotted on Ternary Grid**

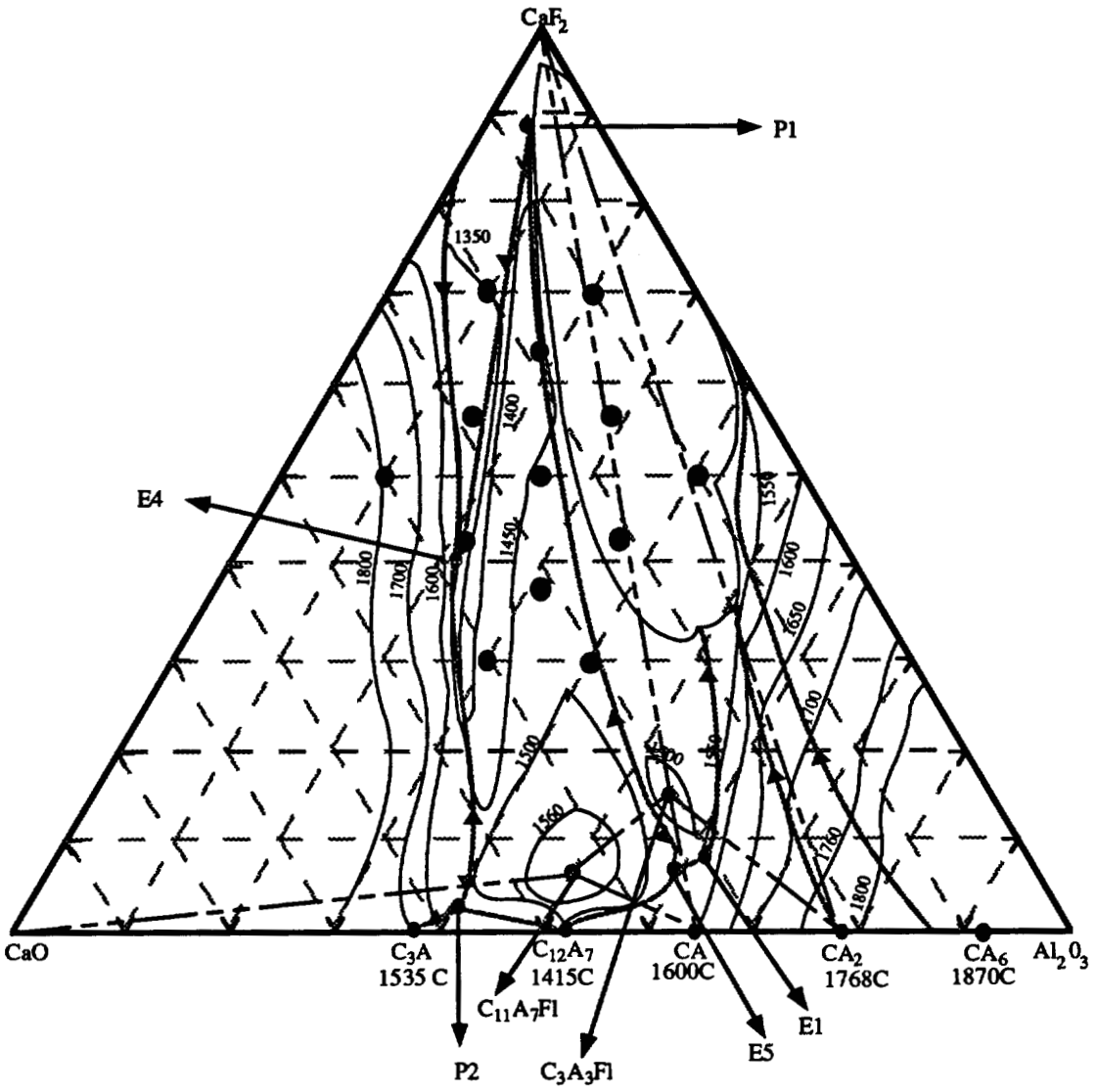


**Figure 6.4**
**Test Points Superimposed on Ternary $CaF_2/CaO/Al_2O_3$ Phase Diagram**

## 6.2.1 Behavior During Prefusion

The slags for this research were prepared by blending specified amounts of pure components with an industrial 70/15/15 slag and melting in a graphite crucible. After each batch of slag had cooled, it was broken into sections and observed. Some slags showed evidence of the presence of immisible liquids and others showed evidence that they had picked up carbon from the graphite crucible.

### 6.2.1.1 Evidence of Immisible Liquids

Slag fusion generated blocks of slag weighing four pounds each. Often, these blocks would crack after they had been cooled and removed from the graphite crucible. When cracking did not occur, the blocks were broken so that the fracture surfaces could be observed for evidence of immisible liquids, as predicted by the phase diagram for heats 91, 80, 77, and 84. The evidence of immisible liquids was the most obvious for the slag which was to be used for heat number 77. This slag is near the center of the immisible liquid region on the phase diagram. The fracture surfaces showed a bright white phase and a distinct dull lavender phase.

### 6.2.1.2 Evidence of Carbon Pickup

The slag to be used for melt number 75 turned a deep gray color. Fresh components were mixed and another batch was made, with the same result. Grinding this slag proved to be much more difficult than grinding any of the others and produced more wear on the grinding surfaces of the hand grinder used for size reduction of the slag. Slags with large amounts of free lime may react with the graphite from the crucible by the following reaction:

$$2CaO + 3C \rightarrow CaC_2 + CO_2$$

Carbon pickup by this mechanism may have been the cause of the gray color of the slag and if carbides were present, they could have contributed to the extreme hardness of the slag.

## 6.2.2 Slag Behavior during Melting

In the process of performing the melts in which slag chemistry was changed from one melt to the next, other parameters were, to as great an extent as possible, held constant. This was difficult because the chemistry of the slag influences the process in several important ways. The slag acts as a resistor in an ESR melt, and thus its resistivity determines the temperature of the slag and thus the melt rate of the ingot. The resistance of the slag also affects the relationships between current, voltage, and power. The impedance of the system is also related to the resistivity of the slag. Table 6.7 lists

the average voltage, current, power, and impedance observed during the steady state portion of each melt. A control system was used in conjunction with a load cell to keep the melt rate constant.

### 6.2.2.1 Determination of Conductivity

Melting data may be used to calculate slag conductivity by use of the following relationship:

$$\kappa = \frac{Id}{VA}$$

where I is the melting current in amps, V is the melting voltage in volts, d is the effective resistance path length (slag depth) in centimeters and A is the cross section of the current path in square centimeters. The conductivity of the slag, $\kappa$, is thus calculated in inverse ohm centimeters. The average values of voltage and current presented in the table above were used to calculate the conductivities exhibited by each of the slags. The effective slag depth was taken to be 2.5" and the cross section of the current path was assumed to have a 3" diameter. The values obtained by this analysis are presented in Table 6.8. Slag conductivity was also calculated by the method of Hara, Hashimoto, and Ogino[1] and these calculated values are also presented. A comparison of the values shows good agreement between theoretical and actual values. The chemistry, and thus the behavior, of the molten slag in an ESR changes throughout the course of a melt due to the loss of volatile constituents as well as preferential solidification which takes place in order to form a slag skin. Both of these phenomena act to decrease the effective resistance path length (d in the equation above) by decreasing the depth of the slag.

## 6.3 Slag Analysis

After each melt, the slag cap and the slag skin were weighed. Samples of slag cap and slag skin from each melt were analyzed for the presence of surrogate elements by ICP mass spec, preceded by a sodium borate fusion for the complete dissolution of all slag constituents. Results of these analysis are presented in Table 6.9. This data was used to back calculate the amount of surrogate retained in the slag during melting, which, except for heat number 94, should be equal to the amount deposited by plasma

spray plus the amount in the starting slag, assuming that the surrogate elements are not subject to substantial volatilization. The results of this mass balance are presented in Table 6.10. The results of this mass balance indicate that for heats 74 through 91, essentially no Neodymium was removed from the steel, which is sensible, as none was added. The last three columns of the table show the parts per million of surrogates present in the slag which originated in the stainless steel. Since the weight of each premelted bar is known, the original concentrations of the surrogate elements may be calculated. The results of this calculation are shown in Table 6.11.

These initial concentrations of surrogate elements calculated by this mass balance are much lower than those aimed for in the planning stages of this study. This may have been brought about by lack of calibration in the plasma spray process. Alternatively, there may be a loss of surrogates as volatile fluorides in the ESR process. The results indicate that very low amounts of both cerium and lanthanum were present during melts number 82, 84, and 85. Melts number 89, 93, and 90 should have contained increasing amounts of cerium as a lone surrogate. The results of mass balance calculations indicate that this may not have been the case, as shown in Figure 6.5.

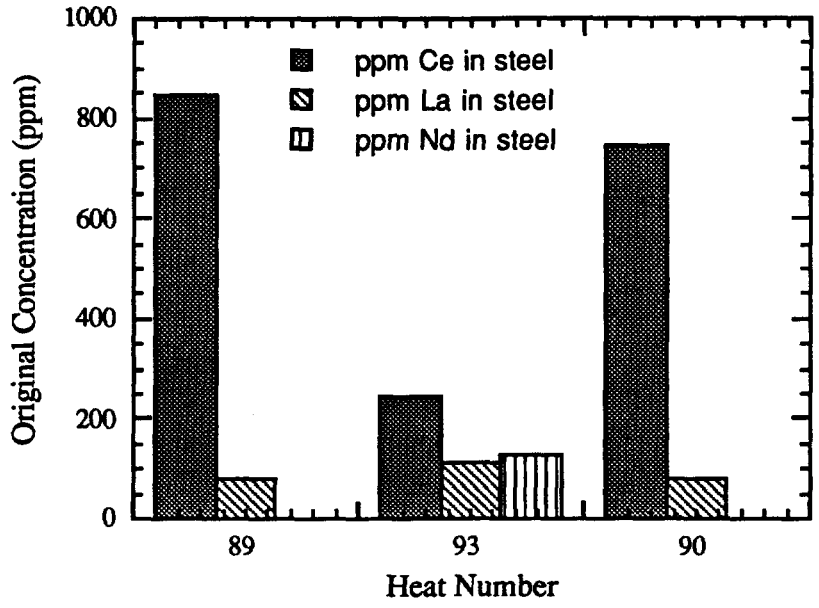


**Figure 6.5**
**Original Concentration of Surrogates in Heats 89, 93, and 90**

Calculation of the concentration of surrogates removed from the Montana Tech ingot by remelting may be added to the concentration of surrogates remaining in the ingot. As shown in Table 6.12, this mass balance shows a distinct lack of closure.

**Table 6.12**
**Mass Balance Discrepancy: Montana Tech Ingot**

| Element | Surrogate Concentration Before ESR (ppm) | Surrogate Concentration After ESR (ppm) | Amount removed* (ppm) | Discrepancy (ppm) |
|---|---|---|---|---|
| Ce | 1000 | 510 | 560.8 | 70.8 |
| La | 670 | 380 | 76.0 | -214 |
| Nd | 840 | 360 | 67.1 | -413 |

*Back calculated from slag chemistry

The discrepancy in the mass balance could have been the result of errors in sampling and weighing slag fractions. In addition, the preliminary ingot analysis of the master ingot may not have adequately represented the chemistry of the slice melted, Researchers at Montana Tech analyzed slices of their master melt ingot by various analytical techniques (X-ray fluorescence, ICP-MS, and INAA) and reported that surrogates were somewhat inhomogeneously distributed throughout the ingot. Their results also indicated that the reported concentration of surrogates varied according to the analytical technique used. Table 6.13 lists the concentrations of surrogates reported by the three analytical techniques for one sample of the master melt ingot.[2]

**Table 6.13**
**Differences in Reported Surrogate Concentrations of Montana Tech Master Melt According to Analytical Technique**

| Analytical Technique | Cerium (ppm) | Lanthanum (ppm) | Neodymium (ppm) |
|---|---|---|---|
| X-ray Fluorescence | 490 | 330 | 620 |
| INAA | 525 | 272 | 332 |
| ICP-Mass Spec | 510 | 300 | 450 |

The concentrations of surrogates present in the Montana Tech ingot, (Heat 94) after remelting by ESR were appreciable, which may indicate that, for the conditions used, ESR was not as effective in removing bulk concentrations of surrogate elements as those present as surface oxides.

## 6.4 Summary

The results of the experiments performed in this study showed that the surrogate concentration in the remelted stainless steel from the plasma sprayed "surface contaminated" material was below detectable limits for all melts performed except when slag was entrapped on an ingot surface. Slag chemistry did influence the change in chemistry of the steel for such elements as sulfur, phosphorous, and carbon. Slag conductivity also influenced the relationships between voltage and current during remelting.

# Chapter 6 Tables

**Table 6.1**
**Elemental Analysis of Ingot Slices by Spectrography**

| Heat | % C | % Mn | % Si | % Cr | %Ni | % Mo | % Cu | % S | % P | % Co |
|---|---|---|---|---|---|---|---|---|---|---|
| E2* | 0.022 | 1.378 | 0.462 | 18.540 | 10.970 | 0.759 | 0.330 | 0.014 | 0.026 | 0.118 |
| E3* | 0.024 | 1.529 | 0.838 | 18.130 | 9.920 | 0.478 | 0.243 | 0.017 | 0.027 | 0.150 |
| 74 | 0.023 | 1.295 | 0.410 | 17.545 | 10.330 | 0.415 | 0.245 | 0.008 | 0.027 | 0.150 |
| 75 | 0.024 | 1.420 | 0.550 | 18.095 | 10.185 | 0.465 | 0.270 | 0.005 | 0.028 | 0.160 |
| 76 | 0.023 | 1.400 | 0.500 | 18.220 | 10.190 | 0.455 | 0.260 | 0.007 | 0.028 | 0.160 |
| 77 | 0.031 | 1.380 | 0.515 | 18.210 | 10.170 | 0.450 | 0.260 | 0.008 | 0.028 | 0.160 |
| 78 | 0.025 | 1.385 | 0.490 | 18.205 | 10.195 | 0.450 | 0.265 | 0.008 | 0.028 | 0.160 |
| 79 | 0.024 | 1.405 | 0.585 | 18.220 | 10.170 | 0.450 | 0.260 | 0.006 | 0.027 | 0.160 |
| 80 | 0.024 | 1.370 | 0.615 | 18.025 | 10.175 | 0.455 | 0.265 | 0.009 | 0.028 | 0.160 |
| 81 | 0.023 | 1.370 | 0.525 | 18.135 | 10.190 | 0.450 | 0.275 | 0.007 | 0.027 | 0.160 |
| 82 | 0.024 | 1.280 | 0.290 | 18.135 | 11.380 | 0.790 | 0.350 | 0.007 | 0.025 | 0.130 |
| 83 | 0.023 | 1.245 | 0.110 | 18.350 | 11.340 | 0.775 | 0.345 | 0.006 | 0.025 | 0.120 |
| 84 | 0.025 | 1.260 | 0.270 | 18.215 | 11.352 | 0.780 | 0.365 | 0.008 | 0.025 | 0.120 |
| 85 | 0.024 | 1.250 | 0.165 | 18.220 | 11.380 | 0.765 | 0.340 | 0.006 | 0.025 | 0.120 |
| 86 | 0.023 | 1.395 | 0.545 | 18.095 | 10.180 | 0.460 | 0.270 | 0.006 | 0.028 | 0.160 |
| 88 | 0.023 | 1.360 | 0.525 | 18.150 | 10.200 | 0.460 | 0.275 | 0.007 | 0.028 | 0.160 |
| 89 | 0.026 | 1.275 | 0.360 | 17.615 | 11.000 | 0.750 | 0.345 | 0.007 | 0.025 | 0.125 |
| 90 | 0.022 | 1.210 | 0.090 | 18.300 | 11.310 | 0.760 | 0.345 | 0.008 | 0.025 | 0.120 |
| 91 | 0.023 | 1.385 | 0.515 | 18.245 | 10.160 | 0.450 | 0.260 | 0.009 | 0.028 | 0.160 |
| 92 | 0.025 | 1.280 | 0.215 | 18.280 | 11.325 | 0.770 | 0.340 | 0.007 | 0.025 | 0.120 |
| 93 | 0.027 | 1.425 | 0.650 | 17.935 | 10.040 | 0.470 | 0.270 | 0.007 | 0.028 | 0.160 |
| 94 | 0.0330 | 1.435 | 0.340 | 18.480 | 10.545 | 0.190 | 0.110 | 0.006 | 0.022 | 0.070 |

* E2 and E3 are spectrographic analysis of the starting material. Analytical results differ from those obtained by DC Plasma.

**Table 6.2**
**Difference Between Starting Material and Final Ingot Chemistry**

| Heat | % C | % Mn | % Si | % Cr | %Ni | % Mo | % Cu | % S | % P | % Co |
|---|---|---|---|---|---|---|---|---|---|---|
| 74 | 0.0010 | 0.234 | 0.428 | 0.585 | -0.410 | 0.0630 | -0.002 | 0.0090 | 0.00 | 0.00 |
| 75 | -0.0005 | 0.109 | 0.288 | 0.0350 | -0.265 | 0.0130 | -0.027 | 0.0115 | -0.001 | -0.010 |
| 76 | 0.00100 | 0.129 | 0.338 | -0.090 | -0.270 | 0.0230 | -0.017 | 0.0100 | -0.001 | -0.010 |
| 77 | -0.0070 | 0.149 | 0.323 | -0.080 | -0.250 | 0.0280 | -0.017 | 0.0090 | -0.001 | -0.010 |
| 78 | -0.0005 | 0.144 | 0.348 | -0.075 | -0.275 | 0.0280 | -0.022 | 0.0085 | -0.001 | -0.010 |
| 79 | 0.00 | 0.124 | 0.253 | -0.090 | -0.250 | 0.0280 | -0.017 | 0.0105 | -0.001 | -0.010 |
| 80 | 0.00 | 0.159 | 0.223 | 0.105 | -0.255 | 0.0230 | -0.022 | 0.0075 | -0.001 | -0.010 |
| 81 | 0.00050 | 0.159 | 0.313 | -0.00 | -0.270 | 0.0280 | -0.032 | 0.0095 | -0.001 | -0.010 |
| 82 | -0.0020 | 0.0980 | 0.172 | 0.405 | -0.410 | -0.031 | -0.020 | 0.0070 | 0.0005 | -0.012 |
| 83 | -0.0015 | 0.133 | 0.352 | 0.190 | -0.370 | -0.016 | -0.015 | 0.0080 | 0.0005 | -0.002 |
| 84 | -0.0035 | 0.118 | 0.192 | 0.325 | -0.382 | -0.021 | -0.035 | 0.0055 | 0.0005 | -0.002 |
| 85 | -0.0025 | 0.128 | 0.297 | 0.320 | -0.410 | -0.006 | -0.010 | 0.0075 | 0.0010 | -0.002 |
| 86 | 0.00050 | 0.134 | 0.293 | 0.0350 | -0.260 | 0.0180 | -0.027 | 0.0110 | -0.001 | -0.010 |
| 88 | 0.00050 | 0.169 | 0.313 | -0.020 | -0.280 | 0.0180 | -0.032 | 0.0095 | -0.001 | -0.010 |
| 89 | -0.0040 | 0.103 | 0.102 | 0.925 | -0.030 | 0.0090 | -0.015 | 0.0070 | 0.0005 | -0.007 |
| 90 | -0.0005 | 0.168 | 0.372 | 0.240 | -0.340 | -0.001 | -0.015 | 0.0060 | 0.0010 | -0.002 |
| 91 | 0.00050 | 0.144 | 0.323 | -0.115 | -0.240 | 0.0280 | -0.017 | 0.0080 | -0.001 | -0.010 |
| 92 | -0.0035 | 0.0980 | 0.247 | 0.260 | -0.355 | -0.011 | -0.010 | 0.0070 | 0.0010 | -0.002 |
| 93 | -0.0035 | 0.104 | 0.188 | 0.195 | -0.120 | 0.0080 | -0.027 | 0.0095 | -0.001 | -0.010 |

**Table 6.3**
**Nitrogen and Oxygen Analysis of Remelted Ingots**

| Heat | $N_2$ % | $O_2$ % |
|---|---|---|
| 74 | 0.1052 | 0.0074 |
| 75 | 0.0885 | 0.0080 |
| 76 | 0.1122 | 0.0071 |
| 77 | 0.1116 | 0.0064 |
| 78 | 0.1146 | 0.0057 |
| 79 | 0.1117 | 0.0069 |
| 80 | 0.1066 | 0.0061 |
| 81 | 0.1228 | 0.0088 |
| 82 | 0.0967 | 0.0069 |
| 83 | 0.1009 | 0.0058 |
| 84 | 0.0993 | 0.0081 |
| 85 | 0.1135 | 0.0064 |
| 86 | 0.1037 | 0.0105 |
| 87 | 0.1078 | 0.0077 |
| 88 | 0.1084 | 0.0107 |
| 89 | 0.0911 | 0.0081 |
| 90 | 0.1083 | 0.0087 |
| 91 | 0.1103 | 0.0068 |
| 92 | 0.1061 | 0.0063 |
| 93 | 0.0955 | 0.0111 |
| 94 | 0.0338 | 0.0061 |

**Table 6.4**
**Analysis of Remelted Ingots for the Presence of Surrogate Elements**

| Heat Number | Bulk | | | Surface | | |
|---|---|---|---|---|---|---|
| | Ce (ppm) | La (ppm) | Nd (ppm) | Ce (ppm) | La (ppm) | Nd (ppm) |
| 74 | <1 | <1 | <1 | | | |
| 75 | <1 | <1 | <1 | <1 | <1 | <1 |
| 76 | <1 | <1 | <1 | | | |
| 77 | <1 | <1 | <1 | | | |
| 78 | <1 | <1 | <1 | | | |
| 79 | <1 | <1 | <1 | | | |
| 80 | <1 | <1 | <1 | | | |
| 81 | <1 | <1 | <1 | | | |
| 82 | <1 | <1 | <1 | | | |
| 83 | <1 | <1 | <1 | | | |
| 84 | <1 | <1 | <1 | | | |
| 85 | <1 | <1 | <1 | 2.5 | 1.6 | <1 |
| 86 | <1 | <1 | <1 | | | |
| 88 | <1 | <1 | <1 | | | |
| 89 | <1 | <1 | <1 | | | |
| 90 | <1 | <1 | <1 | | | |
| 91 | <1 | <1 | <1 | <1 | <1 | <1 |
| 92 | <1 | <1 | <1 | | | |
| 93 | <1 | <1 | <1 | | | |
| 94 | 510 | 380 | 360 | | | |

**Table 6.6**
**Surface Quality Ratings of Remelted Ingots**

| Heat Number | Surface Quality Rating |
|---|---|
| 74 | good |
| 75 | poor |
| 76 | excellent |
| 77 | excellent |
| 78 | average |
| 79 | good |
| 80 | average |
| 81 | good |
| 82 | good |
| 83 | average |
| 84 | good |
| 85 | poor |
| 86 | average |
| 88 | good |
| 89 | good |
| 90 | good |
| 91 | excellent |
| 92 | good |
| 93 | good |
| 94 | average |

**Table 6.7**
**Averages of Voltage, Power, Current, and Impedance from Melt Tests**

| Heat # | Vav (volts) | Iav (Kamps) | Pav (kW) | Impedance |
|---|---|---|---|---|
| 74 | 35.024 | 0.84752 | 29.684 | 41.076 |
| 75 | 27.187 | 0.94563 | 25.685 | 28.891 |
| 76 | 42.887 | 0.71937 | 30.902 | 61.742 |
| 77 | 40.004 | 0.80907 | 32.458 | 49.314 |
| 78 | 40.987 | 0.55957 | 22.953 | 71.798 |
| 79 | 31.984 | 0.96467 | 30.696 | 31.284 |
| 80 | 36.927 | 0.72013 | 26.700 | 51.383 |
| 81 | 35.015 | 0.84911 | 29.700 | 42.356 |
| 82 | 37.031 | 0.92795 | 34.557 | 39.853 |
| 83 | 34.989 | 0.75163 | 26.310 | 46.497 |
| 84 | 35.970 | 0.67360 | 24.230 | 51.164 |
| 85 | 36.222 | 0.68980 | 25.061 | 51.567 |
| 86 | 30.992 | 0.88939 | 27.654 | 33.456 |
| 88 | 34.997 | 0.98653 | 34.774 | 37.018 |
| 89 | 33.093 | 0.85453 | 28.352 | 40.777 |
| 90 | 34.995 | 0.86355 | 30.111 | 41.022 |
| 91 | 41.983 | 0.91286 | 38.053 | 46.342 |
| 92 | 35.007 | 0.87668 | 30.815 | 41.099 |
| 93 | 35.007 | 0.85753 | 30.081 | 39.906 |

**Table 6.8**
**Comparison of Calculated vs. Measured Conductivity**

| Heat # | Melt conductivity ($ohm^{-1}cm^{-1}$) | Calculated conductivity ($ohm^{-1}cm^{-1}$) |
|---|---|---|
| 74 | 3.3878 | 3.3377 |
| 75 | 4.8695 | 4.5978 |
| 76 | 2.3483 | 2.4849 |
| 77 | 2.8314 | 3.2071 |
| 78 | 1.9113 | 1.7515 |
| 79 | 4.2225 | 4.2983 |
| 80 | 2.7302 | 2.0382 |
| 81 | 3.3950 | 3.3377 |
| 82 | 3.5082 | 5.1988 |
| 83 | 3.0075 | 3.4587 |
| 84 | 2.6217 | 2.3367 |
| 85 | 2.6661 | 2.5013 |
| 86 | 4.0176 | 4.3843 |
| 88 | 3.9464 | 3.3377 |
| 89 | 3.6151 | 3.3377 |
| 90 | 3.4547 | 3.3377 |
| 91 | 3.0441 | 4.3482 |
| 92 | 3.5060 | 3.3377 |
| 93 | 3.4294 | 3.3377 |

**Table 6.9**
**Analysis of Slag Caps and Slag Skins for Surrogate Elements**

| Heat # | Ce skin ppm | La skin ppm | Nd skin ppm | wt. skin (g) | Ce cap ppm | La cap ppm | Nd cap ppm | wt. cap (g) |
|---|---|---|---|---|---|---|---|---|
| 74 | 3500.0 | 5100.0 | 220.00 | 245.00 | 7300.0 | 11400 | 170.00 | 1206.0 |
| 75 | 4600.0 | 7100.0 | 150.00 | 973.00 | 11000 | 22000 | 170.00 | 714.00 |
| 76 | 4500.0 | 6200.0 | 160.00 | 334.00 | 6700.0 | 12000 | 130.00 | 1554.0 |
| 77 | 3300.0 | 4600.0 | 260.00 | 344.00 | 7700.0 | 10000 | 200.00 | 1317.0 |
| 78 | 2300.0 | 3500.0 | 92.000 | 381.00 | 7000.0 | 10000 | 120.00 | 1385.0 |
| 79 | 4300.0 | 5400.0 | 210.00 | 227.00 | 9500.0 | 12000 | 230.00 | 1510.0 |
| 80 | 5800.0 | 6800.0 | 180.00 | 743.00 | 11000 | 13000 | 170.00 | 1107.0 |
| 81 | 4900.0 | 7000.0 | 210.00 | 415.00 | 6600.0 | 10000 | 170.00 | 1377.0 |
| 82 | 500.00 | 730.00 | 180.00 | 299.00 | 500.00 | 670.00 | 170.00 | 1556.0 |
| 83 | 3600.0 | 6800.0 | 150.00 | 586.00 | 7600.0 | 12000 | 160.00 | 1263.0 |
| 84 | 1000.0 | 1100.0 | 180.00 | 341.00 | 1200.0 | 1800.0 | 170.00 | 1479.0 |
| 85 | 340.00 | 510.00 | 110.00 | 541.00 | 530.00 | 590.00 | 120.00 | 1294.0 |
| 86 | 5200.0 | 8100.0 | 220.00 | 448.00 | 7400.0 | 13000 | 190.00 | 1383.0 |
| 88 | 3800.0 | 4900.0 | 220.00 | 393.00 | 6200.0 | 9200.0 | 180.00 | 1404.0 |
| 89 | 4300.0 | 520.00 | 200.00 | 226.00 | 6000.0 | 700.00 | 170.00 | 1418.0 |
| 90 | 9100.0 | 1500.0 | 170.00 | 593.00 | 6600.0 | 640.00 | 190.00 | 1084.0 |
| 91 | 2400.0 | 3300.0 | 180.00 | 287.00 | 6200.0 | 8600.0 | 160.00 | 1628.0 |
| 92 | 2400.0 | 2800.0 | 2700.0 | 376.00 | 3700.0 | 4000.0 | 4200.0 | 1293.0 |
| 93 | 4800.0 | 3300.0 | 3700.0 | 558.00 | 1600.0 | 260.00 | 240.00 | 1224.0 |
| 94 | 2500.0 | 270.00 | 210.00 | 1142.0 | 1900.0 | 1300.0 | 1400.0 | 240.40 |

**Table 6.10**
**Mass Balance of Surrogate Elements**

| Heat # | Ce total in slag (ppm) | La total in slag (ppm) | Nd total in slag (ppm) | Ce conc. start (ppm) | La conc. start (ppm) | Nd conc. start (ppm) | Ce taken out (ppm) | La taken out (ppm) | Nd taken out (ppm) |
|---|---|---|---|---|---|---|---|---|---|
| 74 | 6658.4 | 10336 | 178.44 | 351 | 172 | 172 | 6307.4 | 10164 | 6.4400 |
| 75 | 7308.7 | 13406 | 158.46 | 327 | 160 | 160 | 6981.7 | 13246 | -1.5400 |
| 76 | 6310.8 | 10974 | 135.31 | 256 | 125 | 125 | 6054.8 | 10849 | 10.310 |
| 77 | 6788.7 | 8881.6 | 212.43 | 403 | 197 | 197 | 6385.7 | 8684.6 | 15.430 |
| 78 | 5986.0 | 8597.7 | 113.96 | 211 | 103 | 103 | 5775.0 | 8494.7 | 10.960 |
| 79 | 8820.4 | 11137 | 227.39 | 445 | 218 | 218 | 8375.4 | 10919 | 9.3900 |
| 80 | 8911.6 | 10510 | 174.02 | 322 | 158 | 158 | 8589.6 | 10352 | 16.020 |
| 81 | 6206.3 | 9305.2 | 179.26 | 351 | 172 | 172 | 5855.3 | 9133.2 | 7.2600 |
| 82 | 500.00 | 679.67 | 171.61 | 320 | 160 | 160 | 180.00 | 519.67 | 11.610 |
| 83 | 6332.3 | 10352 | 156.83 | 304 | 149 | 149 | 6028.3 | 10203 | 7.8300 |
| 84 | 1162.5 | 1668.8 | 171.87 | 304 | 149 | 149 | 858.50 | 1519.8 | 22.870 |
| 85 | 473.98 | 566.41 | 117.05 | 213 | 104 | 104 | 260.98 | 462.41 | 13.050 |
| 86 | 6861.7 | 11801 | 197.34 | 397 | 194 | 194 | 6464.7 | 11607 | 3.3400 |
| 88 | 5675.1 | 8259.6 | 188.75 | 351 | 172 | 172 | 5324.1 | 8087.6 | 16.750 |
| 89 | 5766.3 | 675.26 | 174.12 | 351 | 172 | 172 | 5415.3 | 503.26 | 2.1200 |
| 90 | 7484.0 | 944.10 | 182.93 | 351 | 172 | 172 | 7133.0 | 772.10 | 10.930 |
| 91 | 5630.5 | 7805.7 | 163.00 | 327 | 160 | 160 | 5303.5 | 7645.7 | 3.0000 |
| 92 | 3407.1 | 3729.7 | 3862.1 | 351 | 172 | 172 | 3056.1 | 3557.7 | 3690.1 |
| 93 | 2602.0 | 1211.9 | 1323.4 | 351 | 172 | 172 | 2251.0 | 1039.9 | 1151.4 |
| 94* | 2395.7 | 449.12 | 416.94 | 351 | 172 | 172 | 2044.7 | 277.12 | 244.94 |

* 94 had surrogates incorporated into it by plasma melting.

**Table 6.11**
**Original Concentrations of Surrogate in Steel (Calculated)**

| Heat number | Original Ce Concentration ppm | Original La Concentration ppm | Original Nd Concentration ppm |
|---|---|---|---|
| 74 | 657.1 | 1058.9 | 0.7 |
| 75 | 731.8 | 1388.5 | 0.0 |
| 76 | 785.9 | 1408.1 | 1.3 |
| 77 | 737.0 | 1002.3 | 1.8 |
| 78 | 716.3 | 1053.7 | 1.3 |
| 79 | 903.9 | 1178.5 | 1.0 |
| 80 | 968.7 | 1167.5 | 1.8 |
| 81 | 721.3 | 1125.1 | 0.9 |
| 82 | 22.5 | 64.9 | 1.4 |
| 83 | 679.5 | 1150.1 | 0.9 |
| 84 | 107.4 | 190.15 | 2.9 |
| 85 | 32.2 | 57.1 | 1.6 |
| 86 | 721.6 | 1295.6 | 0.4 |
| 88 | 618.2 | 939.2 | 1.9 |
| 89 | 846.0 | 78.6 | 0.3 |
| 90 | 743.3 | 80.4 | 1.1 |
| 91 | 683.6 | 985.5 | 0.4 |
| 92 | 350.6 | 408.2 | 423.4 |
| 93 | 246.9 | 114.0 | 126.3 |
| 94* | 560.8 | 76.0 | 67.1 |

* Numbers represent the concentration removed from the ingot by remelting

# Chapter 6 References

[1] Hara, S., Hashimoto, H., Ogino, K. "Electrical Conductivity of Molten Slags for Electroslag Remelting" *Transactions ISIJ*, Volume 23, (1983), 1053-1058.

[2] Worcester, S.A., Twidwell, L.G., Paolini, D.J., Weldon, T.A., Mizia, R.E. (Ed.) "Decontamination of Metals by Melt Refining/Slagging,: First Year Progress Report," WINCO-1138, INEL-DOE, (1995).

# Chapter 7
# Results of Thermodynamic Modeling Studies

The purposes of the thermodynamic modeling performed in this study were to quantitatively predict the transfer of surrogate elements or radionuclides from the liquid steel into the slag phase and to determine the compounds which may be formed by these elements in the slag phase. In previous chapters, Ellingham diagrams have been used to show that both the surrogate elements and the radionuclides which they represent form very stable oxides. In addition, predominance area diagrams have been used to show that these elements may also form fluorides, sulfides, oxysulfides, and oxyaluminates in a complex chemical environment at high temperatures. Examples have been presented which show that the extent of partitioning of an element between a liquid metal and a slag may be estimated if the compound which the element forms in the slag is known so that an equilibrium reaction may be written. For complex systems, however, many reactions may be occurring simultaneously and the products of these reactions may influence other reactions. The final chemical equilibrium assumed by such a system, at which its free energy is at a minimum (or as close to a minimum as the governing kinetics will allow) determines the effectiveness of elemental partitioning.

Thus, free energy minimization techniques were used for the estimation of elemental partitioning between a multicomponent alloy, stainless steel, and various slags composed of oxides and fluorides. Free energy minimization also allows the prediction of the chemical species which may be formed as well as their relative amounts. The accuracy of such predictions depends on the validity of the thermochemical descriptions used to model the phases present. Free energy minimization calculations were performed with the assumption that the slag phase behaves as an ideal solution. Because the electrical behavior of molten ESR slags indicates that they are ionic in nature, separate calculations were performed using an ionic solution model to predict the amounts of surrogate bearing species which may be formed in various slags.

## 7.1 Free Energy Minimization

In order to model the thermochemical phenomena which occur during melting it is necessary to mathematically describe the slag and metallic solutions and the interactions between them. The extent of partitioning of various species during melting is determined by the temperature of the melt and the activities of the components in the oxide and metal phases. The activities are themselves thermodynamic properties and their values must be determined or assumed in order to perform calculations of phase equilibria. Various solution models have been developed for describing metallic solutions. Other models have been developed for slags. In this study, the liquid steel was assumed to behave according to the modified dilute interaction model by Pelton and Bale[1]. The slag was described as an ideal solution.

The central problem in the calculation of thermodynamic equilibria between a liquid metal and a slag phase is to obtain a representation of the Gibbs energy of the total system as a function of temperature, pressure, and composition. The equilibrium state is then obtained by minimizing the total Gibbs energy with respect to the amount and composition of the phases under various conditions. The total Gibbs energy of the system is simply given by the weighted sum of the Gibbs energies of the individual phases at equilibrium. If the phase is a pure substance the Gibbs energy can usually be obtained from standard sources of thermochemical data. The Gibbs energies of solution phases are more complicated to express. An important parameter for a solution phase is the Gibbs energy of mixing $\Delta G^{mix}$ which is the change in Gibbs energy accompanying the formation of a solution by its components. For an ideal solution, $\Delta G^{mix}$ is simply given by the configurational entropy change on forming the solution. In a nonideal solution, however, $\Delta G^{mix}$ will be given by the ideal configurational contribution plus an excess Gibbs energy term $G^{ex}$. The modeling of multicomponent systems is mainly concerned with deriving suitable representations of $G^{ex}$ which reproduce the experimental phase relationships of a particular system. An important requirement in the construction of solution models is that assessments of the individual subsystems are interconsistent, for example, in the assessment of the binary systems the same data must be used for the pure component in each phase.[2] Having derived representations for the Gibbs energies of all the phases in a system, the equilibrium state may then be determined by minimizing the total Gibbs energy.

### 7.1.1 Modeling Experiments

Free energy minimization is an iterative process best performed by computer. Several software packages are available, some of which include extensive thermochemical databases. The F*A*C*T* thermochemical software[3] was used in this research. In order to predict the theoretical partitioning of surrogate elements between the molten steel and slags of various chemistries, the total chemistry of each system to be studied was entered along with the temperatures of interest. All simulations were performed at one atmosphere total pressure. Solution models were chosen for the liquid metal and the slag and the constituents of interest in each phase were chosen. A modified dilute solution model was used to describe the steel solution. This model is valid up to alloying compositions of several percent. High concentrations of nickel and chromium in the stainless steel exceeded the limitations of the modified dilute solution model by several percent but all other elements fell well within the concentration limits of the model. The alternative to using the modified dilute solution model would have been to create a liquid model appropriate for the stainless steel. This was attempted and found to be quite difficult because of the scarcity of high temperature thermodynamic data describing activity coefficients and interaction coefficients. To complicate matters further, the data which is available is often contradictory. Stainless steel is a difficult solution to describe thermodynamically because, while many of its components are present in quantities which make a dilute solution treatment applicable, others, namely nickel and chromium, are not. The slag was described by an ideal solution model and assumed to consist of oxides and fluorides of the elements as well as more complex compounds containing oxygen and fluorine.

So that comparisons could be made between melting and modeling data, each melting experiment which was planned was also modeled by free energy minimization techniques. So that the results of the modeling experiments could be compared with one another, a single steel chemistry was used for each run. The chemistry of the steel used in the model was an average of the chemistries of Master Melts E2 and E3, as shown in Table 7.1. For each experiment that was modeled, appropriate amounts of surrogate elements were included, as were the components making up each individual slag.

Simulations to study the effect of the chemistry of the slag used in melt refining on the final composition of the ingot produced were performed at an assumed melting temperature of 1700°C. The concentrations of surrogate elements used were the same as those planned for the melting studies: 2500 ppm Ce and 2500 ppm La. The final steel chemistries, in terms of major alloying elements, predicted for each melt are given in Table 7.2. The chemistry changes between the initial steel chemistry and the final steel chemistry

(as predicted by free energy minimization) were calculated and are given in Table 7.3 . These chemistry changes were calculated by subtracting the final composition from the initial composition, so a negative number means that the concentration of that element was increased. The model predicts that the steel will increase in Fe, Cr, Ni, Mo, Co, C, O, Al, and Ca. In some cases, these increases are the result of the concentration of some elements in the metal as others are lost to the slag. In other cases, the concentration of an element may increase as a result of transfer from the slag phase. The model predicts that the metal will lose manganese, as well as sulfur, calcium, and silicon in most cases.

The elemental changes predicted for several elements may be shown to be influenced by the chemistry of the slag, although the relationships are not always straightforward. The chemistries of the various slags used have been plotted on a ternary grid by heat number and are shown in Figure 7.1. The amounts of major species formed in the slag for the various experimental melts are predicted by free energy minimization calculations are listed in Table 7.4 as percentages of the weight of the slag.

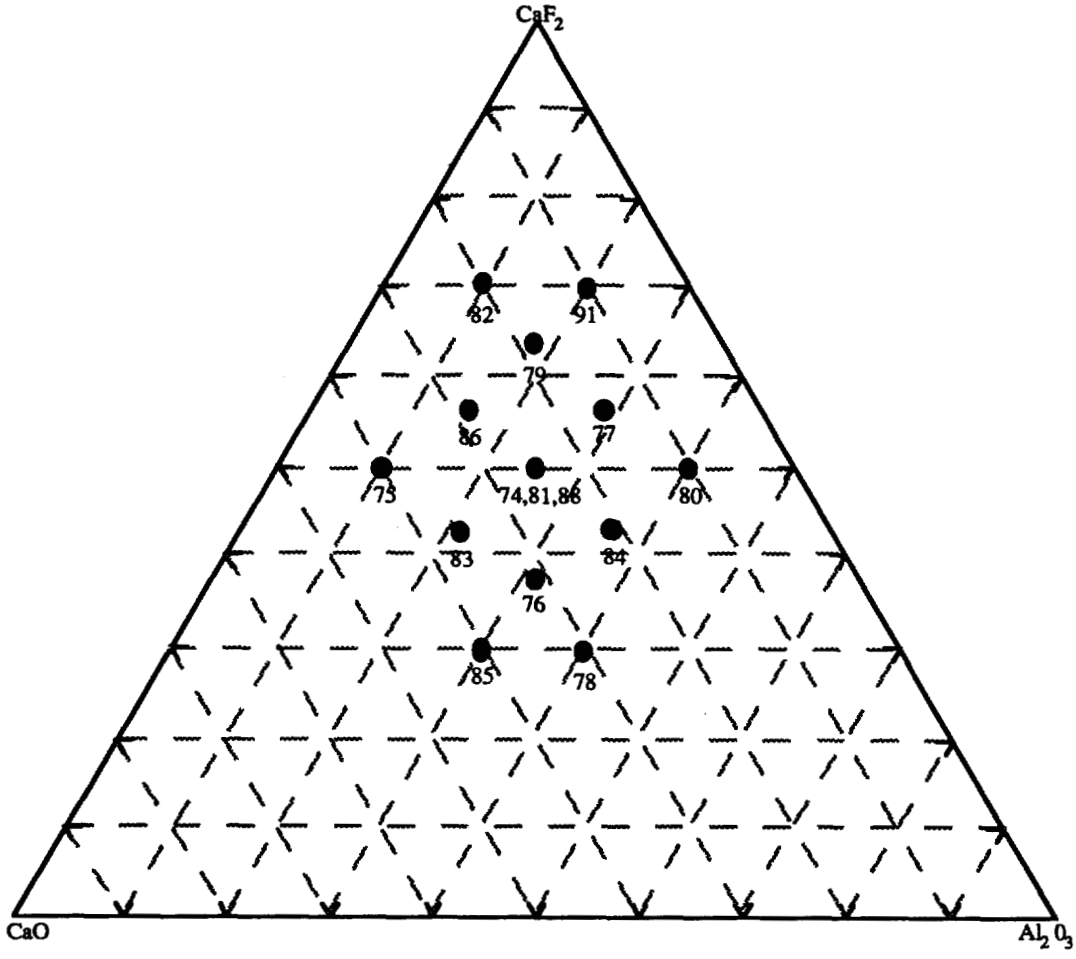


**Figure 7.1**
**Ternary Representation of Slag Chemistries by Heat Number**

The distribution of an element between a metal and a slag is governed by the species formed by the element when it contacts the slag phase. The amount of any species is governed not only by its own stability, but by the stability of other compounds with which it may compete for the elements of which it is composed. In order to illustrate this, the predicted changes in the manganese and silicon contents of the steel as influenced by the chemistry of the slag are examined below.

### 7.1.1.1 Manganese Loss as Affected by Slag Chemistry

Free energy minimization predicts that manganese will be lost from the steel to form $MnAlO_4$ and MnO. It would be expected, therefore that the loss in manganese would be related to the alumina content of the slag. This did not prove to be true, as shown in Figure 7.2.

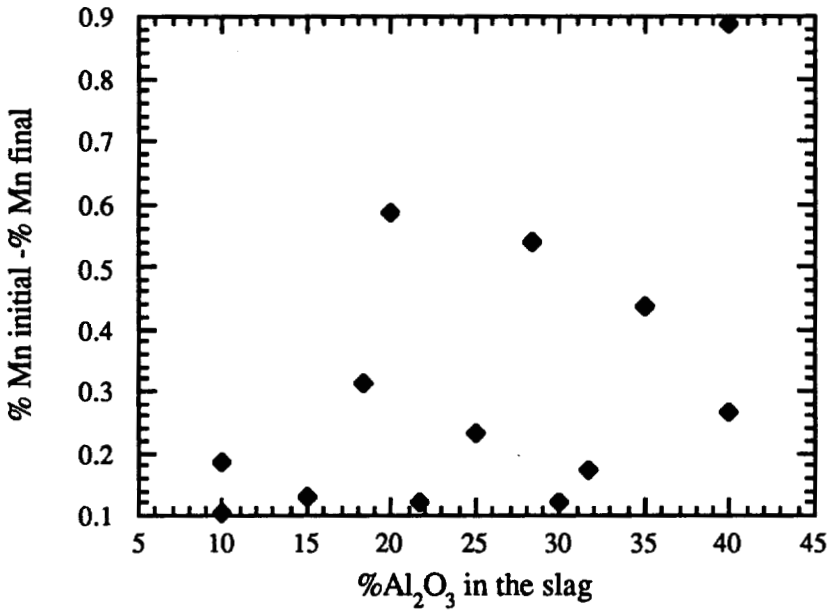


**Figure 7.2**
**Predicted Decrease in Manganese Content of the Steel at 1700°C as Related to Initial Alumina Content of the Slag**

The predicted manganese lost for each heat modeled was found to be related to the calcium oxide content of the slag, however, though not in the expected manner, as shown in Figure 7.3. As the calcia content of the slag was increased, free energy minimization predicted that the manganese loss from the steel would be decreased, indicating that the oxygen contained in slags rich in CaO does not directly contribute to the oxidation of manganese to form MnO.

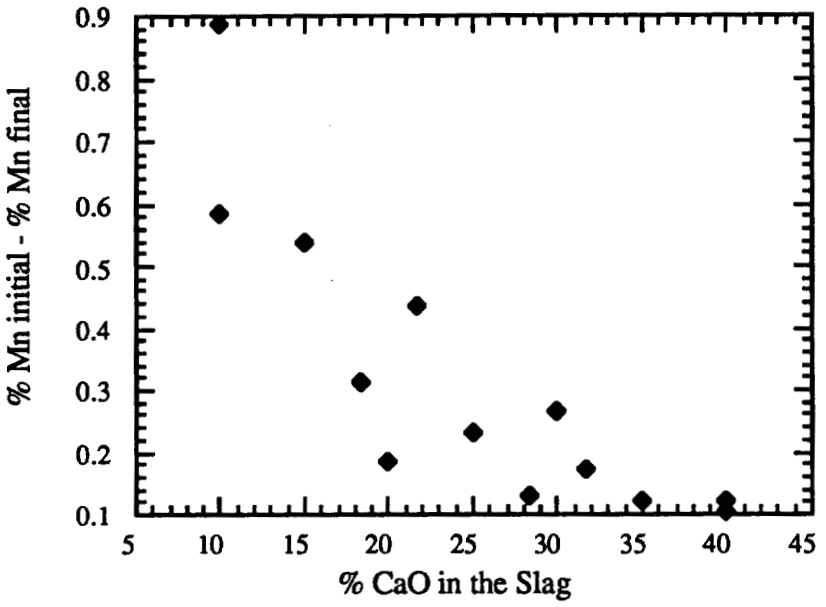


**Figure 7.3**
**Predicted Decrease in Manganese Content of the Steel at 1700°C as Related to Initial Calcia Content of the Slag**

Examination of the predicted loss of manganese for each heat modeled (Figure 7.4) shows the greatest loss associated with heat number 80. The slag associated with this heat initially contained 40% alumina, which could contribute to the formation of manganese aluminates in the slag. The next greatest loss of manganese from the steel, however, was predicted for heat 91, whose slag contained only 10% calcia and 20% alumina. If the predicted manganese loss is a result of the formation of oxides and aluminates, it would be expected that more manganese should be transferred to the slag as a result of melting in

contact with the slag from heat 78, which contained 30% calcia and 40% alumina than for the high fluoride slag used in heat 91.

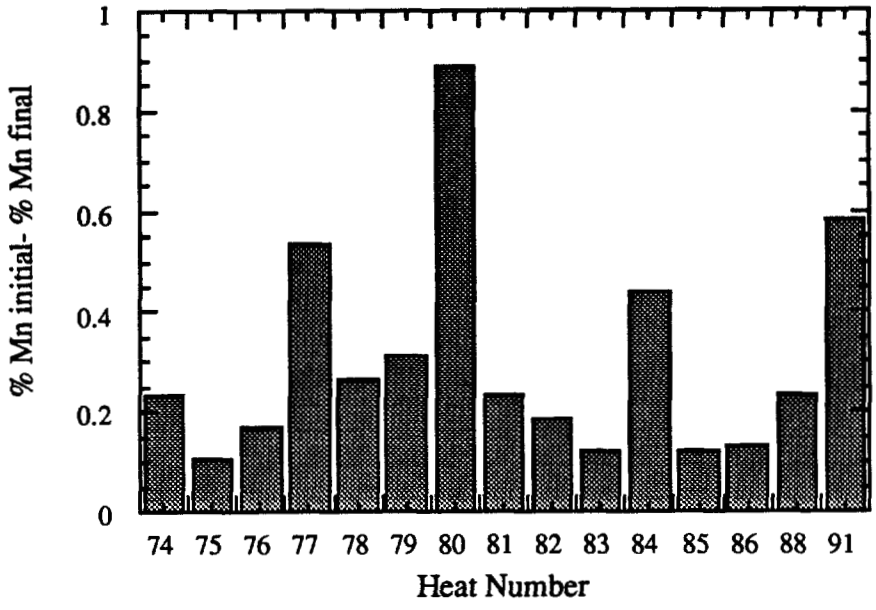


**Figure 7.4**
**Predicted Loss of Manganese from the Steel for each Heat Modeled at 1700°C**

There must be, therefore, another compound which competes with manganese in the formation of oxygen and aluminum bearing compounds. This is illustrated by Figure 7.5, which shows that, for the slag of heat 78, the formation of manganese aluminate is precluded by the formation of the more stable calcium aluminate. Manganese aluminate will form when there is insufficient calcia in the slag to react stoichiometrically with the alumina present.

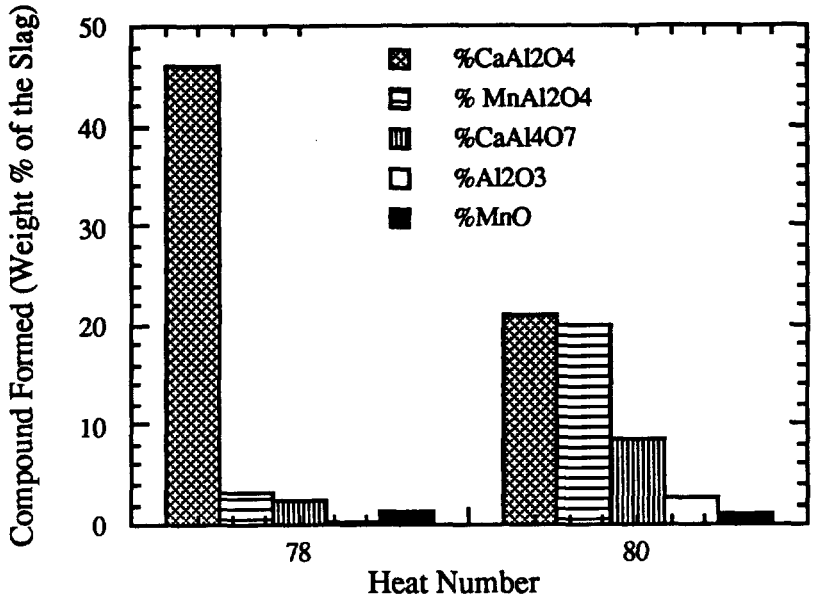


**Figure 7.5**
**Comparison of Predicted Quantities of Calcium, Aluminum, and Manganese Bearing Compounds in the Slag at 1700°C for Two Heats**

The loss of manganese predicted as a result of melting under slags of various chemistries was shown to be dependent not only on the stability of the manganese bearing compounds in the slag, but also on the stability and stoichometry of other competing compounds.

### 7.1.1.2 Silicon Loss as Affected by Slag Chemistry

Free energy minimization predicts that silicon should be lost from the steel to the slag, except in the case of heat 80, whose slag initially contained 50% calcium fluoride, 10% calcia, and 40% $Al_2O_3$. The predicted silicon loss for each heat modeled is shown in Figure 7.6. This figure shows that silicon loss is predicted to be greatest for heats 75, 83, and 85. Each of these heats made use of a slag containing between 35 and 40% calcia.

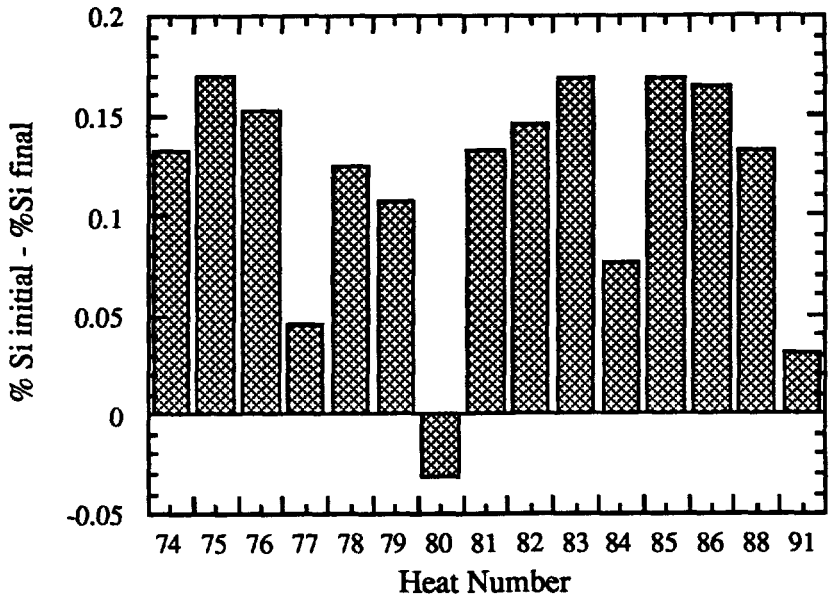


**Figure 7.6**
**Predicted Change in the Silicon Content of the Steel for Each Heat Modeled at 1700°C**

The loss of silicon from the steel is predicted to be greatest when slags containing more than 30% CaO are used. Free energy minimization predicts that silicon will combine with calcia in the slag to form $Ca_2SiO_4$, therefore silicon loss generally increases with increasing CaO content of the slag, as illustrated by Figure 7.7. Alumina in the slag affects silicon removal in two important ways. Silicon combines with calcia and alumina to form $Ca_2Al_2SiO_7$. In this way, the presence of alumina in the slag aids the removal of silicon from the steel. The presence of alumina may also impede the removal of silicon from steel, however, as is evidenced by the modeled results for heat 80, which illustrate that calcium will form calcium aluminates in preference to calcium silicates or calcium aluminum silicates, thus limiting the removal of silicon from the steel.

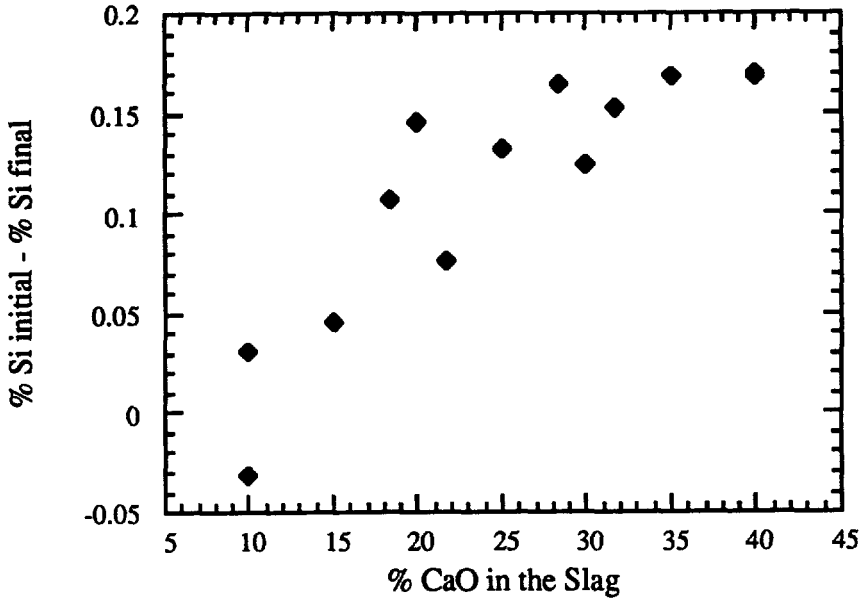


**Figure 7.7**
**Predicted Decrease in Silicon Content of the Steel at 1700°C as Related to Initial Calcia Content of the Slag**

### 7.1.1.3 Surrogate Loss as Affected by Slag Chemistry

Free energy minimization was used to predict the residual concentration of lanthanum and cerium in the steel for each melt. In order to determine the effect of temperature on the residual amounts of surrogates in the steel, modeling was performed for equlibria at 1600, 1700, 1800 and 1900°C. The results of these predictions for cerium are presented in Table 7.5 and those for lanthanum are presented in Table 7.6. The effect of temperature on the predicted quantities of cerium residuals in the steel produced by heat 74 is shown in Figure 7.8. Free energy minimization predicts that partitioning to a slag will be less effective as temperature increases. This is due to the fact that the free energies of formation of compounds which are formed by the surrogates in the slag are more negative at lower temperatures. The thermodynamic model used in this research does not account for the increase in reaction rates promoted by high temperature melting which may offset lower thermodynamic driving forces.

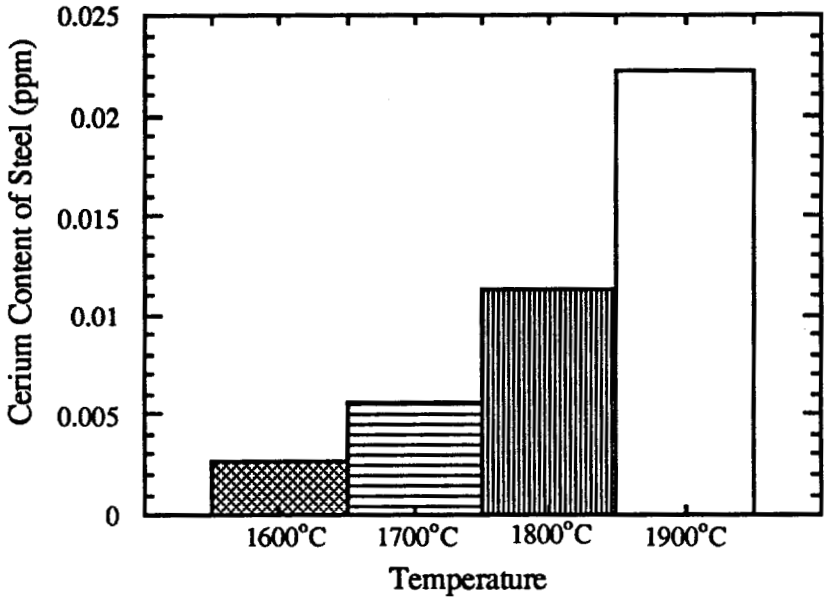


**Figure 7.8**
**Predicted Cerium Content of the Steel Produced by Heat 74 as a Function of Melting Temperature**

A comparison of the residual amounts of cerium and lanthanum which the model predicts will remain in the steel indicates that lanthanum will be more effectively removed from the steel than cerium. The fluoride and oxysulfide compounds formed by lanthanum are slightly more stable than those formed by cerium. The surrogate containing compounds which are predicted to form in the slag at 1700°C and their concentrations as weight percentages of the slag are listed in Table 7.7.

The ability of a slag to effect the removal of an element from a steel hinges upon the types and quantities of compounds which may be formed by the element and available ions in the slag. Cerium and lanthanum may be removed from the steel by the formation of stable oxides, fluorides, oxysulfides, and oxyaluminates. In order to determine which slags are predicted to best remove surrogate elements from the metal, the residual cerium in the steel was compared on a heat by heat basis in Figure 7.9.

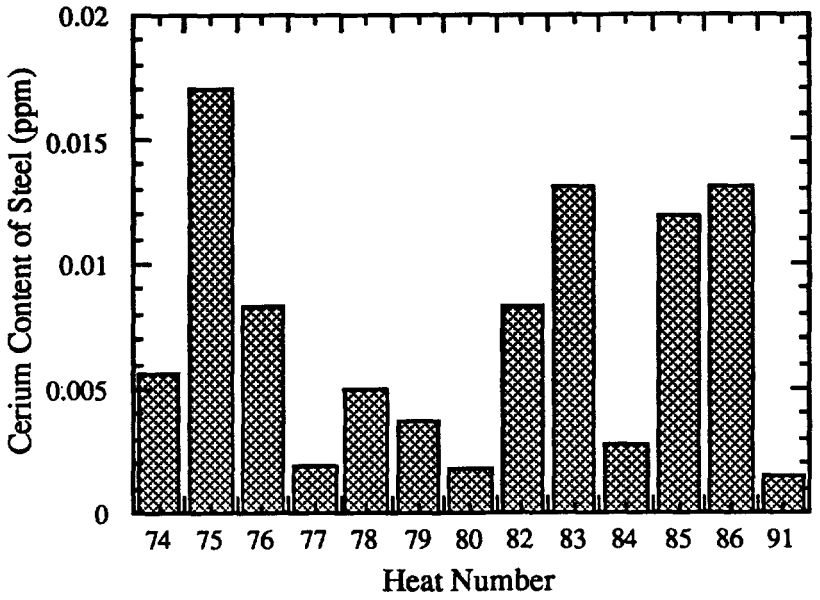


**Figure 7.9**
**Predicted Residual Cerium Content**
**of the Steel for Each Heat Modeled at 1700°C**

Free energy minimization predicts that cerium will be most effectively removed from the steel by the slags used in heats 77, 80, and 91 and least effectively by the slags used in heats 75, 83, and 86. This is also true for lanthanum. Figure 7.10 shows a comparison of the amounts of cerium bearing species formed in the slag for each of these heats. The figure shows that, while each slag is predicted to encourage the formation of $AlCeO_3$, the slags used in heats 77, 80, and 91 also permit the formation of $CeF_3$ and the slag used in heat 77 allows a significant amount of $CeO_2$ to form as well. Except for the fact that lanthanum forms $La_2O_3$ while cerium predominantly forms $CeO_2$, lanthanum behaves in much the same way.

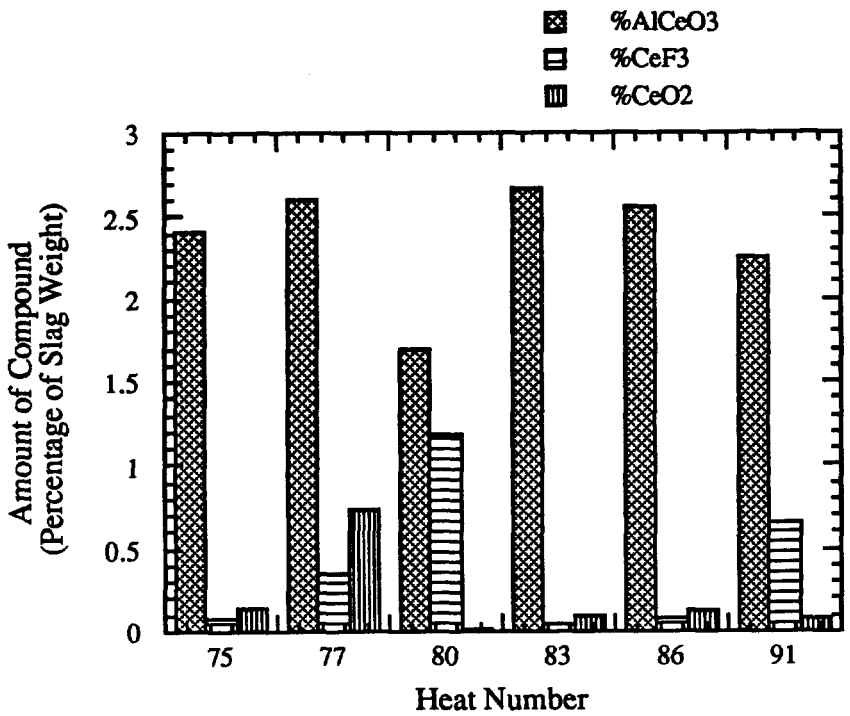


**Figure 7.10**
**Predicted Amounts of Cerium Bearing Compounds in the Slags for Several Heats at 1700°C**

### 7.1.1.4 Uranium Loss as Affected by Slag Chemistry

In order to determine the affect of slag chemistry on predicted uranium partitioning, free energy minimization modeling was performed for stainless steels containing 2500 ppm uranium melted in contact with the same slags used for surrogate modeling at 1700°C. A comparison of the predicted residual uranium content of the steels on a heat by heat basis is presented in Figure 7.11.

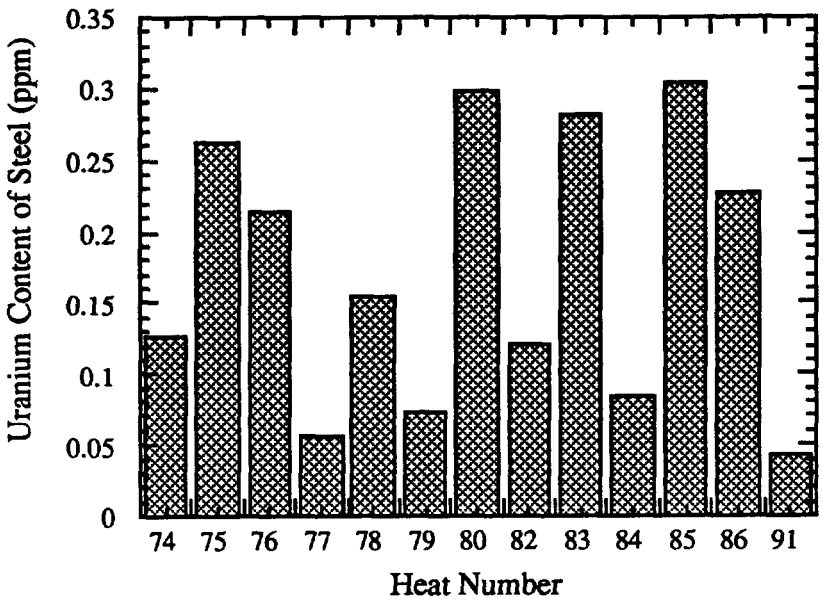


**Figure 7.11**
**Predicted Residual Uranium Content**
**of the Steel for Each Heat Modeled at 1700°C**

This graph shows that uranium is predicted to be most effectively removed from steel by the slags used for heats 91, 77, 79, and 84 and least effectively removed by the slags used for heats 85, 80, 83, and 75. This suggests that cerium and lanthanum are collected into the slag by different mechanisms than uranium. Unlike cerium and lanthanum, uranium is not predicted to form aluminates. Free energy minimization does predict the formation of $UF_4$, but only in minuscule quantities (approximately 1 ppb in the slag). Other uranium species are not predicted, either because thermodynamic data was unavailable or because the presence of gaseous species such as $UF_6$ is not predicted when systems are modeled at one atmosphere of pressure. In the free energy minimization modeling performed, the major mechanism by which uranium is removed from the steel is by the formation of $UO_2$. The slags which should most effectively achieve this removal are those which are able to supply the greatest amounts of available oxygen. When present in a one to one stiochiometric ratio, alumina and calcia are bound together as $CaAl_2O_4$ ($CaO$-$Al_2O_3$). Due to the stability of this compound, the oxygen it contains is not available for the

oxidation of uranium. Figure 7.12 shows the amount of this compound predicted for each slag.

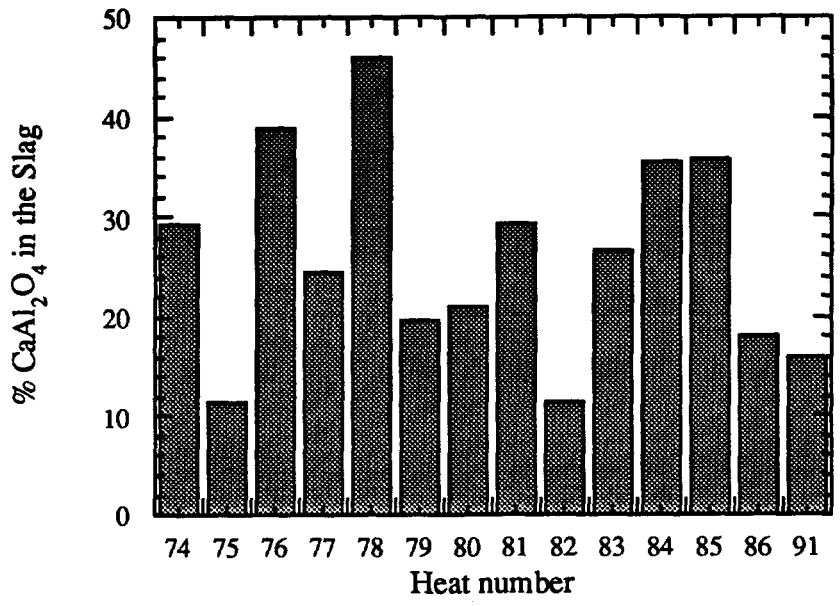


**Figure 7.12**
**Predicted $CaAl_2O_4$ Content**
**of the Slag for Each Heat Modeled at 1700°C**

If, after the formation of calcium aluminate, excess CaO is present in the slag, uranium will not be oxidized. If, however, excess $Al_2O_3$ is present, the oxidation of uranium may take place. The free energy of formation of $UO_2$ per mole of oxygen is more negative than that of alumina though less negative than that of calcia. Uranium, therefore, is able to become an oxide by reacting with available alumina in the slag. Figure 7.13 compares the amount of alumina available for reaction after the formation of calcium aluminates for each slag. This graph shows that, of the slags modeled, the greatest amounts of alumina are available for reaction with uranium in heats 80, 91, 77, and 84.

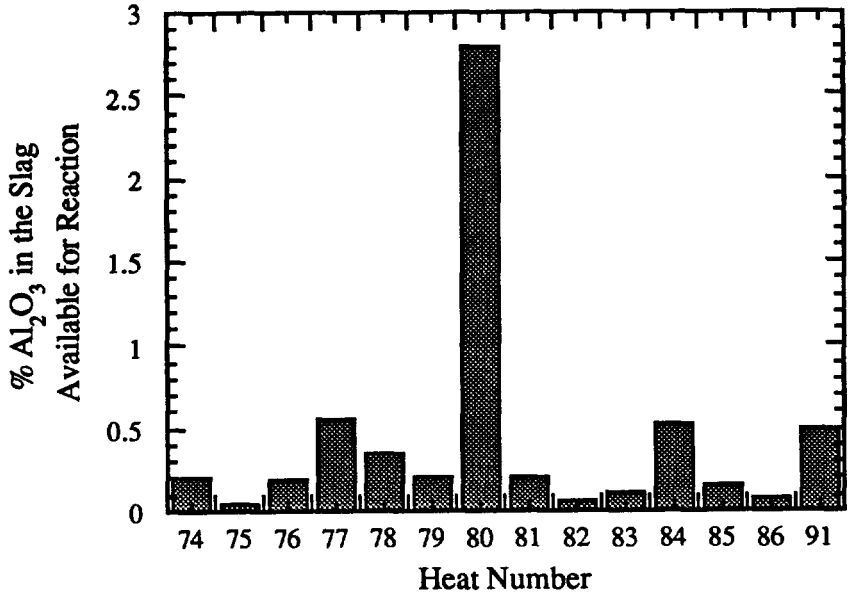


**Figure 7.13**
**Predicted Amount of Alumina in the Slag Available for Reaction for Each Heat Modeled at 1700°C**

The model predicts that for heat number 80 a great deal of alumina is available for reaction with uranium, yet the slag from this heat was not predicted to effectively remove uranium from the steel. The final chemistry predicted for heat 80 indicates that the steel will be higher in aluminum content than any other heat. The oxidation of uranium by reaction with alumina drives up the aluminum content of the steel, and thus the free energy of the system as a whole. Free energy minimization achieves a dynamic balance between the concentrations of uranium, aluminum, and oxygen in the metal and uranium dioxide, and alumina in the slag in order to achieve the lowest free energy attainable by the system. When the concentration of alumina in the slag is high, equilibrium dictates that the level of dissolved aluminum in the steel will also be high. Uranium is free to react with any oxygen available from the dissociation of alumina, but, when the aluminum content of the steel is high, as it was in heat 80, further dissociation of alumina is prohibited because of free energy considerations. In other heats, uranium was free to take oxygen from alumina, thus increasing the dissolved aluminum content of the steel because the aluminum content of the steel was lower to begin with. Heat 80 had, by far, the highest alumina content of any of

the slags, and, due to equilibrium considerations, the stainless steel melted in contact with this slag was predicted to contain more aluminum than any other steel. Uranium, therefore, was unable to take much additional oxygen from alumina because, in order to do so, the aluminum content of the steel would have been further increased, thus increasing the free energy of the system.

The effectiveness of uranium partitioning was also predicted to be related to the melting temperature and to the initial contamination level of the steel. Free energy minimization was conducted at four temperatures for each heat modeled, 1600, 1700,1800, and 1900°C. The residual uranium contents are listed in Table 7.8. Figure 7.14 shows that the efficiency of uranium partitioning to a slag is predicted to be lower at 1900°C than at 1600°C. This trend is predicted because the free energy of formation of $UO_2$ is more negative at the lower temperature than at the higher one.

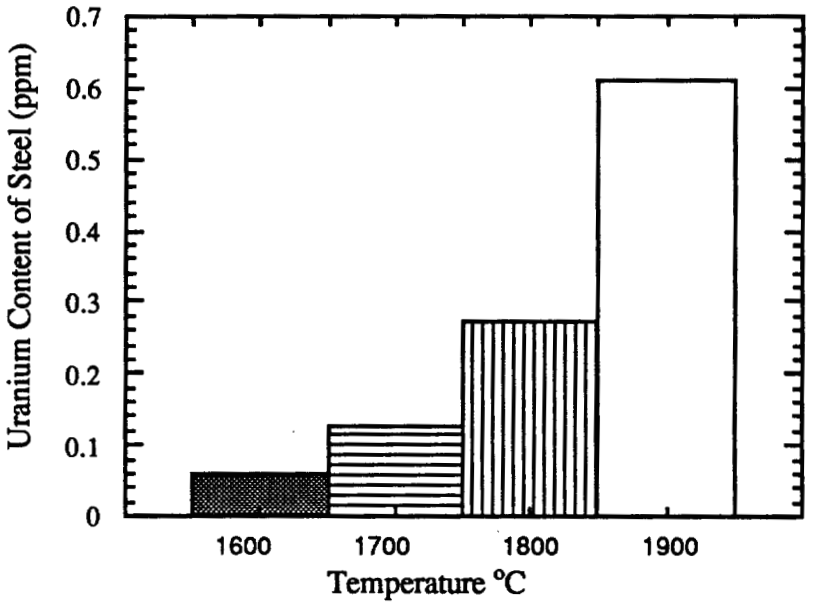


**Figure 7.14**
**Predicted Uranium Content of the Steel Produced by Heat 74 as a Function of Melting Temperature**

The residual uranium content of the steel was shown to be dependent on the degree of contamination of the steel before remelting. Figure 7.15 illustrates that a steel which initially contains ten times the amount of uranium as another steel will, after melting,

contain ten times the residual amount. This predicted result is due to the implementation of a partition coefficient for the oxidation of uranium to form uranium dioxide. At equilibrium, a balance will be obtained between the unoxidized uranium and the uranium dioxide. At a given temperature and oxygen activity, the partition coefficient will be constant, as will the ratio between unoxidized and oxidized uranium.

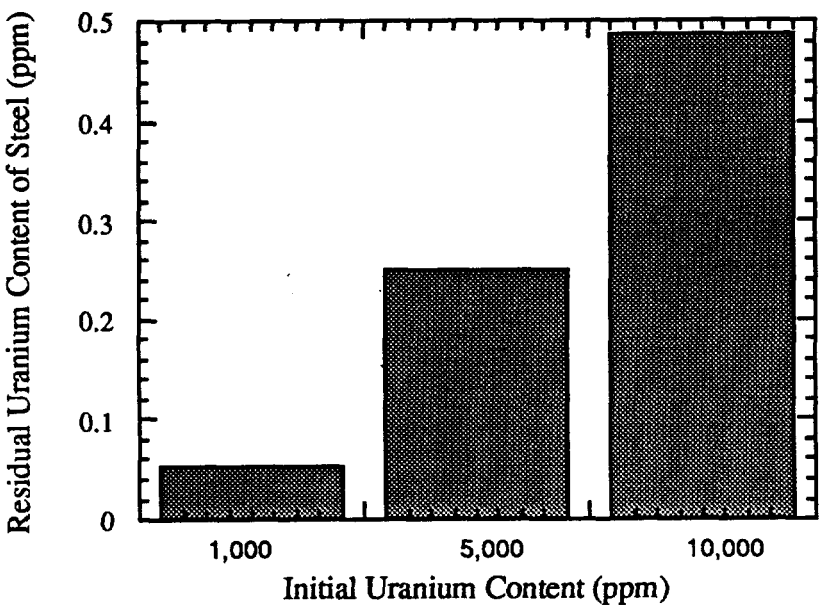


**Figure 7.15**
**Predicted Uranium Content of the Steel Produced by Heat 74 at 1700°C as a Function of Initial Contamination Level**

## 7.1.2 Conclusions Drawn from Free Energy Minimization Modeling

The preceding modeling studies showed that the efficiency of partitioning an element between a molten metal and a slag depends on several factors. These factors include the types of compounds which are formed by interactions between the element of interest and the elements which make up the slag and the thermodynamic driving forces which govern the formation of these compounds. Thus, slag chemistry is predicted to have a great influence on the residual radionuclide content of a steel after remelting. Other factors

which may have an influence on the level of decontamination achieved are the temperature at which melts are conducted as well as the initial amount of contaminant present and its chemical form.

### 7.1.3 Assumptions and Limitations of Free Energy Minimization

Thermodynamic modeling allows prediction of the partitioning of radionuclides between a molten metal and a slag during melting, but thermodynamic predictions are only as good as the assumptions made to generate them and the accuracy of the data used in the calculations. In the free energy minimization model used in this research the stainless steel was assumed to behave according to a modified dilute solution model for iron solutions incorporated into the F*A*C*T* software. Although this model is valid up to several weight percent of specified solute elements, the values of chrome and nickel necessary to model the behavior of the stainless steel used in this research were out of the calibrated range for the model. Predicted changes in the levels of these elements were not studied. The dilute solution model used for the steels allowed the incorporation of cerium, lanthanum and uranium into the metal, but did not include the data necessary for modeling the behavior of other elements of interest, such as neodymium, plutonium, and thorium. Additionally, the slags were assumed to behave as ideal solutions, as the extent of deviation from ideality is not known because values for activity and interaction coefficients have not been generated. Assumption of ideality does not take into account known phenomena such as low melting point eutectics, and thus cannot accurately predict which components of a solution will be solid and which will be liquid at a give temperature.

The free energy minimization model employed in this research imposed several limitations. The most serious of these was that the formation of predicted species was limited by thermodynamic data available in the data base associated with the software or available in the literature. Thermodynamic data for many of the compounds formed by radioactive compounds has not been measured or documented. Thermochemical measurements of liquid metals at high temperatures are difficult and such measurements on liquid slags are more difficult still, due to the corrosive nature of the slags and their complex chemistries. The extent to which an element partitions between a metal and a slag has, however, been shown to be dependent upon the species formed by that element in the slag as well as other species which may compete for required elements. Lack of

thermodynamic data for compounds which, in reality, are likely to be present, precludes the prediction of their formation and, ultimately, causes errors in modeling predictions. The phase diagram for calcium fluoride-calcium oxide-alumina shows five binary compounds and two ternary compounds. Thermodynamic data is available for two of the five binary compounds and for neither of the ternary compounds, and so their influence on the partitioning of the radionuclides or their surrogates is not known.

Another limitation imposed by the model was that, for simulations performed at one atmosphere of pressure, the formation of additional gaseous species is not predicted. This creates inaccuracies in modeling the partitioning of elements such as sulfur which are removed from the metal by the formation of a gaseous species. This limitation probably introduced errors in the modeling of uranium partitioning, as uranium is known to form stable gaseous species such as $UF_6$ and $UO_3$ at the high temperatures associated with melt refining.

## 7.2 Ionic Modeling of the Slags

The slags used in this research were composed of mixed oxides and fluorides. In their liquid state they are ionic in nature, and are composed of cations and anions. The ionic nature of basic slags, such as those used in ESR, has been used to develop models which allow the characterization of these slags by determining the activities of its components. One such model was developed by Temkin, who considered the slag to be composed of two ideal solutions of cations and anions and assumed that all ionic species in the slag were known. Because slags are assumed to be composed of ions, ionic fractions are used in the implementation of the model, instead of mole fractions.

The slags of interest in this study were composed of ions of mixed valence. In order to maintain electrical neutrality at cation and anion sites, a provision was made to account for the charge variation present among ions. The number of cation and anion sites is assumed to be constant, with only cations being allowed to occupy cation sites and only anions being allowed to occupy anion sites. For example, the cations in the slag are $Al^{+++}$ and $Ca^{++}$, which cannot directly substitute for each other because of their differing charges. The anions, $F^-$, $O^{--}$, and $AlO_3^{---}$, also exhibit different valences. In order to consider the formation of electrically neutral species, the electrically equivalent ion fractions may be calculated. The use of electrical equivalency results in the modeling of a solution in which

the activities of the ions are not proportional to their mole fractions and are not a linear function of the concentrations of the ions.

The activity of any constituent formed by the slag is calculated by appropriate multiplication of the electrically equivalent ion fractions, x', of the ions from which the species forms. For example, the activity of calcium fluoride forming from ions in the slag may be calculated by implementing Temkin's Rule:

$$a_{CaF_2} = x'_{Ca^{2+}} x'^{2}_{F^-}$$

## 7.2.1 Modeling Experiments

In order to apply this model, each slag was first described in terms of electrically equivalent ion fractions, from which the activities of various species was predicted. The ions present in the slags were $Ca^{++}$ from calcium oxide and calcium fluoride, $Al^{+++}$ from alumina, $O^-$ from calcium oxide, F- from calcium fluoride, and $AlO_3^{---}$ from alumina. A Temkin analysis was performed for slags containing ions of the surrogate species, $Ce^{+++}$, $Ce^{++++}$, and $La^{+++}$, and another was performed for slags containing $U^{++++}$. For each analysis, the slags were assumed to contain 1 weight percent of the surrogate or radionuclide of interest. The species which were assumed to form were those predicted by free energy minimization modeling, as Temkin analysis only determines the formation of a species based on the presence of its ions, and not on its thermochemical stability. A Temkin model was performed for each slag chemistry used in melting experiments.

Additionally, modeling was performed at many points on the ternary diagram. In this way, diagrams showing the calculated activities of each surrogate species were mapped directly onto a ternary grid. The superposition of these grids onto the ternary phase diagram for the slags allowed the prediction of the relative amounts of surrogate containing compounds present at each point on the phase diagram. In this way, the influence of slag chemistry on the behavior of the surrogates could be seen.

### 7.2.1.1 Modeling of Surrogate Containing Melts

Ionic modeling was performed in order to predict the activities of cerium bearing species present in each slag used in the melting experiments. Activities were calculated for $CeF_3$, $AlCeO_3$, and $CeO_2$ because free energy minimization indicated that these would be the species most likely to form in the molten slags at melt refining temperatures. These activities are listed by heat in Table 7.9. In order to determine the relative activity levels of the various species present in each slag, the percentages of the cerium activity represented by each compound were calculated. These percentages are listed in Table 7.10 and presented graphically in Figure 7.16.

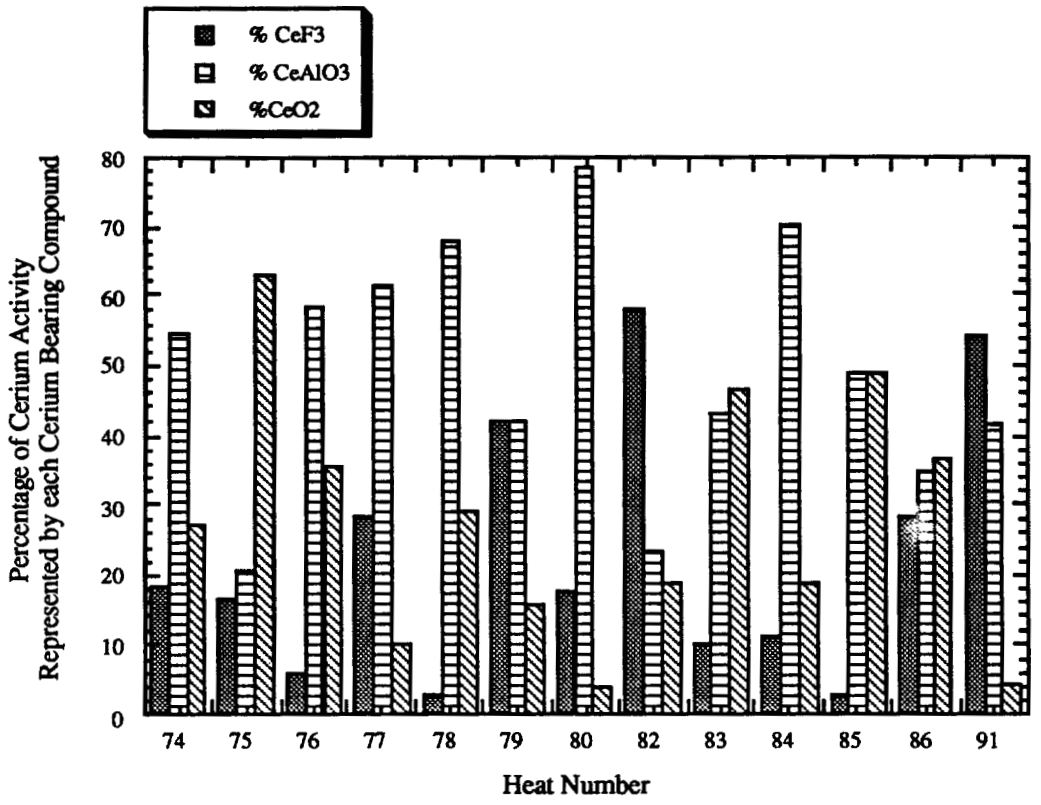


**Figure 7.16**
**Predicted Activities of Cerium Bearing Compounds in the Various Slags**

In the same way, the activities of the three lanthanum compounds predicted by free energy minimization to be the most stable, $LaF_3$, $AlLaO_3$, and $La_2O_3$ were calculated. The calculated activities of the lanthanum bearing phases in each slag used are listed in Table

7.11. The relative percentages of lanthanum activity represented by each compound were compared for each slag and the results are presented in Table 7.12 and are shown graphically in Figure 7.17.

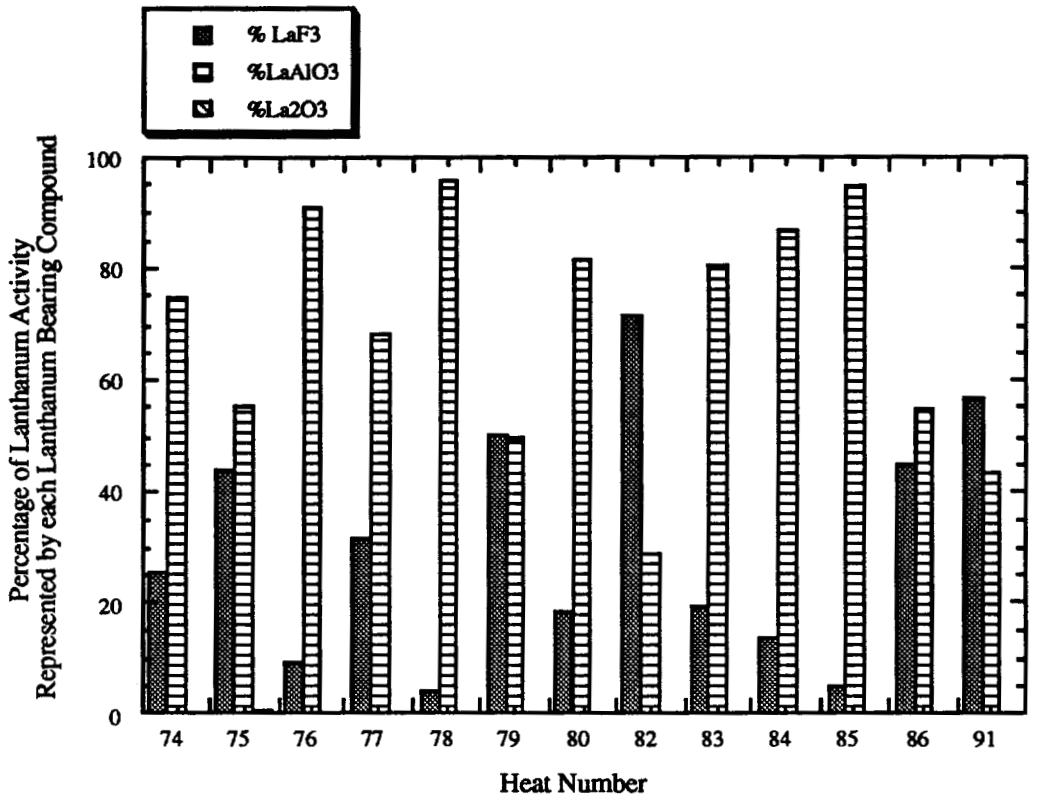


**Figure 7.17**
**Predicted Activities of Lanthanum Bearing Compounds in the Various Slags**

Comparison of the results generated for cerium and those generated for lanthanum reveals that ionic modeling predicts that cerium will form appreciable amounts of $CeO_2$, but that lanthanum will only form small amounts of $La_2O_3$. This is mathematically a consequence of Temkin's rule, as multiplying the square of the ion fraction of lanthanum by the cube of the ion fraction of oxygen generates a low activity value.

The predominance of the phases predicted by ionic modeling was compared with that predicted by free energy minimization. Free energy minimization predicted that the aluminate compounds, $AlCeO_3$ and $AlLaO_3$ would be the dominant species present at all slag compositions. Ionic modeling suggests that the dominant compound will be that formed by the rare earth and the most dominant anion in the slag.

### 7.2.1.1.1 Mapping of Surrogate Species Activities

One of the most useful features of ionic modeling was that it allowed the prediction of the activities of each surrogate bearing species present for any slag chemistry. In order to implement this, a grid containing 65 points was constructed which could be superimposed on the ternary CaF2-CaO-Al2O3 phase diagram. The activity of each surrogate compound was calculated for the slag chemistry represented by each point on the grid. The resulting activity maps may be used to show the distribution of cerium or lanthanum between fluoride, oxide and aluminate phases at any chosen point on the phase diagram. These activity maps are presented in Figures 7.18 and 7.19.

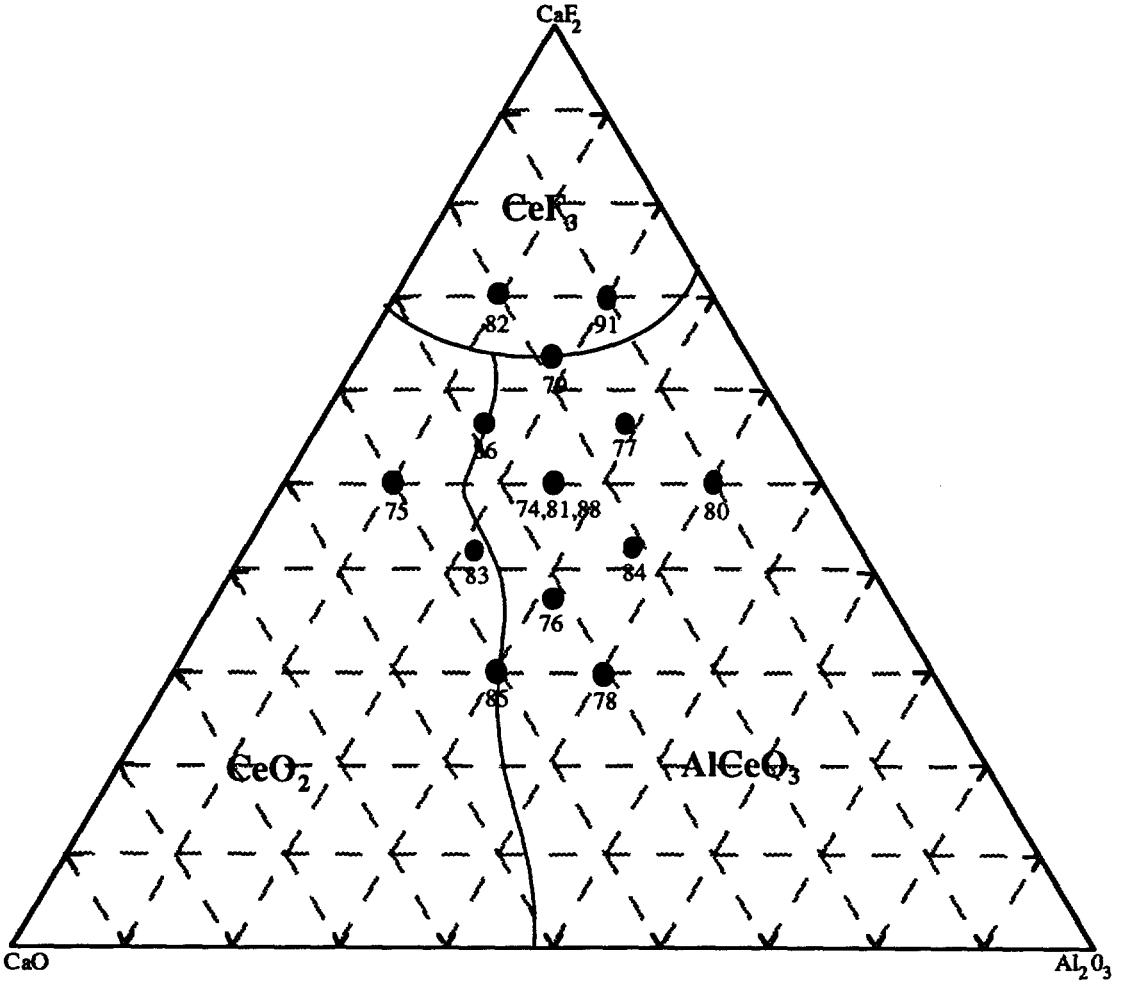


**Figure 7.18**
**Ternary Predominance Area Diagram Showing the Cerium Bearing Compound Which is Prevalent at any Point**

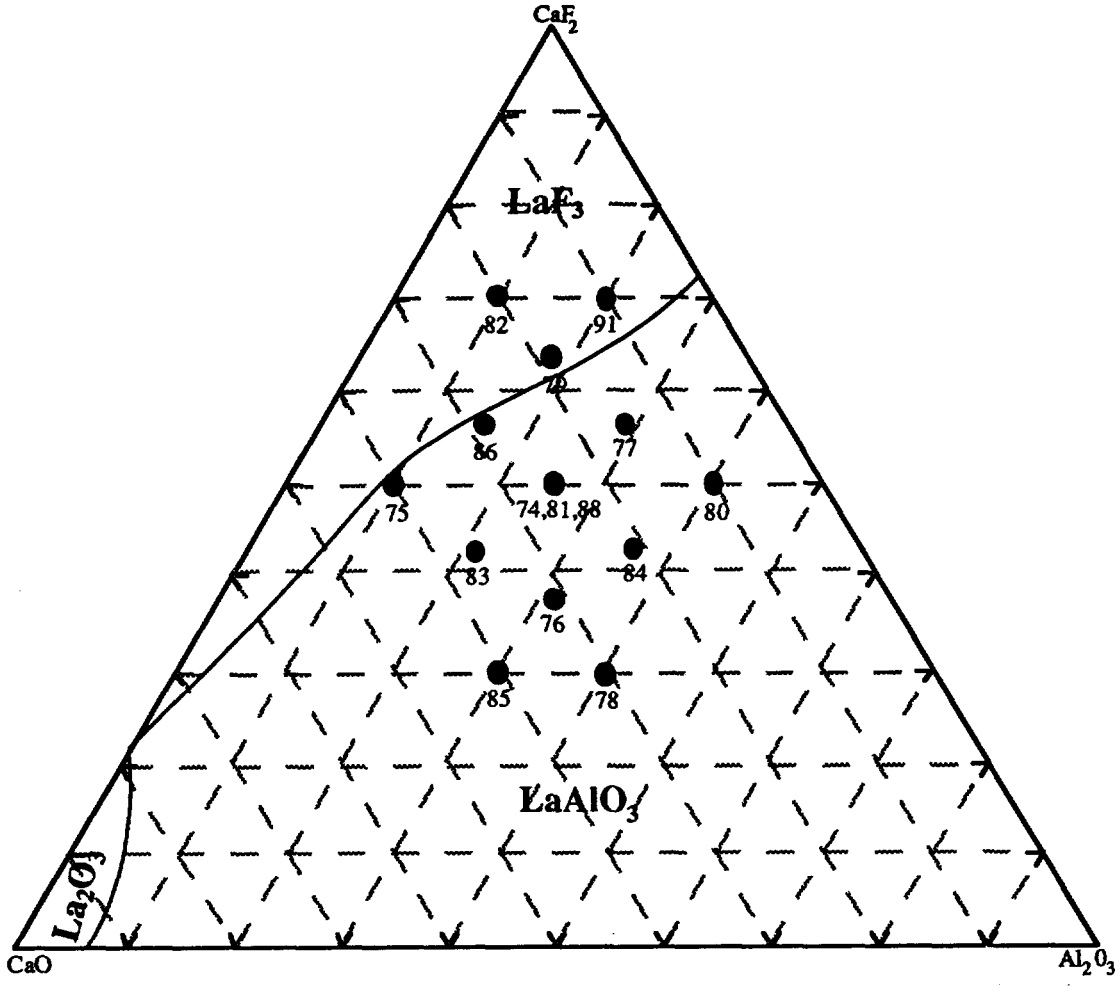


**Figure 7.19**
**Ternary Predominance Area Diagram Showing the Lanthanum Bearing Compound Which is Prevalent at any Point**

## 7.2.1.2 Modeling of Uranium Containing Melts

Ionic modeling was used to determine what the activity of $UO_2$ would be in each of the slags used if the slags initially contained one weight percent of unoxidized uranium. The calculated activity of $UO_2$ which would be allowed by each slag is listed in Table 7.13 and shown graphically in Figure 7.20.

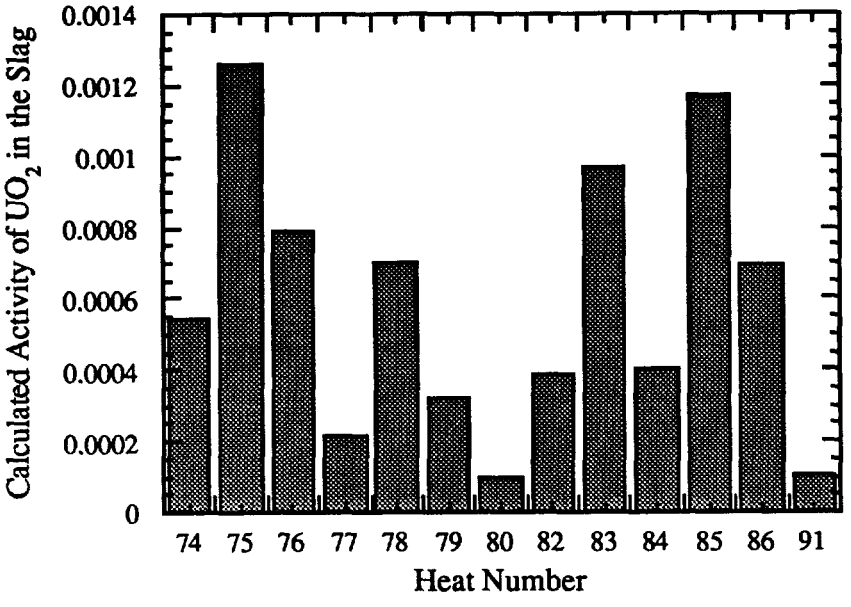


**Figure 7.20**
**Predicted Activities of $UO_2$ in the Various Slags**

In a melt refining situation, the oxidized uranium would remain in the slag phase while that which remained unoxidized would remain as a metallic contaminant. The higher the activity of $UO_2$, therefore, the more effective a slag would be at removing uranium from the metal. The figure shows that the slags used in heats 75 and 85 were predicted to be the most effective for the melt decontamination of uranium bearing metal. According to the ionic model, uranium is oxidized by reaction with oxygen ions resulting from the dissociation of calcia in the slag. The projected ability of a slag to oxidize uranium directly related to the amount of calcium oxide it contained, as shown in Figure 7.21 .

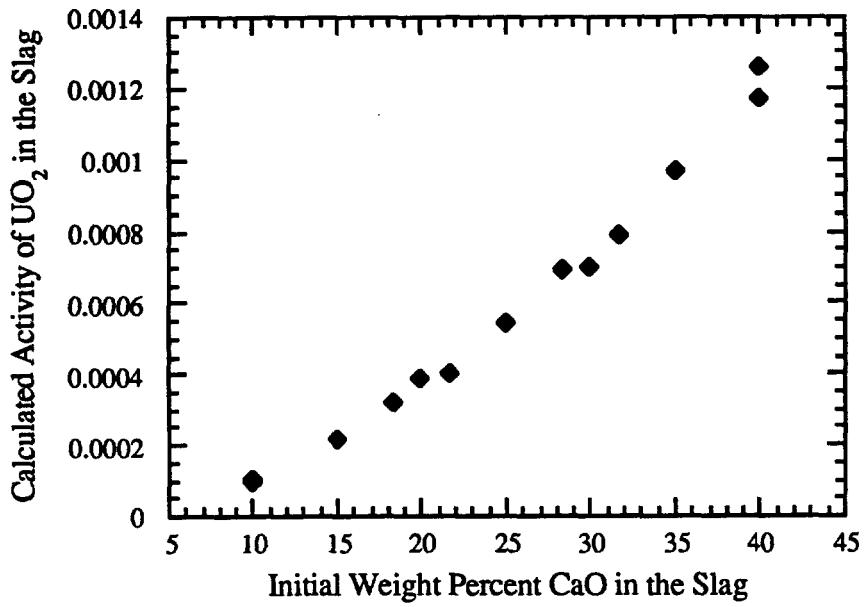


**Figure 7.21**
**$UO_2$ Activity in the Slag**
**as a Function of Initial Calcia Content**

## 7.2.2 Assumptions and Limitations Imposed by the Model

The limitations of this theory derive from the assumptions which must be made in order to employ it. The model assumes that the slags are completely dissociated into ions, which may work well for ESR slags, according to the theories of those researchers who have studied the conductivity and resistivity of the slags. The theory further assumes, however, that there is no interaction between similarly charged ions, that there is complete randomness of ions, and that the slag is composed on two ideal solutions of cations and anions. These assumptions are not met when the slag is concentrated with large, complex ions which have low mobilities and impede the mobility of other ions, or when immisible liquids are present. In order to employ the model, all the ionic species in the melt must be known. This becomes difficult for complex slags. The assumption that $Al_2O_3$ breaks down into $Al^{+++}$ and $AlO_3^{---}$ may be incorrect in view of the fact that conductivity research has suggested the presence of larger, more complex ions. Also, some knowledge of the system

being modeled is necessary because the formation of a species is based solely upon the availability of its ions and not on any thermochemical stability criteria.

## 7.3 Summary

The major purpose of thermodynamic modeling, as utilized in this study, was to predict the behavior of actual radioactive species in stainless steel and to determine the probable accuracy of these predictions. In order to accomplish this, the behaviors of cerium and lanthanum were modeled so that the resulting predictions could be compared with the behavior observed during melting. In this way, the validity of the thermodynamic models could was tested, and the accuracy of predictions made for the radionuclides was estimated.

# Chapter 7 Tables

**Table 7.1**
**Chemistry of Stainless Steel used in Free Energy Minimization Modeling Experiments**

| Element | % Present |
|---|---|
| Fe | 59.58 |
| Cr | 19.97 |
| Ni | 13.73 |
| Mn | 3.58 |
| Mo | 1.77 |
| Si | 0.48 |
| Co | 0.19 |
| C | 0.04 |
| $S_2$ | 0.01 |
| $O_2$ | 0.00 |
| Al | 0.00 |
| Ca | 0.00 |

**Table 7.2**
**Final Stainless Steel Chemistries Predicted by Free Energy Minimization for Planned Melting Experiments at 1700°C**

| Heat # | Fe % | Cr % | Ni % | Mn % | Mo % | Si % | Co % | C % | $S_2$ ppm | $O_2$ ppm | Al ppm | Ca ppm |
|---|---|---|---|---|---|---|---|---|---|---|---|---|
| 74* | 60.2 | 20.1 | 13.8 | 3.35 | 1.78 | 0.34 | 0.19 | 0.037 | 74.18 | 63.46 | 37.42 | 0.026 |
| 75 | 60.1 | 20.1 | 13.8 | 3.48 | 1.78 | 0.31 | 0.19 | 0.037 | 32.93 | 45.33 | 29.82 | 0.065 |
| 76 | 60.1 | 20.1 | 13.8 | 3.41 | 1.78 | 0.32 | 0.19 | 0.036 | 65.18 | 50.67 | 53.05 | 0.046 |
| 77 | 60.3 | 20.2 | 13.9 | 3.04 | 1.78 | 0.43 | 0.19 | 0.037 | 102.3 | 98.24 | 29.72 | 0.006 |
| 78 | 60.2 | 20.1 | 13.8 | 3.31 | 1.78 | 0.35 | 0.19 | 0.036 | 81.77 | 62.51 | 52.81 | 0.025 |
| 79 | 60.2 | 20.1 | 13.8 | 3.27 | 1.78 | 0.37 | 0.19 | 0.037 | 84.69 | 81.35 | 24.80 | 0.013 |
| 80 | 60.5 | 20.2 | 13.9 | 2.69 | 1.79 | 0.51 | 0.19 | 0.037 | 112.3 | 58.32 | 158.7 | 0.002 |
| 82 | 60.1 | 20.1 | 13.8 | 3.40 | 1.78 | 0.33 | 0.19 | 0.037 | 54.63 | 60.42 | 22.38 | 0.029 |
| 83 | 60.1 | 20.1 | 13.8 | 3.46 | 1.78 | 0.31 | 0.19 | 0.037 | 47.32 | 43.34 | 48.07 | 0.068 |
| 84 | 60.2 | 20.2 | 13.8 | 3.14 | 1.78 | 0.40 | 0.19 | 0.037 | 95.78 | 82.24 | 40.05 | 0.010 |
| 85 | 60.1 | 20.1 | 13.8 | 3.46 | 1.78 | 0.31 | 0.19 | 0.036 | 53.92 | 44.54 | 57.19 | 0.066 |
| 86 | 60.1 | 20.1 | 13.8 | 3.45 | 1.78 | 0.31 | 0.19 | 0.037 | 43.46 | 45.33 | 36.56 | 0.059 |
| 91 | 60.3 | 20.2 | 13.9 | 3.00 | 1.78 | 0.44 | 0.19 | 0.037 | 106.6 | 109.3 | 23.17 | 0.003 |

*Heats 74, 81, and 88 are duplicates

**Table 7.3**
**Stainless Steel Chemistry Changes Predicted as a Result of Remelting at 1700°C**

| Heat # | Fe % | Cr % | Ni % | Mn % | Mo % | Si % | Co % | C % | $S_2$ ppm | $O_2$ ppm | Al ppm | Ca ppm |
|---|---|---|---|---|---|---|---|---|---|---|---|---|
| 74* | -0.62 | -0.21 | -0.14 | 0.23 | -0.01 | 0.13 | -19.6 | -22.6 | 28.8 | -63.5 | -37.4 | -0.02 |
| 75 | -0.57 | -0.19 | -0.13 | 0.10 | -0.01 | 0.16 | -17.9 | -22.3 | 70.1 | -45.3 | -29.8 | -0.06 |
| 76 | -0.60 | -0.20 | -0.14 | 0.17 | -0.02 | 0.15 | -18.8 | -11.2 | 37.8 | -50.7 | -53.1 | -0.04 |
| 77 | -0.75 | -0.25 | -0.17 | 0.53 | -0.02 | 0.04 | -21.4 | -23.0 | 0.68 | -98.2 | -29.7 | -0.01 |
| 78 | -0.64 | -0.22 | -0.15 | 0.26 | -0.02 | 0.12 | -20.4 | -11.5 | 21.2 | -62.5 | -52.8 | -0.02 |
| 79 | -0.65 | -0.23 | -0.15 | 0.31 | -0.02 | 0.10 | -20.7 | -22.8 | 18.3 | -81.4 | -24.8 | -0.01 |
| 80 | -0.93 | -0.31 | -0.21 | 0.88 | -0.03 | -0.03 | -32.0 | -25.0 | -9.34 | -58.3 | -159 | -0.01 |
| 82 | -0.60 | -0.20 | -0.14 | 0.18 | -0.02 | 0.14 | -19.0 | -22.5 | 48.4 | -60.4 | -22.4 | -0.03 |
| 83 | -0.58 | -0.19 | -0.13 | 0.12 | -0.01 | 0.16 | -18.0 | -22.3 | 55.7 | -43.3 | -48.1 | -0.06 |
| 84 | -0.71 | -0.24 | -0.16 | 0.43 | -0.02 | 0.07 | -22.4 | -23.2 | 7.22 | -82.2 | -40.1 | -0.01 |
| 85 | -0.58 | -0.19 | -0.13 | 0.12 | -0.01 | 0.16 | -16.6 | -10.8 | 49.1 | -44.5 | -57.2 | -0.06 |
| 86 | -0.58 | -0.20 | -0.13 | 0.13 | -0.02 | 0.16 | -18.6 | -22.4 | 59.5 | -45.3 | -36.6 | -0.06 |
| 91 | -0.77 | -0.26 | -0.18 | 0.58 | -0.02 | 0.03 | -24.9 | -23.7 | -3.60 | -109 | -23.2 | -0.01 |

**Table 7.4**
**Amounts of Major Species in the Slag (Percentages of the Slag Weight) at 1700°C**

| Heat # | $CaF_2$ % | $CaAl_2O_4$ % | $MnAl_2O_4$ % | $CaAl_4O_7$ % | $Al_2O_3$ % | MnO % | CaO % | $Ca_2Al_2SiO_7$ % | $Ca_2SiO_4$ % | $CaSiO_3$ % |
|---|---|---|---|---|---|---|---|---|---|---|
| 74 | 44.4 | 29.29 | 1.85 | 0.78 | 0.20 | 1.48 | 6.15 | 1.52 | 7.68 | 0.32 |
| 75 | 44.7 | 11.53 | 0.37 | 0.08 | 0.05 | 1.10 | 25.5 | 0.52 | 9.65 | 0.26 |
| 76 | 32.7 | 38.97 | 1.31 | 1.00 | 0.19 | 1.08 | 8.43 | 1.59 | 8.27 | 0.24 |
| 77 | 49.5 | 24.41 | 8.06 | 1.76 | 0.55 | 2.38 | 1.88 | 1.65 | 3.07 | 0.42 |
| 78 | 26.7 | 46.01 | 3.18 | 2.40 | 0.35 | 1.30 | 4.91 | 2.40 | 6.17 | 0.28 |
| 79 | 55.9 | 19.73 | 2.53 | 0.51 | 0.21 | 2.08 | 4.23 | 1.31 | 6.76 | 0.44 |
| 80 | 40.4 | 21.11 | 19.84 | 8.57 | 2.80 | 1.04 | 0.28 | 0.09 | 0.03 | 0.02 |
| 82 | 62.6 | 11.33 | 0.57 | 0.09 | 0.07 | 1.55 | 8.02 | 0.52 | 8.79 | 0.33 |
| 83 | 38.8 | 26.52 | 0.81 | 0.43 | 0.12 | 1.07 | 15.6 | 1.09 | 9.0 | 0.25 |
| 84 | 37.8 | 35.27 | 6.48 | 2.63 | 0.53 | 1.85 | 2.64 | 2.20 | 3.97 | 0.36 |
| 85 | 27.0 | 35.65 | 1.12 | 0.87 | 0.16 | 0.97 | 17.1 | 1.54 | 8.98 | 0.23 |
| 86 | 50.7 | 18.13 | 0.54 | 0.18 | 0.08 | 1.17 | 12.3 | 0.70 | 9.65 | 0.26 |
| 91 | 60.1 | 16.06 | 8.12 | 0.98 | 0.50 | 2.84 | 1.46 | 1.05 | 2.30 | 0.43 |

**Table 7.5**
**Effect of Melt Temperature and Slag Chemistry on Cerium Concentration in Steel**

| Heat # | ppm Ce at 1600°C | ppm Ce at 1700°C | ppm Ce at 1800°C | ppm Ce at 1900°C |
|---|---|---|---|---|
| 74* | 0.00265 | 0.00561 | 0.01135 | 0.02222 |
| 75 | 0.00689 | 0.01697 | 0.03866 | 0.08279 |
| 76 | 0.00428 | 0.00828 | 0.01562 | 0.02883 |
| 77 | 0.00071 | 0.00196 | 0.00493 | 0.01149 |
| 78 | 0.00222 | 0.00504 | 0.01070 | 0.02161 |
| 79 | 0.00158 | 0.00370 | 0.00810 | 0.01694 |
| 80 | 0.00058 | 0.00183 | 0.00493 | 0.01166 |
| 82 | 0.00433 | 0.00835 | 0.01581 | 0.02964 |
| 83 | 0.00535 | 0.01309 | 0.02777 | 0.04617 |
| 84 | 0.00107 | 0.00279 | 0.00664 | 0.01473 |
| 85 | 0.00487 | 0.01188 | 0.02668 | 0.05023 |
| 86 | 0.00608 | 0.01306 | 0.02262 | 0.03914 |
| 91 | 0.00053 | 0.00153 | 0.00400 | 0.00973 |

**Table 7.6**
**Effect of Melt Temperature and Slag Chemistry on Lanthanum Concentration in Steel**

| Heat # | ppm La at 1600°C | ppm La at 1700°C | ppm La at 1800°C | ppm La at 1900°C |
|---|---|---|---|---|
| 74* | 2.18e-05 | 8.57e-05 | 3.04e-4 | 9.94e-4 |
| 75 | 5.44e-05 | 2.44e-4 | 9.66e-4 | 3.43e-3 |
| 76 | 3.57e-05 | 1.28e-4 | 4.25e-4 | 1.31e-3 |
| 77 | 5.32e-06 | 2.79e-05 | 1.24e-4 | 4.81e-4 |
| 78 | 1.96e-05 | 8.23e-05 | 3.05e-4 | 1.02e-3 |
| 79 | 1.20e-05 | 5.28e-05 | 2.03e-4 | 7.08e-4 |
| 80 | 2.79e-06 | 1.72e-05 | 8.57e-05 | 3.57e-4 |
| 82 | 3.25e-05 | 1.15e-4 | 3.81e-4 | 1.19e-3 |
| 83 | 4.34e-05 | 1.93e-4 | 7.17e-4 | 2.01e-3 |
| 84 | 9.22e-06 | 4.48e-05 | 1.86e-4 | 6.84e-4 |
| 85 | 4.04e-05 | 1.79e-4 | 7.00e-4 | 2.20e-3 |
| 86 | 4.81e-05 | 1.88e-4 | 5.73e-4 | 1.66e-3 |
| 91 | 3.19e-06 | 1.78e-05 | 8.33e-05 | 3.40 e-4 |

**Table 7.7**
**Amounts of Surrogate Bearing Species in the Slag**
**(Percentages of the Slag Weight) at 1700°C**

| Heat # | LaF3 | $AlCeO_3$ | CeF3 | $AlLaO_3$ | $CeO_2$ | $Ce_2O_2S$ | $La_2O_2S$ | $Ce_2O_3$ | $La_2O_3$ |
|---|---|---|---|---|---|---|---|---|---|
| 74 | 0.348 | 2.729 | 0.088 | 2.299 | 0.094 | 0.118 | 0.370 | 0.066 | 0.013 |
| 75 | 0.338 | 2.415 | 0.087 | 2.017 | 0.141 | 0.191 | 0.587 | 0.205 | 0.040 |
| 76 | 0.145 | 2.764 | 0.036 | 2.407 | 0.084 | 0.136 | 0.456 | 0.073 | 0.015 |
| 77 | 1.135 | 2.604 | 0.356 | 1.785 | 0.728 | 0.041 | 0.084 | 0.022 | 0.003 |
| 78 | 0.179 | 2.843 | 0.043 | 2.541 | 0.071 | 0.088 | 0.309 | 0.421 | 0.009 |
| 79 | 0.754 | 2.622 | 0.213 | 1.992 | 0.106 | 0.100 | 0.255 | 0.058 | 0.009 |
| 80 | 2.133 | 1.686 | 1.189 | 0.650 | 0.014 | 0.007 | 0.005 | 0.002 | 7.7e-5 |
| 81 | 0.348 | 2.729 | 0.089 | 2.299 | 0.094 | 0.118 | 0.370 | 0.066 | 0.013 |
| 82 | 0.585 | 2.402 | 0.161 | 1.876 | 0.144 | 0.183 | 0.492 | 0.149 | 0.025 |
| 83 | 0.198 | 2.670 | 0.049 | 2.283 | 0.102 | 0.160 | 0.517 | 0.108 | 0.022 |
| 84 | 0.577 | 2.786 | 0.151 | 2.287 | 0.069 | 0.053 | 0.157 | 0.027 | 0.050 |
| 85 | 0.119 | 2.752 | 0.029 | 2.405 | 0.086 | 0.144 | 0.484 | 0.086 | 0.018 |
| 86 | 0.295 | 2.548 | 0.076 | 2.1224 | 0.123 | 0.180 | 0.552 | 0.145 | 0.028 |
| 91 | 1.165 | 2.251 | 0.651 | 1.228 | 0.073 | 0.032 | 0.041 | 0.018 | 0.002 |

**Table 7.8**
**Effect of Melt Temperature and Slag Chemistry**
**on Uranium Concentration in Steel**

| Heat # | ppmU at 1600°C | ppm U at 1700°C | ppm U at 1800°C | ppm U at 1900°C |
|---|---|---|---|---|
| 74* | 0.061 | 0.127 | 0.272 | 0.60978 |
| 75 | 0.114 | 0.263 | 0.579 | 1.252 |
| 76 | 0.115 | 0.213 | 0.415 | 0.857 |
| 77 | 0.019 | 0.056 | 0.155 | 0.432 |
| 78 | 0.068 | 0.153 | 0.345 | 0.795 |
| 79 | 0.030 | 0.072 | 0.171 | 0.422 |
| 80 | 0.135 | 0.298 | 0.624 | 1.291 |
| 82 | 0.066 | 0.121 | 0.237 | 0.504 |
| 83 | 0.122 | 0.280 | 0.578 | 1.037 |
| 84 | 0.032 | 0.085 | 0.219 | 0.569 |
| 85 | 0.132 | 0.303 | 0.666 | 1.309 |
| 86 | 0.114 | 0.227 | 0.395 | 0.751 |
| 91 | 0.014 | 0.043 | 0.124 | 0.362 |

**Table 7.9**
**Predicted Activities of Cerium Bearing Species in the Slag**

| Heat Number | Activity of $CeF_3$ | Activity of $AlCeO_3$ | Activity of $CeO_2$ |
|---|---|---|---|
| 74 | 6.24 e-4 | 1.84e-3 | 9.16e-4 |
| 75 | 5.50 e-4 | 6.94e-4 | 2.13e-3 |
| 76 | 2.16 e-4 | 2.20e-3 | 1.34e-3 |
| 77 | 1.03 e-3 | 2.22e-3 | 3.61e-4 |
| 78 | 1.16e-4 | 2.75e-3 | 1.18e-3 |
| 79 | 1.45e-3 | 1.44e-3 | 5.41e-4 |
| 80 | 7.11e-4 | 3.15e-3 | 1.62e-4 |
| 82 | 1.99e-3 | 7.97e-4 | 6.56e-4 |
| 83 | 3.60e-4 | 1.51e-3 | 1.64e-3 |
| 84 | 4.02e-4 | 2.58e-3 | 6.86-4 |
| 85 | 1.07e-4 | 1.98e-3 | 1.98e-3 |
| 86 | 9.16e-4 | 1.11e-3 | 1.18e-3 |
| 91 | 2.18e-3 | 1.66e-3 | 1.75e-4 |

**Table 7.10**
**Percentages of Cerium Activity Represented by Various Chemical Species**

| Heat Number | % of Cerium Activity Represented by $CeF_3$ | % of Cerium Activity Represented by $AlCeO_3$ | % of Cerium Activity Represented by $CeO_2$ |
|---|---|---|---|
| 74 | 18.423 | 54.548 | 27.029 |
| 75 | 16.291 | 20.555 | 63.154 |
| 76 | 5.747 | 58.583 | 35.669 |
| 77 | 28.468 | 61.533 | 9.9988 |
| 78 | 2.8799 | 67.912 | 29.208 |
| 79 | 42.202 | 42.045 | 15.753 |
| 80 | 17.654 | 78.335 | 4.010 |
| 82 | 57.808 | 23.142 | 19.050 |
| 83 | 10.244 | 43.026 | 46.729 |
| 84 | 10.978 | 70.306 | 18.716 |
| 85 | 2.643 | 48.708 | 48.648 |
| 86 | 28.563 | 34.677 | 36.760 |
| 91 | 54.174 | 41.462 | 4.3638 |

**Table 7.11**
**Predicted Activities of Lanthanum Bearing Species in the Slag**

| Heat Number | Activity of $LaF_3$ | Activity of $AlLaO_3$ | Activity of $La_2O_3$ |
|---|---|---|---|
| 74 | 6.29e-4 | 1.86e-3 | 1.56e-06 |
| 75 | 5.55e-4 | 7.00e-4 | 5.47e-06 |
| 76 | 2.18e-4 | 2.22e-3 | 2.73e-06 |
| 77 | 1.04e-3 | 2.24e-3 | 3.94e-07 |
| 78 | 1.17e-4 | 2.77e-3 | 2.25e-06 |
| 79 | 1.46e-3 | 1.45e-3 | 7.22e-07 |
| 80 | 7.17e-4 | 3.18e-3 | 1.18e-07 |
| 82 | 2.01e-3 | 8.04e-4 | 9.67e-07 |
| 83 | 3.63e-4 | 1.52e-3 | 3.70e-06 |
| 84 | 4.06e-4 | 2.60e-3 | 1.01e-06 |
| 85 | 1.08e-4 | 1.99 e-3 | 4.83e-06 |
| 86 | 9.24e-4 | 1.12e-3 | 2.29e-06 |
| 91 | 2.19e-3 | 1.68e-3 | 1.35e-07 |

**Table 7.12**
**Percentages of Lanthanum Activity Represented by Various Chemical Species**

| Heat Number | % of Cerium Activity Represented by $LaF_3$ | % of Cerium Activity Represented by $AlLaO_3$ | % of Cerium Activity Represented by $La_2O_3$ |
|---|---|---|---|
| 74 | 25.232 | 74.706 | 0.063 |
| 75 | 44.021 | 55.545 | 0.434 |
| 76 | 8.9243 | 90.964 | 0.112 |
| 77 | 31.627 | 68.361 | 0.012 |
| 78 | 4.0649 | 95.857 | 0.078 |
| 79 | 50.081 | 49.894 | 0.025 |
| 80 | 18.391 | 81.606 | 0.003 |
| 82 | 71.388 | 28.578 | 0.034 |
| 83 | 19.193 | 80.611 | 0.195 |
| 84 | 13.502 | 86.465 | 0.034 |
| 85 | 5.1360 | 94.635 | 0.229 |
| 86 | 45.115 | 54.773 | 0.111 |
| 91 | 56.644 | 43.353 | 0.003 |

**Table 7.13**
**Predicted Activities of $UO_2$ in the Slag**

| Heat Number | Activity of $UO_2$ |
|---|---|
| 74 | 5.401e-4 |
| 75 | 1.257e-3 |
| 76 | 7.904e-4 |
| 77 | 2.131e-4 |
| 78 | 6.977e-4 |
| 79 | 3.180e-4 |
| 80 | 9.532e-05 |
| 82 | 3.869e-4 |
| 83 | 9.683e-4 |
| 84 | 4.049e-4 |
| 85 | 1.166e-3 |
| 86 | 6.956e-4 |
| 91 | 1.034e-4 |

# Chapter 7 References

[1] Pelton, A.D., Bale, C.W., "A Modified Interaction Parameter Formalism for Non-Dilute Solutions", *Met. Trans.*, Vol. 17A, (1986), 1211-1215.

[2] Ball, R.G.J., Mignanelli, M.A., Barry, T.I., Gisby, J.A. "The calculation of phase equilibria of oxide core-concrete systems" *Journal of Nuclear Materials* , Vol. 201, (1993), 238-249.

[3] Thompson, W.T., Pelton, A.D., Bale, C.W., FACT-Facility for the Analysis of Chemical Thermodynamics, Users Guide and Supplement., McGill University/Ecole Polytechnique, 1979, 1985.

# Chapter 8
# Discussion

The initial goals of this research were to study the effect of slag chemistry on the decontamination of radioactive stainless steel by electroslag remelting and to use the knowledge gained to recommend an optimal slag for this purpose. Melting studies performed with surrogates revealed that electroslag remelting was effective in the removal of surface contamination, as was predicted by thermodynamic modeling. The process of remelting the stainless steel caused changes in its elemental makeup. These changes, which were predicted by free energy minimization modeling, were found to be dependent upon the chemistry of the slag used. Slag chemistry was also found to influence the power required to operate the process. An important finding of this work was that chemistry of the slag determines the chemical species which may be formed in the slag as well as the solidification mechanism of the slag. The combination of these two effects was found to influence the partitioning of elements between the slag skin and the slag cap. Such partitioning could be important in an industrial environment where it would be beneficial to have radionuclides concentrated in a monolithic slag cap rather than in a friable slag skin.

In the following discussion section, the experimental findings are compared with the predictions made in the modeling studies. Whenever possible, the modeling results have been used to explain the phenomena observed in the melting studies. The results are discussed in terms of their implications with regard to the industrial use of ESR as a decontamination strategy for radioactive scrap metals. The parameters used for the selection of an optimum slag chemistry are discussed and the benefits and drawbacks of the use of the selected slag are presented. Finally, the results obtained from the melting of a bulk contaminated material are discussed in terms of how the melt refining of such materials may differ from that of the surface contaminated materials which were the primary subject of this investigation.

## 8.1 Surrogate Removal From Steel

This investigation was aimed at the removal of oxidized surface contamination from stainless steel. Because of the difficulties associated with the use of radioactive elements, surrogates were selected which resembled the radionuclides in physical and thermochemical properties. These surrogates were applied as oxides to the surfaces of the steel to be remelted in order to simulate the presence of the highly oxidized radioactive crud known to coat the interior surfaces of stainless steel reactor piping.

### 8.1.1 Comparison of Melting and Modeling Studies

Melting studies were conducted using slags of various chemistries. The results of these studies showed that the levels of surrogates remaining in the steel ingots after remelting were below the detectable limit of one part per million, regardless of which slag was used. The use of some slags, however, caused the production of ingots with very rough surfaces. Such surface roughness was found to encourage slag entrapment and thus surface contamination.

The outcome of each melt performed was predicted by use of thermodynamic modeling. The results of the melting studies were then compared with the results generated by the model so that the reliability of the predictions made by the model could be documented. Modeling predictions were also made for a set of hypothetical melts, identical to the actual melts, except for the presence of uranium in place of the surrogates.

For each modeling study conducted, free energy minimization predicted that residual cerium concentration would be less than 0.02 ppm and residual lanthanum concentrations would be below 0.0002 ppm for melts conducted at 1700°C. Although modeling predicted that the steel would be decontaminated to below the detectable limits, testwork was performed to determine whether or not the kinetics of the process would allow the predicted decontamination to occur. Modeling predicted that some slags would remove contaminants from steel more effectively than others, depending on the compounds formed by the contaminant in the slag, the availability of the elements needed in order for the compounds to form, and the thermodynamic driving force governing their formation. Melting studies showed that the surrogates remained in the steel at levels less than 1 ppm, regardless of the slag chemistry used.

## 8.1.2 Implications of Surrogate Removal Studies

The finding that the surrogates were effectively removed from each ingot produced, regardless of the chemistry of the slag used, has quite positive implications in terms of implementing ESR as an industrial melt decontamination technique. During ESR melting, the chemistry of the liquid slag changes due to the selective solidification which enables the formation of a slag skin, chemical reactions among the components, and the evolution of gaseous products. These chemistry changes are difficult to monitor and control. The results of this investigation showed that decontamination efficiency would not suffer drastically due to the changes in slag chemistry inherent to the ESR process, although minor changes would be expected.

Slag chemistry was shown, however, to have an impact on the surface quality of the remelted steel and thus on the level of residual surface contamination after melting. The surface quality of the ingots produced by an industrial ESR melt decontamination process would influence the efficiency of this process. Poor surface quality could result in the entrapment of radioactive slag on the ingot surfaces. This contamination would necessitate surface treatment of the ingots before rolling to final shape, resulting in added processing expense, material loss and exposure of personnel.

Thermodynamic modeling predicted that some slags would allow a higher residual concentration of the surrogate elements in the steel than others. The predicted levels, however, were so low that this could not be confirmed by the results of the melting experiments. Small differences in the level of decontamination achieved could be important, however, especially for highly hazardous elements such as plutonium. In order to confirm the modeling predictions, radioactive tracer studies would have to be performed.

The predicted behavior of uranium was different from the predicted behavior of the surrogate elements. The predicted levels of residual uranium in the steel were higher than those for cerium and lanthanum, due to differences in the compounds formed in the slag. Modeling indicated that cerium and lanthanum would be removed from the steel by the formation of oxides, fluorides, and oxyaluminates, and oxysulfides while uranium would be removed solely by the formation of $UO_2$. Uranium does form fluorides which are gasses at melt refining temperatures but their formation was not predicted because, for simulations which are performed at one atmosphere of total pressure, the formation of additional gaseous species is not predicted. Uranium is also known to form an oxysulfide, although no thermodynamic data was available for this compound. Uranium, therefore, may be more effectively removed from the melt than the modeling studies would indicate, but in order to

confirm this, melting studies would have to be performed using uranium or depleted uranium.

## 8.2 Change of Basic Steel Chemistry

In addition to the removal of the surrogate elements, electroslag remelting of the stainless steel ingots was shown to change the base chemistry of the stainless steel. The changes in chemistry observed were found to be related to the chemistry of the slag used. Thermodynamic modeling also predicted chemistry changes which were compared to the actual changes observed with the goal of determining the accuracy of modeling predictions.

### 8.2.1 Comparison of Melting and Modeling Studies

In the comparison of the predictions made by free energy minimization modeling and the results achieved in actual electroslag remelting experiments, differences were expected. Free energy minimization modeling considers the contact of two solutions, a liquid steel and ideal slag, at a temperature of interest. The types and amounts of compounds which are predicted to form are those which are necessary in order to achieve the lowest free energy for the system as a whole. While this is quite applicable to induction melting, in which the liquid metal is in contact with the slag for a prolonged time, the actual situation in electroslag remelting is much more complicated. Although a melt may be started with a slag of known chemistry, changes are brought about by chemical reactions between the metal and the slag, the volatilization of some components, and most especially by the selective solidification of various phases on the water cooled copper crucible during the course of the melt. As chemistry samples were taken from the top third of each ingot produced, the liquid slag which contacted the metal which was eventually analyzed was no longer of the same chemistry as the starting slag. To further complicate matters, the temperature of the slag is different at different locations in the slag pool. The bulk temperature of the slag may well change throughout the course of a heat as the resistivity of the slag changes. In order to accurately model the ESR process, the dynamic changes in slag chemistry, the factors which influence these changes, and the effects of these changes on the slag pool temperature must be better understood and accounted for.

Results of chemical analysis performed on the stainless steel before and after remelting show that the steel was depleted in some elements and enriched in others. Elemental depletion could have been the result of slag-metal reactions. For each heat

melted, the steel lost manganese, sulfur, and silicon, indicating that these elements were removed by each slag tested. In addition, the steel produced by some melts was depleted in carbon, chromium, molybdenum, and phosphorous while the steel produced by other melts was enriched in these elements. This indicates that the behavior of these elements is dependent on the chemistry of the slag used. Elemental enrichment could have been caused either by the transfer of an element initially contained in the slag to the metal or by the selective loss of other elements from the steel. In each melt conducted, concentrations of nickel, copper, and cobalt in the steel produced were higher than in the starting steel. These elements were probably not present in the slag to any great extent, and therefore the enrichment may be assumed to be the result of the loss of other elements such as iron and manganese from the steel.

Free energy minimization predicted the consistent loss of manganese by the steel and indicated that sulfur and silicon would be depleted in the steel produced by all heats except for one. Enrichment in chromium, nickel, molybdenum, cobalt, and carbon was predicted for each ingot produced. Although not expected to be wholly accurate, modeling aided in the understanding of the mechanisms by which various elements were transferred from the metal to the slag. Also, the compounds most likely to form from a free energy standpoint were predicted.

#### 8.2.1.1 The Predicted and Observed Changes in Manganese Content

The loss of manganese predicted by the model was compared with that observed in the melting experiments in Figure 8.1. The figure shows that, for some heats, free energy minimization accurately predicts the manganese removal from steel, while for others, the loss is overestimated. The greatest discrepancy between melting and modeling occurs for heats in which slags low in calcia were used. Figure 8.2 shows the effect of the calcia content of the slag on the predicted and actual manganese losses.

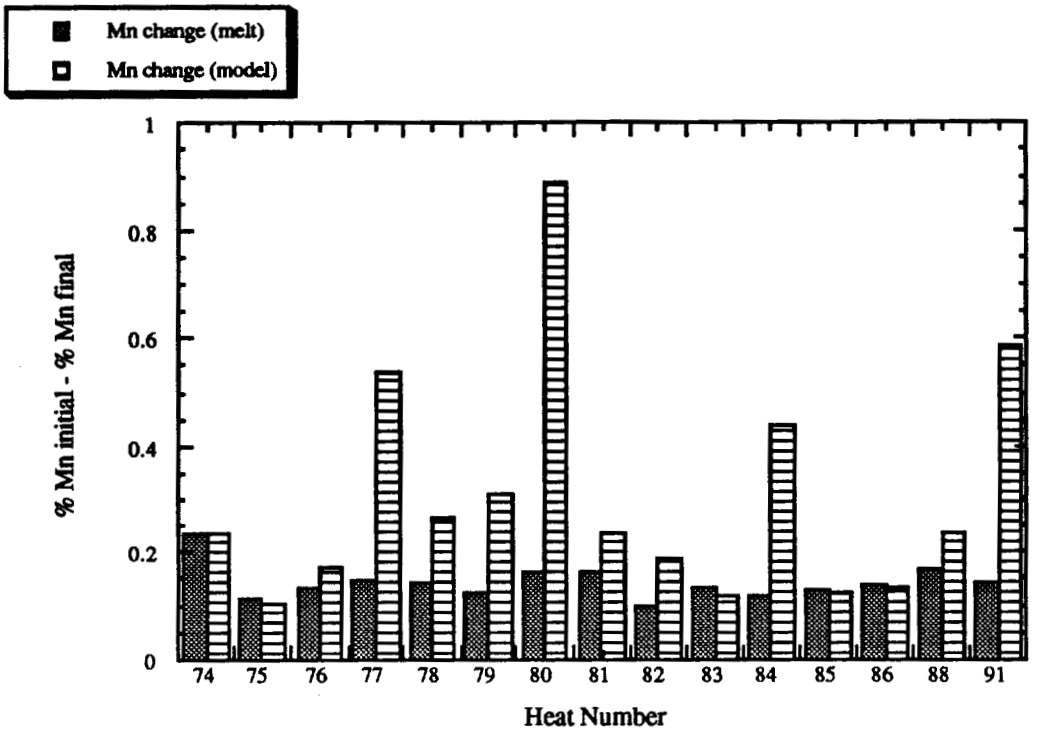


**Figure 8.1**
**Loss of Manganese from the Steel by Heat (Predicted vs. Actual)**

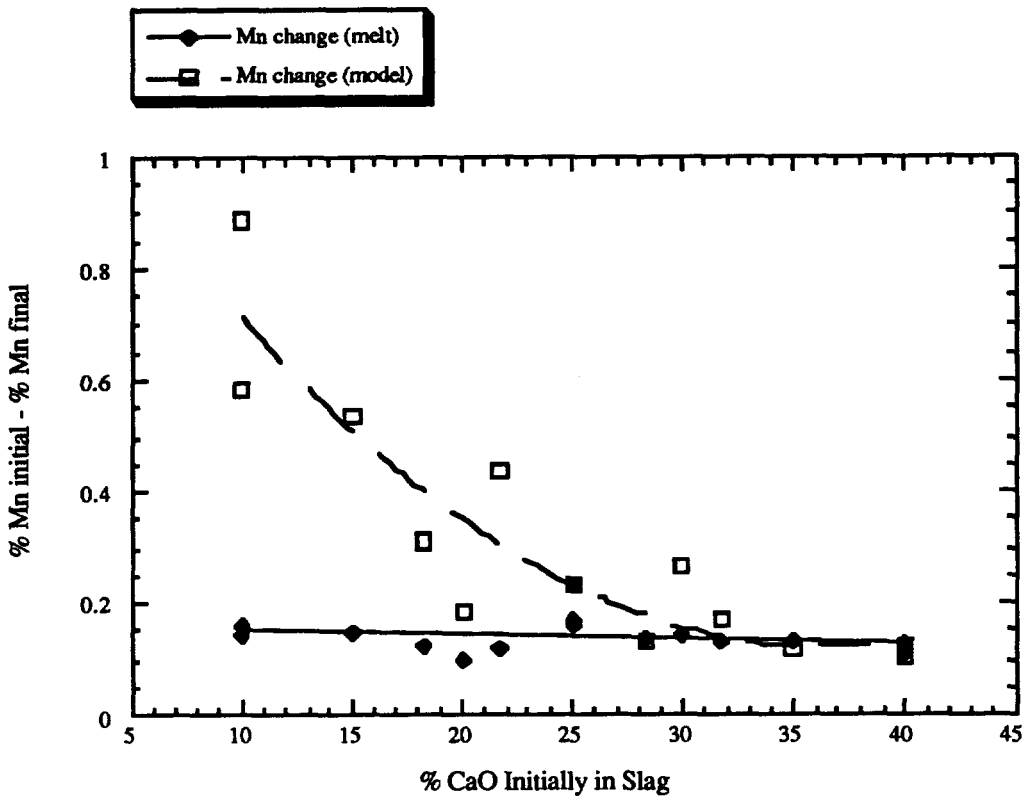


**Figure 8.2**
**Effect of Calcia Content of the Slag**
**on Predicted and Actual Manganese Loss**

For the heats which showed the most deviation between melting results and modeling predictions the model had predicted the formation of increased quantities of $MnAl_2O_4$. The results indicate that this compound may not form to the extent predicted by the model. This could be the result of the solidification of high alumina phases as slag skin during the first two thirds of the melt. The liquid slag in contact with the metal which was analyzed may have thus had a decreased capacity to remove manganese from the steel.

### 8.2.1.2 The Predicted and Observed Changes in Silicon Content

Comparison was also made between the predicted silicon loss and that which was observed, as is shown in Figure 8.3. The model consistently under predicted the amount of

silicon that would be removed from the steel, especially for heats for which slags low in calcia were used.

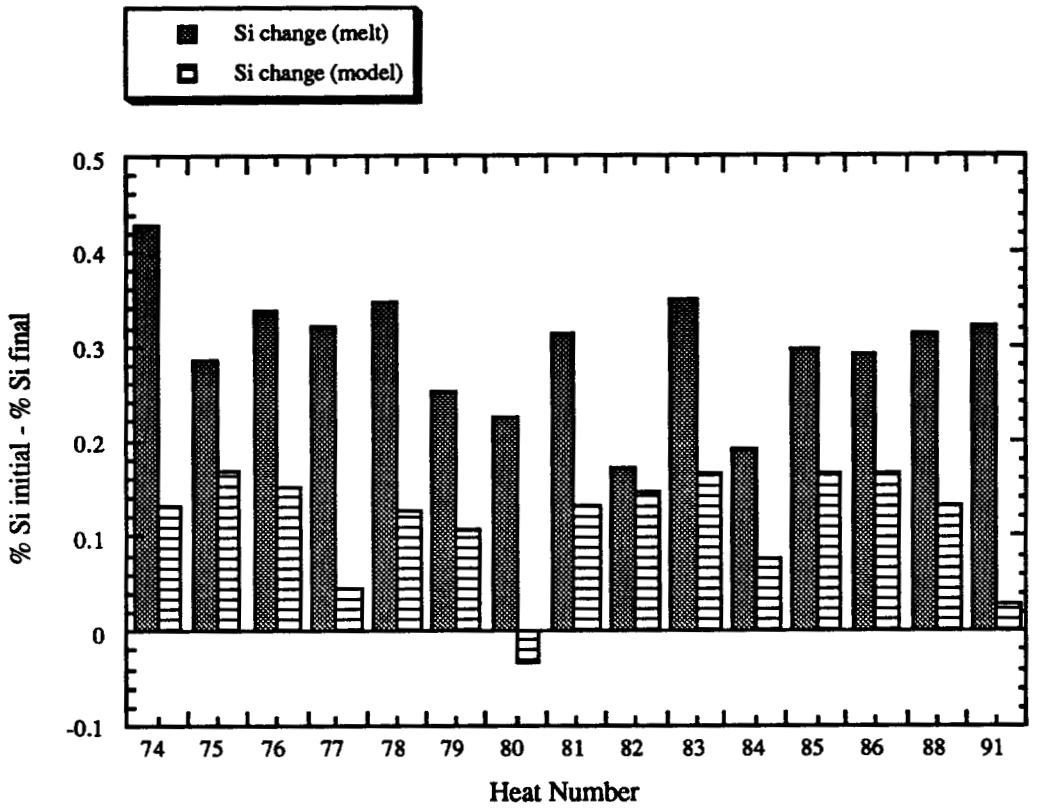


**Figure 8.3**
**Loss of Silicon from the Steel by Heat (Predicted vs. Actual)**

Free energy minimization predicted that the amount of silicon removed from the steel would be related to the amount of calcia initially in the slag. Figure 8.4 shows that melting results did not confirm this prediction, which suggests that silicon may be removed from the metal by several mechanisms which are either not predicted or are underestimated by modeling calculations. For example, silicon combines with fluorine to form $SiF_4$, a stable gas which is released during electroslag remelting. The presence of this gas is not predicted by modeling and loss of silicon associated with it is thus unaccounted for.

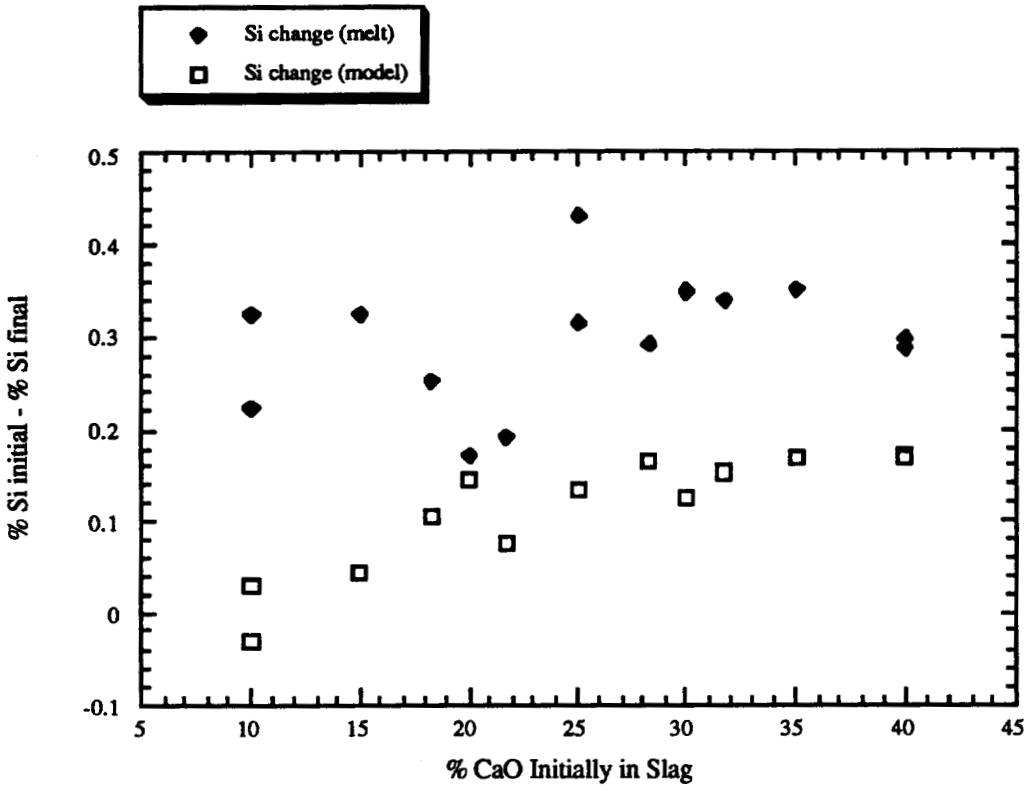


**Figure 8.4**
**Effect of Calcia Content of the Slag on Predicted and Actual Silicon Loss**

### 8.2.1.3 The Predicted and Observed Changes in Carbon Content

The changes in carbon contents of the ingots produced were compared to the changes predicted by modeling for each heat. Figure 8.5 shows that the model predicted that each heat would become enriched in carbon during the process of melting. This predicted enrichment was the result of the loss of other elements from the steel.

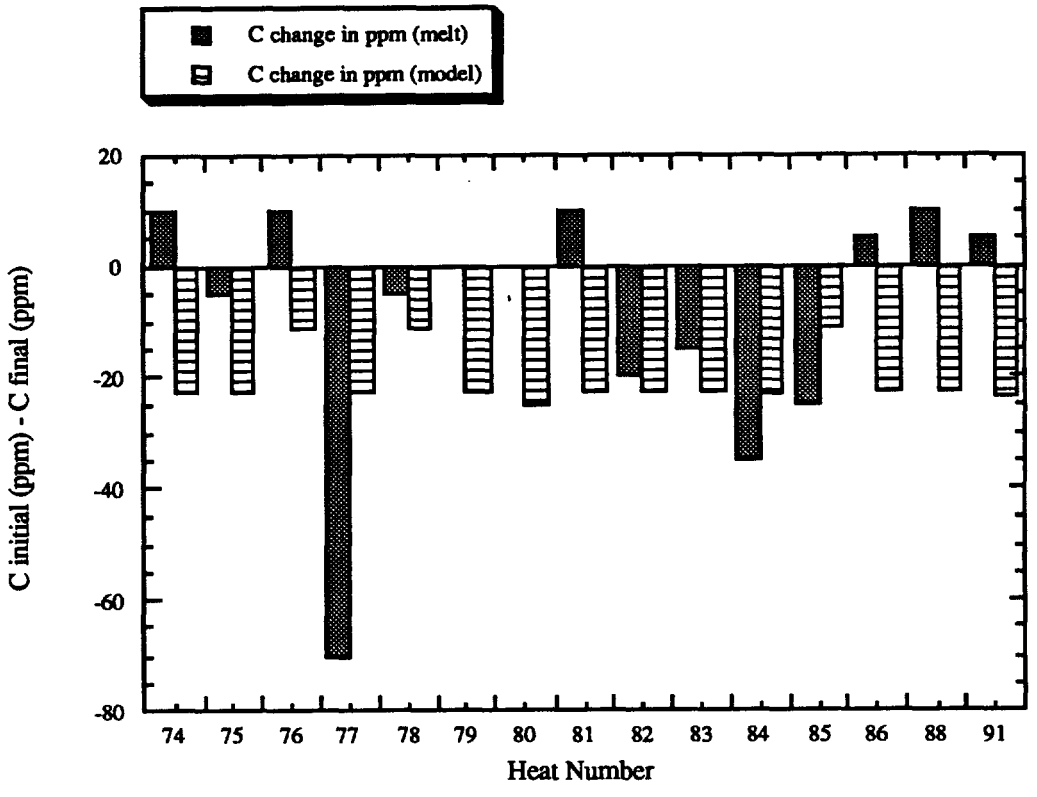


**Figure 8.5**
**Change in Carbon Content of the Steel by Heat (Predicted vs. Actual)**

The magnitude of the change in carbon content of a steel induced by remelting is dependent on several factors. During melting, carbon which is present in the electrode may be transferred to the slag and from the slag to the gas as $CO_2$. Carbon initially present in the slag may be a result of slag prefusion in a graphite crucible and may remain in the slag, be dissolved in the steel, or removed as a gas. The heats for which the carbon content of the steel was decreased were 74,76,81,88,86, and 91. Heats 74, 81, and 88 were all melted using a 50/25/25 slag. Heat 76 was melted using a 36.6/31.7/31.7 slag, heat 86 was melted using a 56.7/28.3/15 slag, and heat 91 was melted using a 70/10/20 slag. The carbon content for heats 79 and 80 did not change. Heat 79 was melted with a 63.4/18.3/18.3 slag and heat 80 was melted with a 50/10/40 slag. All other heats showed an increase in carbon content of the steel produced, particularly heat 77 which was melted with a 56.7/15/28.3 slag. The change in carbon content of the steel was not shown to be related, in any obvious way, to the initial chemistry of the slag used. The greatest amount of carbon pickup was

expected to occur during melts conducted using slags containing free lime. Such slags are known to pick up carbon during prefusion in graphite crucibles by the reaction:

$$CaO + 3C \rightarrow CaC_2 + CaO$$

The slag used when melting heat 75 had the most lime of any of the slags and was observed to react with the graphite crucible during prefusion. In addition, this slag was gray in color and difficult to grind, perhaps indicating the presence of calcium carbides. When this slag was used for remelting, however, the steel was only slightly enriched in carbon. This indicates that carbon pickup by the steel may not be solely a function of the amount of carbon initially present in the slag. In electroslag remelting, carbon may partition between the metal, the slag, and the gas phases. In order to more fully understand the factors governing this partitioning, samples of slag and gas should be taken at known times throughout the melt.

#### 8.2.1.4 The Predicted and Observed Changes in Sulfur Content

The predicted and observed changes in the sulfur content of the steel for each heat are shown in Figure 8.6.

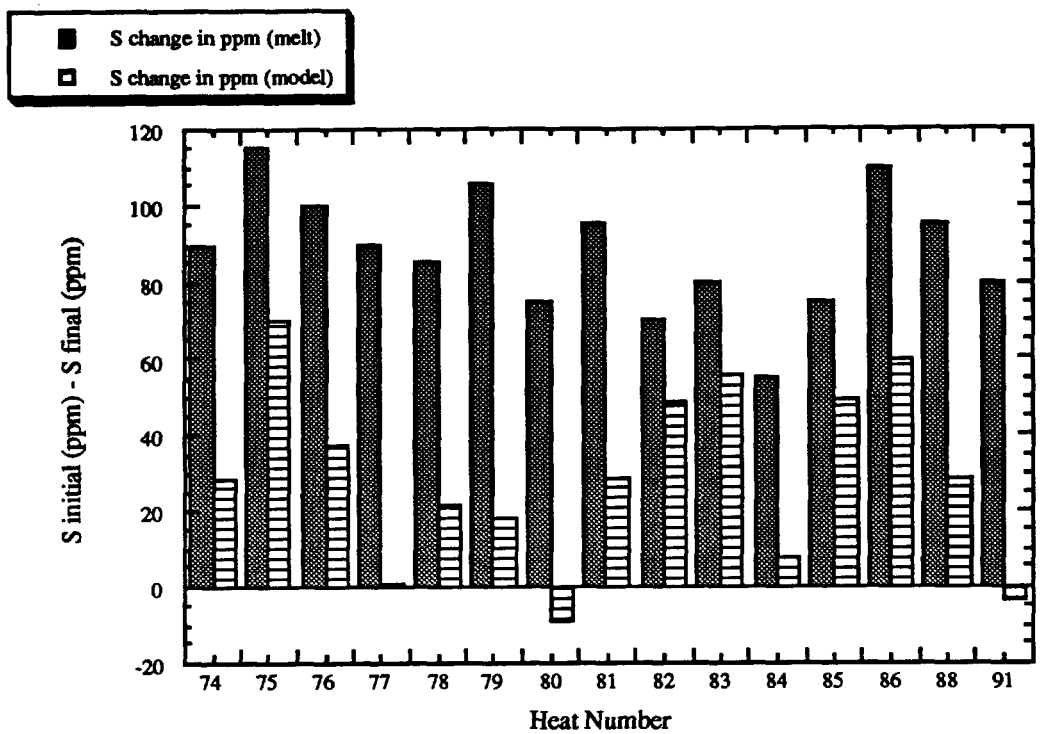


**Figure 8.6**
**Change in Sulfur Content of the Steel by Heat (Predicted vs. Actual)**

The model predicts that sulfur will be removed from the steel by the formation of lanthanum and cerium oxysulfides and thus the extent of removal predicted is linked to the behavior of the surrogates. These oxysulfides are quite stable and are regularly found in steels which have been deoxidized by the use of rare earth elements. The formation of oxysulfides is, however, only one mechanism by which sulfur may be removed from steel. Figure 8.6 shows that the model always underestimated the level of sulfur removal achieved, indicating that other mechanisms may be present. Sulfur is transferred from the metal to the slag. As the slag contacts the atmosphere, the sulfur reacts with oxygen, forming $SO_2$, which is removed as a gas. The slag which removed the largest amount of sulfur from the steel was that used for heat 75, and contained 50% $CaF_2$, 40% CaO, and 10% $Al_2O_3$. Highly basic slags such as this one are industrially known for their ability to remove sulfur from steel. This ability is related to the amount of available oxygen in a slag. The slag used for heat 85 did not remove sulfur as effectively although it contained an equal amount of CaO. The slag used for heat 85 was different than that used for heat 75 in that it contained more $Al_2O_3$ and not as much $CaF_2$. The presence of increased amounts of

alumina in the slag may have caused a decrease in the amount of free oxygen present, perhaps by the formation of stable calcium aluminates. The decrease in calcium fluoride content would have made the slag used for heat 85 more viscous than that used for heat 75. Slag viscosity may have influenced the kinetics of metal-slag and slag-gas reactions. In general, the slags which desulfurize best seem to have high calcia contents as well as high calcium fluoride contents, indicating that sulfur removal is governed by kinetics as well as by chemical partitioning. In order to study the role of slag chemistry in the removal of sulfur from steel during remelting, several melts should be performed using slags of different chemistries and samples of slag and gas should be taken throughout each.

### 8.2.2 Implications

The chemistry changes associated with remelting stainless steel are important in terms of producing an alloy which meets the chemical specifications of the final product to be produced. Specifications for stainless steel include chemistry ranges for high value alloying elements as well as maximum permissible amounts of undesirable trace elements. In the case of nonsensitizing stainless steels, a maximum allowable limit is specified for carbon. Stainless steels which meet the chemical specifications for a particular grade and also have carbon levels lower than the maximum specified amount carry an L designation, such as 304L and 316L.

The steel bars melted in this study initially met most of the chemical specifications for 304L. Electroslag remelting using different slags resulted in the production of ingots with different final chemistries. Most of the ingots met the ASTM specifications for both wrought and cast product. There were, however, some exceptions. The carbon level of the ingot produced by heat 77 was 0.031, which is over the prescribed limit of 0.030 for both wrought and cast product. The slag used in heat 77 was a 56.7/15/28.3. Some of the bars melted (those from master melt E3) were too high in manganese (1.53%) to meet the ASTM cast specification of 1.5% max. and too high in silicon (0.84%) to meet the ASTM wrought specification of 0.75% max. After remelting, all the ingots produced met both specification for manganese and silicon contents. The ingot produced by heat 74 was stripped of enough chromium so that at 17.5% it fell below the wrought specification of 18-20%. The bar used to produce this ingots contained 18.1% chromium before remelting. Each ingot produced met the specifications for nickel and phosphorus contents. The bars contained more than 0.01% sulfur before remelting (0.014% for E2 and 0.017% for E3) and while these values are well below the prescribed maximum of 0.03%, remelting further reduced the sulfur level to between 0.005 and 0.009%. In most cases, remelting did not

cause the steel to deviate from the chemistry for 304L, and, in fact, resulted in a decrease in the levels of tramp elements such as sulfur and silicon present in the metal. Further work should be done in order to determine the mechanisms responsible for carbon enrichment and chromium loss, as either of these could result in the production of steel which did not meet the chemical requirements of the desired grade.

## 8.3 Power Requirements

The power required to perform electroslag remelting was dependent upon the chemistry of the slag used. During the steady state portion of each melt, real time readings of current, voltage, power, and impedance were recorded. The average power consumed during each melt was calculated and is shown in Figure 8.7. During melting, a certain amount of power is required to heat the slag to a temperature above the liquidus of the electrode so that melting takes place. The amount of power necessary depends on the resistivity of the slag. Slags with high resistivity generally require the application of less power to achieve a temperature suitable for melting than slags with low resistivity.

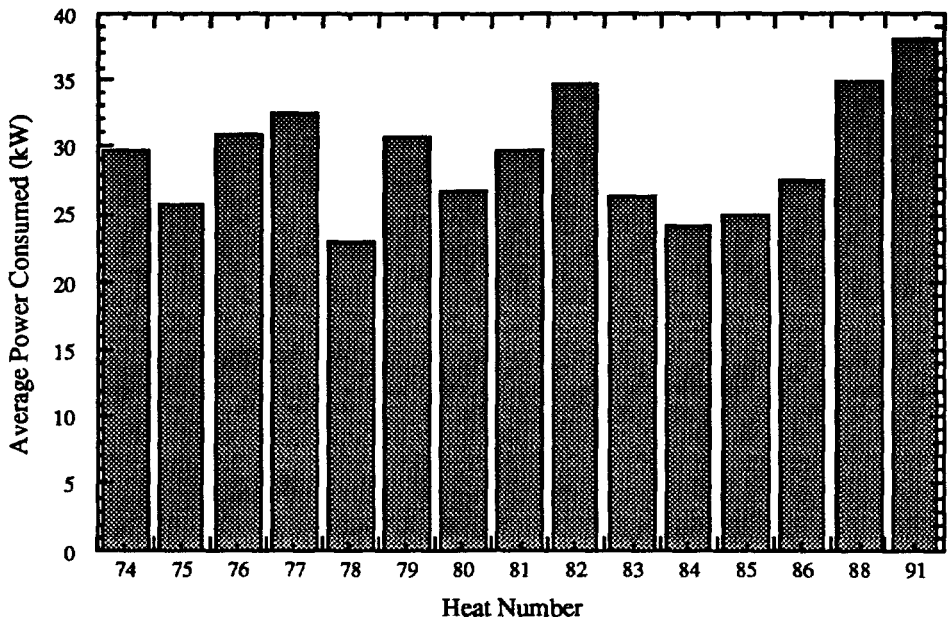


**Figure 8.7**
**Average Power Requirement for Each Heat**

The figure shows that the slag used in heat 91 required the most power in order to achieve electrode melting. This slag contained 70% $CaF_2$, which is highly conductive and thus has a low resistivity. The slags used in heats 78, 84, and 85, required less power. These slags are high in alumina and have high resistivities.

### 8.3.1 Implications

While the choice of a slag for melt decontamination would likely be based on the decontamination efficiency provided and the surface quality produced, power requirement could influence the choice between two or more slags whose performance is similar in other respects. In addition to influencing the power requirement of the ESR process, the resistivity of the slag could have direct influences on the efficiency of the decontamination achieved by remelting. Depending on the control strategy employed, the use of a highly resistive slag could cause an increase in melt rate, which could be detrimental to decontamination reactions which may be kinetically limited. On the other hand, however, the temperature achieved in the slag pool may be higher when a highly resistive slag is used. Increased temperatures could increase the rate at which decontamination reactions proceed.

## 8.4 Surface Quality

The surface quality of the remelted ingots varied according to the slag that was used. Each ingot was assigned a surface quality rating. These ratings are listed in Table 8.1. Ingots whose surface quality was rated as excellent were smooth and shiny, with no slag adhering to the surface of the ingot. Ingots whose surface quality was rated as good were somewhat smooth, with no visible surface slag inclusions. Those ingots which received a poor surface quality rating had a rough surface with some degree of slag entrapment.

**Table 8.1**
**Surface Quality Ratings of Remelted Ingots**

| Heat Number | Surface Quality Rating |
|---|---|
| 74 | good |
| 75 | poor |
| 76 | excellent |
| 77 | excellent |
| 78 | average |
| 79 | good |
| 80 | average |
| 81 | good |
| 82 | good |
| 83 | average |
| 84 | good |
| 85 | poor |
| 86 | average |
| 88 | good |
| 89 | good |
| 90 | good |
| 91 | excellent |
| 92 | good |
| 93 | good |
| 94 | average |

### 8.4.1 Implications

In the remelting of radioactively contaminated scrap metal, the need for good surface quality stems from the fact that entrapped slag inclusions will be radioactive. In an industrial melt decontamination facility, remelted ingots would be subjected to some type of forming operation, depending on the end product being manufactured. The surface roughness of ingots is directly related to the quality of the final product. Thus, if ingots could be produced with uniformly excellent surface, decontamination efficiency would be increased and finishing operations prior to forming could be eliminated.

## 8.5 Partitioning of Surrogates Between the Slag Skin and the Slag Cap

Although each slag tested in this study was shown to remove the surrogate elements from the bulk of the stainless steel to below detectable levels, the slags were shown to behave differently in other respects. The chemistry of the slag was observed to influence

the thickness and texture of the slag skin formed between the water cooled copper crucible wall and the solidified ingot. The average thickness of the slag skin formed during each heat is shown in Figure 8.8.

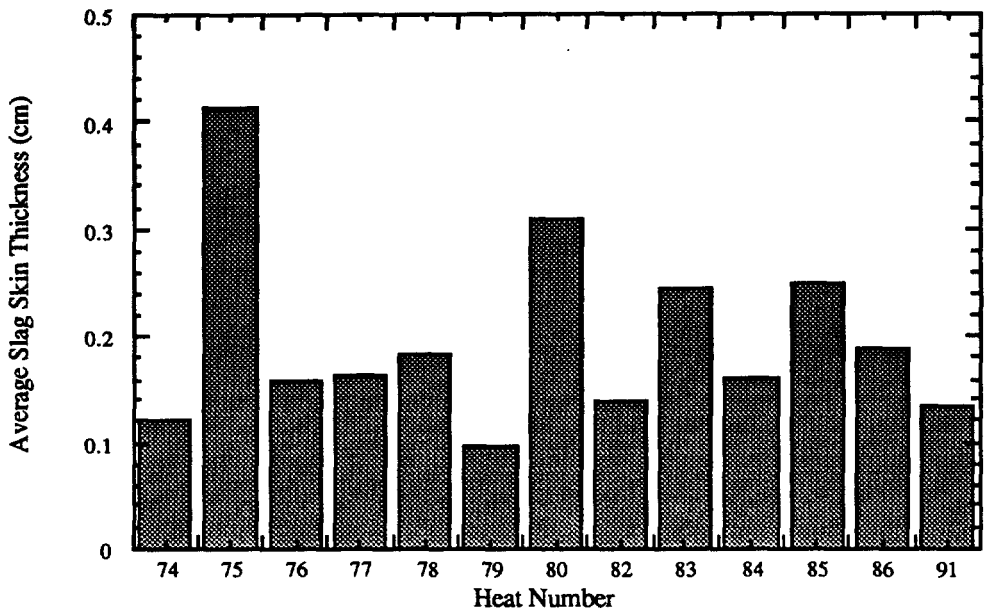


**Figure 8.8**
**Average Slag Skin Thickness for Each Heat**

In addition, the distribution of the surrogate elements between the slag skin and the slag cap was shown to be influenced by the chemistry of the slag. The weights of the lanthanum and cerium in each slag skin were expressed as a percentages of the total weights of lanthanum and cerium present in the final slag (cap + skin) from each heat. The percentages of the total amounts of surrogate elements present that solidified as part of the slag skin formed in each heat are listed in Table 8.2 and shown in Figure 8.9.

**Table 8.2**
**Partitioning Of Surrogate Elements**

| Heat # | % of total Ce captured in Slag Skin | % of total La Captured in Slag Skin | % of total Nd Captured in Slag Skin |
|---|---|---|---|
| 74 | 8.9 | 8.3 | 20.8 |
| 75 | 36.3 | 30.5 | 54.6 |
| 76 | 12.6 | 10.0 | 20.9 |
| 77 | 10.1 | 10.7 | 25.3 |
| 78 | 8.3 | 8.8 | 17.4 |
| 79 | 6.4 | 6.3 | 12.1 |
| 80 | 26.1 | 26.0 | 41.5 |
| 81 | 18.3 | 17.4 | 27.1 |
| 82 | 16.1 | 17.3 | 16.9 |
| 83 | 18.0 | 20.8 | 30.3 |
| 84 | 16.1 | 12.3 | 19.6 |
| 85 | 21.1 | 26.5 | 27.7 |
| 86 | 18.5 | 16.8 | 27.3 |
| 88 | 14.6 | 12.9 | 25.5 |
| 89 | 10.3 | 10.6 | 15.8 |
| 90 | 43.0 | 56.2 | 32.8 |
| 91 | 6.4 | 6.3 | 16.5 |
| 92 | 15.9 | 16.9 | 15.7 |
| 93 | 57.8 | 85.3 | 87.5 |
| 94 | 86.2 | 49.7 | 41.6 |

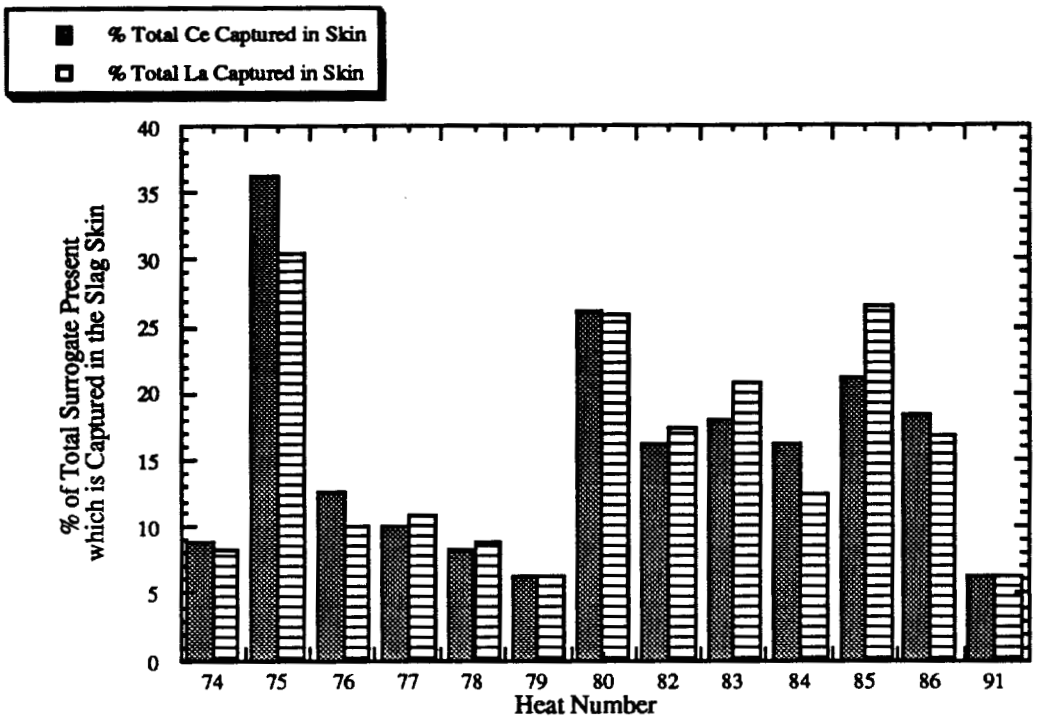


**Figure 8.9**
**Percentage of Total Surrogate Weight Captured in the Slag Skin for Each Heat**

Figure 8.9 indicates that lanthanum and cerium behave similarly, though in most cases not identically, in their tendency to partition to the slag skin. A comparison of Figures 8.8 and 8.9 suggests that when the thickness of the slag skin increases, the quantity of surrogate it contains also increases. The relationships between slag skin thickness and the percentage of the total surrogate element contained in the slag skin are shown in Figures 8.10 and 8.11.

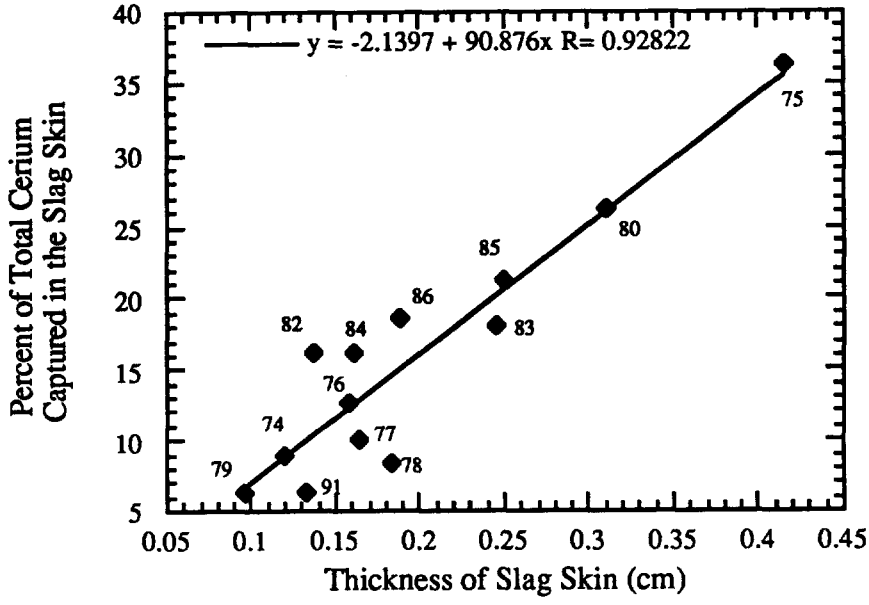


**Figure 8.10**
**Percentage of Cerium Captured in the Slag Skin as a Function of the Average Thickness of the Slag Skin**

This figure shows that the relationship between the thickness of the slag skin and the percentage of the total cerium present in the slag skin is, in general, linear. There are, however, some important exceptions. The slags used in heats represented by points which lie below the line show a tendency to cause concentration of cerium in the slag cap. Points above the line represent heats during which cerium was concentrated in the slag skin.

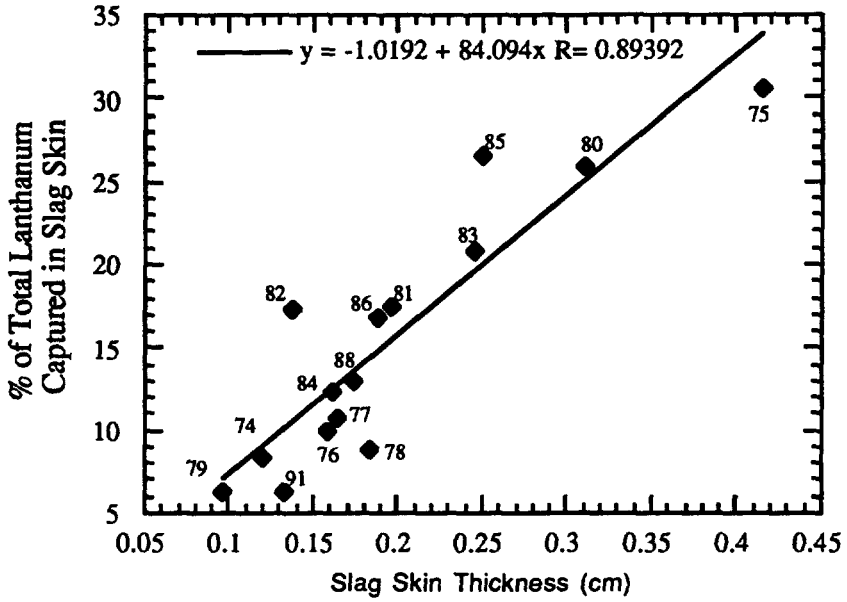


**Figure 8.11**
**Capture of Lanthanum in the Slag Skin as a Function of the Thickness of the Skin**

The observed concentration of lanthanum in the slag skin was somewhat different from that of cerium. This figure shows that lanthanum was strongly concentrated in the slag skin for heats 85 and 82 and was concentrated in the cap for heats 91, 76, 77, and 78. The relationship of the slag chemistries which produce this partitioning may be observed in the following diagram, Figure 8.12.

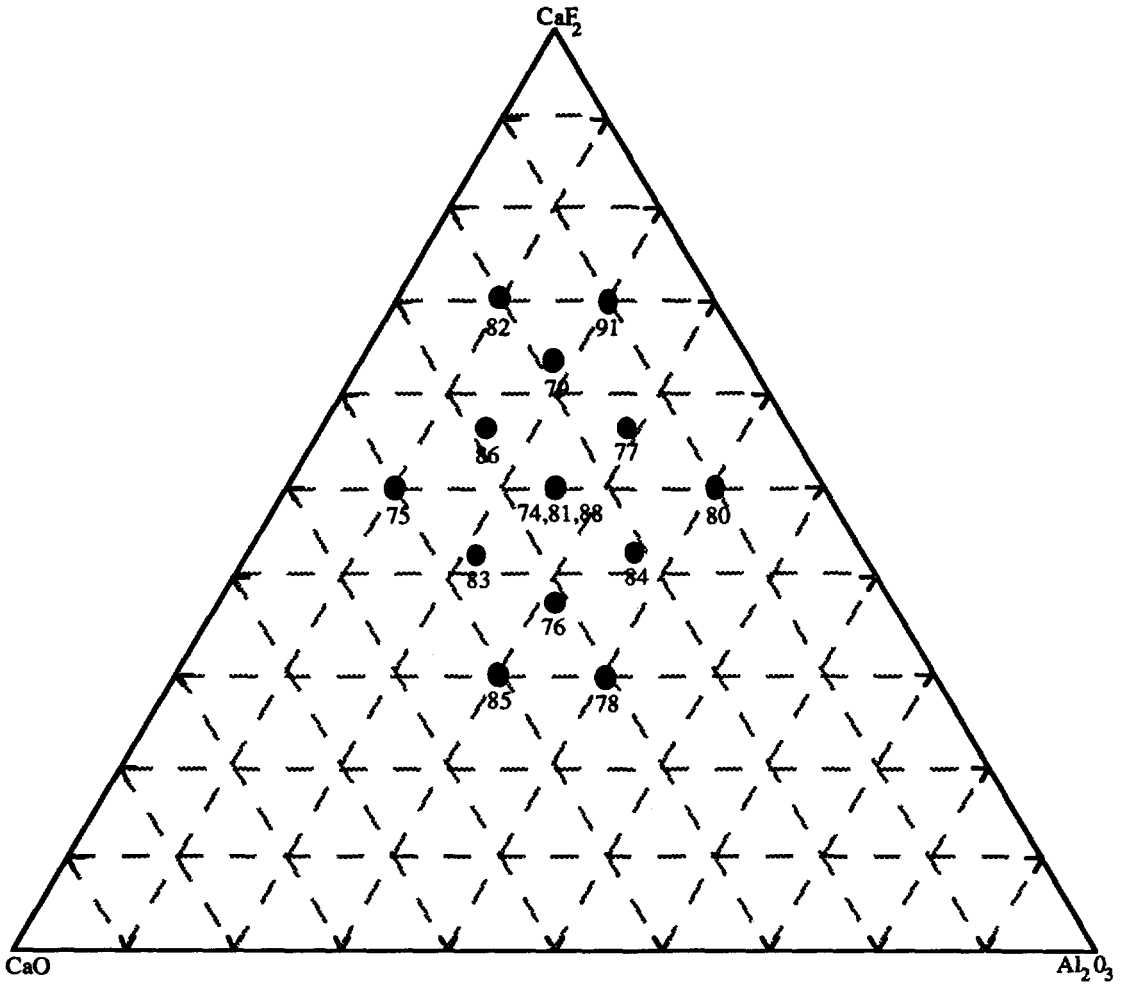


**Figure 8.12**
**Slag Chemistries by Heat Plotted on Ternary Grid**

Determination of the effect of the slag chemistry on the partitioning is most clearly observed along lines for which the amount of one component is held relatively constant while the proportions of the other two components change in relation to each other. One such line contains the points 78, 76, 83, and 75. Along this line, the concentration of CaO in the slag changes only slightly while calcium fluoride increases and alumina decreases. Figure 8.13 shows the change in the amount of surrogates captured in the slag skin as the slag increases in calcium fluoride along this line.

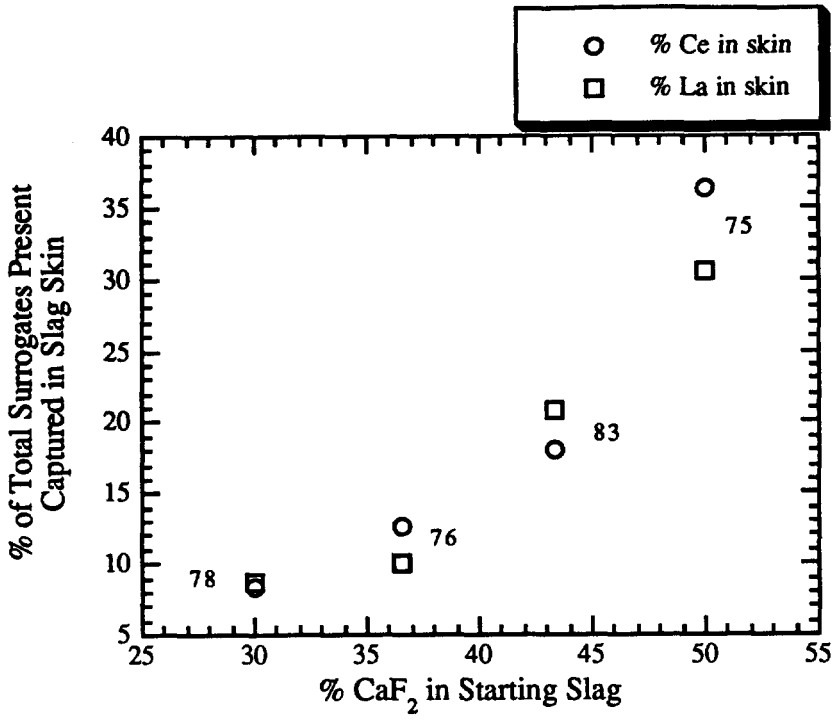


**Figure 8.13**
**Partitioning of Surrogates as a Function of Increasing $CaF_2$ and Decreasing $Al_2O_3$**

Along the line containing points 78, 76, and 86, (approximately 40% CaO) a similar trend is observed. As calcium fluoride is increased at the expense of alumina and calcium oxide is held fairly constant, the percentage of the total amount of surrogates present that reports to the slag skin is increased. The effect of increasing calcium fluoride while keeping alumina relatively constant (between 10 and 20 %) was observed by plotting values for the heats 75, 86, 79, and 91 (Figure 8.14) For this sequence, the surrogate in the slag skin decreases as calcium fluoride is increased. This trend was also observed for the sequence of melts 83, 79, 91 at 20 % alumina .

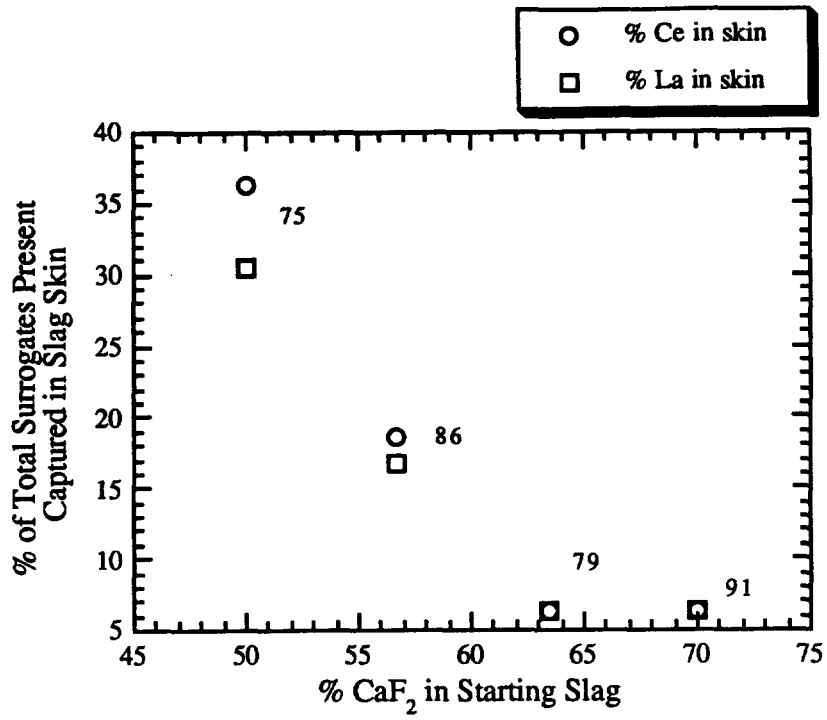


**Figure 8.14**
**Partitioning of Surrogates as a Function of Increasing $CaF_2$ and Decreasing CaO**

The ternary phase diagram has two areas for which slags tended to cause more than 87% of the surrogates to be concentrated into the slag cap. The first area is in the region of points 91, 79, and 77. The second region includes the points 76 and 78. Radiating out from these two regions is an area which includes points 86, 84, 83, in which up to 80 % of the surrogates reported to the cap. Outside these regions, at high levels of lime or alumina, increased percentages of surrogate reported to the skin.

Another, more accurate way, of determining the ability of a slag to concentrate surrogate elements in the slag skin or reject them to the slag cap is to examine the relationship between the percentage of the total cerium captured in the slag skin as a function of the percentage of the of the total weight of the slag that solidified as slag skin. This eliminates the bias of ingot length inherent in Figure 8.10. The slag skin of a long ingot may have the same average thickness as that of a shorter ingot, but the skin of the longer ingot will weigh more. The percentage of the surrogate contained in the slag skin will also tend to be greater when a longer ingot is formed. Therefore, when the percentage

of the total surrogate weight which is present in the slag skin is plotted against the percentage of the slag weight which makes up the slag skin, any tendencies of the slag to cause surrogate partitioning will become evident. This relationship is plotted in Figure 8.15. The points representing heats 82, 84, and 85 have been omitted from the graph because a mass balance revealed that an insufficient amount of surrogate had been applied to the bars melted in these heats.

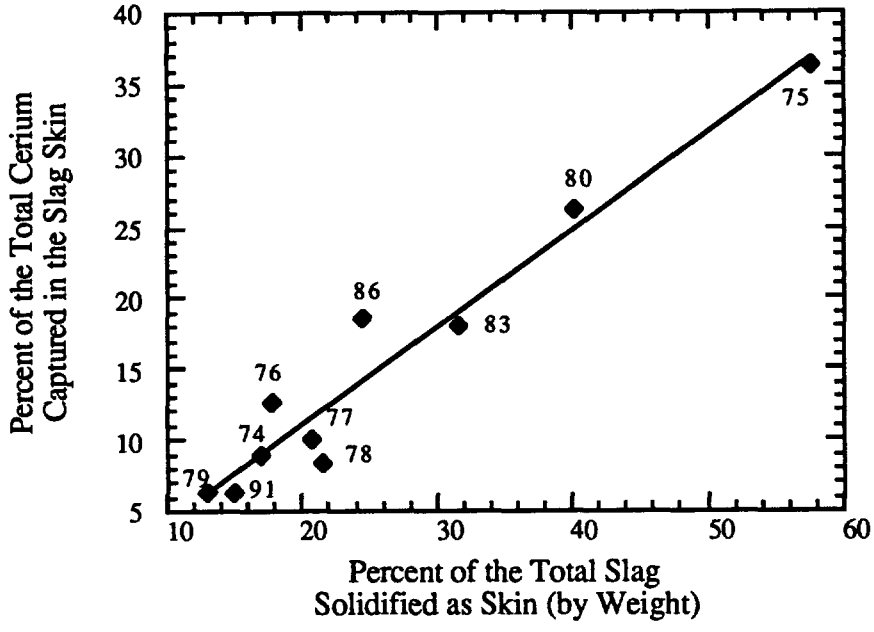


**Figure 8.15**
**Percentage of Cerium Captured in the Slag Skin as a Function of the Percentage of the Slag Which Solidified as Skin**

The graph shows that, during heats 91, 78, and 77, cerium was selectively partitioned to the slag cap while during heats 76 and 86, the surrogate was concentrated in the slag skin. Such partitioning, if not merely a result of experimental data scatter, must result from phenomena related to the behavior of the surrogate elements in the slag. The mechanism proposed to explain this partitioning is based on the solidification mechanics of the various slags and the preferred chemical forms of the surrogates as determined by the species present in the molten slag.

The surrogates used in this study were introduced as oxides with very high melting points (2600°C for $CeO_2$ and 2301°C for $La_2O_3$). It is therefore unlikely that the surrogate oxides melted in the slag, but they may well have been dissolved just as table salt does not melt in water at room temperature, but is dissolved by the action of water dipoles. Although the extent of this dissolution is not known, X-ray fluorescence performed on one slag did not reveal the presence of undissolved $CeO_2$ or $La_2O_3$, but revealed the presence of rare earth oxygen aluminum compounds. This suggests that dissolution and subsequent reaction had occurred in the slag.

Upon dissolution, surrogates are free to remain in the liquid slag as ions or to combine to form compounds. The types and amounts of the compounds which are formed will depend on the species present in the liquid slag. Surrogate bearing compounds may either be solidified out as part of the slag skin or be redissolved in the slag, depending on the melting point of the compound formed and its physical proximity to the cold copper crucible. The chemical constitution of the liquid slag changes throughout the melt, so that the species which may be formed at the beginning of the melt could be different from those formed as melting proceeds.

A slag skin is formed by the selective solidification of one or more phases on the water cooled copper wall. The phases which solidify and their order of solidification are determined by the composition of the liquid slag and the governing phase relationships as shown by the phase diagram. Because the chemistry of the slag in contact with the cold copper crucible wall is constantly changing, the phases which solidify also change as the heat progresses. For the purposes of this work, the slags were assumed to be simple ternary mixtures of calcium fluoride, calcium oxide, and alumina. The presence of small quantities of silica and other oxides was ignored. The influence of lanthanum and cerium on the established $CaF_2$-$CaO$-$Al_2O_3$ ternary has not been determined, and was assumed to be negligible.

A simple model was used to describe the ways in which surrogate bearing species become part of the slag skin. Surrogate ions in the slag are thermodynamically more likely to combine with other ions to form compounds when they are present in the cooler slag near the crucible walls. These compounds may simply become entrapped as slag skin solidification proceeds. Alternatively, the compounds which form may have a higher melting point than the first slag phase to solidify, as predicted by the phase diagram. These high melting point compounds could solidify preferentially as part of the slag skin. Conversely, a surrogate ion is likely to remain in the liquid slag (which eventually becomes the slag cap) if the compounds which it forms are dissolved by the slag or have lower melting points than the components solidifying to form the slag skin. The temperatures of

interest in the application of this model, including the melting points of the important surrogate bearing compounds and the invariant temperatures in the ternary slag system, are presented in Table 8.3.

**Table 8.3**
**Important Transformation Temperatures and Melting Points of Predominant Compounds**

| Compound or Invariant Point | Temperature of Interest (°C) | Change Taking Place at this Temperature |
|---|---|---|
| $CeF_3$ | 1460 | Melting |
| $LaF_3$ | 1500 | Melting |
| $CeAlO_3$ | ≈1800 | Melting |
| $LaAlO_3$ | 2110 | Melting |
| $CeO_2$ | 2600 | Melting |
| $Ce_2O_3$ | 1692 | Melting |
| $La_2O_3$ | 2307 | Melting |
| $C_3A_3Fl$ | 1507 | Melting |
| $C_{11}A_7Fl$ | 1577 | Melting |
| $CaF_2$ | 1422 | Melting |
| CaO | 2600 | Melting |
| $Al_2O_3$ | 2040 | Melting |
| P1 | 1405 | $L + C_3A3Fl = C_{11}A_7Fl + C_{aF2}$ |
| E4 | 1230 | $L = CaO+C_{11}A_7Fl+CaF_2$ |

In order to determine how the compounds formed by the surrogates depended on the species present in the liquid slag, the results of the Temkin ionic slag model were used to predict the activities of the surrogate bearing compounds which would be present at any point on the ternary diagram. A diagram was then plotted showing the area in which each of these compounds would be prevalent. The resultant diagram, showing the dominant compounds which the model predicts will be formed by cerium in ternary $CaF_2$-CaO-$Al_2O_3$ slags, is shown in Figure 8.16.

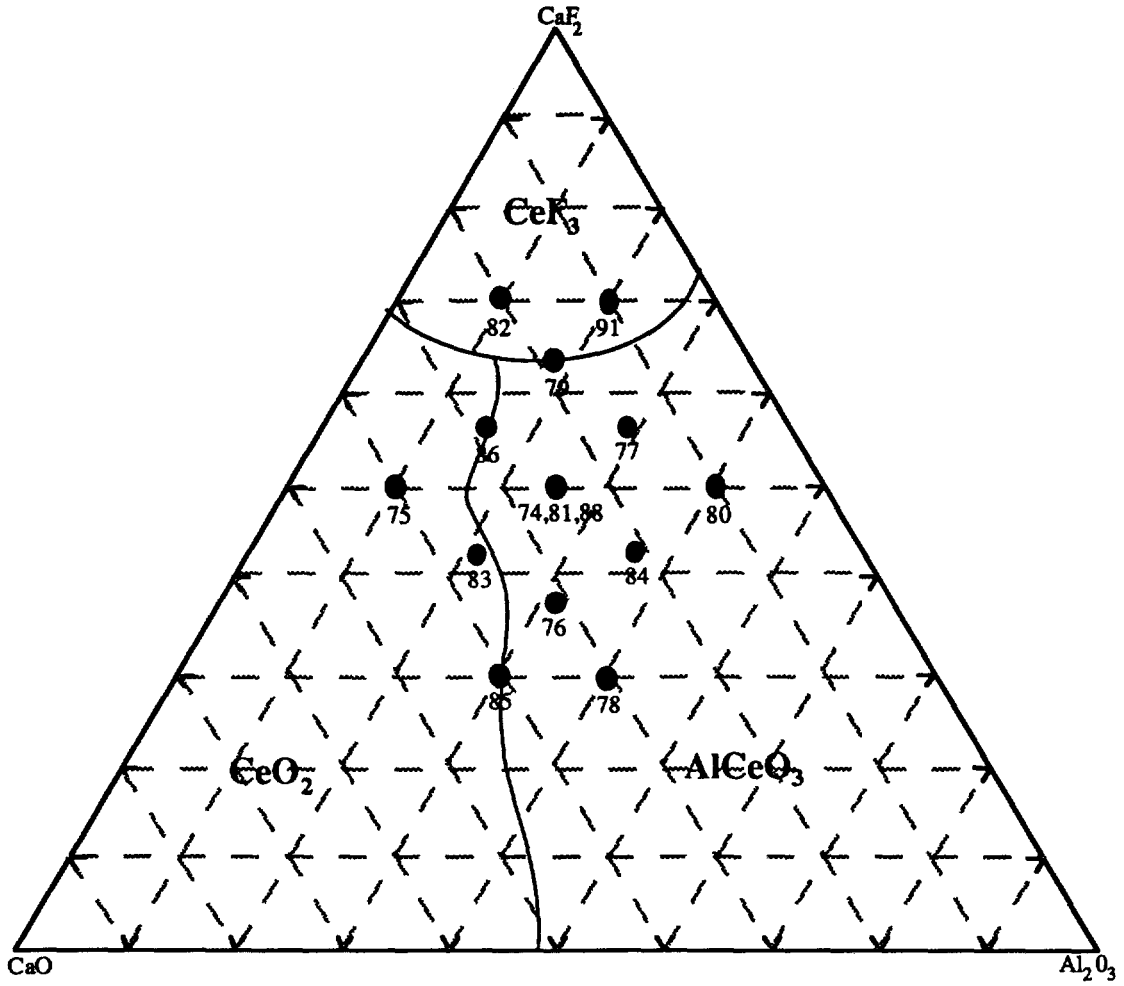


**Figure 8.16**
**Ternary Predominance Area Diagram Showing the Cerium Bearing Compound Which is Prevalent at any Point**

The diagram shows that, according to the Temkin ionic slag model, the dominant compound formed by cerium in a liquid slag depends on the chemistry of the slag. The presence of cerium as a fluoride, and oxide, or an aluminate depends on the presence of $F^-$, $O^=$, or $AlO_3^{---}$ in solution. Within each region shown, one compound of cerium is predicted to have a greater activity than either of the other two compounds. Along the lines dividing the areas, the activities of two compounds are essentially equal. The diagram also shows that as the slag chemistry changes, so does the prevalent cerium bearing compound which is formed.

In order to understand why some slags seem to concentrate cerium in the slag skin while others appear to concentrate it in the slag cap, the solidification mechanics of the

various slags must be examined. Mills[1] developed a solidus diagram which, in Figure 8.17, has been superimposed over a ternary grid on which the chemistry of each slag used in this study has been plotted.

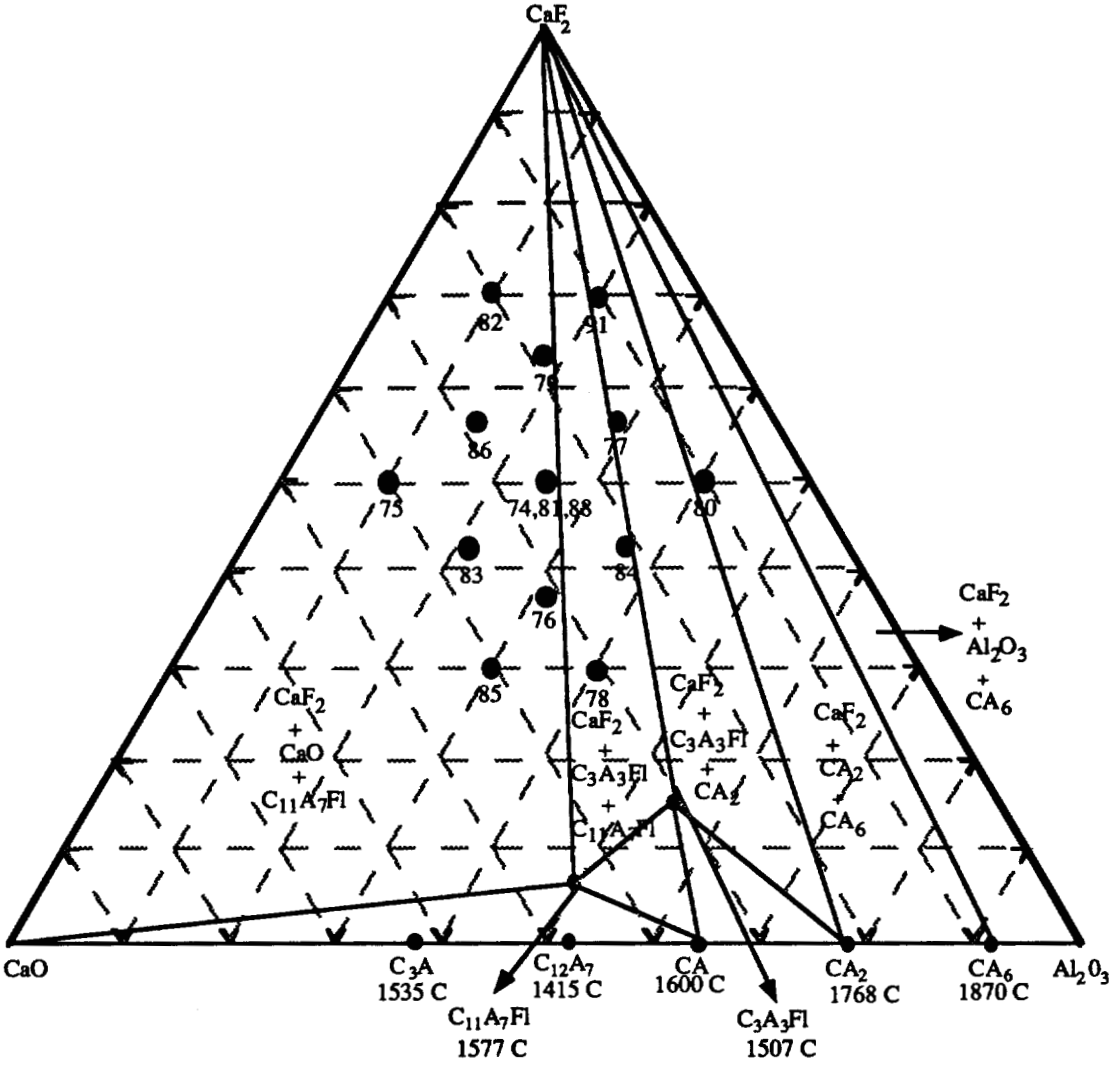


**Figure 8.17**
**Primary Crystallization Fields for the System $CaF_2$-Ca0-$Al_2O_3$ Showing the Phases Which Should Form on Solidification of the Various Slags Tested**

The figure shows that the various slags tested fall into categories according to the phases which are expected to form upon solidification. Interestingly, two of the slags which were shown to concentrate cerium into the slag cap, those used in heats 77 and 91, fall near the border between two solidification regions. One of these regions includes the point representing the slag used for heat 78, which also showed a tendency to concentrate cerium into the slag cap. All the points which lie in the region $CaF_2$+CaO+$C_{11}A_7Fl$ lie either

on the line in Figure 8.15, therefore showing no tendency to cause cerium partitioning, or above it, indicating a tendency to concentrate cerium in the slag skin.

Figure 8.17 is useful in that it shows the phases which will form upon solidification for each of the slags tested. In ESR, however, solidification of the slag phase proceeds selectively, therefore it is useful to consider the order in which the phases solidify, as shown by the ternary phase diagram shown in Figure 8.18.

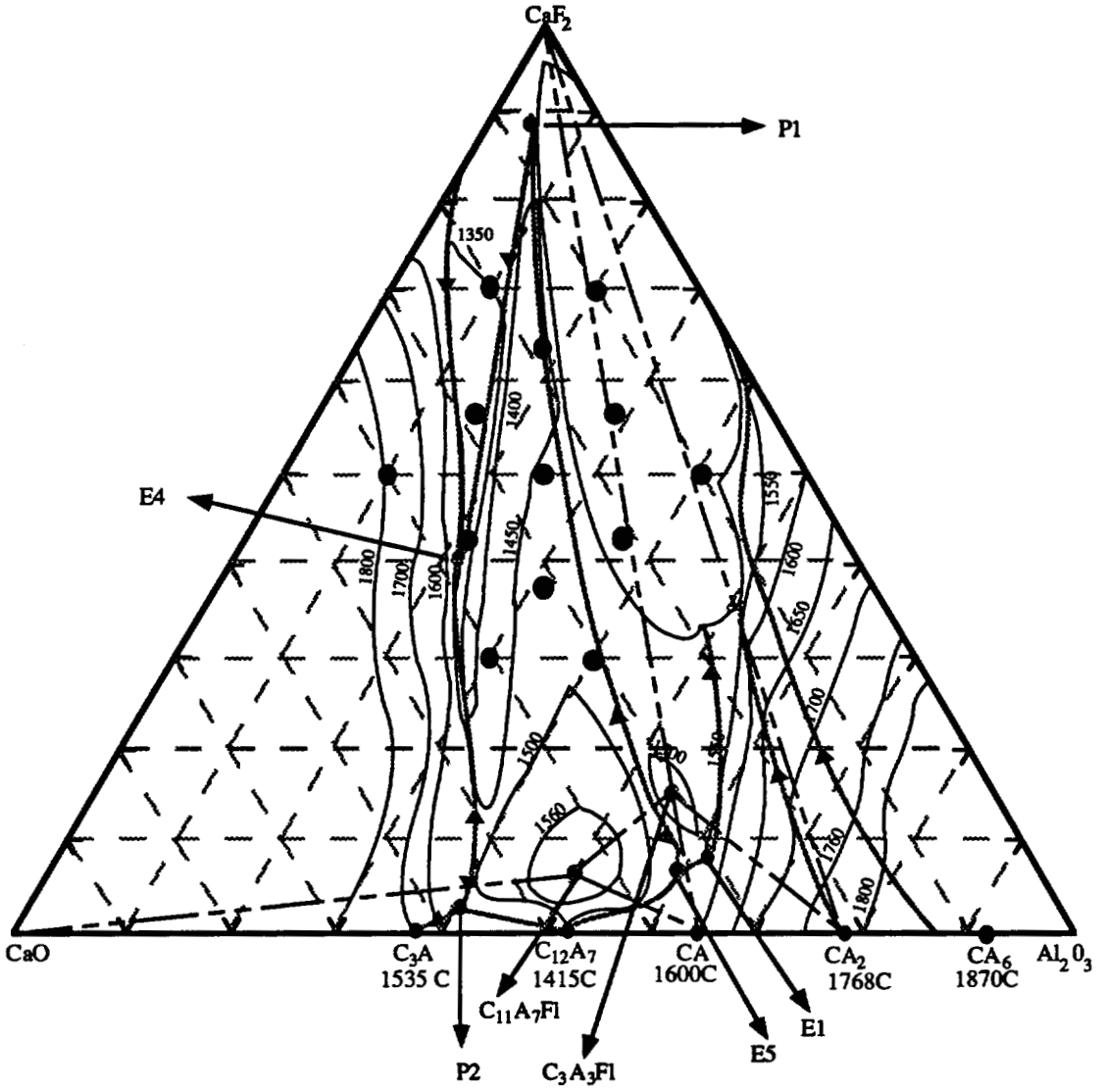


**Figure 8.18**
**Ternary Phase Diagram for the System $CaF_2$-CaO-$Al_2O_3$ Showing the Chemistries of the Various Slags Tested**

For each of the slags used in this study, a solidification path may be traced. The number of steps in the solidification path and the manner in which the last liquid solidifies

determines the composition of the slag skin and influences the slag skin thickness. The slag used in heat 75, for example, yielded the thickest slag skin of any slag studied. The first constituent to solidify is CaO, causing the slag composition to follow a path directly away from the CaO corner of the phase diagram until it intersects a eutectic trough. The composition of the slag followed this trough until the final liquid solidified eutectically at point E4. The slag used in heat 83 was very near the eutectic point E4. The slag used in heat 83 had a much thinner slag skin than that used in heat 75 because the solidification path was much simpler. The slag used in heat 79, which yielded the thinnest skin of any slag tested, lies directly on a solidification path terminating with peritectic solidification at point P1. The composition of the slag used in heat 78 lies along the same solidification path as that used in heat 79, although farther from point P1. The longer solidification path followed by slag 78 resulted in a thicker slag skin than that observed for heat 79.

The order of phase solidification also influences whether cerium is partitioned to the slag cap or to the slag skin. Peritectic solidification seems to favor the concentration of cerium in the slag cap. Consider the slag used for heat 91. Before solidification begins, the slag is composed of two immisible liquids. The first compound to solidify at 1472°C is $C_3A_3Fl$. The predominant cerium bearing compound at this composition is $CeF_3$ which has a melting point of 1460°C. Cerium is thus concentrated in the liquid slag until the peritectic composition is reached. Peritectic solidification begins to take place at 1405°C, at which point cerium fluoride may solidify. The slag used for heat 77 solidifies in the same manner but has a thicker slag skin due to its longer solidification path. The vertical section of the phase diagram which contains the compositions of both slag 77 and slag 91 is shown in Figure 8.15.

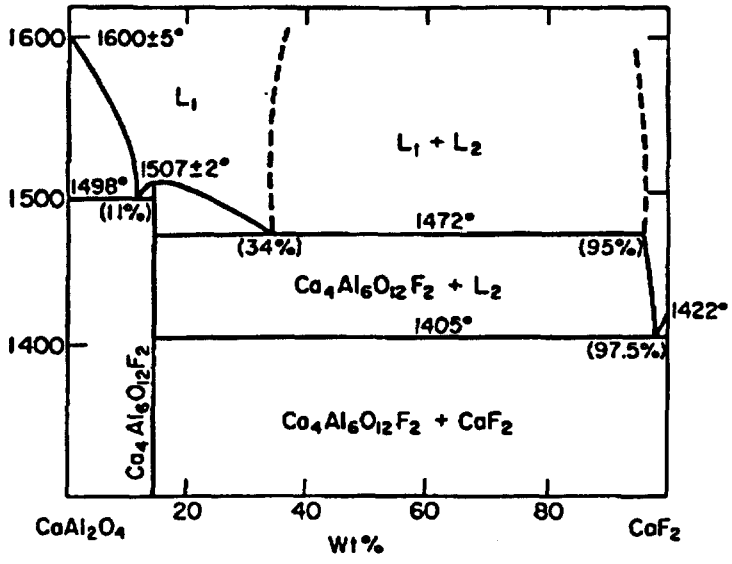


**Figure 8.19**
**Vertical Section of the Ternary Phase Diagram for the System $CaF_2$-Ca0-$Al_2O_3$**

The slag used in heat 78 also solidifies peritectically. As solidification begins, the primary cerium bearing phase is $CeAlO_3$, which has a melting point of approximately 2030°C. This compound should, initially, solidify in preference to the $C_3A_3F_1$ ($3CaO\text{-}3Al_2O_3\text{-}CaF_2$)which melts at 1507°C and thus be concentrated in the slag skin. As solidification proceeds, however, the liquid slag becomes increasingly rich in fluoride ion and more and more $CeF_3$ is formed, which remains with the liquid slag. By the end of the heat, the liquid slag is rich in cerium. Peritectic solidification may also encourage the rare earth to partition to the slag cap due to the presence of a high fluoride liquid at the solidification interface. This liquid may inhibit the formation of $AlCeO_3$ or cause it to be redissolved.

The slags which were observed to cause the cerium to concentrate in the slag skin were those used for heats 76 and 86, both of which solidified eutectically. In the case of heat 86, the primary slag phase to solidify is $CaF_2$ which has a melting point of 1422°C. All of the cerium compounds present, $CeF_2$, $CeO_2$ and $CeAlO_3$ have melting points greater than 1422°C and thus tend to concentrate in the slag skin. As solidification proceeds, the slag is depleted in fluorine and the predominance of high melting point phases increases as the solidification temperature of the slag decreases. In the case of heat 76, the most

abundant cerium phase is $AlCeO_3$ which solidifies in preference to the mixture of major slag constituents present whose liquidus temperature is approximately 1500°C.

Lanthanum, having been co-deposited with cerium on the bars to be melted, was also present in the slag. The tendency of lanthanum to partition between the slag skin and the slag cap is shown in Figure 8.20.

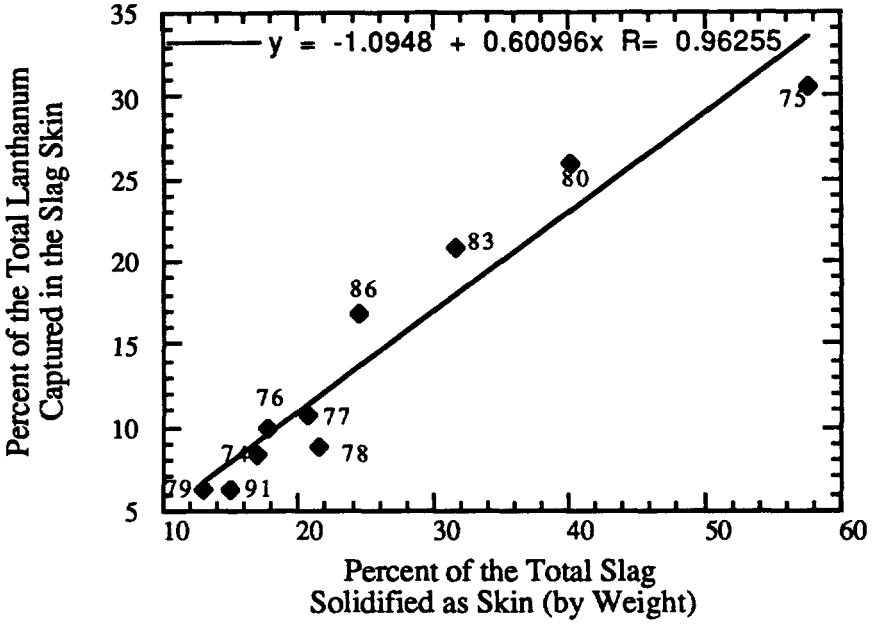


**Figure 8.20**
**Percentage of Lanthanum Captured in the Slag Skin as a Function of the Percentage of the Slag Which Solidified as Skin**

This figure shows that lanthanum is concentrated in the slag cap by the slags used in heats 78 and 91, just as cerium was. The slags which concentrated lanthanum into the slag skin were those used in heats 86, 83, and 80. The slag used in heat 86 also caused the concentration of cerium into the skin. The predominant lanthanum bearing phases present at any point were predicted by Temkin analysis and the results are shown in Figure 8.17 .

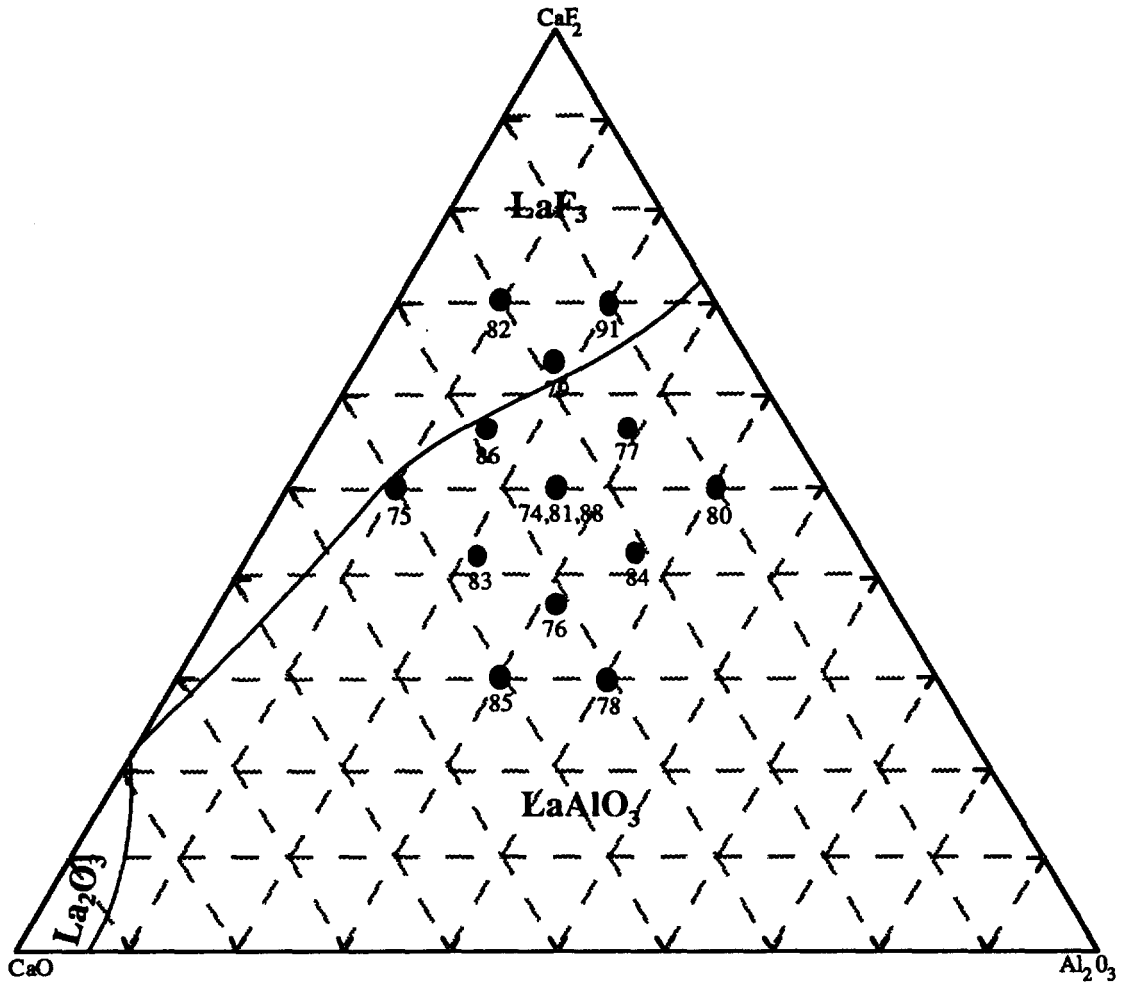


**Figure 8.21**
**Ternary Predominance Area Diagram Showing the Lanthanum Bearing Compound Which is Prevalent at any Point**

This figure shows that, according to the ionic Temkin model of the slag, $LaAlO_3$ predominates over much of the phase diagram. This is also predicted by free energy minimization. The concentration of lanthanum into the slag skin of heat 83 could be the result of this high melting aluminate compound solidifying preferentially to a eutectic slag having a low liquidus temperature. The slag used in heat 83 did not show a tendency to concentrate cerium in the slag skin. According to free energy minimization modeling, $LaAlO_3$ will form in preference to $CeAlO_3$, and thus the lanthanum could become concentrated in the slag skin while the cerium was not.

Several complicating factors have been neglected in the proposal of this mechanism for the partitioning of surrogates. The presence of the surrogate elements could change the phase relationships and liquidus temperatures presented in the simple ternary eutectic.

Calcium fluoride forms a eutectic with both lanthanum fluoride and cerium fluoride. The presence of either of these compounds lowers the melting point of the calcium fluoride. Also, in reality, the predominant surrogate compound will be the most thermochemically and kinetically favorable one, based on slag temperatures and availability of ions. The Temkin slag model used to determine the predominant surrogate compound only considers the availability of necessary ions. Cerium, for example, may form either the high melting point $CeO_2$ or the lower melting point $Ce_2O_3$, depending on the availability of oxygen. The presence of oxides of different melting points could affect the degree to which partitioning takes place. Nevertheless, the result that slags which solidify peritectically in the presence of a high fluoride liquid produce thin slag skins which have a tendency to contain small amounts of surrogate elements is interesting and the further testing of this theory could prove to be most worthwhile.

### 8.5.1 Implications

If the results observed in these experiments were proved to hold true when steel contaminated with radioactive elements is melted, the tendency of some slags to cause the partitioning of radionuclides to the slag cap could simplify the melt decontamination process considerably. The goal of melt decontamination is to concentrate the radioactive elements in a mineral-like solid slag which may be easily packaged for storage. The slag cap resulting from an ESR process tends to be dense and monolithic and, if it fractures at all, tends to break into large pieces without the production of a great deal of dust. The slag skin, on the other hand, often fractures into many small pieces which, in the process of removing the slag skin from the furnace, can generate a great deal of dust. It would be beneficial, therefore, to produce as small a volume of slag skin as possible. If the radioactive elements could be concentrated in the slag cap, the process of removing the ingot and the slag from the ESR furnace would be simplified and the probability of worker contamination could be decreased.

The surface treatment of ingots produced by the ESR process is expensive and the surface grinding of contaminated ingots could cause additional problems related to the production of radioactive dust. The concentration of radionuclides in the slag cap could mean that the contaminant level of any grinding dust produced could be considerably reduced. The optimum slag would enable the production of ingots with smooth surfaces, thus eliminating the need for surface treatment.

The mechanism for surrogate partitioning should be fully evaluated for each radionuclide of interest, as the compounds formed by uranium, plutonium, and the other

actinides may be different than those formed by the surrogates and may have different melting points.

## 8.6 Recommendation of an Optimum Slag

An optimum slag for the melt decontamination of stainless steel would have several attributes. The slag should maximize the extent of decontamination achieved while retaining the chemical pedigree of the alloy. In addition, the slag should solidify in such a manner that a uniformly thin slag skin is produced. This enables the production of ingots with smooth surfaces and uniform grain structure. In addition, the slag skin should contain as little of the radionuclide as possible.

Of the slags tested, those predicted by free energy minimization to most effectively remove lanthanum, cerium, and uranium from stainless steels were those used in heats 77, 79, and 91. The ingot produced by heat 77 was sufficiently enriched in carbon to be out of specification for 304L stainless steel. The slag used in heat 79 solidified peritectically to produce the thinnest slag skin of any slag tested. This slag skin also contained only 6.4% of the surrogate present in slag. This study indicates that the slag composition used in heat 79, 63.4/18.3/18.3, could be close to optimum for a decontamination slag. Other suitable compositions are expected to lie along the same solidification path. The slag used in heat 79 contains a high percentage of calcium fluoride and is moderately efficient in terms of power consumption. This slag is close in chemistry to 60/20/20, a slag commonly used in industry. The surface quality of the ingot produced with the slag used in heat 79 was rated as good. The ingot was smooth with no entrapped slag.

## 8.7 Remelting of Bulk Contaminated Material

In a related study, researchers at the Montana College of Mineral Science and Technology studied the factors influencing the removal of surrogate elements from bulk contaminated stainless steel by induction melting in the presence of a slag. The stainless steel used as feedstock in this study was produced by the addition of elemental cerium, lanthanum, and neodymium during plasma melting. A sample of this material was dissolved in an iodine stripping apparatus at the Oregon Graduate Institute. The alloy matrix was dissolved and the undissolved inclusions were captured and examined by Transmission Electron Microscopy (TEM). These inclusions were found to be oxysulfides of cerium, lanthanum, and neodymium which had agglomerated to form small inclusions

ranging in size from several hundred angstroms to a few microns.[2] It was postulated that these inclusions accounted for the bulk of the surrogates present in the bulk contaminated material.

One section of this bulk contaminated master ingot was electroslag remelted using a 50/25/25 slag. After remelting, the ingot retained 510 ppm Ce, 380 ppm La, and 360 ppm Nd. A sample of the remelted ingot was analyzed by TEM and no inclusions were found. Electroslag remelting was apparently effective in the removal of the surrogate containing inclusions, but ineffective in the removal of the surrogates dissolved in the steel.

Free energy minimization predicted that, at 1700°C, the residual amount of cerium remaining in the steel after remelting would be 0.26 ppm and that the residual amount of lanthanum would be 0.003 ppm. Electroslag remelting did not approach its predicted decontamination efficiencies for this steel. A comparison of the observed removal of sulfur, manganese, and silicon with that predicted by thermodynamic modeling revealed that the chemistry change of the steel was sometimes over estimated and sometimes underestimated. Predictions and observations were never more than a factor of four different, however.

Induction melting studies conducted at the Montana College of Mineral Science and Technology showed that the removal of the surrogates from the stainless steel was a time dependent process. Decontamination to levels approaching those predicted by thermodynamics were only observed after the molten steel had been stirred in the presence of a slag for 30 minutes.[3]

### 8.7.1 Implications

Apparently, the removal of elemental cerium and lanthanum from bulk contaminated stainless steel is a time dependent process and is thus more difficult than the removal of oxidized cerium and lanthanum from surface contaminated stainless steel. If electroslag remelting were to be used as part of a decontamination and decommissioning project, surface contaminated material should perhaps be directly ESR melted, electrode configuration permitting, and not be cut up and induction melted prior to electroslag remelting. Further work is necessary in order to determine whether, with proper process design and slag chemistry, ESR could be as effective at removing bulk contamination as it is at removing surface contamination.

# Chapter 8 References

[1] Mills, K.C., Keene, B.J. "Physicochemical Properties of Molten $CaF_2$ based slags" *International Metals Reviews*, No 1, (1981), 21-69.

[2] Shendye, Sanjay, B. "Characterization of Rare-Earth Element Containing Stainless Steel and Steel Alloys Using Electron Microscopy", Unpublished Report, Oregon Graduate Institute, (November, 1994).

[3] Worcester, S.A., Twidwell, L.G., Paolini, D.J., Weldon, T.A., Mizia, R.E. (Ed.) "Decontamination of Metals by Melt Refining/Slagging,: First Year Progress Report," Westinghouse Idaho Nuclear Company, Inc. WINCO-1138, INEL-DOE, (1995).

# Chapter 9
# Conclusions and Recommendations for Further Research

This investigation included experiments in which stainless steel bars which had been coated with simulated contamination were electroslag remelted using a variety of chemically different slags. Free energy minimization modeling of the interaction between the molten stainless steel and a slag (which was assumed to be idea) was used to predict the outcome of each melting experiment performed. The predicted outcome and the actual outcome of each experiment were compared. Simulations were also performed for the melting of uranium contaminated stainless steel. The activities of various species in the slag were calculated using a Temkin model. Samples of the slag were analyzed in order to determine the manner in which the surrogate elements were divided between the slag cap and the skin. One melting experiment was performed on a material which had been bulk contaminated with surrogate elements rather than surface contaminated with oxides. Samples from each ingot produced were analyzed to determine the changes in major alloying elements induced by remelting as well as to determine the decontamination achieved. Several interesting conclusions may be drawn from the results of this research. Questions were also raised which provide opportunities for further research.

## 9.1 Conclusions

Several conclusions may be drawn from the data collected, the analytical results obtained, and the observations made during this study:

1. Free energy minimization modeling predicted that, for each slag tested, cerium and lanthanum would be removed from the stainless steel to below the detection limit of 1 ppm. Results of the melting studies proved this prediction accurate for the melting of surface contaminated material.

2. Some slags enabled the production of ingots with excellent surface quality. The use of other slags, however, resulted in very rough ingot surfaces with associated slag entrapment. Steel from the surface of a smooth ingot was shown to contain undetectable levels of surrogates, while analysis of steel from the surface of an ingot which had poor surface quality revealed the presence of surrogate elements. The surface treatment of ingots prior to final forming operations is costly, and, if the grinding dust produced by such operations is radioactive, surface treatment could cause potential exposure of personnel in a melt refining facility. This study indicates that the proper choice of slag can eliminate the need for surface treatment of ingots.

3. Free energy minimization modeling predicted that the residual level of cerium and lanthanum in the steel would be dependent on the chemistry of the slag. Predictions also indicate that this would be true for the melt refining of uranium contaminated stainless steel. In most, but not all cases, the same slags which are predicted to most effectively remove the surrogate elements from steel are also predicted to be most effective for uranium removal. Differences arise from the thermochemical mechanism by which various elements are captured by a slag. Lanthanum and cerium are predicted to react with various ions in the slag to form compounds such as fluorides, oxides, and oxyaluminates, while, according to free energy minimization, uranium is captured in the slag primarily by the formation of $UO_2$.

4. Cerium and lanthanum are similar to the transuranic elements in many respects including the free energies of formation of their stable oxides. The mechanisms by which transuranic elements react with ions in a slag and are removed from the molten metal may be different than those mechanisms for the surrogate elements. Free energy minimization modeling suggested that the transuranic elements may behave differently during electroslag remelting than the surrogate elements by which they have been represented in this study. Lanthanum and cerium form very stable ternary compounds with oxygen and aluminum, $LaAlO_3$ and $CeAlO_3$. There is a substantial driving force for the formation of these compounds in ESR slags because the alumina is able to dissociate by the formation of $Al^{3+}$ and $AlO_3^{3-}$ ions. The ions are then able to combine with $La^{3+}$ and $Ce^{3+}$ forming stable compounds which are responsible for the predicted ability of some slags to remove the surrogate elements from steel more effectively than other slags.

The transuranic elements either do not form ternary compounds with oxygen and aluminum or data regarding the formation of these compounds is presently unavailable. The surrogate elements and the transuranic elements may also behave differently because the densities of the inclusions formed by the reaction of the transuranic elements with oxygen are greater than those of the surrogate oxides. Heavier inclusions will be less likely to float and thus will be less effectively captured by the slag.

5. The chemistry of the slag was found to influence changes in the chemical constitution of the stainless steel. Remelting was shown to remove manganese, sulfur, and silicon from the steel. The extent of removal was dependent on the chemistry of the slag. Some slags also removed carbon, chromium, molybdenum, and phosphorous. In most cases, chemical changes induced by remelting did not result in the production of steel which was out of specification for the 304L grade. In fact, the sulfur reduction may indicate that the process removed sulfur containing inclusions and thus increased the cleanliness of the steel, which could lead to improved corrosion resistance and mechanical properties. None of the slags were expected to remove nickel, copper, or cobalt from the steel and this proved to be the case.

6. The chemistry of the slag was found to influence the power required to heat the slag sufficiently so that the stainless steel electrode could be melted. Slags with high resistivity generally require the application of less power to achieve a temperature suitable for melting than slags of low resistivity.

7. A study of the manner in which slags of different chemistry begin to solidify to form a slag skin revealed that the thickness of the slag skin is related to the mechanism by which solidification takes place as well as the chemistry of the phases which solidify.

8. The surrogate elements present in the slag showed a tendency to selectively partition to the slag skin when some slags were used and to partition to the slag cap when other slags were used. The electroslag melt decontamination process could be simplified if the radionuclides could be made to partition to the slag cap, which, after remelting, is a highly dense solid block. A model proposed to explain the observed partitioning was based on the dominant chemical species

formed by the surrogates in slags of various chemistries and the solidification mechanics taking place during the melt.

9. Based on the results of this testwork, the optimum slags to use for the electroslag decontamination of radioactive stainless steels are proposed to be those which lie along the peritectic solidification path terminating at point P1 on the ternary phase diagram and contain more than 60% $CaF_2$. While these slags may not be the most power efficient, they form very thin slag skins, produce ingots with smooth surfaces, and due to the presence of a high fluoride liquid present throughout solidification, they have the potential to partition radionuclides to the slag cap.

## 9.2 Recommendations for Further Research

The findings of this study raised several questions which could present opportunities for further research:

1. The consequences of performing vacuum induction melting for the consolidation of scrap prior to the electroslag remelting of the resultant electrode should be studied in detail. Such a two step process could take advantage of the vacuum induction melting step to remove volatile radionuclides such as cesium and strontium and the electroslag remelting step to remove nonvolatile radionuclides. The lack of success in the removal of surrogates from the one bulk contaminated melt attempted indicates the necessity of fully researching the implications of two stage melt refining and the optimization of this process.

2. Thermodynamic modeling predicted that some slags would allow a higher residual concentration of the surrogate elements in the steel than others. The predicted levels, however, were so low that this could not be confirmed by the results of the melting experiments. Small differences in the level of decontamination achieved could be important, however, especially for highly hazardous elements such as plutonium. In order to confirm the modeling predictions, radioactive tracer studies would have to be performed. Such studies could also be used to study the mechanisms by which various transuranic elements

react to form compounds which are either captured in the slag, retained as inclusions in the steel, or released as gasses.

3. In order to study the mechanisms by which the chemistry of the steel is changed by remelting, several melts should be performed using slags of different chemistries and samples of slag and gas should be taken throughout each. Specifically, further work should be done in order to determine the mechanisms responsible for carbon enrichment and chromium loss, as either of these could result in the production of steel which did not meet the chemical requirements of the desired grade.

4. The solidification model proposed in this research should be confirmed by performing a series of melts using slags blended from pure components for which the solidification paths may be traced. Samples of slag skin should be taken from several locations along the length of each ingot. Identification of the phases present should provide information about the mechanisms by which the slag skin is formed. Samples of the liquid slag should be taken at intervals throughout each heat. Analysis of the elemental makeup of these samples would provide information on the manner in which the chemistry of the liquid slag changes throughout the course of a heat. This series of experiments should be repeated using known amounts of various slag impurities in order to determine how each impurity or combination of impurities affects slag skin formation and thus, final slag skin thickness.

5. Perform radioactive tracer experiments to determine whether the transuranic elements partition between the slag skin and the slag cap in the same manner observed for the surrogate elements. The mechanism for surrogate partitioning should be fully evaluated for each radionuclide of interest, as the compounds formed by uranium, plutonium, and the other actinides may be different than those formed by the surrogates and will have different melting points.

6. A model is needed which accurately describes the ESR process and includes the dynamic changes in slag chemistry, the factors which influence these changes, and the effects of these changes on the operation of the process as a whole. This model, would, of necessity include an accurate thermochemical description of the slag, including activity and interaction coefficients. Free energy

minimization would also be a useful component of this model, but must be able to account for the formation of gaseous phases. Continuing testwork would be necessary to benchmark the model and to insure its accuracy.

# Appendix I
# Radioactivity:
# Terms and Definitions

## Radionuclides: Nomenclature

A neutral atom consists of a small dense central nucleus surrounded by a diffuse cloud of electrons. The nucleus contains most of the mass of the atom and carries a positive electric charge that equals a whole number times the electronic charge $1.606101 \times 10^{-19}$ C. This whole number is the atomic number, Z, of the atom and is identical with the serial number of the element in the periodic table. For an element with atomic number Z, the nucleus is made up of Z protons and a definite number of N neutrons. The total number of particles, A, in the nucleus (N+Z) is called the mass number. All neutral atoms having a given atomic number and given mass number are members of the same nuclide species, and have similar nuclear properties. Nuclides having the same mass number but different atomic numbers are called isobars, while nuclides having the same atomic number but different mass numbers are called isotopes. Isotopes are of concern in this study because, although they have very similar chemical properties their nuclear properties may be different. A nuclide is represented by writing the mass number after the chemical name or as a superscript preceding the chemical symbol. The complete notation for a nuclide is the element symbol preceded by a subscript which is Z, the atomic number of the element, and a superscript, A, the mass number of the nuclei (the number of protons plus the number of neutrons). Nuclei with given A and Z can exist temporarily in metastable states having more energy than the ground state. Nuclei with the same A and Z but different energies are called isomers; those of higher energy are represented by placing an m or * after the mass number in the superscript as in $^{85m}Kr$.[1]

Radioactivity is the spontaneous emission of particles or radiation from isotopes which have unstable nuclei, anxious to drop to more stable energy states by splitting (fission) or emitting particles and various types of radiation. The stability of a nucleus and type of decay is associated with the ratio of neutrons to protons it contains. If the ratio is too high, a neutron is converted to a proton and a beta particle (electron). If the ratio is too low a proton is converted to a neutron and a positron. When a neutron is captured by the nucleus, an unfavorable balance of protons to neutrons may result. The neutron rich

nucleus commonly corrects this by forming a new element with the emission of a beta particle and a neutrino. The nucleus formed by this beta decay may be in an excited state and may drop to a more stable energy level by emission of gamma rays.[2] Radioactive nuclides break down spontaneously, generating different types of radiation. The probability that a radioactive nucleus will decay in a given time is independent of temperature, pressure or the decay of other neighboring nuclei. The disintegration of individual nuclei are statistically independent events, but in a large number of nuclei, the fraction that decays in a unit time is a constant and is numerically equal to the probability that a single nuclei will decay in that time. The rate of radioactive decay is expressed by the decay constant $\lambda$ and has units of reciprocal time. Because the number of nuclei that decay in a unit time is proportional to the number present, radioactive decay is first order reaction. If N is the number of nuclei present at time t and if N changes with time due to radioactive decay, then

$$\frac{dN}{dt} = -\lambda N$$

which integrates to an equation which describes the number present at time t:

$$N = N^{o}e^{-\lambda t}$$

Where $N^{o}$ is the number of nuclei present at time zero. It is customary to describe the specific rate of radioactive decay by the half-life $t_{1/2}$ which is the length of time required for half of the nuclei originally present to decay. The half life is related to the decay constant as follows:

$$\frac{N^{o}}{2} = N^{o}e^{-\lambda t_{1/2}}$$

$$t_{1/2} = \frac{\ln 2}{\lambda} = \frac{0.693}{\lambda}$$

The curie (Ci) is a unit defined as the amount of radioactive material that will produce $3.7 \times 10^{10}$ disintegration per second. This is approximately equal to the number of disintegration per second in 1 gram of radium. The becquerel (bq) is the amount of radioactive material that produces one disintegration per second. Because the number of disintegration per second in 1 gram atom is $\lambda N$, where N is Avogadro's number (6.02252

X $10^{23}$ atoms/gram-atom) the number of curies per gram of a nuclide of atomic weight M and decay constant $\lambda$ is

$$\frac{\lambda N}{3.7\times10^{10}M} = 1.13\left(\frac{10^{13}}{t_{1/2}(s)M}\right)$$

This means that the heavier the element and the longer its half life, the amount of material required to produce 3.7 X $10^{10}$ disintegration per second is decreased. This becomes important in determining an acceptable level of contaminant, as it not only depends on the concentration of radioactive element which is present, but also on the specific elements present and the types of radiation which they emit when decay takes place.[1]

## Types of Radioactivity

When the types of radionuclides likely to be present at any nuclear site are known the types and levels of radioactivity may be predicted and appropriate safety standards implemented. Radioactive nuclides break down in different ways which may yield particles of various charges, fission products, energy in the form of photons or x-rays, or a combination of these.

Alpha radioactivity results from the discharge of alpha particles which are double charged ions of helium which, in passing through matter such as an ordinary sheet of paper, give up their energy and become neutral helium atoms. Because of their short range alpha particles do not present a hazard unless they are ingested, at which point they become very toxic because of the large amount of energy released in a short distance within living tissue. Alpha radioactivity is found principally among elements beyond bismuth on the periodic table. All the nuclides important as fissionable materials are alpha emitters with half lives as listed in Table AI.1.

**Table AI.1 Half Lives of Important Alpha Emitters**

| Nuclide | Half-life, years |
|---|---|
| $^{232}Th$ | $1.41X10^{10}$ |
| $^{233}U$ | $1.62X10^{5}$ |
| $^{235}U$ | $7.1X10^{8}$ |
| $^{238}U$ | $4.51X10^{9}$ |
| $^{239}Pu$ | $2.44X10^{4}$ |

The beta-radioactive nuclides important in nuclear reactors decay by emitting negative electrons. The daughter nuclide thus has an atomic number one higher than the parent. Beta radioactive isotopes are known for every element. The half lives of several important nuclides are listed in Table AI.2 . Although beta particles have a greater range than alpha particles they can be stopped by relatively thin layers of water, glass, or metal. Precaution must be taken when handling beta emitters as the range of beta particles in tissue is great enough to cause burns when the skin is exposed. Additionally, beta active isotopes may become fixed in the body and are very toxic. For example, $^{90}Sr$ becomes fixed in bone. Other isotopes such as $^{85}Kr$ or $^{14}C$ which are turned over quickly by the body are much less toxic.

**Table AI.2 Beta Emitting Radioactive Nuclides**

| Nuclide | Half-life |
|---|---|
| $^{85}Kr$ | 10.76 yr |
| $^{89}Sr$ | 50.5 days |
| $^{90}Sr$ | 28.1 yr |
| $^{131}I$ | 8.05 days |
| $^{233}Th$ | 22.2 min. |
| $^{233}Pa$ | 27.0 days |
| $^{237}U$ | 6.75 days |
| $^{239}U$ | 23.5 min. |
| $^{239}Np$ | 2.35 days |

Gamma rays are photons given off when a nucleus undergoes transition from a state of higher energy to one of lower energy. The wavelength $\lambda$ of the radiation is related to the energy change $\Delta E$ of the nucleus emitting this quantum of radiation by the equation

$$\lambda = \frac{hc}{\Delta E}$$

where h is Plank's constant, $6.62559 \times 10^{-34}$ J•s, and c is the velocity of light, $2.997925 \times 10^{8}$ m/s. Gamma rays are hard, or high frequency x-rays which penetrate great thicknesses of matter before being absorbed. Because of the penetrating nature of gamma radiation, overexposure of the body to it results in extensive organic damage. Of the types of radiation from radioactive substances, gamma radiation represents the most serious hazard and those working around gamma sources must use heavy shielding and remotely controlled operations. Table AI.3 shows the half lives of some gamma emitters resulting from the decay of fission products.

**Table AI.3 Examples of Gamma Emitting Radioactive Nuclides**

| Nuclide | Source of nuclide | Half-life |
|---|---|---|
| $^{60m}Co$ | Neutron capture: $^{59}Co$ | 10.5 min. |
| $^{80m}Br$ | Neutron capture: $^{79}Br$ | 4.38 hr |
| $^{91m}Y$ | Decay of $^{91}Sr$ | 50 min. |
| $^{99m}Tc$ | Decay of $^{99}Mo$ | 6.0 hr |
| $^{127m}Te$ | Decay of $^{127}Sb$ | 109 days |
| $^{135m}Xe$ | Decay of $^{135}I$ | 15.6 min. |
| $^{137m}Ba$ | Decay of $^{137}Cs$ | 2.55 min. |

Many of the nuclides in the actinide family (U, Np, Pu, etc.) will fission spontaneously as one of the modes of radioactive decay. For a nuclide with multiple modes of radioactive decay, the half-life of the nuclide is usually determined from the total decay rate, representing all decay processes for that nuclide. In the case of spontaneous fission, however, a separate half life for that process alone is used. Examples of nuclides that undergo spontaneous fission are given in Table AI.4. The neutrons from spontaneous fission are emitted with average energies of a few million electron volts. These fission neutrons carry no electrical charge, so they readily penetrate solids and liquids, being stopped or slowed down only when they collide with nuclei of the material through which they are traveling. A neutron loses the greatest amount of energy per collision when it collides with a hydrogen nucleus, whose mass is almost identical with its own. When these neutrons pass through tissue, the hydrogen nuclei (protons) recoiling from neutron collisions cause ionization within the tissue resulting in severe biological damage. Radionuclides which exhibit spontaneous fission should be shielded with mixtures of hydrogenous materials and neutron absorbers (boron).

**Table A1.4 Examples of Nuclides Undergoing Spontaneous Fission**

| Nuclide | Half life for spontaneous fission, yr |
|---|---|
| $^{235}U$ | $1.9X10^{17}$ |
| $^{238}U$ | $10^{16}$ |
| $^{239}Pu$ | $5.5X10^{15}$ |
| $^{240}Pu$ | $1.4X10^{11}$ |
| $^{242}Pu$ | $7X10^{10}$ |
| $^{244}Cm$ | $1.3X10^{7}$ |
| $^{252}Cf$ | 85 |

# Appendix I References

[1] Benedict, M, Pigford, T., Levi, H., Nuclear Chemical Engineering, McGraw Hill, New York, (1981), 1-35.

[2] Lippincott, W.T., Garrett, Alfred B., Verhoek, Frank H., Chemistry: A Study of Matter, John Wiley and Sons, New York, (1977),598-613.

# Appendix II
# Copper Mold and Water Jacket Assembly

This Appendix contains drawings of the copper mold and water jacket used in the melting experiments, as well as a description of mold cooling.

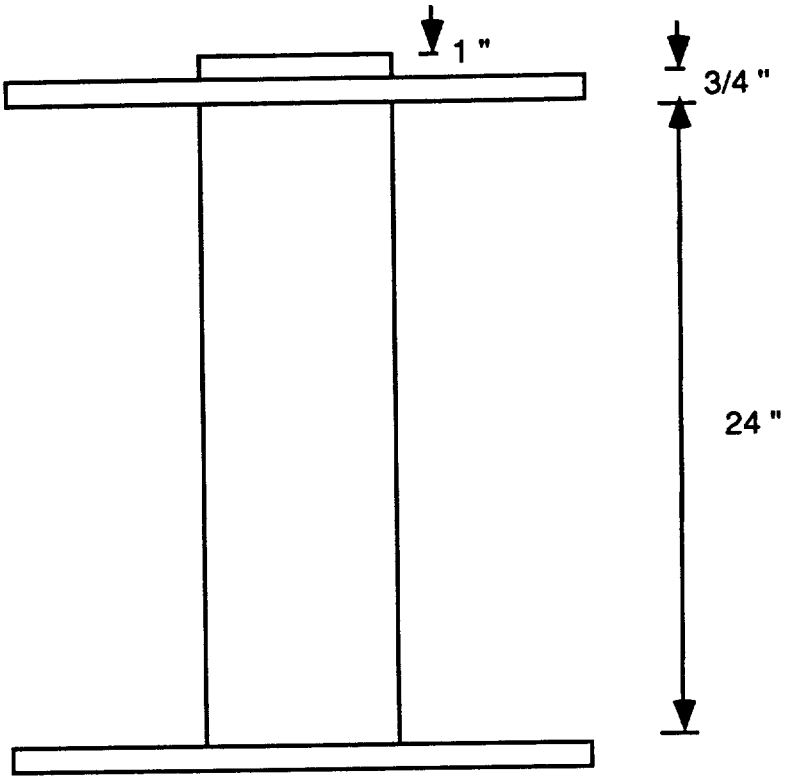


Copper molds

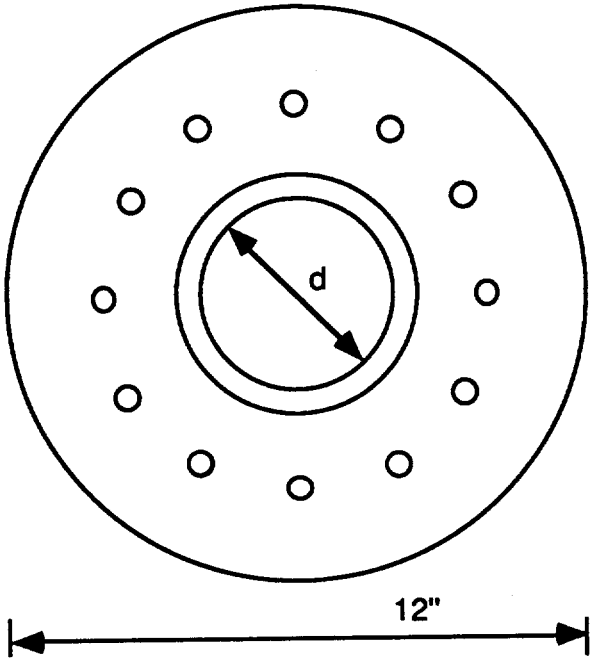


d (inner diameter of copper mold) = 3 3/4"

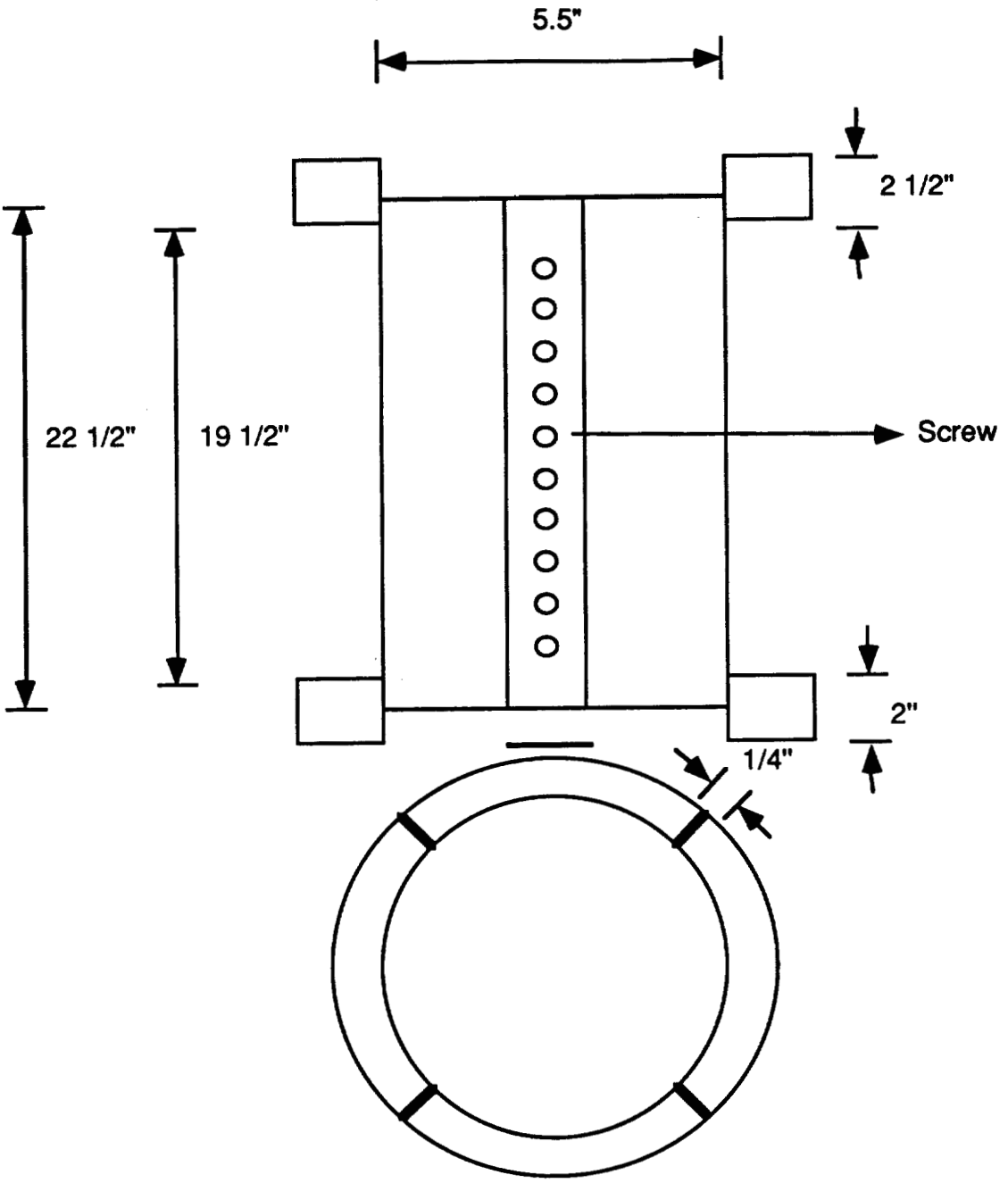


Inner Water Jacket

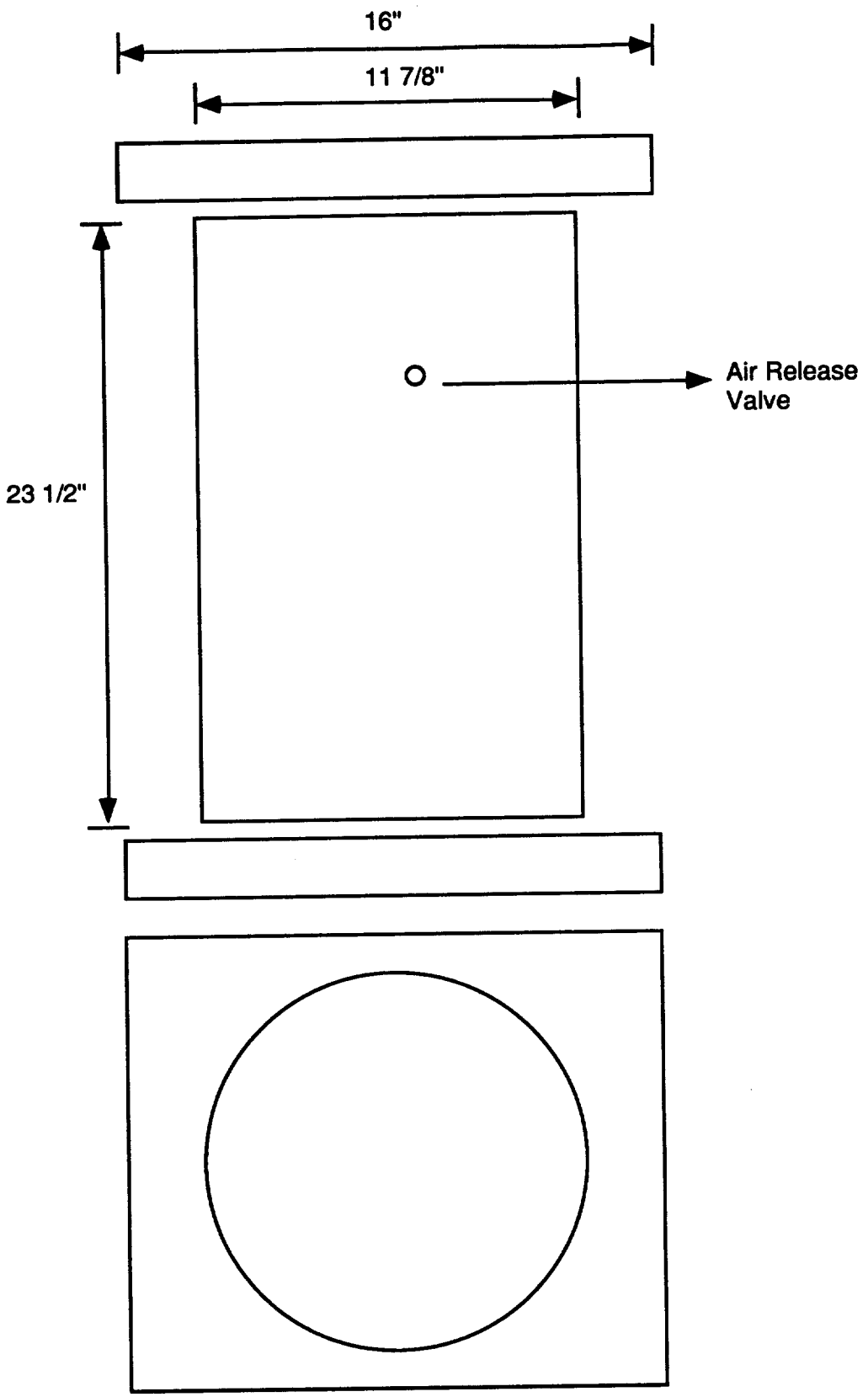


Outer Shell of Water Jacket

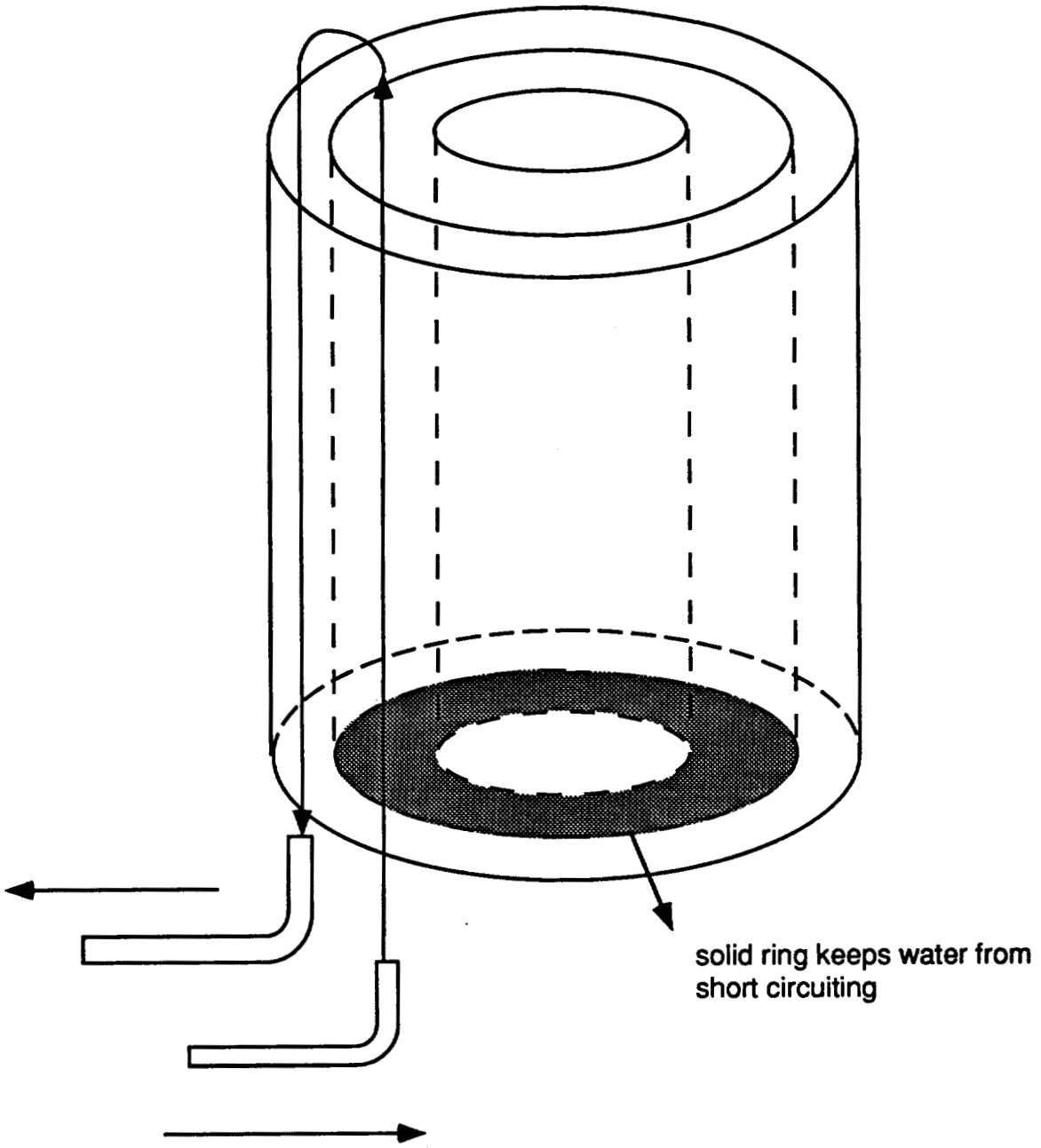


Schematic of water flow around copper mold

## Cooling Water Considerations in Water Jacket Design

The flow of heat through ESR crucibles depends on several factors including slag skin thickness, shrinkage gap width, cooling water flow rate, and crucible surface condition. In ESR, heat is generated by joule heating of the slag, which acts as a resistor. The heat which is transferred by direct contact with the copper crucible results from the contact of liquid slag with the copper. As the slag solidifies, it pulls sway from the copper wall and heat transfer must proceed by radiation and air conduction through an air gap. There are two regions of importance when considering the mold/water interface: the nonboiling region and the surface boiling region. On examining the temperature distribution on a copper mold, it may be observed that the temperature of the copper mold containing the liquid slag and metal pool is above the boiling point of water at atmospheric pressure. When the surface temperature exceeds the saturation temperature, local boiling in the vicinity of the surface may take place even if the bulk water temperature is below the boiling point. This boiling in a liquid whose bulk temperature is below the saturation temperature, but whose boundary layer is sufficiently superheated that bubbles form next to the heating surface, is usually called surface boiling. The amount of heat transferred to the cooling water in the nonboiling region is a small proportion of the total heat flux into the mold cooling water. A high rate of water flow through the annulus is necessary to insure a fast cooling rate and to maintain the crucible temperature below the water boiling temperature for the sake of safety. The fluid mechanics equations for flow through an annulus are as follows:

For an incompressible fluid flowing in steady state between two coaxial cylinders the velocity distribution in the upward direction as defined in Figure Figure AII.1 is given by:

$$v_z = \frac{(P_O - P_L)R^2}{4\mu L}\left[1 - \left(\frac{r}{R}\right)^2 + \left(\frac{1-\kappa^2}{\ln\left(\frac{1}{\kappa}\right)}\right)\ln\left(\frac{r}{R}\right)\right]$$

where R is the inside radius of the large cylinder (stainless water jacket) and $\kappa R$ is the outside radius of the small cylinder (copper crucible). $P_O$ is the inlet pressure and $P_L$ is the

outlet pressure of a fluiid of viscosity μ over a mold of length L. The velocity vz at any radial position, r, can be calculated by use of this formula.
The maximum velocity (midway between the cylinders) is:

$$v_{z,\max} = \frac{(P_O - P_L)R^2}{4\mu L}\left\{1 - \left(\frac{1-\kappa^2}{2\ln\left(\frac{1}{\kappa}\right)}\right)\left[1 - \ln\left(\frac{1-\kappa^2}{2\ln\left(\frac{1}{\kappa}\right)}\right)\right]\right\}$$

The average velocity is ;

$$\langle v_z \rangle = \frac{(P_O - P_L)R^2}{8\mu L}\left(\frac{1-\kappa^4}{1-\kappa^2} - \frac{1-\kappa^2}{\ln\left(\frac{1}{\kappa}\right)}\right)$$

The volume flow rate is:

$$Q = \pi R^2 (1-\kappa^2)\langle v_z \rangle$$

$$Q = \frac{\pi(P_o - P_L)R^4}{8\mu L}\left((1-\kappa^4) - \frac{(1-\kappa^2)^2}{\ln\left(\frac{1}{\kappa}\right)}\right)$$

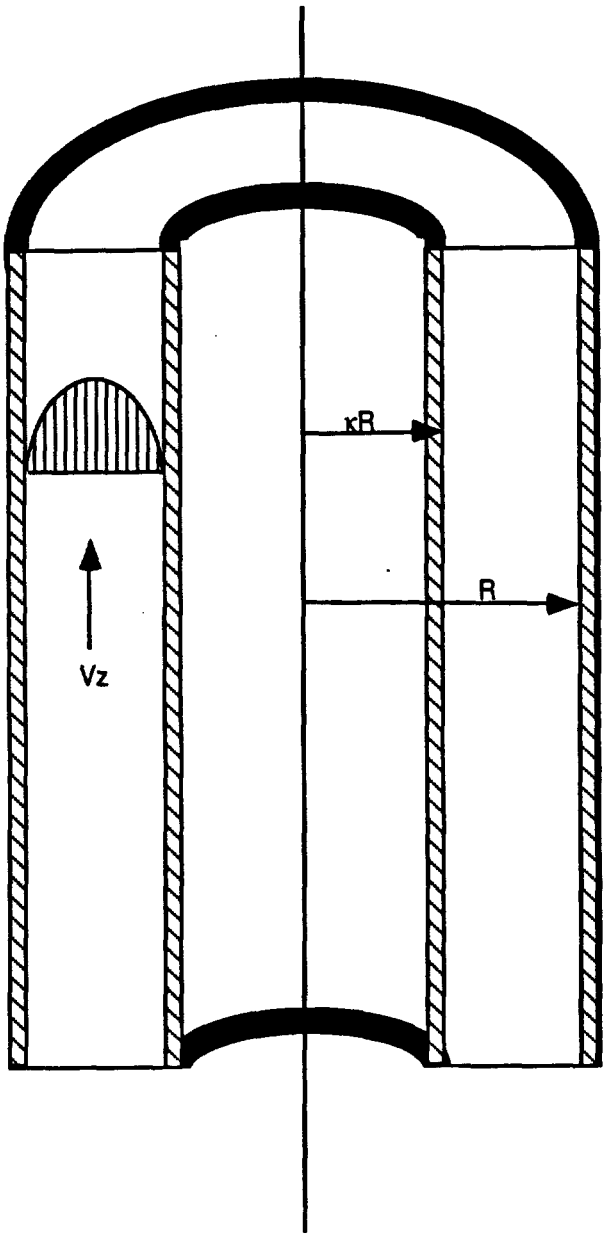


**Figure AII.1 Flow in an Annulus**

For the ESR mold and water jacket assembly currently in use the outside diameter of the copper mold is 4.475 inches and the inside diameter is 3.890 inches, so the average thickness of the copper is 0.293 inches. The gap between the outside of the copper and the inside of the stainless was originally 5/8 of an inch, but was reduced to 1/2 inch. A rule of thumb for a "safe" water velocity is between 2 and 10 ft/sec at the copper wall. Even after

modifications, the water jacket was on the low end of the safe zone (about 4 ft/sec), as shown in Figure AII.2, and so thermocouple readings were monitored closely.

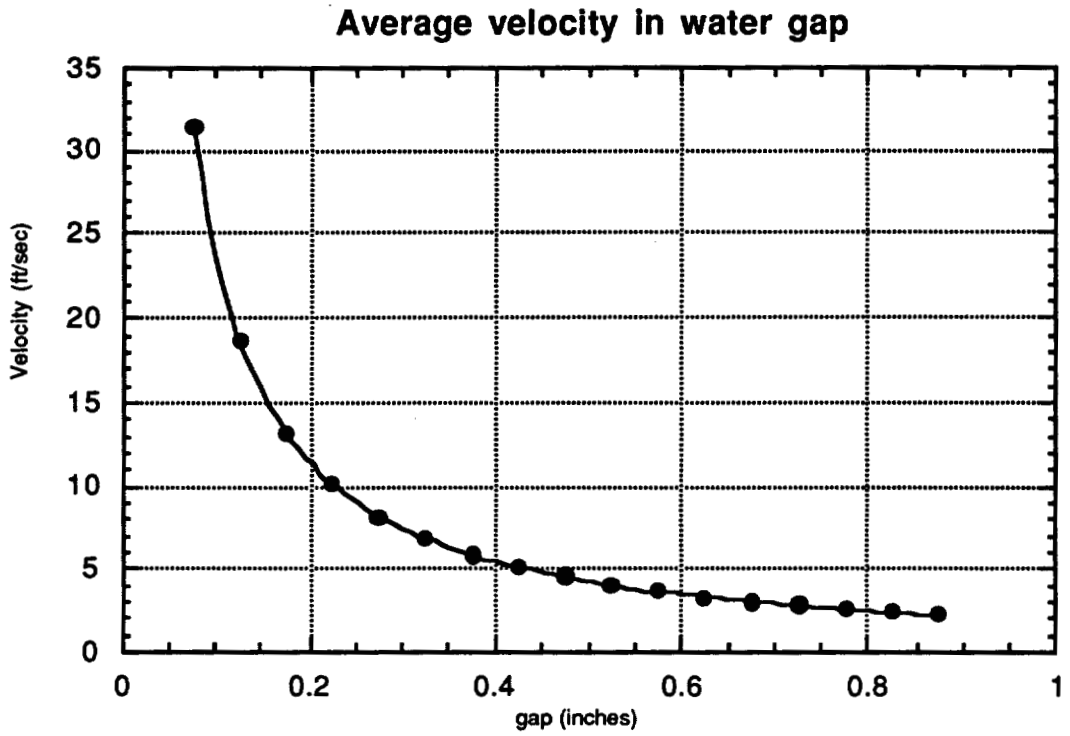

# Biographical Sketch

Joanna Meredith Robertson was born in Henderson, Nevada on June 30, 1959. She grew up in small copper mining towns in Arizona and, in 1977, graduated from Ajo High School. She attended University of Arizona in Tucson where she majored in Metallurgical Engineering and graduated with a B.S. in 1981. In May of 1983, she graduated from the Montana College of Science and Technology in Butte, Montana with a Masters Degree in Mineral Processing Engineering. Her thesis was entitled "Recovery of Copper from Converter Slag by Flotation: An Optimization Study"

From 1983 until 1985 she worked as a Mineral Processing Engineer for the Illinois State Geological Survey in Urbana, Illinois on a project to remove pyritic sulfur from coal by means of a modified froth flotation technique. From 1986 to 1989, she was employed by North Star Steel in Beaumont, Texas as a Quality Assurance Metallurgist assigned to melting and casting. Her interests and special projects included modifying slag practice to influence steel desulfurization and use of special refractories to influence steel cleanliness.

In 1990, she enrolled in graduate school at the Oregon Graduate Institute in Beaverton, Oregon where she began work on an advanced degree in Materials Science Engineering. While at OGI, she did research relating to the presence of nonmetallic inclusions in vacuum induction melted Inconel 718. She also worked on a project involving the precipitation hardening of aluminum alloy 7075. In 1994, she began working on her dissertation research and in July of that year she transferred to Sandia National Laboratories as an Associated Western Universities Fellow in order to complete her testwork.

Joanna M. R. Buckentin is a member of ASM and its associated honor society, Alpha Sigma Mu. She was assisted in obtaining her degree by her two children, Michael John, who was born in May of 1984, and Patrick Joseph, who was born in August of 1988. Her other activities include writing children's stories, watercolor painting, and playing with her German Shepherd dog